UNIVERSITY OF
BIRMINGHAM

CORRELATION BETWEEN GEOTECHNICAL AND GEOPHYSICAL PROPERTIES OF SOIL

by

NASTARAN SHIRGIRI

A Thesis submitted to
The University of Birmingham
For the degree of
MASTER OF PHILOSOPHY

School of CIVIL ENGINEERING
College of ENGINEERING AND PHYSICAL SCIENCES
The University of Birmingham
April 2012

ABSTRACT

In the UK road network, it is estimated that up to 4 million holes are cut each year in order to install or repair buried service pipes and cables, and it is important to identify the location of existing buried assets prior to such works if the numerous potential practical problems such as unforeseen costs and dangers for utility owners, contractors and road users are to be avoided. The Mapping the Underworld research team is attempting to develop the means to locate, map in 3-D and record the position of all buried utility assets without excavation. To realise this aim four different kinds of technologies are being studied: ground penetrating radar, acoustics, low frequency active electromagnetic fields and passive electromagnetic fields. All these techniques need waves to travel through the ground and they are affected by the ground properties.

Geophysical techniques, such as the seismic surface wave technique, offer a non-intrusive and non-destructive way of analysing the ground and potentially providing measurements of geotechnical properties. However, we need to be careful in comprehending the relationships between geophysical techniques and geotechnical ground properties to ensure reliable interpretation and so as not to overrate the results that geophysics can accomplish.

This research discusses the model testing for Kaolin and OxfordClay, which was carried out to help to understand seismic surface wave results in relation to the geotechnical properties of the soils. The surface wave tests were initially carried out to establish an optimal methodology for the evaluation of this correlation as well as to prove the accuracy of the equipment and its system for surface wave testing at the laboratory scale. The surface wave

technique generated and recorded the shear waves in the soil samples, enabling a shear modulus profile to be determined for the two soils over a range of water contents from significantly wet to significantly dry of the optimum water content (and hence maximum dry density) of the compacted clay soils. This made it possible to vary the subsurface velocity with different variations in water content and density over short distances.

The relationships obtained from the controlled tests showed close agreement to those reported in literature, but that the literature only considers a narrow range of water contents. The test results demonstrated that the shear wave velocity, and hence the shear modulus, decrease with increasing moisture content. Importantly the test results also indicated that the shear wave velocity, hence shear modulus, has an inverse relation with density before it reaches the optimum water content (or maximum dry density) after which they exhibit a direct relationship, i.e. the shear wave velocity decreases while the density decreases.

DEDICATION

To my parents, of course;
Kian & Mahmood
There is no doubt in my mind that without their
Continued support and counsel
I could not have completed this process

ACKNOWLEDGMENTS

This thesis was made possible by the support and assistance of a number of people whom would like to personally thank.

I am heartily thankful to my supervisor Prof. Chris Rogers for giving me the opportunity to carry out this Thesis and for being a great supervisor. Thank you for all your patience, help, support and guidance throughout the process.

I would also like to thank Dr. Nicole Metje as my co-supervisors., for all the advice and encouragement.

I would like to acknowledge gratefully for the assistance receive from the following:

Dr G.Ghataora and Dr I. Jefferson for their opinion and advice.

Mr. Aziman Madun for all his time, help and advice.

Mr Phillip Robert Atkins for lending his laboratory testing equipment, as well as sharing his knowledge and experience on the testing and the signal processing.

Dr David Gunn for his helps in my early understanding of seismic surface wave.

Lab technicians' Mr Michael Vanderstam, Mr David Cope, Mr Jim White, Mr Nathan and Mr Bruce Reed for their support.

Miss Lyn Hipwood for her helps, time and support.

Mr Mark Britton, for all his helps.

Friends and post graduate members' in room F59B (November 2009 to April 2012) for their help and support.

Finally members of my family and my lovely friends, specially Saba Ghasemi, for their help and support.

Table of Contents

ABSTRACT…….. i

DEDICATION…….. iii

ACKNOWLEDGMENTS……..……..... iv

LIST OF FIGURES……... viii

LIST OF TABLES……..……..... xii

LIST OF ABBREVIATIONS……..... xiv

Chapter 1 ……..... 1

1.1 Introduction……..... 1

1.2 Research Aim and Objectives……..... 3

1.3 Outline of thesis……..... 4

Chapter 2 ……..... 6

2.1 Introduction…….…….. 6

2.2 Overview of Geophysical Techniques…….……. 7

2.2.1 Ground Penetration Radar (GPR) …….……. 9

2.2.2 Electrical Resistivity …… 11

2.2.3 Seismic –based Methods …….…… 12

2.3 Seismic Waves ……... 14

2.3.1 Body Waves …….…….. 16

2.3.2 Surface Waves ……....…… 20

2.3.2.1 Spectral Analysis of Surface Waves (SASW) …..…… 22

2.3.2.2 Continuous Surface Wave (CSW) …….…… 24

2.3.2.3 Multi-Channel Surface Waves (MASW) ….…….. 27

2.4 Surface Wave Method …….……. 29

2.5 Relationship of Seismic to Geotechnical Parameters …..……. 31

2.6 Experimental Relationships and Data From The Literature …..... 34

2.7 Summary ……. 44

Chapter 3 …….. 45
3.1 Introduction ……. 45
3.2 Establishing Laboratory Seismic Surface Wave Equipment ……. 47
3.2.1 Seismic Surface Wave Equipment ……..... 49
3.3 Experimental Procedure …….. 53
3.4 Method for Data Processing ……..……. 54

Chapter 4 ……. 59
4.1 Introduction ……... 59
4.2 Data Processing ……...…..... 59

Chapter 5 ……. 64
5.1 Introduction ……..... 64
5.2 Clay Materials Used in Test Beds ……..... 64
5.2.1 Plasticity Measurements …….. 65
5.2.2 Specific Gravity ……..... 66
5.2.3 Compaction Test …… 66
5.3 Preparation of Kaolin clay Test Bed …….. 67
5.4 Preparation of Oxford clay Test Bed …….. 69
5.5 Preparation of The Test Bed …….…… 71
5.6 Seismic Test ……..... 72

Chapter 6 ……. 76
6.1 Introduction ……..... 76
6.2 Kaolin clay- 28% Moisture Content ……... 76
6.2.1 Repeatability of the tests- Kaolin clay ……..... 82
6.2.2 Kaolin clay, 24% and 33% Moisture Content ……... 86
6.3 Homogeneous Oxford clay- 32% Moisture Content ……..... 93
6.3.1 Repeatability of the tests- Oxford clay ……. 97
6.3.2 Oxford clay, 19% and 24% Moisture Content 101
6.4 Discussion …….……..... 107

Chapter 7 …….. 109
7.1 Introduction ……..... 109
7.2 Equipment and System …….. 109
7.3 Clay Model …….. 110
7.3.1 Phase and Shear Wave Velocity Variations …… 110
7.3.1.1 Kaolin Clay ……..... 110
7.3.1.2 Oxford Clay ……..…….. 115
7.3.2 Shear Modulus …… 119
7.3.3 Shear Wave Velocity, Density and Moisture Content 123

Chapter 8 …….. 127
8.1 Introduction …… 127
8.2 Main Outcomes ……..…….. 128
8.3 Recommendations for Future Studies …….. 130

REFERENCES ……. 132

LIST OF FIGURES

Figure	2.1	GPR, electrical resistivity equipment seismic based method……	8
Figure	2.2	V, I and R, the parameters of Ohm's law……..	11
Figure	2.3	Resistivity……..	12
Figure	2.4	the Schematic elastic wave propagation in ground……	15
Figure	2.5	(a) Reflection and (b) Refraction……	17
Figure	2.6	Rayleigh wave dispersion……..	22
Figure	2.7	In an SASW measurement…….	24
Figure	2.8	Schematic diagram showing the steps for CSW technique…….....	27
Figure	2.9	MASW field data collection……..	29
Figure	2.10	Modulus Variations with Strain Level….....	32
Figure	2.11	Bender Element Wave Generation…….	33
Figure	2.12	Characteristic ranges of soil stiffness modulus……..	34
Figure	2.13	Variation of shear wave velocity with depth…….....	36
Figure	2.14	Distribution of shear velocity and water content with depth…….	39
Figure	2.15	Shear modulus versus wave length- Oxford Clay 32%.....	42
Figure	2.16	Shear modulus versus wave length- Oxford Clay 40%.....	42
Figure	2.17	Variation of S-wave velocity with degree of saturation ……	43
Figure	3.1	The seismic surface wave factors…….....	48
Figure	3.2	Outline details of the Initial and Main laboratory scale model tests……..	49
Figure	3.3	Electromechanical vibrator -absorber pad…….	50
Figure	3.4	Piezo-ceramic transducer located on sample……..	50
Figure	3.5	Detail of the equipment……..	51
Figure	3.6	Laboratory setup for seismic surface wave test…….....	52
Figure	3.7	photograph of the equipment……..	52
Figure	3.8	Illustration of the laboratory-scale model and equipment setup…….....	53
Figure	3.9	data collection process…….....	54
Figure	4.1	The phase differences for the 2 sensor-pairs Kaolin Clay …….	61
Figure	4.2	The Normalised coherence between channels A and B Kaolin Clay….....	62

Figure 4.3 Phase velocity versus frequency Kaolin clay……. 63

Figure 5.1 Compaction test for Oxford and Kaolin clay……. 67

Figure 5.2 Compacting Oxford clay and collect sample to measure the density…… 69

Figure 5.3 Plastic box of test bed……..... 70

Figure 5.4 Illustration of the laboratory-scaled model and equipment setup…….. 72

Figure 5.5 Seismic source at the middle of the receiver sensor-pairs……. 73

Figure 6.1 Normalised coherence, Kaolin clay, 28%, 100-10000Hz…….. 77

Figure 6.2 Normalised coherence, Kaolin clay, 28%, 1000Hz-9000Hz……. 78

Figure 6.3 Normalised coherence, Kaolin clay, 28%, 1500-8000Hz…….. 78

Figure 6.4 Unwrapped phase differences, Kaolin clay, 28%, 1500-8000Hz……. 79

Figure 6.5 Phase velocity versus frequency, Kaolin clay, 28%, 1500-8000Hz…….. 80

Figure 6.6 Wavelength versus phase velocity, Kaolin clay,28%, 1500-8000Hz……..... 81

Figure 6.7 Normalised coherence, Kaolin clay, 28% , (repeated),100Hz-10000Hz…... 83

Figure 6.8 Normalised coherence, Kaolin clay, 28% (repeated), 1500Hz-8000Hz…… 84

Figure 6.9 Unwrapped phase differences, Kaolin clay,28% (repeated)……..... 84

Figure 6.10 Phase velocity versus frequency, Kaolin clay, 28% (repeated)…… 85

Figure 6.11 phase velocity versus frequency ,Kaolin clay ,28%..... 86

Figure 6.12 Wavelength versus phase velocity, Kaolin clay, 28% (repeated)…….. 86

Figure 6.13 Normalised coherence, Kaolin clay with a 24%, 100Hz-10000Hz……... 87

Figure 6.14 Normalised coherence, Kaolin clay, 24%, 3000Hz-6000Hz……. 87

Figure 6.15 Unwrapped phase differences, Kaolin Clay, 24%..... 88

Figure 6.16 Phase velocity versus frequency, Kaolin clay, 24%..... 89

Figure 6.17 Wavelength versus phase velocity, Kaolin, 24%..... 89

Figure 6.18 Normalised coherence, Kaolin clay, 33%, 100Hz-10000Hz……. 90

Figure 6.19 Normalised coherence, Kaolin clay, 33%, 1000Hz-4000Hz……. 90

Figure 6.20 unwrapped phase differences , Kaolin clay ,33%..... 91
Figure 6.21 Phase velocity versus frequency, Kaolin clay, 33%..... 92
Figure 6.22 Wavelength versus phase velocity, Kaolin clay, 33%..... 92
Figure 6.23 Typical coherence, Oxford clay, 32% 100Hz-10000Hz……..... 94
Figure 6.24 Normalised coherence, Oxford clay, 32% 1000Hz-5000Hz……..... 94
Figure 6.25 Unwrapped phase differences s, Oxford clay, 32%..... 95
Figure 6.26 Phase velocity versus frequency, Oxford clay, 32%..... 96
Figure 6.27 Wavelength versus phase velocity, Oxford clay, 32% ……..... 97
Figure 6.28 Normalised coherence, Oxford clay, 32 %(repeated), 100Hz-10000Hz..... 98
Figure 6.29 Normalised coherence, Oxford clay, 32 %(repeated), 1000Hz-5000Hz….. 99
Figure 6.30 Unwrapped phase differences, Oxford clay, 32%..... 99
Figure 6.31 phase velocity versus frequency, Oxford clay ,32%..... 100
Figure 6.32 phase velocity versus frequency ,Oxford clay , 32%..... 100
Figure 6.33 Wavelength versus phase velocity, Oxford clay, 32% (repeated)…..... 101
Figure 6.34 Normalised coherence, Oxford clay, 24%..... 102
Figure 6.35 Normalised coherence, Oxford clay, 24%..... 102
Figure 6.36 Unwrapped phase differences, Oxford Clay, 24%..... 103
Figure 6.37 Phase velocity versus frequency, Oxford clay, 24%..... 104
Figure 6.38 Wavelength versus phase velocity, Oxford clay, 24%..... 104
Figure 6.39 Normalised coherence, Oxford clay, 19% moisture content……..... 105
Figure 6.40 Normalised coherence, Oxford clay, 19%..... 105
Figure 6.41 unwrapped phase differences ,Oxford clay ,19%..... 106
Figure 6.42 Phase velocity versus frequency, Oxford clay, 19%..... 107
Figure 6.43 Wavelength versus phase velocity, Oxford clay, 19%..... 107

Figure 7.1 Phase velocity versus frequency, 1500-8000 Hz, Kaolin clay……... 112

Figure 7.2 Phase velocity variation, 3000-4000 Hz, Kaolin clay…… 112

Figure 7.3 Shear wave velocity versus frequency, 1500-8000 Hz, Kaolin clay……..... 114

Figure 7.4 Shear wave velocity variation, 3000-4000 Hz, Kaolin clay……..... 114

Figure 7.5 phase velocity versus frequency,1000-7000 Hz, Oxford clay……..... 115

Figure 7.6 phase velocity variation , of 2000-5000 Hz, Oxford clay……..... 116

Figure 7.7 shear wave velocity versus frequency,1000-7000 Hz, Oxford Clay…….. 117

Figure 7.8 shear wave velocity,2000-5000 Hz, Oxford Clay……. 118

Figure 7.9 shear wave velocity, shear modulus, Kaolin clay…….. 120

Figure 7.10 shear wave velocity ,shear modulus , Oxford clay……. 121

Figure 7.11 Variation of shear modulus, Kaolin Clay……..... 121

Figure 7.12 Variation of shear modulus, Oxford clay……..... 122

Figure 7.13 Shear Modulus profile at different depth, Kaolin clay……... 123

Figure 7.14 Shear Modulus profile at different depth, Oxford clay…….. 123

Figure 7.15 Shear wave velocity, moisture content and density, Kaolin clay……... 125

Figure 7.16 Shear wave velocity, moisture content and density, Oxford clay……..... 125

LIST OF TABLES

Table	2.1	P and S-wave typical values for different earth materials…….…….	16
Table	2.2	Minimum, maximum and mean values of measure shear wave velocity…...	39
Table	5.1	Summary of the index properties of Oxford clay and Kaolin ……	65
Table	5.2	Density results- Kaolin clay……	69
Table	5.3	Density Results- Oxford clay……..	70
Table	5.4	Date for Kaolin and Oxford clay……	72
Table	7.1	Results of average phase velocity for kaolin clay……...	111
Table	7.2	Results of average shear wave velocity for kaolin clay……..……	113
Table	7.3	Results of average phase velocity for Oxford clay…….	115
Table	7.4	Results of average shear wave velocity for Oxford clay……	116

LIST OF ABBREVIATIONS

ϕ	Phase angle
2-D	Two dimensional
A-B	Sensor pair between A and B
B	Bulk modulus
C-D	Sensor pair between C and D
CPT	Cone penetration test
CSW	Continuous surface waves analysis
c_u	Undrained shear strength
d	Distance between the source and the first receiver
e	Void ratio
E	Young's Modulus
f	Frequency
FFT	Fast Fourier Transform
f_n	Frequency of n (n is integer)
f_s	Sampling rate
G_{max}	Maximum or small strain shear modulus
GPR	Ground penetrating radar
G_s	Specific gravity
I	Current
LL	Liquid limit
MASW	Multi-channel analysis of surface waves
MSW	Multi-channel surface wave
NI	National Instruments
PI	Plasticity index
PL	Plastic limit
P-wave	Compression / longitudinal wave
R	Resistance
SASW	Spectral analysis of surface waves
SNR	Signal-to-noise ratio

S-wave	Shear / transverse wave
V	Voltage
w	Water content
Δx	Spacing between the receivers
λ	Wave length
ω	Angular frequency (ω = 2πf)
³	Poisson's ratio
¬ $_p$	Compression / longitudinal wave velocity
¬ $_s$	Shear wave velocity
¬ $_r$	Rayleigh wave / phase velocity
$y_n(k)$	Time-domain signal at n discrete sample and time k
$Y_n(f)$	Spectrum of the signal at n discrete sample and frequency f
$\Delta¤_{mn}(w)$	Phase difference between receivers m and n at frequency w.
°	Soil bulk density
° $_w$	Water density

Chapter 1

INTRODUCTION

1.1 Introduction

In the UK road network, it is estimated that up to 4 million holes are cut each year in order to identify the location of existing buried assets when installing or repairing buried service pipes and cables. This results in numerous practical problems such as indirect and other costs and danger for utility owners, contractors and road users (Mapping the Underworld [online]). Therefore, the Mapping the Underworld research group is trying to develop the means to locate, map in 3-D and record the position of all buried utility assets without excavation. To reach this aim three different kinds of technologies are being studied: ground penetrating radar, acoustics, and low frequency active and passive electromagnetic fields. All these techniques need waves to travel through the ground and these waves are affected by the ground properties.

Geophysical techniques such as ground penetrating radar, electrical resistivity, and magnetism are convenient and use specific imaging equipment. However to use these methods entails skill, good knowledge and information on the geological model of the area, and support from

borehole data to interpret the results (Crice, 2005). Considering an example, there are shortfalls of using ground penetrating radar in obtaining deeper results when dealing with high conductivity material such as marine clays or saturated clays. The resistivity of soils differs depending on the moisture content and the soil type. The degree of soil resistance is chiefly controlled by the movement of charged ions in pore fluids. As a result, the salinity, porosity and fluid saturation tend to govern electrical resistivity measurements (Giao et al., 2003). Conversely, seismic wave techniques that are reliant on the modulus and density of the materials can be used to determine very useful parameters for engineering purposes, such as elastic modulus, shear modulus and Poisson's ratio, and are most effective when soils are saturated (as is often the case in the UK).

As such, geophysical techniques, like the seismic surface wave technique, offer a non-intrusive and non-destructive way of performing geotechnical properties measurements. Moreover, geophysical approaches such as this provide a cost effective way to investigate conditions on a test site. At the same time these methods help to overcome major shortfalls of classical analytical approaches. It is evident that geophysical testing can create very considerable high quality results. However, there is a need to be careful in comprehending the geophysical techniques, and essentially the disadvantages, so as not to overrate the results that geophysics can accomplish (Clayton et al., 1995).

The transmission of the seismic waves is in the form of body waves and surface waves. However the difference is that body waves are usually non-dispersive. In a solid and homogeneous medium, the velocity of surface waves does not oscillate drastically as a function of the distance propagated. However, when the properties of the medium vary with depth, surface waves become dispersive in a manner that the velocity of the propagation varies with respect to wavelength and frequency. Surface waves are also relatively less

attenuated as a function of the transmission distance when compared to body waves. These two characteristics make it practical to apply surface wave analysis for the survey of near-surface soil properties, and thus in turn the survey of any changes to these properties that subsequently occur.

Classical surface wave techniques that use a single pair of receivers generally yield one-dimensional results of phase velocity versus depth. In a laterally heterogeneous medium, however, it is more appropriate to use multi-channel receivers so as to avoid discrepancies. It is important to present a plot of the phase velocity against depth as a function of the lateral distance. Tallavo et al. (2009) have applied this method for the detection of buried timber trestles.

Therefore, the surface wave technique is used in the research reported herein to generate the phase velocities, which then were transformed to shear waves. With this, a shear modulus profile was then created and examined. The data processing technique was vital since it made it possible to vary the subsurface velocity with different variations in density over short distances. The results were further studied while considering the model properties and the configuration. Hence this research has been carried out to help to understand seismic surface wave result in relation to the geotechnical properties of the soils which is a related to the aim of the Mapping the Underworld group for design and construction of a prototype acoustic sensor to determine the acoustic technologies for locating the buried utility service location.

1.2 Research Aim and Objectives

The aim of the study is to assess how soil properties influence acoustic wave transmission and how they can be used to develop a correlation between acoustic and geotechnical properties.
To achieve this aim, the following objectives were established:

- Conduct an extensive literature review to critically assess the current knowledge and determine where there are gaps in knowledge with respect to seismic wave propagation through the ground

- Identify suitable seismic surface wave equipment for laboratory scale tests
- Develop a laboratory test to identify the influence of geotechnical soil properties on the propagation of the seismic waves and geophysical properties of soil
- Determine a suitable range of soils and soil conditions for the laboratory experiments in order to determine the correlation between geophysical and geotechnical properties of soils

1.3 Outline of Thesis

Chapter 2 presents a brief introduction to the use of geophysics, which includes an overview on various geophysical methods, types of seismic wave and a general description of the relationship between Seismic and Geotechnical Parameters. Chapter 3 describes the initial testing method for laboratory testing, which involved the development of equipment and its operational system. Sample preparation, development of the test equipment and measurement procedures are established for the seismic surface wave experimental work. Chapter 4 shows the possibility of the test procedure and a brief introduction to data processing and result analysis. Chapter 5 presents the geotechnical properties of clay materials used in the tests, the preparation of the test bed, the seismic surface wave testing arrangement and the data processing techniques. In Chapter 6 the test results are analysed, compared and discussed in detail. In Chapter 7, results are discussed and correlations are made between the seismic wave results and geotechnical properties of soil. This is followed by Chapter 8 which includes a summary and conclusions from the present work. Moreover it explains recommendations for future work, in the hope that further work will yield valuable and useful results. A complete list of references is included and lastly, the Appendices are found at the end of the thesis.

This research built upon prior research at the University of Birmingham and in particular draws upon the work by Aziman Madun.

Chapter 2

LITERATURE REVIEW

2.1 Introduction

Geophysical techniques have been used in a number of different fields such as mining and archaeology with a range of different applications including hydrological investigations, environmental site assessment and geotechnical assessment. The use of geophysical techniques represents numerous advantages such as providing a cost effective way to investigate conditions on a test site without physical intervention. This deals primarily with shallow depths of no more than 100m, but it also serves deeper operations. Such operations include, but are not limited to, exploration of engineering sites, groundwater exploration, the location of buried utilities, buried artefacts as well as deeper exploration of hydrocarbons (McDowell et al., 2002). A key application of geophysical techniques is the effective measure of the physical properties of a multitude of different soil types. It enables calibration of geotechnical properties such as moisture content, soil strength and composition, rippability, deformity and liquefaction potential of the soil under investigation. As mentioned by Clayton (2012) on his work on seismic activity, geophysical techniques are potentially useful and constitute an efficient complement to ground investigations. The following section will review

the geophysical techniques which are used for soil investigation and will illustrate how soil properties can be determined and investigated.

2.2 Overview of Geophysical Techniques

In order to determine the geophysical properties of physically tested geo-materials, it is important to use an appropriate geophysical technique. Moreover the use of different geophysical techniques on the same test location aids in consolidating and enhancing the quality of the results of any given soil being tested. In geotechnical engineering shallow ground is always involved, therefore geophysical techniques such as ground penetrating radar (GPR), electrical resistivity and seismic-based approaches (see Figure 2.1) are frequently used because they are able to give higher spatial resolution at shallow depth by using higher frequencies, which give better resolution (McDowell *et al.,* 2002) than the lower frequencies that are needed for deeper testing.

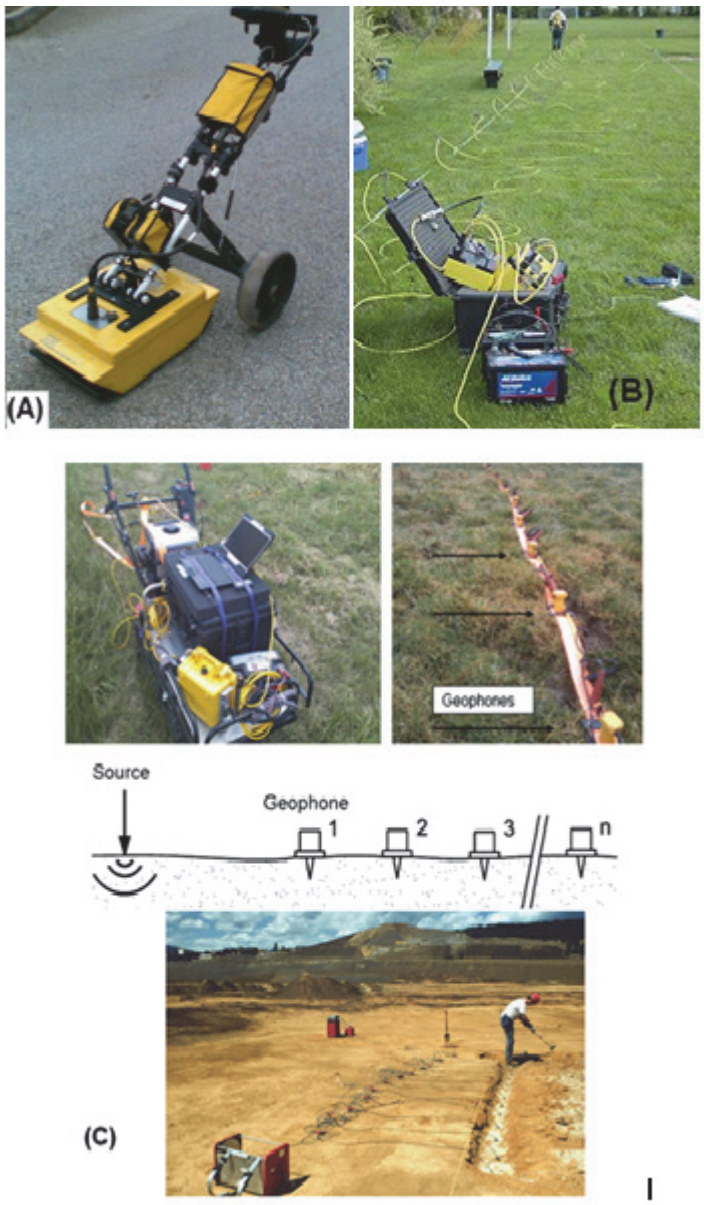

Figure 2.1: (A) Ground Penetrating Radar (GPR;2013 - Cube Surveys Ltd, 2013), (B) electrical resistivity equipment (Wightman et al., 2003), and (C) a seismic-based method (K. Samyn et al., 2012)

Geophysical methods can be divided into five groups: (1) Seismic-based methods which include refraction, reflection and surface wave methods, (2) Electro-magnetic wave-based methods, including ground electrical conductivity and Ground Penetrating Radar (GPR) methods, (3) Electrical-based methods, (4) Gravity methods and (5) Magnetics. Each of these methods is used to find geophysical and geotechnical properties of soil (Reynolds, 1997; McDowell et al., 2002). While this thesis is focussing on seismic-based methods, GPR and

electrical resistivity will be briefly reviewed to offer parallel thinking on the subject of primary interest – the correlation between geophysical and geotechnical properties.

2.2.1 Ground Penetrating Radar (GPR)

The GPR technique is a high resolution electromagnetic technique that is designed to examine the shallow subsurface of the earth. The main purpose of using such a technique is to locate buried objects such as pipes or reinforcement cables, or changes in the fabric of the subsurface such as flaws and cracks in materials or ground water moisture differences (Finck and Florian, 2003).

GPR operates by transmitting high frequency electromagnetic pulses into the ground through a transmitter antenna and the pulses are partially reflected back to the surface from various buried objects or distinct contact surfaces between different materials in the ground, i.e. those across which there is a contrast in dielectric constant. The reflected waves are then received by an antenna or antenna array and software displays them in real time on a screen. The data are also saved in appropriate memory for future processing and interpretation (Prestij and Intimarga, 2010).

Other common areas in which GPR can be used include geological and hydro-geological investigations: mapping of bedrock topography, water levels, soils and aggregate location, and site investigations. The operational parameters for this purpose are likely to vary from those needed for such purposes as evaluation of buried structures including foundations and reinforcing bars, location of buried engineering structures and subsurface mapping for cables, pipes and other buried structures prior to trenchless operations. The GPR technique has some merits due to its high resolution coverage of the area under survey as it uses high-frequency ranges. High-resolution coverage of the survey area and detecting even small objects,

possibility of on-site interpretation because of instant graphic display and rapid ground coverage are commonly quoted benefits of GPR. However, there are some significant limitations for GPR, e.g. it requires significant operator training and is subject to a level of subjectivity when interpreting the images (Prestij, 2013).

It is worth noting that in spite of all the above advantages, the GPR technique also has some technical shortfalls. The penetration depth for investigation is controlled by the radar pulse frequency, magnetic permeability, electrical conductivity and permittivity of the ground, so the greater the conductivity and permittivity of the ground the shallower the penetration of the electromagnetic pulse. Also the depth of investigation is inversely related to frequency; hence, the lower the frequency of the signal, the greater the penetration depth of the signal but the poorer the resolution of the result. There is also a greater loss in electromagnetic radiation, and consequently depth of signal penetration, in wet compared to dry areas (Thomas, 2010). Since permittivity is highly dependent on the water content of the soil, the greater the presence of high or perched groundwater (for example in clay areas), the greater the compromising effect on the depth of penetration. This thus makes the use of this electromagnetic–based method more problematic in such cases. The depth of penetration is also hindered by materials of high electrical conductivity (Madun, 2011; Thomas, 2010). Even though most soils are not magnetically impermeable due to their low iron content, it is possible to encounter soils with high magnetite content. In such a case, the presence of magnetic material will cause significant changes in propagation properties (Cassidy, 2007). It is possible to make a beneficial comparison between results of the GPR and those obtained from electrical resistivity methods since ground conductivity surveys cannot directly determine the physical properties of the ground or the soil. This is due to the fact that the result of the conductivity measure for GPR is the inverse of its electrical resistivity value (McDowell et al., 2002).

2.2.2 Electrical Resistivity

The Oil Company Schlumberger in France was the first to design the electrical resistivity method in the 1920's for prospection of minerals. Henceforth, the electrical resistivity method has been employed to find portable groundwater supplies, trace contamination as it migrates through the saturated zone, estimate pipeline corrosion, and determine soil resistivity for efficiently designing electrical substations and ground arrays. This method is also used for detecting shallow structures using slight changes in apparent soil resistivity. This ability thus makes it beneficial for use in archaeological surveys (Radar-Solutions, 1996).

The electrical resistivity method is used to measure the conductivity and resistivity of the ground. The resistivity method usually uses a four-electrode array – two potential, and two current (voltage), electrodes. Direct current or a very low-frequency is applied to one of the current electrodes, and the current flows through the earth to the second current electrode, closing the circuit. The potential difference, or voltage, between the two potential electrodes is measured by the instrument, and resistance determined using a very simplified version of Ohm's Law as given in Equations 2.1 and 2.2. (See Figures 2.2 and 2.3)

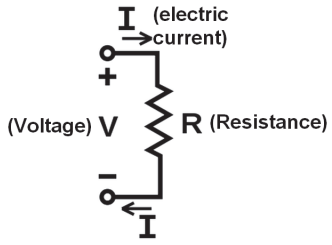

Figure 2.2: V, I, and R, the parameters of Ohm's law.

$$V = IR \qquad \text{Equation 2.1}$$

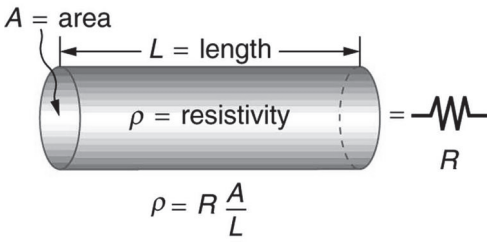

Figure 2.3: rResistivity (after Erik, 2012)

$$\rho = \frac{RA}{L}$$ Equation 2.2

where V is the voltage (V), I is the electric current (A), R is the resistance (Ω), A is the cross sectional area of medium (m^2), L is the length of medium (m) the ρ is the resistivity (Ωm).

A basic electrical property of all materials is shown by the ability to transmit ions. The movement of ions in electrolytic solutions, moist soils and water-bearing rocks leads to electrical conduction. For soils, the major factors on which electrical resistivity depends include porosity, the nature of the pore fluid, the level of compatibility of the solids, extent of saturation, particle shape and orientation, pore structure, clay content and mineralogy (Keller and Frischknecht, 1966; Garcia-Bengochea et al., 1979; Arulanandan and Muraleetharan, 1988; Thevanayagam, 1993; Abu-Hassanein et al., 1996). The relationship between resistivity and soil strength as a quality indicator has, however, revealed a very weak correlation. This is because the resistivity values are being affected by other parameters such as water content, pore water salinity and porosity (Staab et al., 2004; Cosenza et al., 2006).

2.2.3 Seismic-based Methods

The seismic-based method is a powerful geophysical exploration procedure that can measure different parameters relative to other geophysical methods. This method is the most responsive to physical properties of geo-materials and relatively insensitive to the chemistry of the geo-materials. It also is sensitive to their fluids and requires careful attention to avoid possible pitfalls in the collection, processing and interpretation of data. Careful planning is

also necessary to make the method increasingly cost effective relative to test drilling and other geophysical methods. The selection of seismic recording equipment, energy source and data-acquisition parameters is often critical to the success of a project (Steeples and Miller, 1990).

The seismic-based techniques generally cause the ground to vibrate and produce very small strains. Thus, the soil velocities derived from the seismic-based measurements are related to the soil shear modulus. As such, seismic-based techniques can be used to directly derive the geotechnical properties that relate to strain, including the maximum shear modulus (G_{max}), bulk modulus (B), Young's modulus (E), and Poisson's ratio (υ) (Steeples and Miller, 1990; McDowell et al., 2002; Charles and Watts, 2002; Crice, 2005; Clayton, 2011).

In the seismic method, an elastic pulse or a more extended elastic vibration is generated at shallow depth. The resulting motion of the ground at nearby points on the surface is detected by small seismometers or "geophones". The travel-time of the pulse to the geophones is measured at various distances to obtain the velocity of transmission of the pulse in the ground. Usually, the ground is not homogeneous in its elastic properties thus causing the velocity to vary both laterally and in depth. In cases where the ground structure is simple, the values of elastic wave velocity and the positions of boundaries between regions of different velocity can be computed from the measured time intervals. Velocity boundaries usually coincide with geological boundaries and the cross-section on which velocity interfaces are plotted. This may be similar to the geological cross-section even though the two are not necessarily the same (Griffiths and King, 1965).

In the fields of both engineering site investigation and hydrology, this seismic methodology has been of considerable importance. The depth of interest ranges from approximately some tens of metres to no more than a few hundred metres. The problems which may be solved range from well-defined water table location or the estimation of the depth of high-velocity

"bedrock", to the evaluation of the hydrological and mechanical properties including the degree of saturation, the degree of fracturing, porosity, etc., of a concealed foundation material aquifer (Griffiths and King, 1965).

2.3 Seismic Waves

There are different kinds of seismic waves and they all move in diverse ways. The two main wave types are body waves and surface waves. While body waves can travel through the earth's inner layers, surface waves on the other hand can only move along the surface of the planet like ripples on water. Earthquakes usually radiate seismic energy as both body and surface waves. A body wave is a combination of compression waves, which are called the P-waves, and shear waves, which are called S-waves. A surface wave is a combination of Rayleigh and Love waves, as shown in Figure 2.4. These four types of elastic seismic waves are produced by impulses and all travel at different velocities (Michigan Technological University, 2007).

When a sound wave travels in air, the molecules fluctuate forwards and backwards in the direction of energy transport. Thus, this pressure or push wave travels as a series of refractions and compressions. In a solid medium, the pressure wave has the highest velocity of any of the possible wave motions and is then also known as the compression wave, primary wave or simply P-wave (Milsom, 1939).

The vibration of particles at right angles to the direction of the energy flow creates an S-wave. This is only possible in solids due to the relative low velocity. In many consolidated rocks, the S-wave velocity is about half the P-wave's velocity. This may depend slightly on the plane of the vibrating particle, but such variations are usually inconsequential in small-scale surveys. These kinds of waves are distortional stress waves that spread near to the ground surface with

a cylindrical wave front and wave amplitude attenuated in proportion to $\frac{1}{\sqrt{r}}$, where r is the distance from the seismic source. Therefore, surface waves are less attenuated and so propagated over longer distances than body waves (Al-Hunaidi, 1993). Love waves are generated at the interfaces, while particles on the earth's surface can follow elliptical paths to create Rayleigh waves. Love and Rayleigh waves may carry significant quantities of the source energy, but travel very slowly. Usually they are simply lumped together as the ground rolls based on many surveys which have been done (Milsom, 1939). These waves are only propagated through a solid medium with the depth of penetration being a function of their wavelength and frequency (Reynolds, 1997).

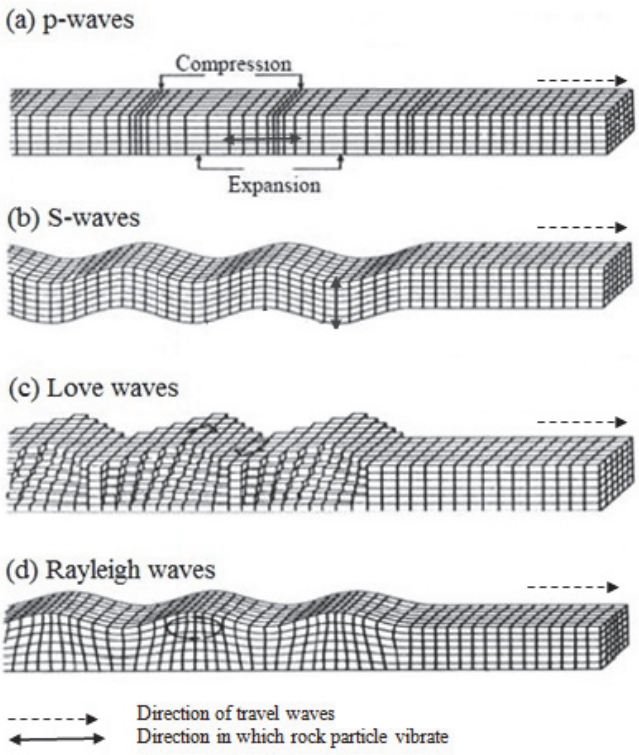

Figure 2.4: The schematic elastic wave propagation in ground (after Menzies, 2001; Central Weather Bureau, 2013)

2.3.1 Body Waves

The two wave types that constitute elastic seismic body waves are: the compressive wave (P-wave) and the shear wave (S-wave). The P-wave or primary wave is the fastest kind of seismic wave. It therefore generally reaches the seismic station first. The P-wave can travel through any type of medium be it a liquid, gaseous or solid medium. The P-waves systematically push and pull the sound waves and are thus called compressional waves. The direction of wave propagation is synonymous to the direction of the energy flow (Michigan Technological University, 2007).

The S-wave or secondary wave is the other type of body wave. S-waves are generally slower than P-waves and can only move through solid rocks. The unique property of the S-wave which makes it unable to move through liquids is the reason that seismologists concluded that the earth's outer core is a liquid. S-waves move rock particles both horizontally and perpendicularly to the direction of wave propagation (Michigan Technological University, 2007). Table 2.1 shows the typical values of P-waves and S-waves for different materials, which illustrate key differences.

Table 2.1: Typical P-wave and S-wave velocities for different material (McDowell et al., 2002; and Parasnis, 1997)

Material	P-wave velocity, m/s	S-wave velocity, m/s
Air	330	0
Water	1450	0
Sands and clays	300-1900	100-500
Glacial till	1500-2700	600-1300
Chalk	1700-3000	600-1500
Strong limestone	3000-6500	1500-3500
Weathered granite	100-3000	500-1500
Fresh granite	3000-6000	1500-3000
Slate	5000-7000	2500-3800
Rock salt	4000-5500	2000-3200

Refraction and reflection are the two most common types of seismic surveys that use body waves. When a seismic wave meets an interface between two different types of rocks, some of the energy is reflected while the residual energy is refracted at different angles. The law of reflection is very simple and can be easily computed as being equal to the angle of incidence (Figure 2.5a). The seismic refraction is based, fundamentally, on Snell's Law (Equation 2.3), which relates the angles of incidence and refraction to the seismic velocities in the two media.

$$\sin i = V1/V2 \qquad \text{Equation 2.3}$$

where i is the critical incident angle (degree), V_1 is the velocity of the upper layer (m/s) and V_2 is the velocity of the lower layer (m/s).

Refraction will be towards the interface if V_2 is greater than V_1, and if sin i equals V_1/V_2 the refracted ray will be parallel to the interface. In such a situation, part of the energy will return to the surface as a head wave that leaves the interface at the original angle of incidence (Figure 2.5 b). This is fundamentally how the refraction method works. If the incidence angle is too large, then there will be no possibility of refraction and thus all the energy is reflected (Milsom, 1939).

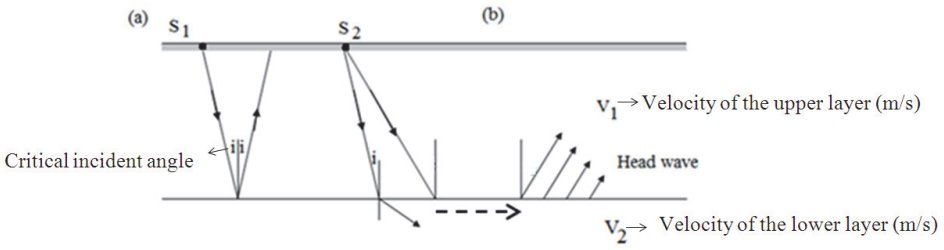

Figure 2.5: (a) Reflection from source 1 (S1) and (b) refraction from source 2 (S2) (after Milsom, 1939).

When the seismic refraction method is used, it requires the soil layers to increase in density with depth. Contrary to this, the reflection method requires the density contrast to reflect

waves back to the surface (Lankston, 1990). The travel time of the either the P-wave or S-wave energy is recorded with the seismic refraction method. Therefore, by interpretation of these data, the layer thicknesses and seismic velocities will be determined (McDowell et al., 2002).

Traditionally, a small charge of dynamite is used as the common seismic source. Although explosives are still quite commonly used to some extent, the use of impact and vibrator sources have become popular in recent years. A simple sledge hammer provides a handy source for small-scale surveys. The energy that is produced is useful and usually is reliant on both the strength and skill of the operator as well as the ground conditions. Hammers can nearly always be used in refraction work on spreads 10 to 20 m long but very seldom where energy has to travel more than 50 m. More powerful impact sources are required for larger surveys: for example, large weights of several hundreds of kilograms can be raised using portable hoists and then dropped to create a larger source of impact. The use of vibration sources is common when it involves large surveys that require extensive and complicated data processing. Almost any type of safe explosive can be used for seismic work, but explosives involve problems with safety, security and bureaucracy (Milsom, 1939).

There is considerable difference in the mode of generation of either a P-wave or an S-wave. By using explosives or vertically dropping a mass into the ground, P-waves are automatically generated. This makes the generation of P-waves easier than the generation of S-waves. S-wave generation is more complex in that the energy needs to be induced in the ground perpendicularly to the direction of the row of receivers. As a result, the soil particle motions will be perpendicular to the direction of the wave propagation (Luna and Jadi, 2000). This technique amplifies the S-wave amplitude while simultaneously decreasing the P-wave amplitude, thus making the S-waves more easily identifiable in the seismic record (Lankston, 1990).

Instruments used for land seismic wave detection are called geophones, while those used in the detection of waves under water are called hydrophones. They both convert mechanical energy into electrical signals. Geophones are usually positioned by pushing a spike screwed to the geophones into the ground or by using some form of adhesive pad or putty when working on bare rock (Milsom, 1939).

By using the appropriate source for the waves and receivers, laboratory tests and field surveys can be conducted using these two body waves. The time taken by the waves to travel from the transmitter to the receiver is used to calculate wave velocities. The seismic waves can be directly used to compute engineering properties. Using the P-wave and S-wave velocities, the maximum shear modulus, G_{max}, bulk modulus, B, Young's modulus or dynamic elasticity modulus, E, and Poisson's ratio, υ, at varying small strains can be calculated using Equations 2.4 to 2.7 :

$$G_{max} = \rho v_s^2 \qquad \text{Equation 2.4}$$

$$B = \rho v_p^2 = \frac{E}{3(1-2\upsilon)} \qquad \text{Equation 2.5}$$

$$E = 2\rho v_s^2(1+\upsilon) = \frac{\rho v_p^2(1-2\upsilon)(1+\upsilon)}{(1-\upsilon)} \qquad \text{Equation 2.6}$$

$$\upsilon = \frac{\left[\left(v_s / v_p\right)^2 - 2\right]}{2\left[\left(v_p / v_s\right)^2 - 1\right]}$$ Equation 2.7

Where ρ is the bulk density of the soil (kg/m³), V_p is the P-wave velocity (m/s) and V_s is the S-wave velocity (m/s) (Clayton et al., 1995; Menzies and Matthews, 1996; Massarsch, 2005). The maximum shear modulus can be obtained from measurements of V_s alone by using Equation 2.4 (Massarsch, 2005). Geo-materials have values of Poisson's ratio in the range of 0.05 for very hard rocks and nearly 0.5 for saturated unconsolidated clays (Sheriff and Geldart, 1982). According to the theory of elasticity, Young's modulus, E, and bulk modulus, B, are related to the shear modulus, G_{max} by Equation 2.8:

$$G_{max} = \frac{E}{2(1+\upsilon)}$$ Equation 2.8

$$G_{\max} = \frac{B(1-2\upsilon)}{(1-\upsilon)}$$ Equation 2.9

Where υ is the Poisson's ratio, E is the Young's modulus (N/m²) and B is the bulk modulus (N/m²).

2.3.2 Surface Waves

When a vertical load is used to vibrate the surface of the ground, two-thirds of the energy is transformed into surface waves, which propagate parallel to the ground surface (Socco and Strobbia, 2004). These waves can generally be either Love waves or Rayleigh waves (Central Weather Bureau, CWB, 2013). These surface waves fall into the category of lower frequency

waves compared to body waves. They are easily differentiated on the seismogram regardless of the fact that they arrive after body waves.

Love waves are named after the British mathematician A.E.H. Love, who worked out the mathematical model for this kind of wave in 1911. Love waves are the fastest surface waves, they move the ground from side-to-side and they produce entirely horizontal motion (Michigan Technological University, 2007). The Rayleigh wave on the other hand was named after John William Strutt Lord Rayleigh, who mathematically predicted the existence of this kind of wave in 1885. Rayleigh waves result from the interfering P-waves and S-waves at the ground surface (Xia et al., 2002). The way a Rayleigh wave rolls along the ground is similar to how a wave rolls across a lake or an ocean. The fact that it rolls makes it capable of moving the ground both horizontally and vertically perpendicularly to the wave motion.

Surface waves possess the property of dispersion and, therefore, can be used to categorize near-surface elastic properties. This dispersive property comes about due to the fact that different frequencies or wavelengths move at different depths (Reynolds, 1997). If a material is homogeneous, then the surface wave velocity does not vary with frequency. However, if the soil is heterogeneous with different densities, the surface wave velocity will fluctuate with the frequency in areas where there is diversity in both stiffness and depth (Stokoe et al., 1994). A graphical explanation of this phenomenon is illustrated in Figure 2.6, where Medium 1 with thickness L overlies Medium 2. The Rayleigh wavelength (λ_1) shorter than L would propagate mainly within Medium 1, thus the phase velocity is representative of Medium 1. However, the Rayleigh wavelength (λ_2) is larger than L and this occurs when the phase velocity is affected by the properties of both Mediums 1 and 2 (Rhazi et al., 2002). This is a phenomenon known as dispersion, which thereby causes different frequencies and wavelengths to travel at different velocities.

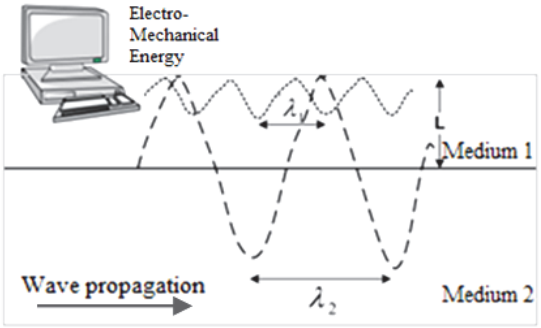

Figure 2.6: Rayleigh wave dispersion; Rayleigh wavelength (λ_1) within Medium 1, Rayleigh wavelength (λ_2) within Medium 2 (after Rhazi et al., 2002)

The different ways of distinguishing surface waves vary according to the source and the field receiver. Three major ways have been developed for site investigations using surface waves and these are explained in detail in next sections. The first method makes use of a transient vertical impact source and is known as the Spectral Analysis of Surface Waves (SASW) method. The second uses a steady-state vibration source and is known as the Continuous Surface-Wave (CSW) method (Sutton and Snelling, 1998). The third method uses multi-channel receivers and either assorted active seismic sources such as sledge hammers or ambient sources. This method is known as the Multi-channel Surface Wave (MSW) method (Park et al., 2005).

2.3.2.1 Spectral Analysis of Surface Waves (SASW)

The Spectral Analysis of Surface Waves method was developed in the early 1980s, for different engineering purposes. Compared to traditional borehole methods this allows for less costly measurements while testing is performed on the ground surface. The basis of the SASW method is the dispersive characteristic of Rayleigh waves when travelling through a layered medium.

The Spectral Analysis of Surface Waves method uses a single pair of receivers that are placed collinear with the impact point of the transient source. A series of hammer weights are essential to create a range of frequencies – heavier weights are used to produce lower frequency signals. To capture signals from ground motion receivers the SASW recordings use a spectrum analyser, the signals usually being captured in the time domain and then converted into the frequency domain. The phase difference between the signals from these spectral data and the coherence of the cross-correlated signals at each geophone can be determined. The coherence is a measure of the signal-to-noise ratio at a given frequency (Addo and Robertson, 1992).

SASW testing consists of obtaining and interpreting the corresponding shear wave velocity profile through measuring the surface wave dispersion curve at the site. Surface waves are generated by using a dynamic source wave of different wavelengths and are monitored by multiple receivers at known offsets. Data from forward and backward profiles are averaged together. An expanding receiver spread is used to avoid near-field effects associated with Rayleigh waves. The geometry of the source receiver is used to minimize the body wave signal. By using an interactive masking process, all the phase data are verified manually in order to discard low quality data.

Figure 2.7 shows each step involved in the SASW method from data collection to data analysis (Luke, 1999). Initially source energy is applied at the ground surface and then the resulting ground motion is detected at the receivers and digitised at the analyser. The time signals need to be transformed to the frequency domain and the phase difference between receivers is determined. After that the phase data are unwrapped and the dispersion curve is generated from the unwrapped, masked phase data at several different receiver spacings.

Finally a theoretical dispersion curve is matched to the experimental dispersion curve to yield the shear wave velocity profile for the site (Luke, 1999).

As the SASW method uses a single pair of receivers, it requires a configuration and reconfiguration of the receivers so as to sample the desired frequency range and to reduce body wave noise. As a result it may be sometimes not feasible to assess and differentiate signals from noise with only a pair of receivers.

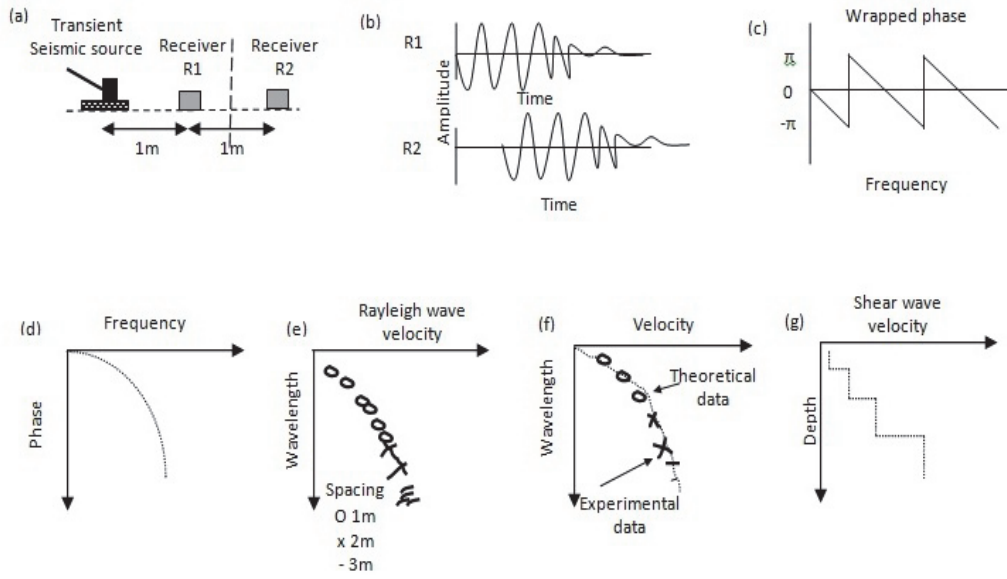

Figure 2.7: In an SASW measurement, a) source energy is applied at the ground surface; b) the resulting ground motion is detected at the receivers and digitised at the analyser; c) the time signals are transformed to the frequency domain and the phase difference between receivers is determined; d) the phase data are unwrapped and masked to eliminate spurious components; e) the dispersion curve is generated from the unwrapped, masked phase data at several different receiver spacing; f) a theoretical dispersion curve is matched to the experimental dispersion curve to yield g) the shear wave velocity profile for the site. (after Luke, 1999).

2.3.2.2 Continuous Surface Wave (CSW)

The Continuous Surface Wave method employs a steady-state vibrator as an energy source. Such sources have the key benefit of controlling the frequency and thereby enhancing the frequency content as well as ensuring good frequency resolution. GDS Instruments Ltd was

the first to utilise the Continuous Surface Wave System (CSWS; Sutton and Snelling, 1998). This came as a huge step forward in site investigation technology. This system fundamentally uses low natural frequency geophones to pick up surface waves that are generated by a computer-controlled vibrator on the ground surface. This has enabled the creation of a ground stiffness profiling system which is completely monitored by a computer. CSWS gives a picture of the average maximum shear modulus (G_{max}) with depth profile.

The seismic source uses a vibrator, which generates a number of continuous sinusoidal waves, to produce surface wave frequencies in the range of 3Hz to 200Hz. A small electromagnetic vibrator, weighing less than 15kg, is typically employed in order to obtain greater frequency ranges and to facilitate mobility. [It is worth noting that such a vibrator is ineffective in giving good quality sinusoidal waveforms when the frequencies are below 7Hz.] There is a need to use heavier machinery to achieve lower frequencies in the range between 3Hz-50Hz. Longer wavelengths are generated by lower frequencies and they penetrate further into the ground, thus they can give a reasonable idea about deeper ground layers (Matthews et al., 1996).

It is possible to minimise the differences in the data by using many geophones, which allow for a best fit line to be drawn through the phase angle-distance plot. It has been found that in cases where two geophones are used, the results are unreliable. Therefore, in order to obtain the best quality results, as many as 24 receivers are used as an evolution of the CSW technique. Therefore, in order to establish the signal quality, a minimum of two sensors must be used for the CSW test and must be arranged in a collinear fashion with the seismic source.

Figure 2.8 depicts a summary of the CSW technique. It starts with equipment preparation and selective frequency (f_1). This frequency sampling does not stop until n frequency (f_n). Since the captured data are in the time domain, they are converted to the frequency domain. As

such, the phase angles for each geophone are determined and plotted with some distance so that the best fit line is achieved based on the assumption of laterally homogeneous soil (this is only applicable if using more than 3 geophones). The difference in phase angle between geophone pairs, known as the phase difference, is then utilised to estimate phase velocities. The calculated phase velocities are then divided by their respective frequencies to give the wavelength. The dispersive curve illustrates a plot of phase velocity against wavelength (Madun, 2011).

There are major differences between the SASW and the CSW due to the fact that the transient impact seismic source generates swept frequencies while the vibrator seismic source forms a single-frequency sinusoidal force. The frequency is of vital importance in the surface wave techniques and hence the CSW is much better than the SASW in terms of the selective mono-frequency that may be used when the results of both are compared. Consequently, no frequency bypasses, and any superfluous background noise is more easily recognised, avoided and filtered in the CSW technique (Clayton, 2011); with the SASW some of the impulse energy sources are required to spawn diverse bands of frequencie,s thus leading to some of the frequencies being omitted as a consequence of lack of control over the wave frequency generated using impact sources (McDowell et al., 2002).

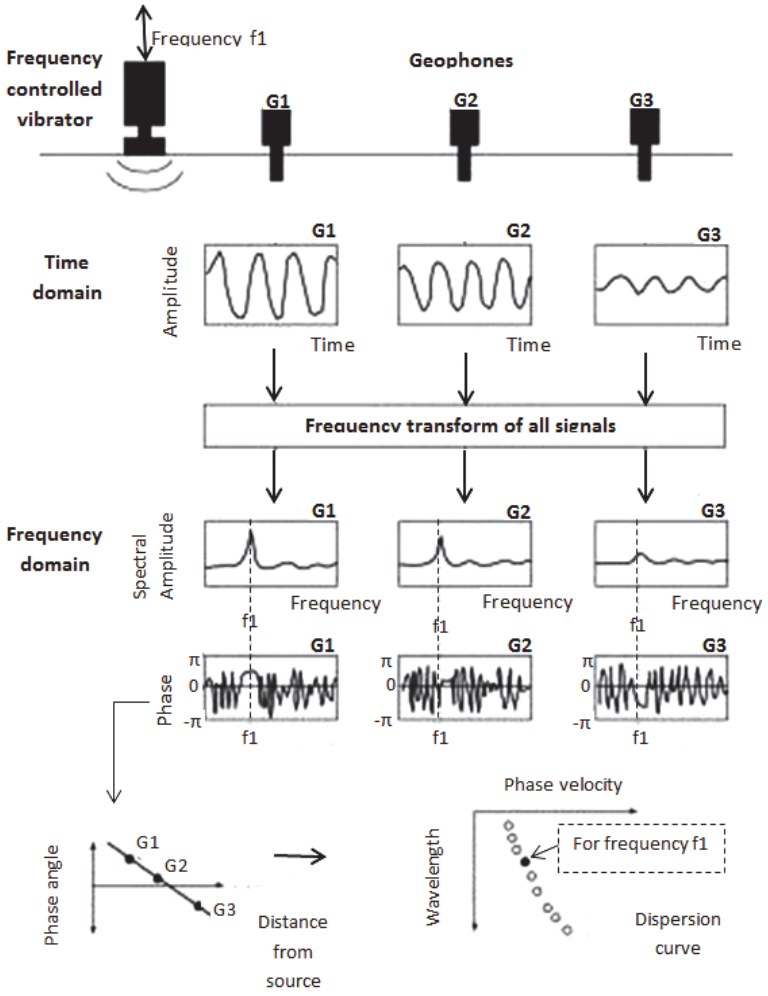

Figure 2.8: Schematic diagram showing the steps followed in the determination of the dispersive curve using the CSW technique (after Matthews et al., 1996)

2.3.2.3 Multi-Channel Surface Waves (MASW)

One outstanding seismic method used for estimating ground stiffness or elastic state of the soil is the Multi-channel Surface Wave (MSW) method, which was initially discovered in Japan more than half a century ago. Initially it was called the micro-tremor survey method (MSM). The Kansas Geological Survey in the late 1990s developed electrical equipment for the MSW and used it for multi-channel analysis of surface waves, MASW (Park et al., 1999). MASW operates by initially measuring the seismic surface waves obtained from various types of seismic sources. The transmission velocities of these surface waves are then analysed to deduce shear wave velocity variations below the surveyed area, which are related to its geotechnical features.

Regular surface wave analysis approaches are based on a single transmitter-receiver pair in contrast to the MSW, which brings in additional benefits as compared to conventional methods. The MSW method is not affected by buried pipelines or cables, or by urban noise, to the same extent as the seismic method that utilises body waves, because surface waves have much bigger signals and are not constrained by the assumption inherent to seismic refraction that the velocities increase with depth. On the other hand the use of a multiple-receiver strategy for measuring has the advantage of shortening the time for the survey thus gives a way for achieving lateral resolution, while the sub-surface characterisation in both the vertical and lateral axes provides a convenient 2-D representation (Socco and Strobbia, 2004). Generally, when the MSW method is used, all the seismic wave energy, both body and surface waves, is recorded by the multi-channel receivers, which is the significant advantage of MSW method.

MASW, which was presented by Park et al. (1999), allows one to efficiently identify, isolate and filter noise from dispersed and reflected waves during data analysis just by using several receivers and with only one shot. It therefore becomes possible for the best fit line to be drawn on the phase angle plot. There are three main steps for the complete procedure of the MASW. The initial step is obtaining the multi-channel field records. This is followed by the extraction of the dispersion curves and finally inverting these dispersion curves to achieve a one- or two-dimensional shear wave velocity and depth profile as shown in Figure 2.9.

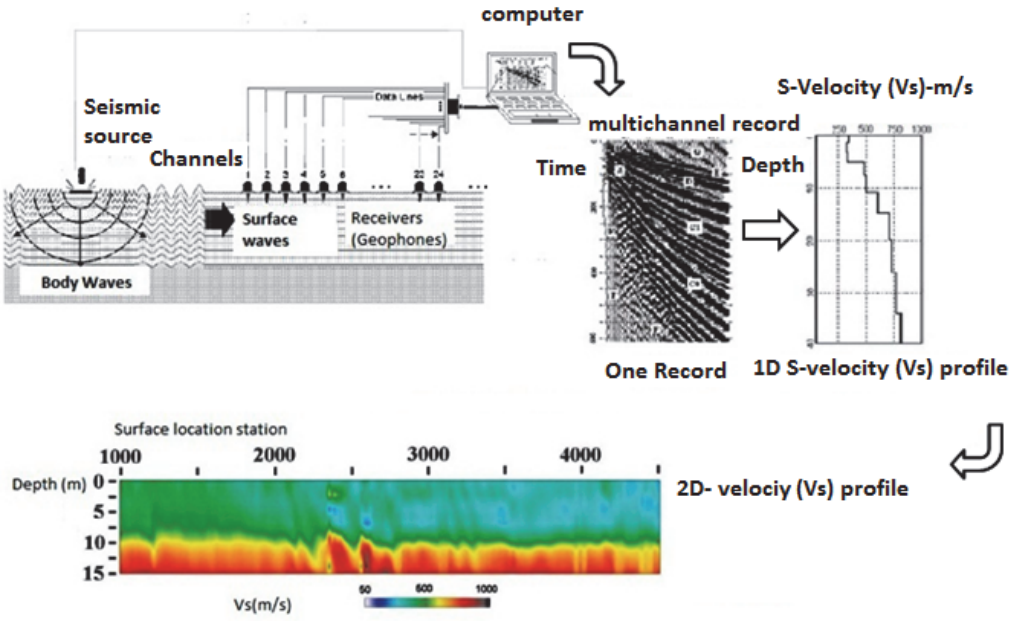

Figure 2.9. inverting the dispersion curves to obtain1-D or 2-D shear wave velocity depth profiles (after Park et al., 2007 & 1999).

When a pair of receivers is used in the SASW and CSW techniques, a one-dimensional result of phase velocity against depth is obtained. It is of primary importance that a plot of the phase velocity versus depth as a function of lateral distance is obtained in a lateral heterogeneous medium. This aids the removal of all anomalies, thus rendering the MSW method more effective than others. This method can be used to get an improved assessment of the geotechnical features such as strength and stiffness because it provides relevant information in the tangential dimension. This facilitates the detection of voids, fractures and soft spots (Gordon et al., 1996).

2.4 Surface Wave Method

Data collection and signal processing are usually the two major steps used in spectral analysis. With regard to data collection, a seismic source is generally used to generate a signal x(t), and multiple receivers are deployed to acquire the seismic data. This is represented by $y_1(t)…y_n(t)$, where n is the index of the array of receivers. The familiar option for a seismic source is a

manually-controlled mass dropped to induce a broadband impulsive signal into the ground. Another option could be the use of an electro-mechanical shaker that is generally controlled by a digital source. The latter option makes it possible to vary and effectively adjust the bandwidth and duration, and usually is relatively easy to implement. The receivers usually consist of geophones for field testing, or accelerometers in laboratory-scale testing (Madun et al., 2010).

The arrangement of the transmitter and receiver arrays is subject to the near- and far-offset constraints (Heisey et al., 1982). These constraints are related to the signal wavelength and as such they determine the highest and lowest frequencies that are relevant for spectral analysis. As an empirical rule for the near-offset constraint it is recommended that the distance between the source and the first receiver, d_{min}, as a function of the surface-wave wavelength, λ, is approximated (Al-Hunaidi, 1993; Matthews et al., 1996; Park et al., 1999) using Equation 2.10:

$$d_{min} > \frac{\lambda_{max}}{3} \qquad \text{Equation 2.10}$$

When the receiver is far away from the seismic source, the far-offset is associated with the attenuation of the surface waves. This constraint can be approximated by Equation 2.11:

$$d_{\max} < 2\lambda_{\min} \qquad \text{Equation 2.11}$$

Furthermore, the spacing between the receivers, Δx, is given by Equation 2.12:

$$\Delta x \approx \lambda_{\min} \qquad \text{Equation 2.12}$$

The wavelengths that pertain to both the smallest and highest frequencies are denoted by λ_{min} and λ_{max} respectively.

The analysis used in such approaches assumes that the soil behaves as a layered half-space that is laterally homogeneous and isotropic. Thus, the results represent the mean velocity of the whole horizontal layer corresponding to the respective wavelength (Sutton and Snelling, 1998; Moxhay et al., 2001; Moxhay et al., 2008; Redgers et al., 2008; Roy, 2010).

2.5 Relationship of Seismic to Geotechnical Parameters

Seismic waves or elastic stress waves travelling through soils interact with soil particles and interstitial fluids. So seismic wave responses are affected by the soil texture and structure, and they are sensitive to the variations in soil properties. Propagation of seismic waves through soils is a small-strain phenomenon that introduces a small perturbation without altering the fabric of the soil. As a result, seismic parameters are constant fabric characteristics and can be used to estimate and observe on-going internal changes of soil properties.

The resistance of the body to deform under applied force is termed stiffness (Clayton, 2011). So when a body is being referred to as being stiff, it can be inferred that it is difficult to easily deform it when a force is applied to it. The three stiffness parameters are known as Young's modulus, E, bulk modulus, B, and shear modulus, G.

Atkinson states that the relationship between strain and stiffness of soils is generally non-linear and only at very small strains does the correlation between strain and stiffness behave in a linear fashion. It is at these smaller strains that the shear stiffness reaches its maximum value, usually referred to as G_0 or G_{max} (Atkinson, 2007).

In summary the material's maximum modulus depicts the modulus value over the linear section of stress-strain curve and is popularly symbolized as E_{max}, maximum Young's modulus, or G_{max}, the maximum shear modulus. Figure 2.10 gives a clear picture of this relationship.

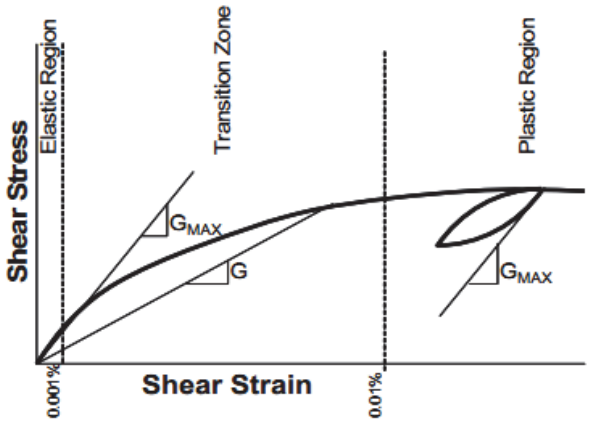

Figure 2.10: Modulus variations with strain level (after Davich et al., 2004)

Measurement of soil stiffness parameters is made by conducting stress path triaxial tests in the laboratory, since in the conventional triaxial test it is unreliable to measure strain smaller than 0.1%. However, using the hydraulic triaxial test it is possible to measure strain smaller than 0.01%. To achieve 0.001% strain reliably, an internal strain gauge should be mounted directly on the sample. It is very difficult to measure stiffness of soil at very small strain, i.e. less than 0.001%, using triaxial tests by direct measurement of strains. However, the simplest way is to measure and calculate shear modulus at very small strain using the seismic shear wave velocity (Atkinson, 2007). Another way to obtain small strain moduli is by using bender elements. They are usually short piezoelectric cantilever strips that have direct contact to the specimen. Although there are several different types of bender elements, the fundamental concept of each of the apparatuses does not change. On opposite sides of the soil specimen, two small elements are inserted. By using the piezoelectric material to generate motion, an

electric pulse is sent to one of these elements which ultimately produces compression (P) or shear (S) waves in the soil. These waves depend upon the direction of the piezoelectric material. Figure 2.11 shows a schematic of this process. As the bender element on the opposite side receives the wave, a time path is documented. It thus becomes possible to calculate the Poisson's ratio and the shear modulus of the soil being tested when both the shear and compression waves have been identified (Davich et al., 2004).

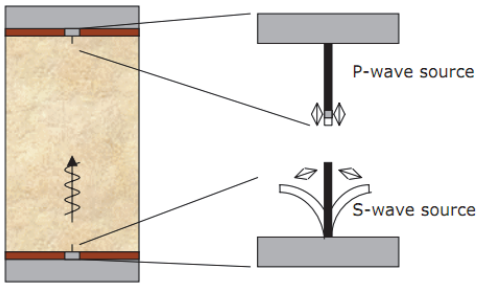

Figure 2.11: Bender element wave generation (after Davich et al., 2004)

The soil moduli generated from both the seismic and geotechnical testing is at different strain levels. The basic difference between both strains is that those from the seismic waves are caused by very low range vibration of soil particles, meanwhile strains from geotechnical testing in the triaxial test range from 0.01 to 0.001% (Matthews et al., 2000). Differences in strain dimension can be prone to faulty correlations. Figure 2.12 illustrates the way in which Atkinson (2007) abridged the relationship between the stiffness or the shear modulus and the strain. It can be seen that as the soil stiffness or the shear modulus decreases, as the strain increases. The three principal regions of soil stiffness are very small strains, small and large strains. The value of the first strain region generates up to a 0.001% strain reaches the highest approximately constant value. For the small strain region (i.e. the second or intermediate region), the shear modulus rapidly decreases in a non-linear way with increasing strain. In the large strain region, the soil state has reached the state boundary surface and the soil behaviour is elasto-plastic and it is usually greater than 1 %.

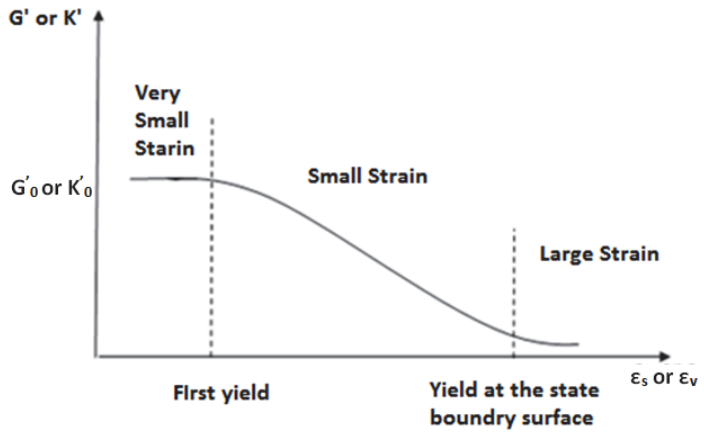

Figure 2.12: Characteristic ranges of soil stiffness modulus (after Atkinson, 2007).

As mentioned before there are three stiffness parameters; Young's modulus, *E*, bulk modulus, *B*, and shear modulus, *G*. Fundamental differences exist between all three types of moduli. The key characteristic of the Young's modulus is that it comprises both the volumetric strains and shear distortion. The bulk modulus on the other hand is composed of strain modifications in volume with no variations in the shape. On the other hand, the shear modulus is determined when the strain change is due to changes in shape but no alterations in volume (Menzies and Matthews, 1996).

Some researchers like Mattsson et al. (2005) and Chan (2006) showed that there is a close relationship between the stiffness parameters (Young's modulus, *E*, bulk modulus, B, and shear modulus, G) determined from seismic tests and other soil parameters such as soil strength, for example. Soil parameters such as soil strength showed a high correlation between the maximum soil modulus (G_{max}) and undrained shear strength (c_u) of stabilised clay (Chan, 2006).

2.6 Experimental Relationships and Data from the Literature

Baxter and Sharma (1977), commenting that changes in G_{max} or v_s during shearing have been studied for clayey soils (e.g. Rampello et. al., 1997; Teachavorasinskun and

Amornwithayalax, 2002; Teachavorasinskun and Akkarakun, 2004), presented the variation of shear wave velocity, v_s, during shear. In their research, drained and undrained triaxial tests on cemented sands were performed with shear wave velocity measurements throughout the shearing process. The results showed that shear wave velocity during shear does not depend solely on mean normal effective stress (p'). During drained shear, v_s was found to be dependent on σ'_1 and during undrained shear v_s was dependent on σ'_3. During drained shear, v_s peaks before the strength of the soil is fully mobilized, and this feature of v_s can be used as an indicator of bond breakage in cemented soils. For cemented soils the v_s behaviour during shear is not well represented by a power law function of p'.

Yunmin et al. (2005) studied the correlation of shear wave velocity with liquefaction resistance based on laboratory tests. A simplified procedure is proposed based on the combination of in situ measurements of shear wave velocity and laboratory tests for evaluating liquefaction resistance and other factors such as relative density. Two series of dynamic triaxial tests were devised: (1) control of the shear wave velocity by changing the relative density or strain history with the confining stress (100kPa) unchanged; and (2) control the shear wave velocity by changing its confining pressure with the relative density (60%) unchanged. Bender elements were installed on samples tested using the conventional dynamic triaxial tests system, so that both measurements of shear wave velocity and dynamic triaxial tests could be conducted consecutively on the same samples. The generation and receiving of the shear wave are carried out by the bender elements, which were then used to determine the shear-wave velocity. The sands used in these tests were obtained from two sites in China: Hangzhou and Fujian. Furthermore, these authors referred to a case study by Andrus and Stokoe (2000) about a site at Treasure Island Fire Station, in California, where the value of shear wave velocity measured by cross-hole testing, assuming soil density of 1.76Mg/m^3, was found to be between 140-200m/s. (see figure 2.13)

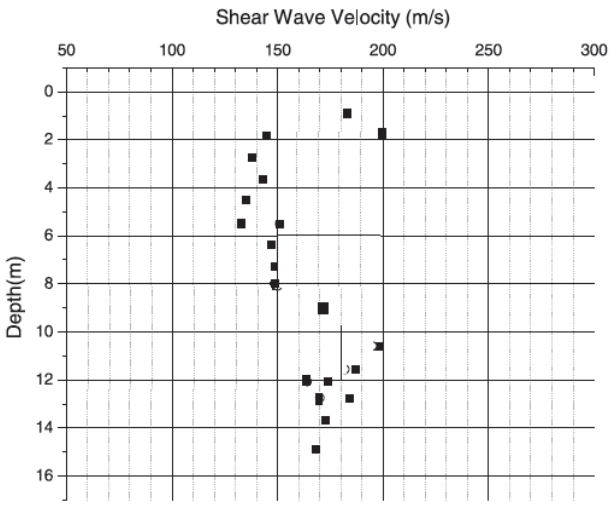

Figure 2.13 variation of shear wave velocity with depth (Yunmin et al. (2005))

Molnar et al. (2007) compared geophysical shear-wave velocity methods. The methods examined included both invasive (SCPT: Seismic cone penetration tests), and non-invasive techniques, including both active (SASW: Spectral Analysis of Surface Waves and CSWS: Continuous Surface Wave System), and passive sources (the single-instrument microtremor method). They concluded that sites with relatively soft soil are generally investigated with SCPT method while for sites which are too dense for cone penetration, SASW and CSWS methods were employed. They report a range of values for different geological horizons: for example, based on the 21 SCPT and 4 SASW field tests, a shear-wave velocity model has been determined by Monahan and Levson (2001) for bedrock in Greater Victoria, which consists of igneous and metamorphic rocks (Nasmith and Buck, 1998); the bedrock is estimated to have high shear-wave velocities of 1000-2500m/s (see also Hunter et al., 1999). They report the average shear-wave velocity of other geological units as follows: till and over-consolidated sediments earlier than the last glaciation, 390-550 m/s ; Colwood sand and gravel, 270-380m/s ; Colwood delta slope, 150-230m/s; brown Victoria clay, 160-260 m/s ; grey Victoria clay 100-160m/s ; and Holocene organic soils, 40-100m/s.

Uyanil (2011) studied the porosity of saturated shallow sediments from seismic compressional and shear wave velocities. This study presents a new analytical relationship between Poisson's ratio and shear modulus values, which were obtained from seismic velocities and porosity values of water-saturated material computed from water content and grain densities, which were determined by laboratory analysis of disturbed samples. The aim of the study was to estimate the porosity of water-saturated undrained soils without obtaining samples or disturbing the natural situation of soils, and this was achieved by using a nondestructive seismic refraction method to determine the seismic wave velocities. The analytical relationship between data sets indicates that when the shear modulus of water-saturated loose soil increases, porosity decreases logarithmically. If shear modulus increases in dense or solid saturated soils, porosity decreases linearly. This research indicates that porosity is one of several factors affecting the propagation of seismic waves in soils; other factors are: 1. Lithological properties of soil (grain sizes, shape, type, distribution, amount, compaction, consolidation and binding); 2. Physical properties (porosity, permeability, density, anisotropy, saturation degree, solid–liquid interference, pressure and temperature); and 3. Elastic properties (shear modulus (G), bulk modulus (K), Young modulus (E), Poisson's ratio (μ) and Lamé constant (λ)). Any change in the lithological properties of soil also affects seismic wave velocities, e.g. the higher the compaction rate the higher the velocities of both shear waves (S-waves) and compressional waves (P-waves). These relationships have been the

Pickett (1963) showed that the ratio of compressional (P) to shear (S) wave velocities could serve as a lithological indicator. The velocity of seismic waves changes according to the physical properties of soils; the seismic wave velocity in dense soil is higher than that in loose soil (Uyanık and Ulugergerli, 2008). Increasing soil density indicates higher soil compaction. P-wave velocity is therefore utilized in identifying lithology, porosity and pore fluids. S-wave velocity is utilized for mineral identification, determining soil porosity and for identifying

fluids. Hardin and Black (1968), and Hardin and Drnevich (1972), established experimental relationships between void ratio and shear modulus.

The development of the analytical relationship derived for this research indicates dependency of the bulk modulus (K) on shear modulus (G) and Poisson's ratio (μ), and then the shear modulus (G) is related to shear wave velocity (v_s), density (γ) and gravitational acceleration (g). Lastly, Poisson's ratio (μ) is related to v_s and v_p. In Uyanik's (2011) study, seismic P- and S-waves were recorded using vertical and horizontal component geophones respectively, connected to a 12-channel analogue recorder. Geophones were firmly attached to the ground and the first break arrival time of direct and refracted waves was obtained by digitizing and a commercial software package, SeisOPT® (Pullammanappallil and Louie, 1993). The results of the 2D inversion of the first arrivals for each profile were thus obtained. Geo-seismic sections (velocity-depth profiles, see figure 2.14) were determined as variations in velocities with respect to distance and depth. From these variations in velocities, the average seismic compressional and shear wave velocities were obtained. These average velocities were used in geotechnical cross-sections. The samples used for this research were classified as gravely, sandy and clayey-silty soils. Generally, shear wave velocity was found to increase slightly with depth in the studied sediments and water content decresase with depth (see figure 2.14). In the gravel soils, shear wave velocity lay within the range 66–503m/s (average 260m/s), while in sandy soils the shear velocities were within the range 105-516m/s (average 294m/s) and in the clayey–silty soils shear wave velocity fell within the range 58-584m/s (average 264m/s). (see table 2.2)

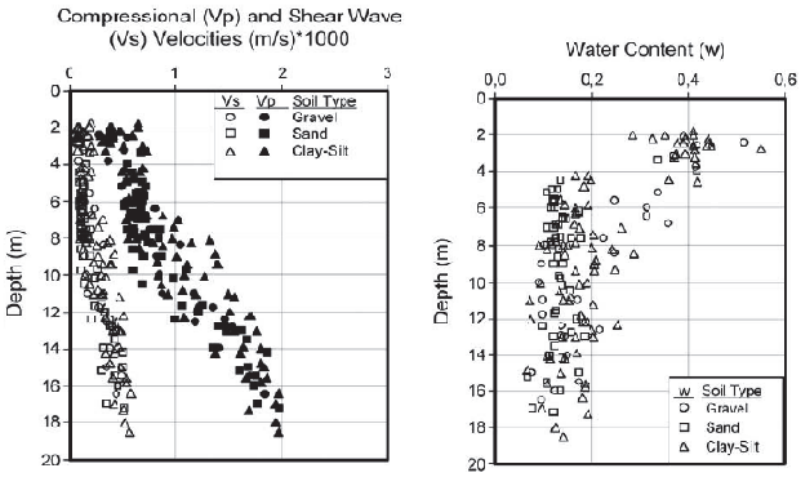

Figure 2.14 distribution of shear and compresional wave velocity and water content with depth (Uyanik's (2011))

Table 2.2 minimum maximum and mean values of measure shear wave velocity in gravel, sand and clay-silt (Uyanik's (2011))

Soil type	gravel				Sand				Clay-Silt				
	a	b	c	d	e	f	g	h	i	j	k	l	
Shear wave velocity	169	138	66	126	165	332	155	105	177	134	78	58	Min
	503	460	441	357	507	516	428	356	584	562	437	420	Max
	300	283	244	212	328	440	265	144	370	352	172	162	Ave.

Maheswari et al. (2008) studied the development of empirical correlation between shear wave velocity and standard penetration resistance in soils of Chennai city. They indicated that knowledge of accurate and realistic dynamic characteristics, such as shear wave velocity and other related dynamic soil properties like shear modulus, damping ratio, etc., is an essential requirement in the analysis of seismic wave propagation. In Chennai city, the soil formation mainly consists of soft marine clay, stiff clay and loose sand. In their study Multichannel Analysis of Surface Wave (MASW) tests were carried out using a seismic recorder with 24 vertical geophones, which were used to receive the wavefields generated by the active source of a sledgehammer. In order to have a confidence on the obtained shear wave velocities from MASW test, a seismic cross-hole test and bender element tests have also been carried out and the results from all methods match well. Their results show that in general shear wave

velocity increased slightly with depth (0-16m) and the shear wave velocity was within the range 150-250m/s.

Thitimakorn (2010) compared shear-wave velocity profiles of Bangkok subsoils from Multi-Channel Analysis of Surface Wave and down-hole seismic methods.

This study compares estimates of v_s derived from the traditional borehole method with those derived from the newer MASW technique at three sites near Bangkok, Thailand, namely at the Asian Institute of Technology (AIT), Chulalongkorn University (CU) and the Thailand Metrological Department (TMD). The Bangkok subsoil is reasonably uniform throughout the entire region and consists of marine and terrestrial deposits, the uppermost layer being known as Bangkok soft clay. All the results indicate that the MASW technique was acceptably congruent with the standard downhole seismic technique and therefore the MASW method was considered acceptable for estimating v_s of soils in and around the Bangkok area. The results shows the average shear wave velocity was between 150-300m/s by MASW method and 100-260m/s from the traditional borehole method at these three sites near Bangkok.

These finding are put into context by the work of Ashford et al. (1997), who reported that the shear-wave velocity (v_s) of the Bangkok soft clay layer was really low (about 60 to 100m/s), whilst that for the underlying stiff clay layer was in the range of 150-200 m/s, increasing to about 250 m/s for the first layer beneath that. He also stated that the low shear-wave velocity of Bangkok clay is comparable to Mexico City clay.

Adamo et al.,(2009), have presented the theoretical basis and practical; experimental setup for measuring the water content. The soil specimen used to perform the experiments was sandy soil and it was contained in a reinforced wood box measuring 170cm× 90 cm ×80cm (L×W×H). The compressional and shear waves velocities have been measured for four different values of the saturation (0.6%,30%,50%, and 70%). The theoretical analysis shows

that by measuring the shear waves velocity it is possible to estimate the water content, and the velocities ratio gives information about water distribution into the examined soil. The experimental setup has produced results in a good agreement with the theoretical values. The measured values of velocities reported, ranging from 130 to 150 m/s in case of compression wave and from 80 to 90 m/s in case of shear wave for sandy soil specimen.

Adamo et al., (2004), also have shown that by introducing suitable simplifications and hypotheses in the equations of elastic waves propagation of compressional waves and the moisture content of soil can be obtained. But this approach had some limitations a good knowledge of many parameters of the medium (e.g., porosity, density, granular composition, etc) are required.

They also have studied the possibility of using shear waves velocities in conjunction with compressional ones.

Madun et al., (2012), describes a methodology for performing surface wave testing in the laboratory. In comparison with field tests, a laboratory-scale experiment offers the advantage of allowing the process of data collection to be calibrated, and analytical studies can be carried out as the properties of the material under test are controllable and known a priori. In addition, a laboratory scale experiment offers insight into the interaction between the seismic surface wave, the soil, the boundary and, hence, the constraints associated with the seismic surface wave technique.

Two simplified models of different sizes were developed using homogeneous remoulded Oxford Clay at different water contents and corresponding undrained shear strengths. In this setup, two sizes of containers were constructed measuring (1): 600 mm x 300 mm x 300 mm and (2): 1080 mm x 680 mm x 500 mm in length, width and depth respectively. The containers contained Oxford Clay at different water contents of 32 % and 40 %.

The measured phase velocities were converted to shear wave velocities using equation and the the maximum shear modulus, G , was calculated using equation $G_{max}=\rho$(density)$\times v^2$(shear

wave velocity) The maximum shear modulus plots versus wavelength for homogeneous Oxford Clay at 32 % and 40 % water content, are shown in Figure 2.15 and 2.16 respectively. The measurements demonstrate that the clay in the two containers had very different shear moduli, which indicated that the surface wave technique was reliable to carry out at the laboratory scale using the equipment and methodology described in this paper.

Also the laboratory experimental methodology demonstrated that the seismic surface wave equipment used in the laboratory was directly influenced by the clay properties as well as the size of the test model and showed that the arrangement of the seismic source and the receivers had an impact on the range of reliable frequencies and wavelengths obtained.

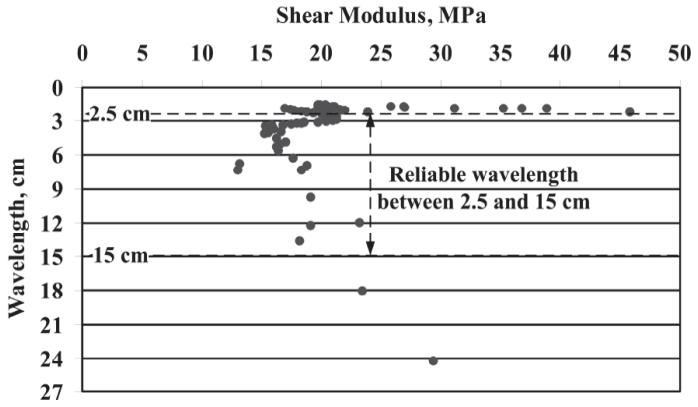

Figure 2.15 shear modulus versus wavelength for measured conducted on the smaller container filled with Oxford clay 32% (Madun, 2011)

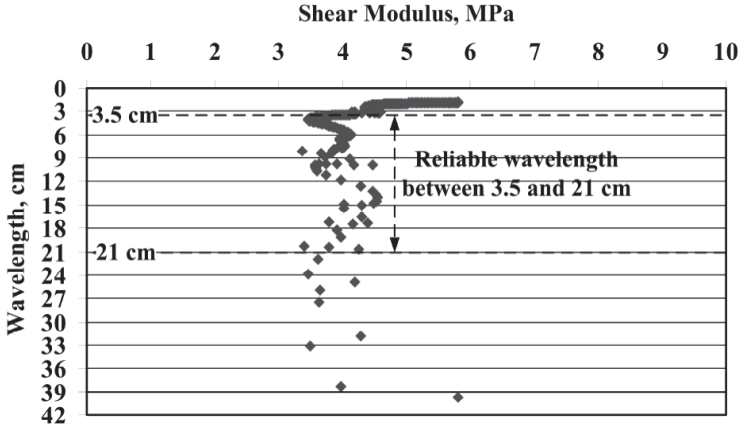

Figure 2.16 shear modulus versus wavelength for measurements conducted on the larger container filled with Oxford clay 40% (Madun, 2011)

Yang et al., (2008), determine the dynamic properties of compacted clayey soil with matric suction measurements. The effects of matric suction of unsaturated residual lateritic soil on small strain shear wave velocity and small-strain shear modulus were investigated.

The soil, residual lateritic soil, used in this study was taken from Linkuo located at about 20 km south of Taipei city in Taiwan with natural moisture content 31% ~ 37%, 10% Sand, 30% silt and 60% clay,.

Soil specimens were compacted at optimum moisture content, wetted to various moisture contents, then, tested for small-strain shear wave velocity and matric suction using the bender element and the filter paper method, respectively. Test results demonstrated that the small-strain shear wave velocity and small-strain shear modulus decrease with increasing moisture content and decreasing matric suction. (see figure 2.17)

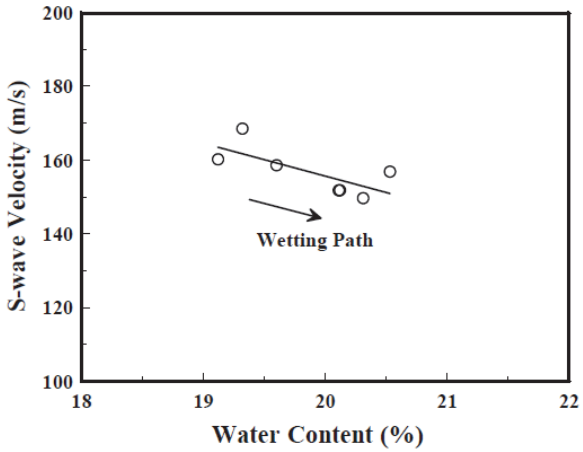

Figure 2.17 variation of S-wave velocity with degree of saturation (Yang et al., (2008))

2.7 Summary

This chapter summarised the advantages of seismic-based techniques compared with other geophysical and geotechnical techniques. The seismic wave results are directly related to active soil properties such as the maximum shear modulus, G_{max}, the bulk modulus, B, Young's modulus, E, and Poisson's ratio, v (Charles and Watts, 2002; Crice, 2005).

Seismic-based methods have been proven to be both more versatile than other methods as well as being more economical in terms of field operation to determine physical properties of tested geo-materials (Matthews et al., 2000). Since the surface waves travel in the vicinity of the ground surface, they are less attenuated and dispersive. The dispersive features pertains uniquely to the surface wave in which case the frequency and wavelength change as a result of the different velocities when the soils are layered. The dispersive phenomenon is used to identify the soil properties with depth. SASW, CSW and MSW are common surface wave techniques. Of all these techniques, MSW is preferred due to its flexibility in the signal processing approach to extract the dispersion curve.

Chapter 3

INITIAL TESTING METHOD

3.1 Introduction

In this section, emphasis is placed on the development of small-scale seismic surface wave testing in the laboratory as well as assessing the viability of the proposed method to investigate the relationship between the geophysical and geotechnical properties of soil, so that geotechnical soil databases can be used to inform geophysical surveying protocols and results analysis.

The choice of which geophysics tests to use depends on the parameters to be examined (Mitchell and Jardine, 2002). Amongst geophysical methods, the seismic method based results empirically derive geotechnical properties such as maximum shear modulus $(G_{\max})$, bulk modulus (*B)*, Young's modulus (*E)*, and Poisson's ratio (υ) (Charles and Watts, 2002; Crice, 2005) and the seismic-based techniques have proved particularly useful in determining shear modulus which can be expand to calculate the shear wave velocity and find that how soil properties influence acoustic wave transmission during the seismic surface wave testing (Moxhay *et al.,* 2001; Redges *et al.,* 2008).

As testing in the field is difficult and complex, and this is coupled with non-homogeneity of typical natural ground conditions, the laboratory test was established to provide a straightforward means of creating repeatable data and the process was further simplified by the use of homogeneous material. The outcomes from testing can be then used to develop procedures for full seismic testing in natural soil as part of supplementary work

The selection of seismic sources was determined by the level of frequency and energy required for the test materials and the selection of the seismic apparatus, specification and the size of the test models has to consider the factors of time, cost and workability. The seismic surface wave equipment for use in the laboratory seismic tests was directly related to the material properties and the size of the test model.

The development of the small-scale model for seismic surface wave testing in the laboratory aimed to develop the most appropriate seismic surface wave method for attaining and utilising the data to investigate the influence of soil properties on acoustic wave transmission

To achieve this aim, it is necessary to investigate the suitability of the seismic equipment and its system for laboratory use. The use of seismic surface wave methods in the laboratory should have sufficient sample volume size to reduce the effect of seismic wave back-scattering, due to the model boundary together with interference by body waves.

Kaolin Clay and Oxford Clay were used for these tests, Oxford Clay being more practically relevant than Kaolin since Oxford Clay is representative of natural soil. This is because Oxford Clay has various clay types and hence a mixed mineralogy. Use of Kaolin Clay, which is a pure form of kaolinite, ensures a high degree of sample control, simplifies the analysis and reduces variability throughout the test programme. Laboratory-scale experiments are preferable over field tests because the data collection process occurs under far more controlled conditions to obtain the true measure of the data that are being collected.

3.2 Establishing Laboratory Seismic Surface Wave Equipment

The most relevant factors that were vital for the success of the seismic surface wave tests in the laboratory can be seen in Figure 3.1. In essence, there are two major pieces of apparatus for the seismic test, namely the seismic source, which generates vertical ground motions using a point source of energy, and the seismic recorder. To have more flexibility in the size of the test model, a high frequency range for the seismic receivers was selected.

To investigate correlation between the geophysical and geotechnical properties of soil, development of the most appropriate small-scale model for laboratory seismic surface wave testing is necessary both in terms of obtaining and utilising the data. The effect of seismic wave back-scattering needs to be reduced, so the laboratory seismic surface wave method chosen should have sufficient sample volume size. This is mainly because the model is bound to interfere with body waves which then intensify the signal-to-noise ratios.

This research uses two different types of soils, i.e. Kaolin and Oxford Clay. For laboratory testing, the equipment and its systems need to be appropriate to determine change of soil properties, and hence the suitability of the seismic source-receivers array should be considered. A summary of the overall testing, involving a variety of materials and how they related to one another, is shown in Figure 3.2. In this chapter the initial test methods are discussed, while the corresponding results are presented in Chapter 4. Afterwards, the main test methodology is discussed in Chapter 5 and the associated results presented in Chapter 6.

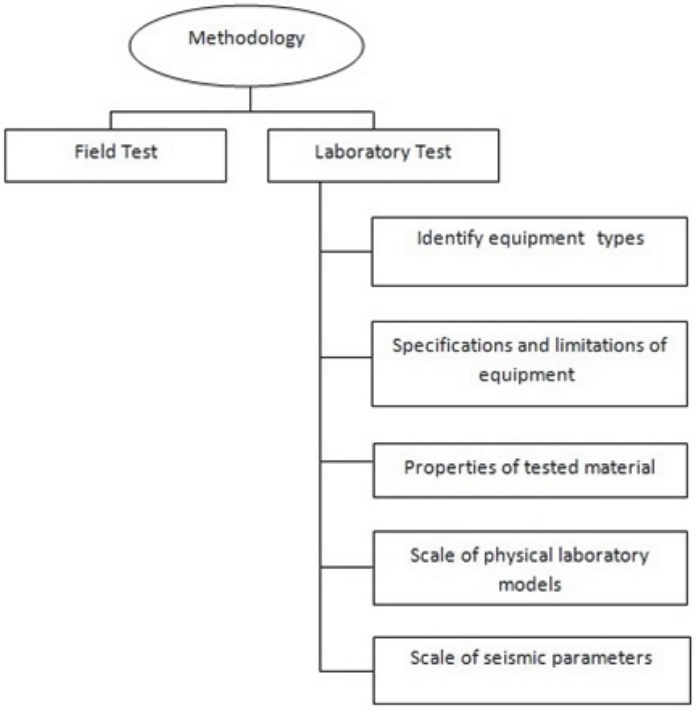

Figure 3.1: The seismic surface wave factors that contributed to the success of tests at the laboratory scale.

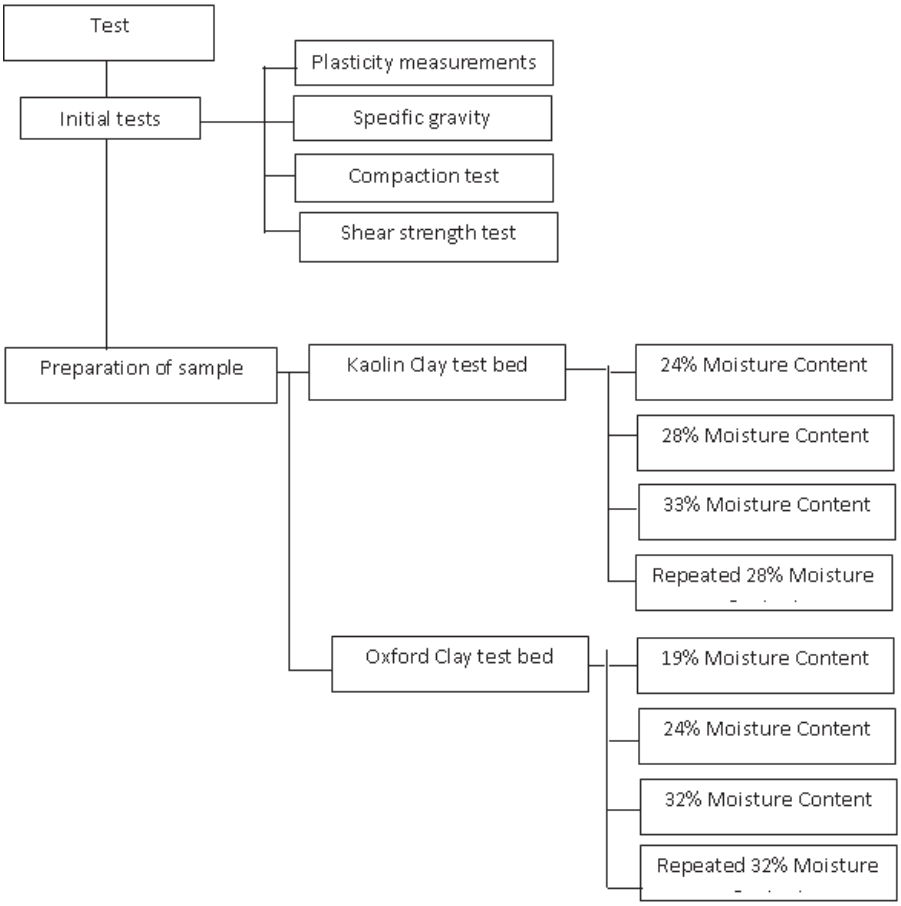

Figure 3.2: Outline details of the Initial and Main laboratory scale model tests

3.2.1 Seismic Surface Wave Equipment

The surface wave was generated by a piezo-ceramic transducer with an electromechanical vibrator placed above it, creating a point energy source (see Figure 3.3). The piezo-ceramic transducer, which is a transducer that converts mechanical energy to electrical energy, was located on the sample and an electromechanical vibrator connected to an audio power amplifier was used to create mechanical energy; together they acted as a seismic source to generate the excitation signals. The frequency level and the amount of energy needed must be taken into consideration when selecting the seismic source. For example the piezo-ceramic transducer gives better energy at higher frequencies when compared to an electromagnetic vibrator. In the test procedure in order to ensure good contact with the test material, the piezo-

ceramic transducer included weights padded with acoustic absorbers, while the electromechanical vibrator used absorber pads to maintain its position and support its weight, as illustrated in Figure 3.3 and Figure 3.4. Four channels of the signal conditioner and four piezoelectric-accelerometers were used to measure the seismic output. The number of receivers deployed in a multi-channel approach is usually a compromise between the economic cost of the equipment and the time required to conduct the survey.

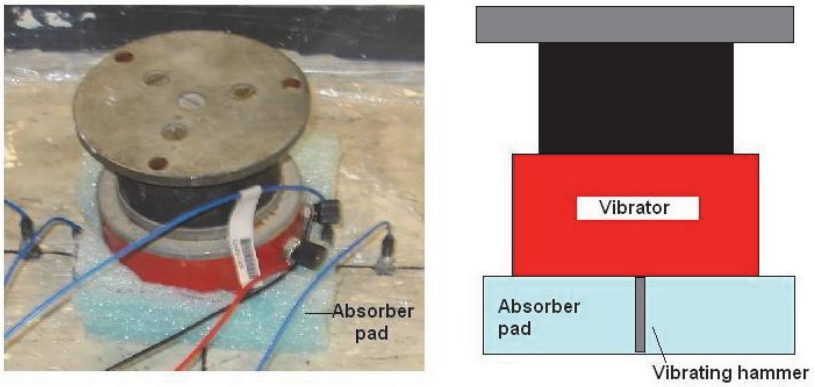

Figure 3.3: Electromechanical vibrator supported by the absorber pad to maintain its position.

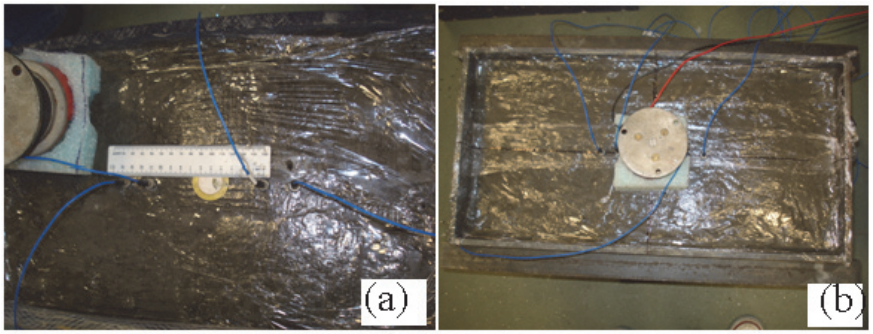

Figure 3.4: (a) piezo-ceamic transducer which is located at the middle of the sample on the surface of the sample (b) electromechanical vibrator which is placed on top of it in the vertical direction used as a point energy source and it used absorber pads to support its weight and maintain its position as

Matlab software was used to monitor communication between the various sets of equipment. A script on how to conduct the experiment using a computer was written within the Matlab environment – see Appendix **B**. The computer was then connected to a National Instruments data acquisition system, in which a 16-bit analogue output module (NI-9263) generates the transmission waveforms. An audio power amplifier was used to drive the seismic sources (piezo-ceramic transducer or electromechanical vibrator) with excitation signals. On the

receiver side, to measure the vertical ground acceleration the sensors were made up of four piezoelectric accelerometers (ICP®, model 352C42 from PCB Piezotronics) with a frequency range of 100 Hz to 10 kHz. The accelerometers were connected to an analogue signal conditioner (model 482C05) via a Teflon cable of low-noise coaxial BNC plug model 003C10 from PCB Piezotronics. A 24-bit sigma-delta analogue-to-digital converter module (NI-9239) with a sampling rate of 50 kHz was used to sample the seismic signals. The data being generated were then collected, stored and later processed when the data acquisition session was complete. To diminish ambient noise, acoustic absorbers were used to isolate the models from the ground. Figure 3.5 summarises the equipment for use in a laboratory seismic surface wave experiment. Figure 3.6 illustrate, in general, the laboratory seismic surface wave test setup, where the seismic source located at the middle of the receiver sensor-pairs, and Figure 3.7 shows a photograph of the equipment.

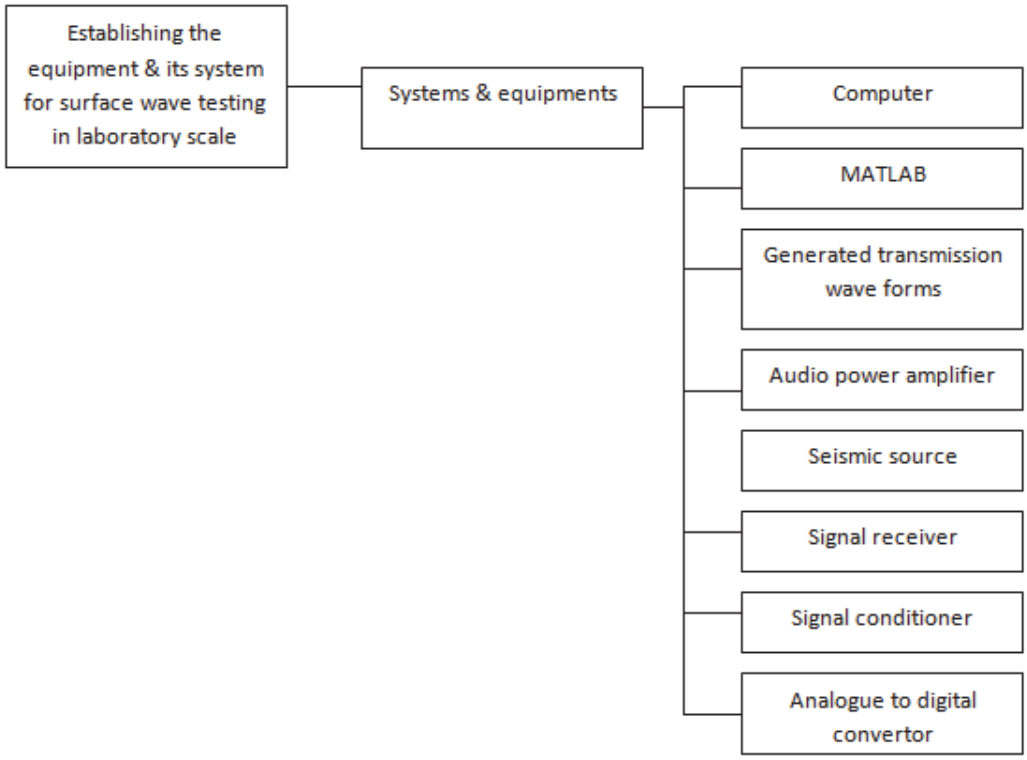

Figure 3.5: Details of the equipment, specification for the laboratory scale seismic surface test.

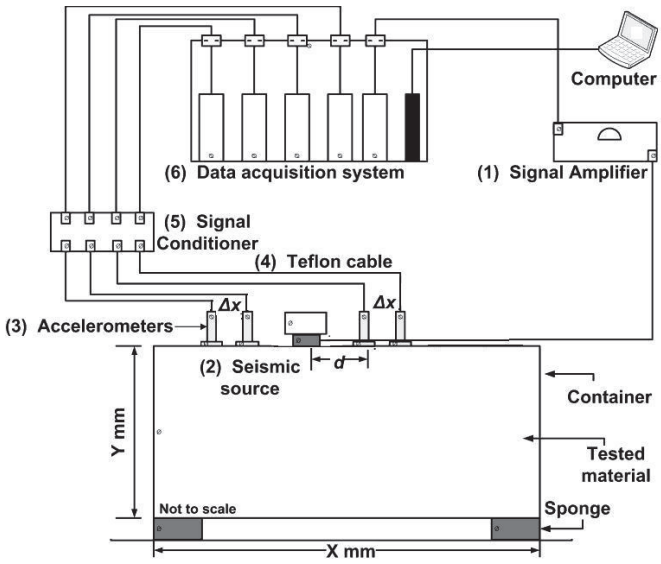

Figure 3.6: Laboratory setup for seismic surface wave test.

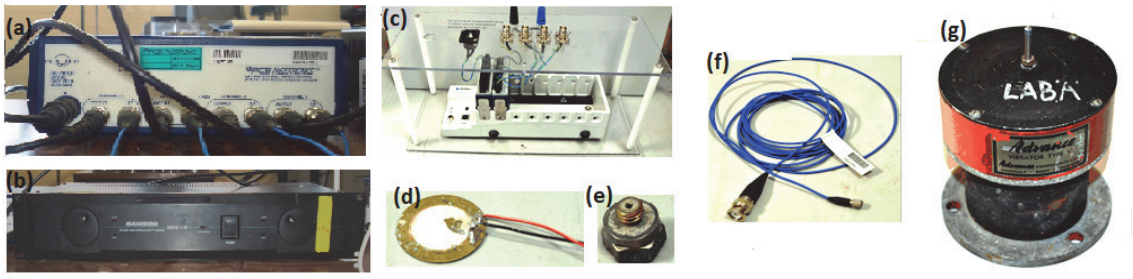

Figure 3.7: (a) Signal conditioner, (b) Signal amplifier, (c) Data acquisition system, (d) Piezo-transducer, (e) Piezo-electric accelerometer, (f) Teflon cable, (g) Electromechanical vibrator

Rayleigh waves will be formed when the wavelength is smaller than half of the model depth (Zerwer et al., 2000 and 2002). As the piezo-ceramic transducers are suitable for transferring high frequency energy they are most appropriate for the clay model, which requires a higher frequency. The excitation signal was generated by using an audio power amplifier to drive the piezo-ceramic transducer and, as stated above, the piezo-ceramic transducer was acoustically coupled to the surface with the use of a weight padded with acoustic absorber. In view of the fact that the frequency range of the accelerometers is up to 10 kHz, the captured data will not exceed 10 kHz. Figure 3.8 shows the laboratory-scale model and equipment setup on the clay model with sensing accelerometers.

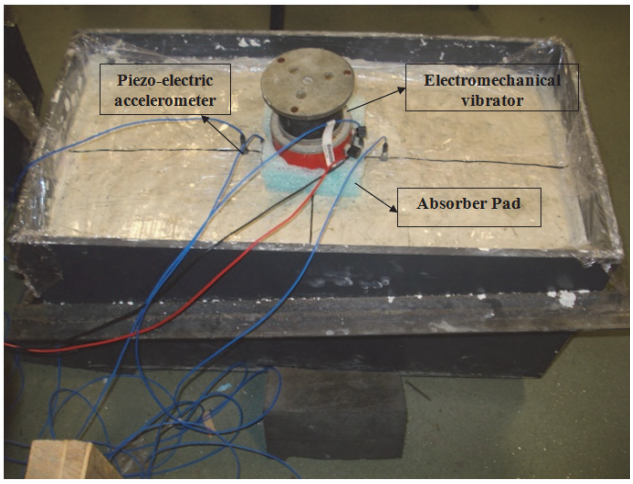

Figure 3.8: Illustration of the laboratory-scale model and equipment setup, i.e. the clay model with sensing accelerometers

3.3 Experimental Procedure

As mentioned above, the multi-channel approach used in this study is based on small number of receiver channels. Up to 4 piezoelectric accelerometers formed the array of receivers. d_{min}, the distance between the source and the first receiver, and d_{max} ,the distance between the source and second receiver, were set as 55 mm and 80 mm respectively (same dimensions for receivers at the right and left side of the source). The applicable frequency range was calculated for each test by assuming a surface wave velocity and using the constraints given in Equations 2.9 and 2.10, which consider near and far offset constraint. Nevertheless, the frequency limit of the sensing accelerometers is bound by the upper frequency limited of 10kHz. A stepped-frequency method was employed with the frequency of the sinusoidal wave being raised from 100Hz to 10 KHz with a 10Hz step size. In order to compute the normalised coherence for each frequency, 5 recurring measurements were acquired for averaging. The experiment was initially performed using a series of measurements for the

Kaolin Clay model. Figure 3.9 shows the basic sequence.

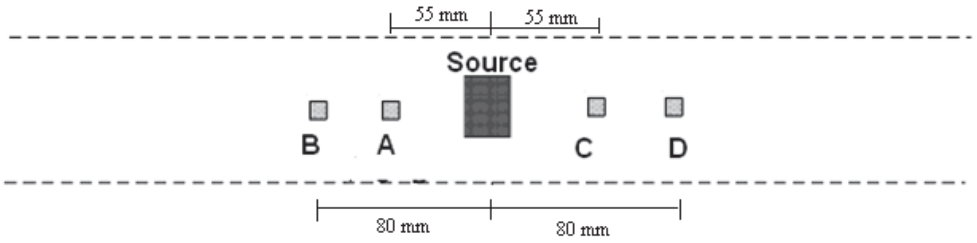

Figure 3.9: Data collection arrangement with accelerometers A, B, C and D

3.4 Method for Data Processing

Two major techniques were used to analyse all the surface wave data; signal processing and spectral analysis. These methods were built upon prior research by Aziman Madun (Madun, 2011).

An analogue-to-digital converter was used to separately sample the time domain signals $Y_n(k)$ and the N-points were stored on the computer on which subsequent spectral analysis was done. The sampling rate of the signals, f_s, can be sufficiently captured through the use of the analogue-to-digital converter (the converter must have at least two times the optimum bandwidth of the signal, although it usually is higher). To get the discrete spectrum of the signal, discrete Fourier Transform (implemented using the FFT algorithm) was applied as given in Equation 3.1:

$$Y_n(f) = \sum_{k=0}^{N-1} y_n(k) \exp\left(-j2\pi f\ k/N\right) \qquad \text{Equation 3.1}$$

where f is the discrete frequency of the signal, $N = Tf_s$, and k and T are the discrete-time and time spans of the signals.

The quality of the phase velocity is heavily reliant on the reliability of the phase information. It therefore requires that the consistency of the received signal to be noted (i.e. the coherence of the received signals) with regard to the frequency. This is important because if the signal-to-noise ratio is too high at a given frequency, it will compromise the quality of the data, i.e. the phase data for that frequency would be unreliable. The coherence of the received signals is represented by its normalised cross-spectrum between the pairs of received signals. This paves the way for measuring the signal-to-noise quality as a function of frequency. In a situation in which the phase difference is calculated between a pair of receivers, the normalised coherence becomes a measure of variance, over several snapshots of time between the received signals. The normalised coherence can then be calculated as given in Equation 3.2 (Ifeachor and Jervis, 1993):

$$S_{norm,mn}(f) = \frac{\sum_{p=1}^{P}\left[\left(Y_{n,p}(f) - \mu(Y_{n,p}(f))\right)\left(Y_{m,p}(f) - \mu(Y_{m,p}(f))\right)^{*}\right]}{(P-1)\sqrt{\sum_{p=1}^{P}\left|Y_{n,p}(f) - \mu(Y_{n,p}(f))\right|^{2}\sum_{p=1}^{P}\left|Y_{m,p}(f) - \mu(Y_{m,p}(f))\right|^{2}}} \quad \text{Equation 3.2}$$

where p is the index of P, the total number of repetitive collections for each frequency step. $\mu(Y(f))$ is the mean of the complex spectrum across the repetitive collections at each step frequency f and * represents the complex conjugate operation. The Equation 3.3 can then be used to obtain the signal-to-noise ratio from the normalised coherence.

$$SNR(f) = 10\log_{10}\left(\frac{S_{norm,mn}(f)^{2}}{1 - S_{norm,mn}(f)^{2}}\right) dB \quad \text{Equation 3.3}$$

where S is coherence and S_{norm} is normalised coherence.

The phase velocity calculated as a function of frequency between any two receivers can be obtained from their corresponding phase difference. The angle of the trivial spectrum value

($\Delta\emptyset$) represents the phase difference at a particular frequency and is expressed by Equation 3.4:

$$\Delta\phi_{mn}(f) = \tan^{-1}\left(\frac{\mathrm{Im}(S_{mn}(f))}{\mathrm{Re}(S_{mn}(f))}\right) \qquad \text{Equation 3.4}$$

From Equation 3.4, m and n represent the receivers between which the four-quadrant phase difference is computed, *mn* is the complex conjugate of Fourier spectrum of receivers m and n, S_{mn} is the cross power spectrum between receivers m and n, $\mathrm{Re}(S_{mn(f)})$ is real part of the complex $S_{mn,,}$ $\mathrm{Im}(S_{mn(f)})$ is imaginary part of the complex S_{mn} and $\Delta\Phi_{mn}(f)$ is the phase shift between receivers m and n.

The time-delay related to the phase difference observed between the two receivers can be derived from Equation 3.5:

$$\tau(f) = \frac{\Delta\phi(f)}{2\pi f} \qquad \text{Equation 3.5}$$

The frequency-dependent phase velocity, *v(f),* can then be obtained using the distance between the two receivers m and n, $\Delta_{mn}x$, as given in Equation 3.6:

$$v_{mn}(f) = \frac{2\pi\ f\Delta_{mn}x}{\Delta\phi_{mn}(f)} \qquad \text{Equation 3.6}$$

The Rayleigh-wave phase velocity, V_r, can be converted into shear-wave velocity, V_s, in a solid and homogeneous medium. In an elastic medium V_s is approximately:

$$V_s \cong \frac{1+\upsilon}{0.862+1.14\upsilon}V_r \qquad \text{Equation 3.7}$$

where υ is the Poisson's ratio (Richart et al., 1970).

The maximum shear modulus of material, G_{max}, is defined as the ratio of shear stress to the shear strain and is one of several quantities for measuring the stiffness of materials. G_{max} describes the material's response to shear strains and it is related to the mass soil density, ρ, and the shear wave velocity through the relationship:

$$G_{\max} = \rho v_s^{\,2} \qquad \text{Equation 3.8}$$

Because of the approximation of the Poisson's ratio for soil and rock materials, errors arise in the maximum shear modulus.

The next chapter shows how the data are analysed in general while Chapter 5 details the sample preparation.

Chapter 4

SUMMARY OF THE DESIGNED TEST PROCEDURE

4.1 Introduction

This chapter summarises the designed test procedure, while the test process and analysis of results will be described in the subsequent chapters. The data analysis presented in this chapter is in accordance with Madun (2010, 2011), who demonstrated the validity of the methodology. The outcomes from the tests can be used to develop the surface wave test method on models of natural soil for future work.

4.2 Data Processing

Each comprehensive set of measurements contains received signals from the 4 sensing channels with the frequency range of 100 Hz to 10 kHz with a step-size of 10 Hz. The collected data were processed after each session by using the Matlab software. Applying a Fast Fourier Transform (FFT) to all the data, to acquire spectral representation of the received signals, was the initial step in the process. The magnitude and angle from the complex results

represented the amplitude and phase respectively. On running a stepped-frequency transmission, the corresponding complex frequency of transmission that related to the received signal was selected and stored. Initially this was repeated for the transmissions at the same frequency, and later it was carried out for the entire frequencies across the whole frequency range. The result was a new FFT spectral series as a function of the stepped frequencies. Consequently, the data were simplified to the stepped-frequency spectral version for the 4 sensor channels. This had 5 multiple sets, given that there were 5 repetitive snapshots per frequency step when the data were being collected.

After the initial step, obtaining the phase difference between the receivers was the next step. By performing a mathematical operand, termed a complex conjugate multiplication, in the spectral domain, the phase difference was achieved for each of the neighbouring sensor pairs. In order to get the phase difference between two neighbouring pairs, say A and B, the complex conjugate of the FFT of the signal from sensor B was multiplied with the FFT of the signal from sensor A.

4.3Analysis of Results

This section explains the process which is used in Chapter 6 for the results analysis based on the figures and results for a Kaolin Clay sample with a moisture content of 28%; this moisture content, which is the optimum moisture content for Kaolin clay (based on Figure 5.1), is used here as an example.

Figure 4.1 shows the phase difference measurements achieved from the Kaolin Clay sample with a 28% moisture content. In an ideal, homogeneous medium with no boundaries, the differential phase response is expected to be a linear function of frequency. However, as shown in Figure 4.1, measurements were affected by boundary reflections and there was mutual interference between the body and the surface waves. Figure 4.2 indicates the normalised coherence between channels A and B from measurements on a Kaolin Clay

sample with a 28% moisture content. By using Equation 3.2, the normalised coherence was then calculated for each of the sensor pairs. The normalised coherence can be used to evaluate the signal quality in terms of the signal-to-noise ratio. This was thus used as a decisive factor in choosing the frequencies that produced reliable phase measurements, i.e. it was used to discard low quality measurements and retain the frequencies that contained phase measurements with higher accuracy. This relies on a rigid threshold regime, where only measurements above the threshold are taken into account. As a result, all the values below the threshold are treated as equally insignificant, while the values above are likewise considered of equal importance. A minimum threshold of 0.995 for the normalised coherence was applied to attain a sufficiently high degree of accuracy of the phase difference, since phase measurements are very sensitive to degradation in signal-to-noise ratio. Therefore, the frequencies with a coherence that surpassed the threshold were chosen. This threshold corresponded to a signal-to-noise ratio of approximately 20 dB and an equivalent phase measurement standard deviation of approximately 6 degrees (Madun et al., 2010).

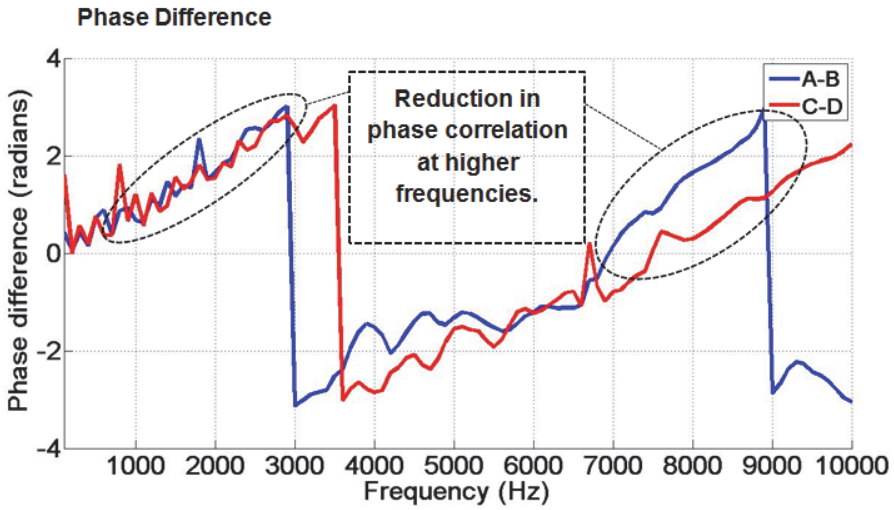

Figure 4.1: The phase differences for the 2 sensor-pairs from measurements on a Kaolin Clay sample with a 28% moisture content

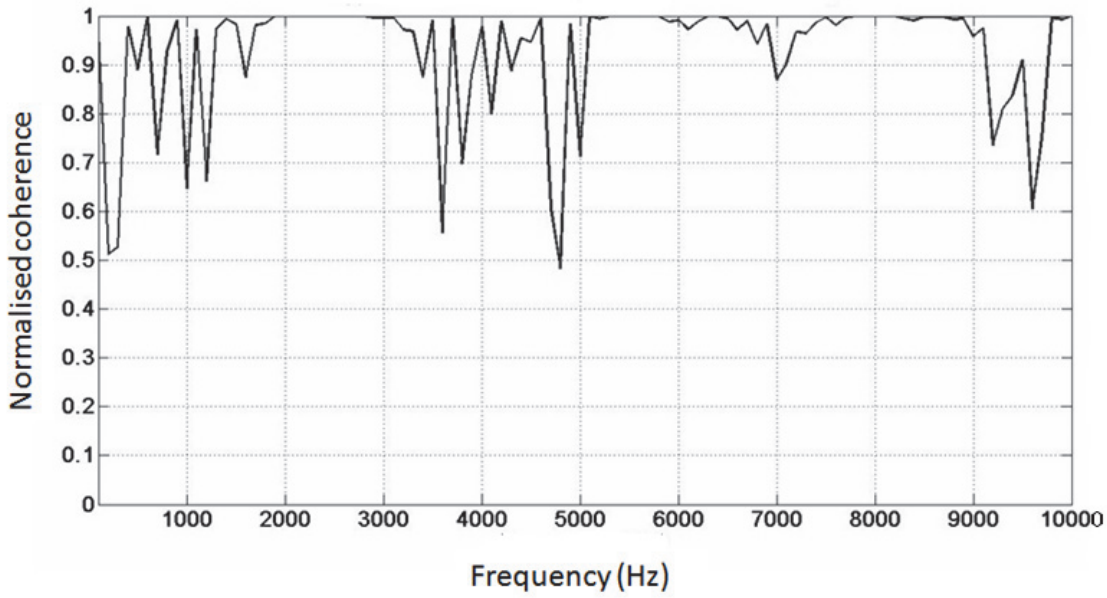

Figure 4.2: The normalised coherence between channels A and B from measurements on a Kaolin clay sample with a 28% moisture content.

The effective frequency which was predicted and chosen for processing for each test was calculated using Equations 2.10 and 2.11, and it was in the range of 100 Hz up to 10 kHz (the maximum frequency limitation). The frequency range was split into sub-bands of 400Hz each, because only a few frequencies exceeded the threshold. Rayleigh-wave phase velocity measurements are the next step. Equation 3.6 was employed to compute the velocities from the phase measurement. The velocity within each sub-band that corresponded to the qualifying frequencies was averaged.

Figure 4.3 shows the result of phase velocity versus frequency for the Kaolin clay sample with a 28% moisture content for frequency range of 1500 Hz to 8000 Hz. From Figure 4.3 it can be seen that at lower frequencies than 2 kHz, larger deviations from the averaged Rayleigh-wave phase velocity can be observed for the sample. This was likely to have been caused by interference from other wave modes at these lower frequencies.

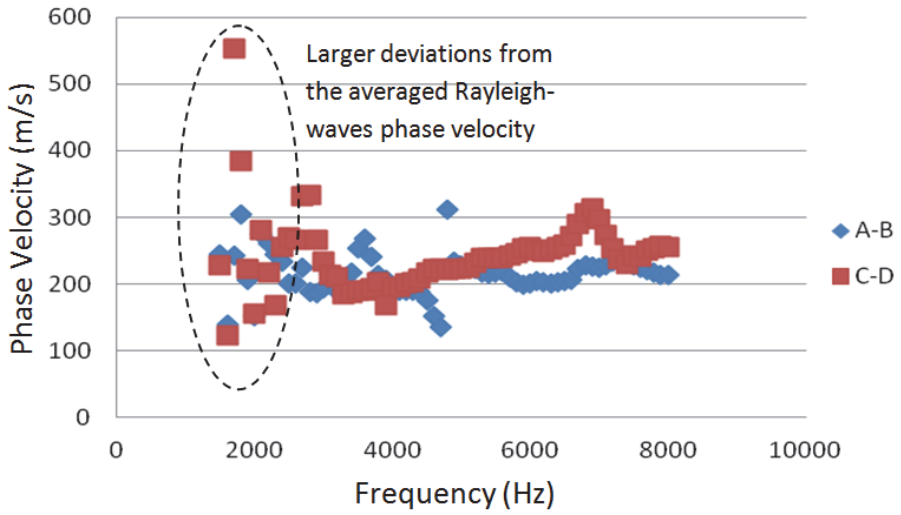

Figure 4.3: Phase velocity versus frequency for the Kaolin clay sample with a 28% moisture content

The Rayleigh-wave phase velocities were converted into shear-wave velocities by a factor of 1.08, based upon the adoption of a Poisson's ratio of 0.3 in Equation 3.7. In the situation where more discrete samples are obtainable either through the use of a wider frequency range, or in situations where there are more frequencies that contain precise phase measurements, the shear-wave velocity values can be interpolated to get a smoothed dataset. The relationship between the shear wave velocity and the moisture content of the soil will be investigated, so this will show how soil properties such as moisture content and density influence acoustic wave transmission. This will allow the formulation of a correlation between acoustic and geotechnical properties.

Chapter 5

DETAILED PROGRAMME OF WORK

5.1 Introduction

This chapter gives a summary of the experiments conducted to measure the shear wave velocity for the samples with different moisture content. The experimental models are constructed based on the aim of this study, which is to assess how soil properties influence acoustic wave transmission and how the results can be used to develop a correlation between acoustic and geotechnical properties. The programme involved 8 tests using a plastic box filled with Kaolin Clay or Oxford Clay, each using 4 different moisture contents.

5.2 Clay Materials Used in Test Beds

In this research, the Clay test beds were made of compacted Oxford Clay and Kaolin Clay with different moisture contents. Kaolin Clay mixed from dry, processed powdered Clay was used initially. This reduced the level of variation in the course of the test programme and also ensured a high level of sample control. A single batch of Oxford Clay was obtained from the

Hanson Brick quarry in Peterborough, England. Oxford Clay comprises marine sedimentary rock formed in the Jurassic age. It can be found underneath the ground surface around Oxford and over much of southeast England, Peterborough and Weymouth. The choice of Oxford Clay was primarily

due to its ready availability, relative ease in sampling and uniformity across all the samples taken. All the samples were well mixed before the tests in order to ensure that they were homogeneous. This allowed for any differences in the sample material to be averaged out before compacting the material in the box.

Table 5.1 shows the differences between the Kaolin and Oxford Clays. The properties of both the Oxford Clay and Kaolin Clay samples were determined by use of the appropriate British Standard. All the physical properties of the materials used throughout the test were characterised as the index properties of Oxford Clay and Kaolin Clay.

Table 5.1: Summary of the index properties of Oxford Clay and Kaolin Clay

Type of soil	Oxford Clay	Kaolin Clay
Plasticity test: Plastic limit Liquid limit Plasticity index	 25.5 % 45.3 % 19.8 %	 38.4 % 54.5 % 16.1 %
Compaction test: Optimum water content, OWC Maximum dry density, MDD Bulk density	 24 % 1550 kg/m^3 1920 kg/m^3	 28 % 1410 kg/m^3 1810 kg/m^3
Specific gravity	2.60	2.69

5.2.1 Plasticity Measurement

By using the cone penetrometer device in conformance with Section 4.3 of BS1377: Part 2: 1990 (BSI, 1990), a liquid limit (LL) test was performed. Also, a plastic limit (PL) test was done in accordance with Section 5.0 of BS 1377:Part2:1990 (BSI, 1990). The test results revealed that Oxford Clay had a LL of 45.3% and PL of 25.5 %. These results are typical for

Oxford Clay as proposed by Lee (2001). In contrast, Kaolin Clay had a LL of 54.5% and PL of 38.4%, which agrees with the standard values reported by John (2011).

5.2.2 Specific Gravity

Using the small pyknometer method in accordance with Section 8.3 of BS 1377: Part 2:1990 (BSI, 1990), specific gravity tests were carried out. The soil used for testing was oven-dried soil which passed through a 2mm sieve. The precise specific gravity of the Oxford Clay was 2.60 and for Kaolin Clay was 2.69, which is also in line with accepted values for these soil types.

5.2.3 Compaction Test

The Clay compaction tests were conducted based on BS 1377: Part 4.7: 1990 (BSI, 1990), using the 2.5 kg hammer method. This technique makes use of a 2.5 kg hand compaction hammer and a compaction mould measuring one litre. This method is often referred to as the 'Proctor' test. A dry density-moisture content relationship for Oxford Clay and Kaolin Clay is shown in Figure 5.1. The Oxford Clay and Kaolin Clay have a highest dry density of approximately 1550 kg/m^3 and 1410 kg/m^3 at optimum water contents of 24% and 28% respectively.

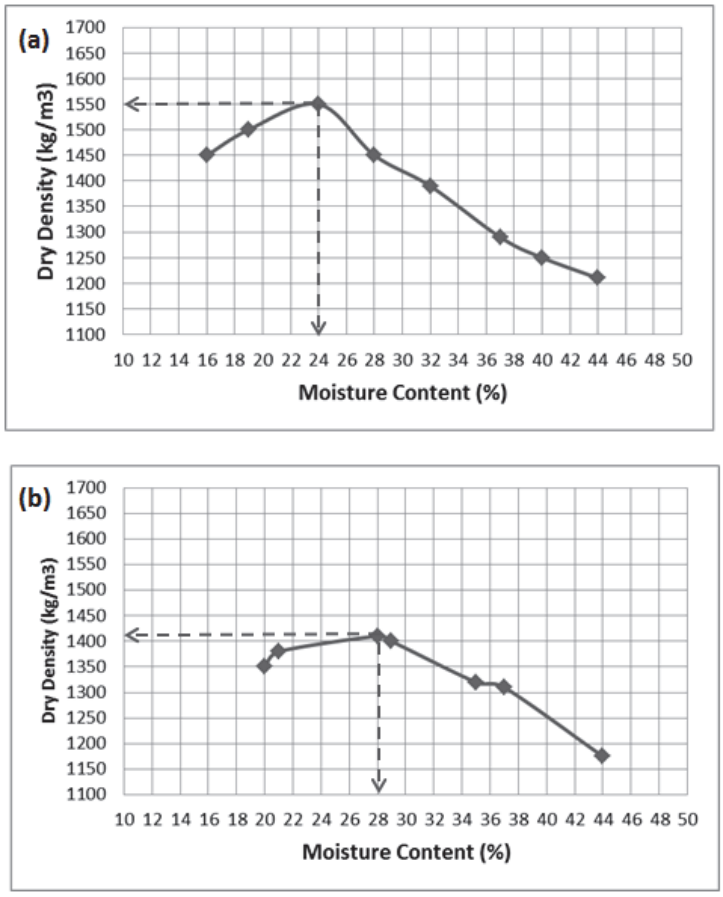

Figure 5.1: Compaction test for (a) Oxford Clay, (b) Kaolin Clay

5.3 Preparation of the Kaolin Clay Test Bed

The experiments were done using a container with length, width and height of 600mm × 300mm × 300mm to obtain the response of the soil during the seismic wave test. The selection of the seismic apparatus, and specifications and size of the test model, has to consider the factors of time, cost and workability. The selected size of the container is suitable from a uniform scale model point of view, i.e. so an acceptably large sample could be made that can be compacted well and uniformly. Also it is acceptable size from practical viewpoint, but had issues and limitations from the acoustic experiments point of view, such boundary reflection; accordingly it was necessary to define the reliable wave lengths for that size of sample. Hence by adopting this selected size of sample, some parameters are liable to be more accurate, such as compaction of the sample, but on the other hand there will be some

limitation such as reliable wavelength, because of the boundary reflections. The chosen dimensions were therefore considered to be an acceptable compromise.

The test results were used to understand the response of the soil due to wave transmission and also to identify the phase velocity of the Clay. Based on the index properties of the Kaolin Clay (Table 5.1), four different samples of dry Kaolin was repeatedly mixed with water to achieve three different levels of moisture content: 24% (significantly below the OWC), 28% (the OWC), 33% (significantly above the OWC), and a repeat test at 28%. The 3 different moisture contents were considered to provide a good range of moisture content for the test results. To prove the repeatability of the test procedure, one of these 3 moisture content (the OWC) was chosen for repeat testing. Weights of 75kg, 76kg, 80kg and 75 kg of Kaolin were mixed using 18.0kg, 21.3kg, 26.4kg and 21.0kg of water respectively. Each Kaolin sample was mixed with water using a large mixer for half an hour. After pouring the mixture to achieve successive layers of 50mm thickness into the plastic box, each layer was then compacted using a vibrator. Every 100mm, three standard thin-walled tubes were used to collect samples from each compacted layer to measure the density of the layer to make sure that all parts of the sample had the same density. These tubes were knocked into the compacted layer surface at three different points, and then the size and weight of the three cylindrical soil samples were measured to calculate the density. The process is shown in Figure 5.2 and the results are indicated in Table 5.2. It was not possible to refill the holes with the same sample as the samples needed to be placed in the oven to calculate the moisture content, needed to obtain the density. So the same mixture was used to fill the holes and compacted by using the vibrator at the same time with the same energy; in this way the replaced material was considered to have the same density to a good approximation. This process continued until the final layer was constructed. In order to ensure good contact for the next Clay filled layer, the Clay surface was grooved to avoid a plane of weakness between the layers (i.e. stratification).

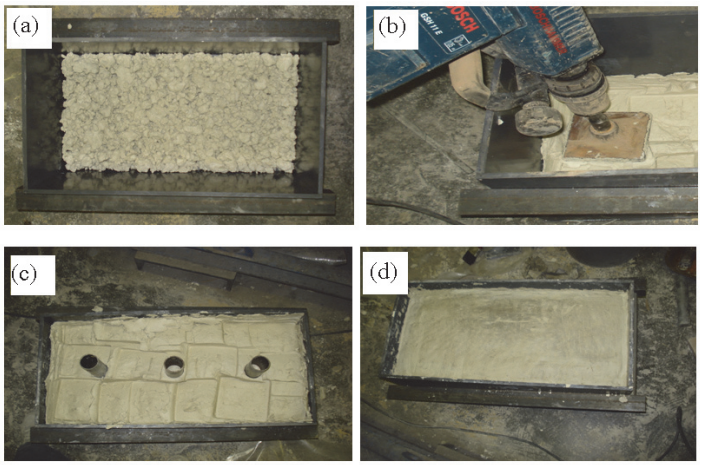

Figure 5.2: (a) Mixed Kaolin Clay ready to be compacted with a vibrator, (b) wooden plates used to smooth the surface of Clay layer, (c) tubes in place to retrieve samples for density testing, and (d) final Kaolin Clay bed test

Table 5.2: Results for the density measurement for each layer during the preparation of the Kaolin Clay test bed for different moisture contents

Clay type	Moisture content %	Compounds	Layers	Density (kg/m^3)	Averaged density of each layer	Bulk density, kg/m^3	Dry density, kg/m^3
Kaolin Clay	24%	Clay: 75 kg Water: 18.0 kg	1	1365	1359	1750	1380
			2	1360			
			3	1352			
	28%	Clay: 76 kg Water: 21.3 kg	1	1498	1495	2260	1410
			2	1502			
			3	1485			
	33%	Clay: 80 kg Water: 26.4 kg	1	1506	1488	2110	1340
			2	1480			
			3	1478			
	28%	Clay: 75 kg Water: 21.0 kg	1	1472	1446	2260	1410
			2	1430			
			3	1438			

5.4 Preparation of the Oxford Clay Test Bed

The index properties of the Oxford Clay are given in Table 5.1. Oxford Clay and water were repeatedly mixed to obtain different moisture contents of: 19%, 24%, 32% and a repeat test at 32%, again to provide a spread significantly above and below the OWC and to provide a

sample to test for repeatability. Oxford Clay with weights of 79.1kg, 83.7kg, 80.0kg and 73.0kg was mixed using 15.2kg, 20.0kg, 24.0kg and 23.4kg of water respectively. For each Oxford Clay-water mixture, a process similar to that using Kaolin Clay was carried out. Results for the density measurement for each layer during the preparation of the Oxford Clay Test bed are shown in Table 5.3. Figure 5.3 shows the compaction and density measurement procedures for the Oxford Clay test bed.

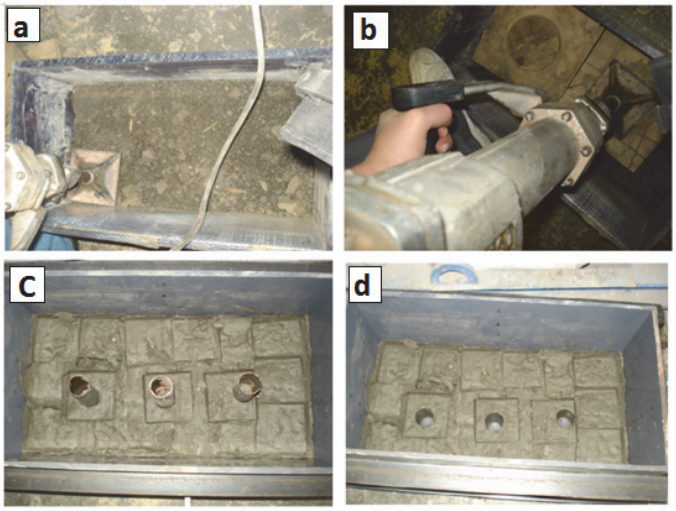

Figure 5.3: (a) Compacting Oxford Clay with a vibrator, (b) wooden plates used to smooth the surface of Clay layer, (c) and (d) thin walled tubes used to collect sample to measure the density of the Clay layer.

Table 5.3: Results for the density measurement for each layer during the preparation of the Oxford Clay Test bed for different moisture contents

Clay type	Moisture content %	Compounds	Layers	Density (kg/m^3)	Averaged density of each layer	Bulk density, kg/m^3	Dry density, kg/m^3
Oxford Clay	19%	Clay: 79.1 kg Water: 15.2 kg	1	1380	1423	1870	1500
			2	1402			
			3	1488			
	24%	Clay: 83.7 kg Water: 20.0 kg	1	1602	1606	1820	1550
			2	1620			

			3	1598			
	32%	Clay: 80.0 kg Water: 24.0 kg	1	1410	1396	1740	1370
			2	1415			
			3	1364			
	32%	Clay: 73.0 kg Water: 23.4 kg	1	1421	1411	1740	1370
			2	1394			
			3	1445			

5.5 Preparation of the Test Bed

After the initial tests including index properties (plastic limit test, Liquid limit test, and Plasticity index), compaction tests (optimum moisture content, Maximum dry density, Bulk density) and Specific gravity. The dimensions of the main test arrangement dictated which technique is most efficient in developing the correct seismic wave to investigate how soil properties influence acoustic wave transmission this is commented upon in subsequent sections of this study. Figure 5.4 shows that an impervious plastic sheet was used to wrap the top Clay in order to limit evaporation of water from the test specimens.

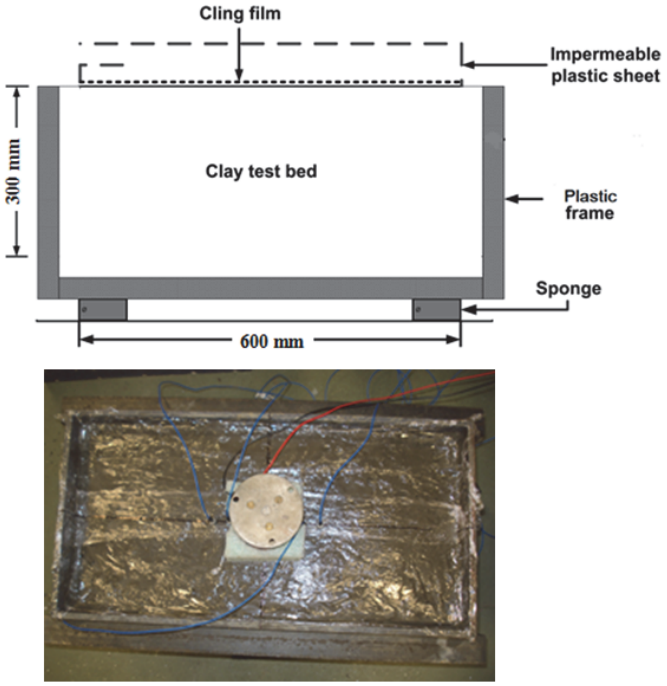

Figure 5.4: Plastic box used for the test bed

As explained before, for each kind of Clays, Kaolin and Oxford Clays, four different moisture contents ,(one is repeated) were used, one at the Optimum moisture content and two others were less and one more than the optimum moisture content, were selected to prepare four test beds for each of them.

Table 5.4 shows the averaged geotechnical data for the test beds.

Table 5.4: Data for Kaolin Clay and Oxford Clay

Kaolin Clay	Water content %	Bulk density, kg/m³	Dry density, kg/m³
1	24%	1750	1380
2	28%	2260	1410
3	33%	2110	1340
Oxford Clay			
1	19%	1870	1500
2	24%	1820	1550
3	32%	1740	1370

5.6 Seismic Test

Figures 5.4 and 5.5 shows the seismic test laboratory setup with the seismic source at the middle of the sensor-pairs. The distance between the first receiver and the source, *d*, was

verified by trial-and-error experimentation to achieve both a suitable distance between the source and the first receiver and the receivers' spacing, Δx. The values of d and Δx were chosen so that higher coherence values (>0.9) were achieved for a large frequency range.

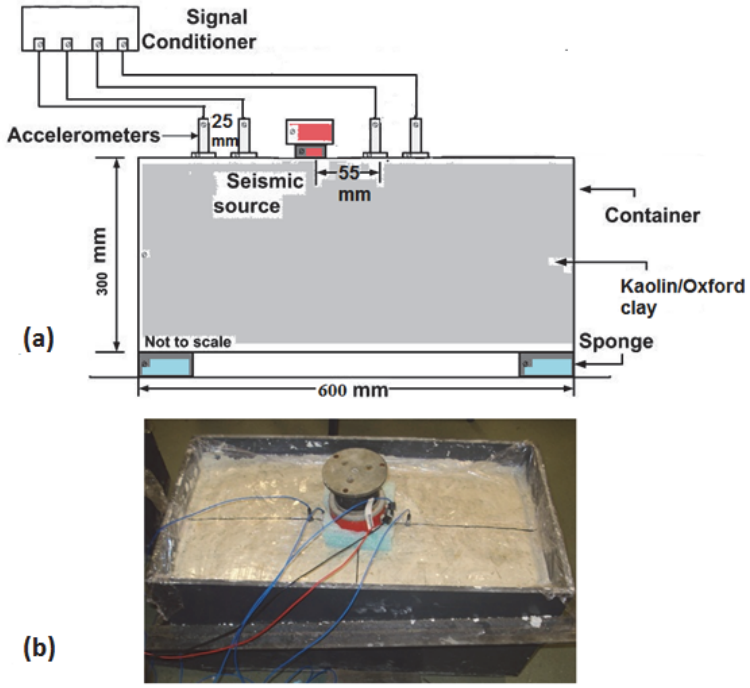

Figure 5.5: (a) Illustration of the laboratory-scaled model and equipment setup, and (b) photo of the Kaolin model with the seismic source located in the middle.

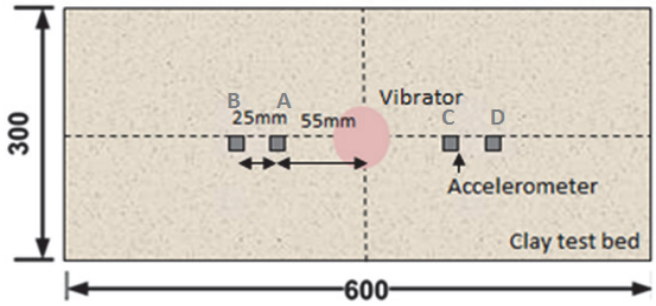

Figure 5.5(b): Seismic source at the middle of the receiver sensor-pairs.

For the seismic test using homogeneous Clay, the receivers consisted of 4 piezoelectric accelerometers in a linear array with the seismic source placed in the middle of the array. Figure 5.5 a, and 5.5 b show a simple Illustration of the laboratory-scaled model and equipment setup and a photo of the Kaolin model with the seismic source located in the middle. The signal frequency for the surface excitation was scaled up due to the fact that the

laboratory model was scaled down. The distances between the source and the first receiver, *d*, was set as 55 mm and the receivers spacing, Δx, was 25 mm based on the trial tests, in order to have a higher signal-to-noise ratio.

As mentioned earlier, the surface wave was generated by a piezo-ceramic transducer with an electromechanical vibrator placed above it, creating a point energy source (see Figure 3.3). The piezo-ceramic transducer, which is a transducer that converts mechanical energy to electrical energy, was located on the sample and an electromechanical vibrator connected to an audio power amplifier was used to create mechanical energy; together they acted as a seismic source to generate the excitation signals. To ensure a good coupling contact between the accelerometer and the soil surface, nails were used to couple them, and the accelerometer was placed on top of a nail by using wax. Four receiver sensors, named A, B, C and D, were used in the configuration of the seismic test. The arrangement with the seismic source at the centre of the receiver-pairs, A-B and C-D, is shown in Figure 5.5.

The seismic tests will be discussed in detail in Chapter 6. For each test, the adopted frequency ranges for the seismic tests was different. These frequencies were chosen to avoid the near-far offset constraint as discussed in Chapters 3 and 4. The wavelengths fell within the range of *d/2* and *3d* based on Al-Hunaidi (1993), Matthews et al., (1996) and Park et al., (1999), which stated that $d_{min} > \lambda_{max}/3$ and $d_{max} < 2\lambda_{min}$; this corresponded to 27.5mm and 165.0 mm for a *d* of 55mm, where d is the distance between the first receiver and the source (using Equations 2.10 and 2.11). The normalised coherence was computed by obtaining repetitive measurements at every frequency.

Chapter 6

ANALYSIS

6.1 Introduction

In this chapter, the results of the experimental work are presented, analysed and discussed. Kaolin clay and Oxford Clay were used to develop the test bed and detailed test results of phase velocity measurements in a physical model of homogeneous Kaolin clay and Oxford Clay have been analysed.

6.2 Kaolin clay – 28% Moisture Content

A linear array of accelerometers consisting of 4 sensors and a seismic source at the middle of the array was used for testing of the Kaolin clay physical model. The excitation was initially done with a frequency range of 100Hz to 10,000Hz, using a stepped-frequency approach with a step-size of 100Hz. At each frequency step, a set of tests with a total of 5 snapshot measurements was obtained, both for averaging and to calculate the normalised coherence. The signal quality in terms of the signal-to-noise ratio showed a degradation when the frequency was less than 1500Hz, when it was between 4000Hz and 5000Hz and when it reached 9000 Hz. This is illustrated in Figure 6.1. Based on the results from Figure 6.1 and

based on the criterion used when choosing the frequencies, as discussed in Chapter 4, the frequency range of 1000Hz-9000Hz was selected initially to produce good quality results, while on closer inspection, as indicated in Figure 6.2, the final frequency range of 1500Hz-8000Hz was used for the seismic method, as indicated in Figure 6.3. The differences between the results from sensor pairs A-B and C-D was attributed to possible minor defects in the equipment, some unevenness of the sample surface and/or some difficulties coupling the piezo-ceramic accelerators to the soil surface.

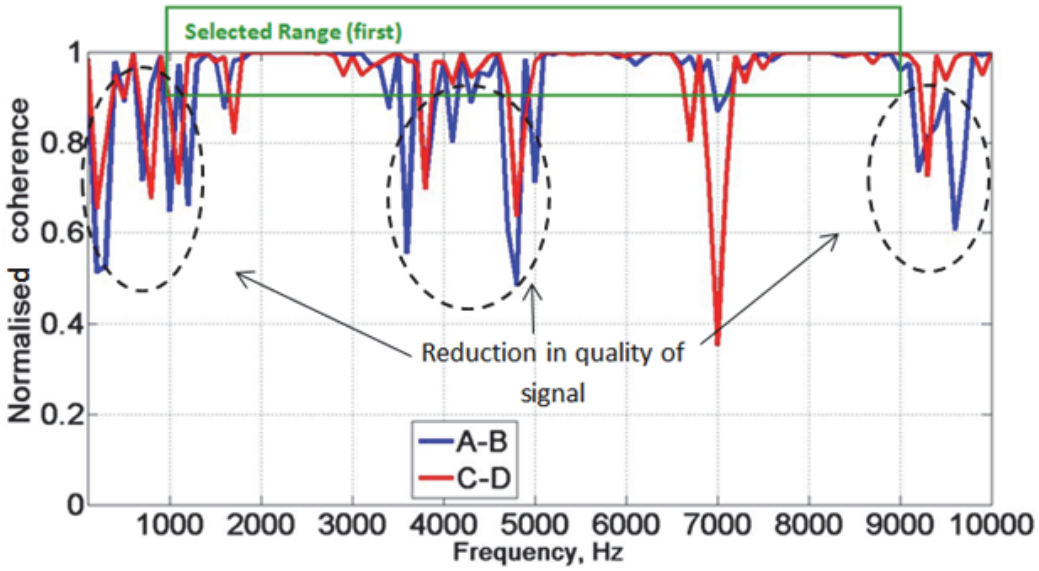

Figure 6.1: Normalised coherence for the 2 sensor-pairs for the Kaolin clay with a 28% moisture content, selected frequency range 100 Hz-10000Hz

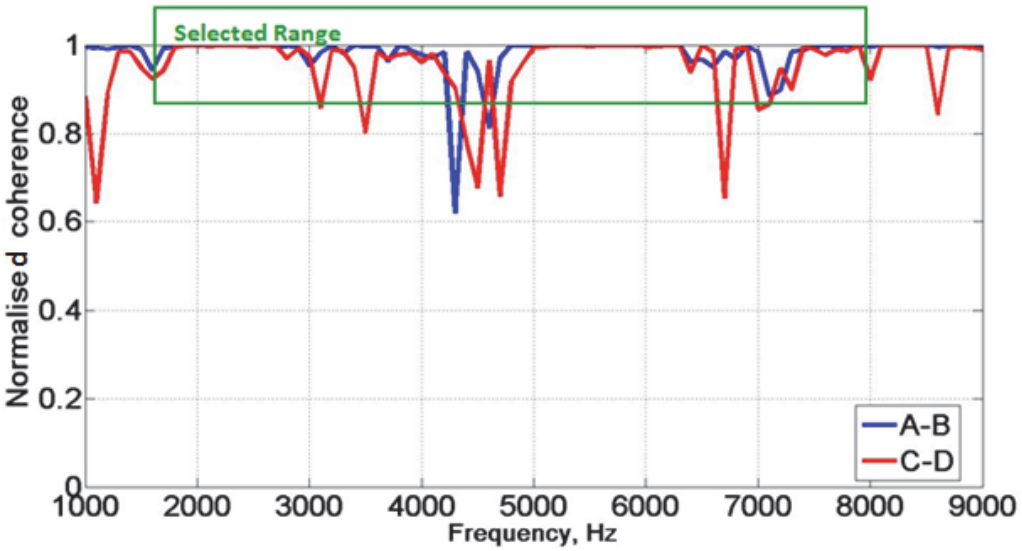

Figure 6.2: Normalised coherence for 2 sensor pairs for the Kaolin clay with a 28% moisture content, selected frequency range 1000Hz-9000Hz

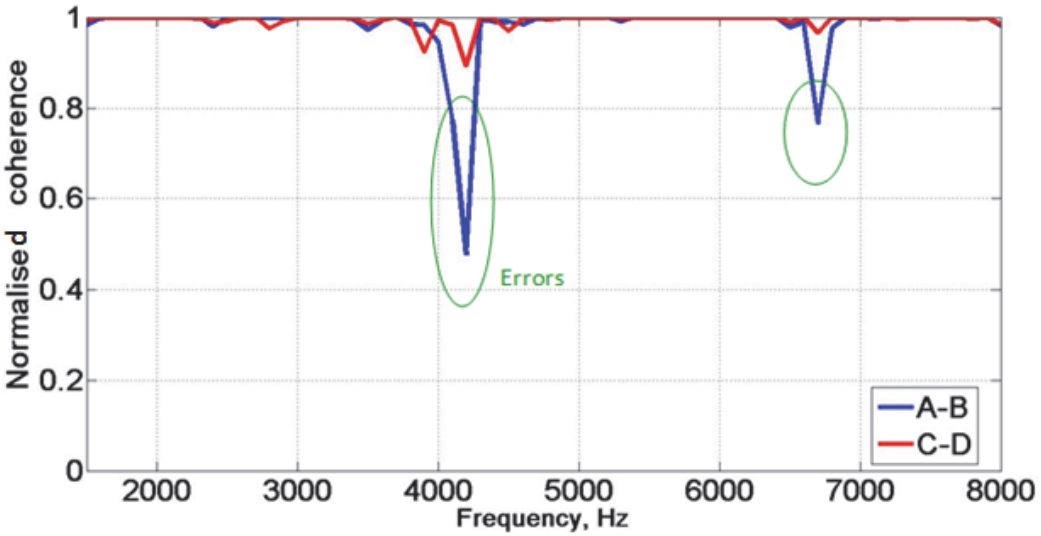

Figure 6.3: Normalised coherence for the selected frequency range for 2 sensor pairs for the Kaolin clay with a 28% moisture content, selected frequency range 1500Hz-8000Hz

The graph of frequency against unwrapped phase difference for all sensor pairs should show a perfect linear function relationship for a homogeneous material. The corrupted unwrapped phase measurement shown in Figure 6.4 indicates that sensor-pair C-D was the most disturbed. The distortion in the phase response was most likely due to attenuation due to a combination of the reasons stated above, i.e. defects in the equipment, unevenness of the sample surface and difficulties in coupling the piezo-ceramic accelerators to the soil surface.

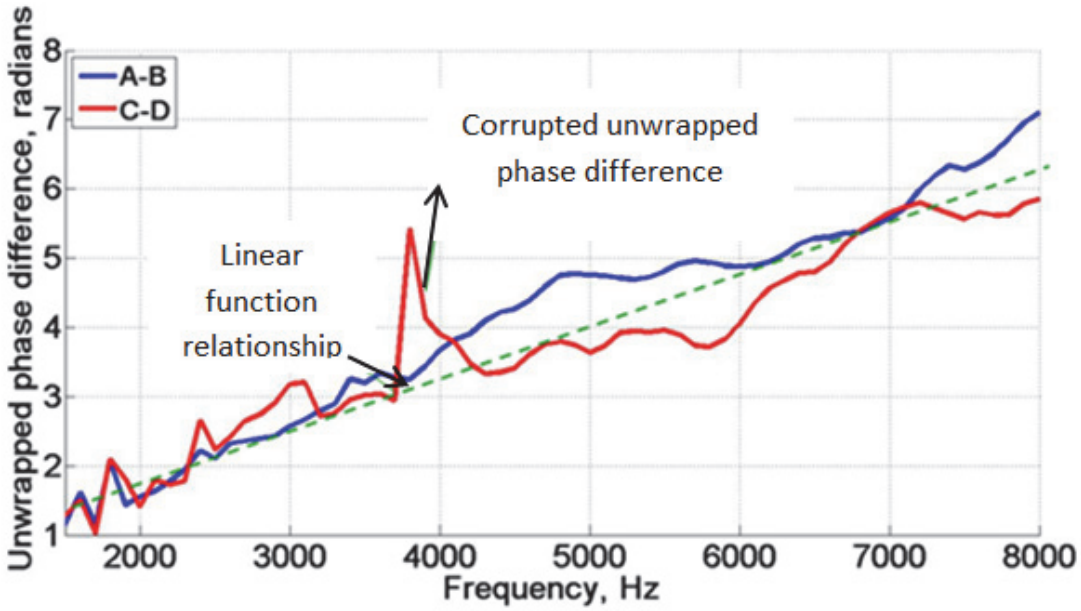

Figure 6.4: Unwrapped phase differences against frequency showing an almost linear function for the sensor pairs A-B and C-D for Kaolin clay with a 28% moisture content and a frequency range of 1500 Hz-8000Hz

The phase velocity was calculated for each frequency from the phase difference and the distance between the sensors (using Equation 3.6). The graph of the frequency versus phase velocity is shown in Figure 6.5, which indicates that the phase velocity range for the frequency range of 1500Hz-8000Hz is approximately 140 m/s to 250m/s for the Kaolin clay with a 28% moisture content.

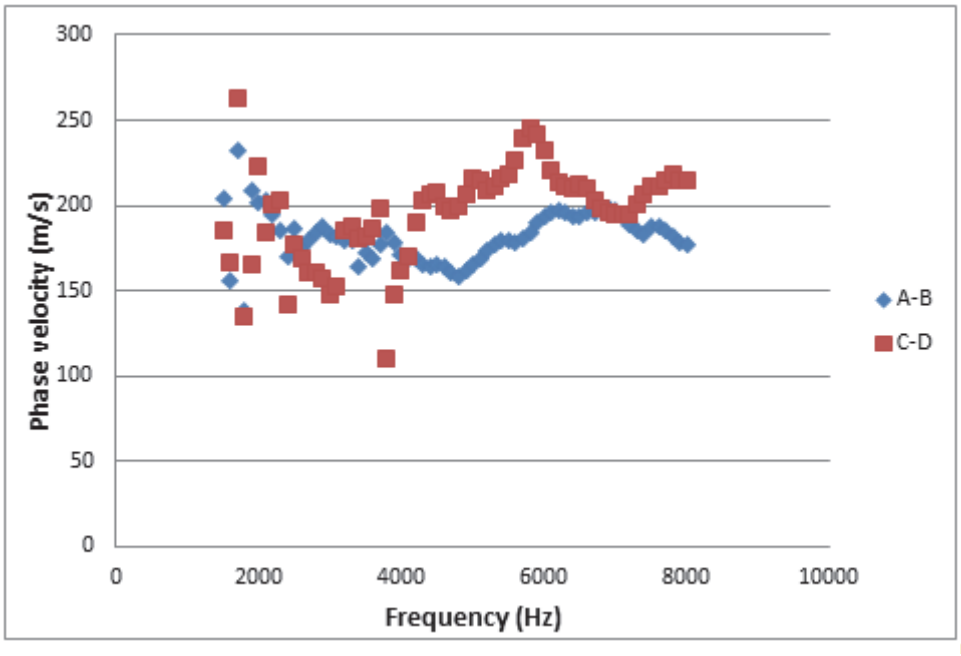

Figure 6.5: Phase velocity versus frequency showing the dispersive curve for Kaolin clay with a 28% moisture content and a frequency range of 1500Hz-8000Hz

The variation of the phase velocity with wavelength is shown in Figure 6.6. It shows that signals with small wavelengths, between 4 and 6 cm, tended to attenuate quicker, the majority of results falling between 170-230m/s approximately, than signals with larger wavelengths, between 6 cm and 16 cm, for which there are more results of phase velocity less than 170 m/s. The phase velocities deviation was thought not to be caused by the change of clay properties, but by the frequencies/wavelength constraint that influences the near- and far-offset distance of the source from the receivers, as well as some reflected waves from the boundary of the clay container (Madun, 2011).

This plot is important to evaluate the reliability of the phase velocity data, which in an ideal situation should be constant across a wide range of wavelengths for homogeneous clay. It is important to verify the reliability of the data not only on the basis of coherence threshold, but also on acceptable (i.e. approximately constant) range of phase velocity with changes in wavelengths.

To avoid a far-offset constraint, the wavelengths should be larger than 2.75 cm (using Equation 2.11), and to avoid the near-offset constraint, the wavelengths should be less than 16.50 cm (using Equation 2.10), hence the consideration in Figure 6.6 of the variation of average phase velocity versus wavelength between 2.75 and 16.50 cm.

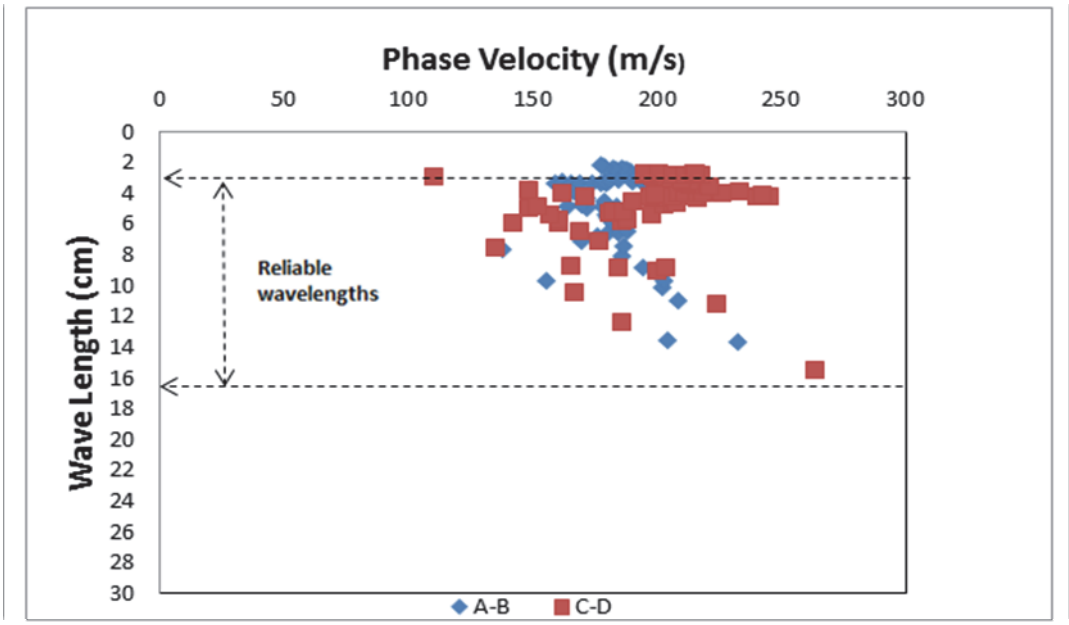

Figure 6.6: Wavelength versus phase velocity for Kaolin clay with a 28% moisture content. Variation of phase velocity with wavelength shows greater deviation of phase velocities for sensor pair C-D throughout the wavelength range of 2.75cm to 16.50 cm, corresponding to a frequency range 1500 Hz-8000Hz

It can be observed from Figure 6.5, that the velocities at frequencies lower than 3000 Hz had larger deviations from the averaged phase velocity than those between frequencies of 3000 Hz to 7000 Hz. It was reported by Zerwer *et al*. (2002) that the deviated phase velocities resulted from the unformed Rayleigh wave for wavelengths larger than half of the container's medium depth. It is worth noting that with a container depth of 300mm, these low frequency

distortions were likely to be caused by the small physical size of the clay container, in which significant noise from the boundary and bottom reflections occurred.

The C-D sensor-pair shows larger phase velocity deviations compared with the A-B sensor pair. This could be due to differences in the effectiveness with which these accelerometers were coupled to the surface, while generally large deviation could be due to insufficient energy exacerbated by interfering reflected waves from the boundary of the container. The phase velocities across the frequencies were not totally non-dispersive, thus suggesting that the Kaolin clay is not absolutely homogeneous due to experimental errors in the sample preparation and compaction of the sample.

The useful frequency ranges can be based on using Equations 2.10 and 2.11, and limitation of the maximum wavelength to half of the container depth. It is worth noting that the expectation is that the phase velocity in soft clay is 200 m/s (McDowell et al., 2002, and Parasnis, 1997).

6.2.1 Repeatability of the Tests - Kaolin clay

In order to test the repeatability of the experiments, a second test using Kaolin clay with a moisture content of a 28% was carried out. For this, the test tank was emptied and a new batch of clay was mixed, and placed and compacted in the test bed as described before. This test was designed to demonstrate that the measurement system can give reliable results of phase velocities and shear parameters (which are presented and discussed in Chapter 7). Figures 6.7 and 6.8 indicate the results for Kaolin clay with a 28% moisture content as a repeated test.

In previous test, the acceptable frequency range was 1500Hz-8000Hz based on a coherence threshold of 0.9. Figure 6.7 indicates a slightly improved signal with fewer signal quality reduction compared to the results in Figure 6.1. This could be related to the process of sample preparation, compaction procedure and better coupling of the accelometers to the surface.

Figure 6.8 confirms this finding since the most appropriate frequency range is again 1500Hz to 8000Hz with only one frequency (~7000Hz) where the normalised coherence is very low. Comparing Figures 6.7 and 6.8, there is a second region around 3800Hz where normalised coherence is also lower than the general trend.

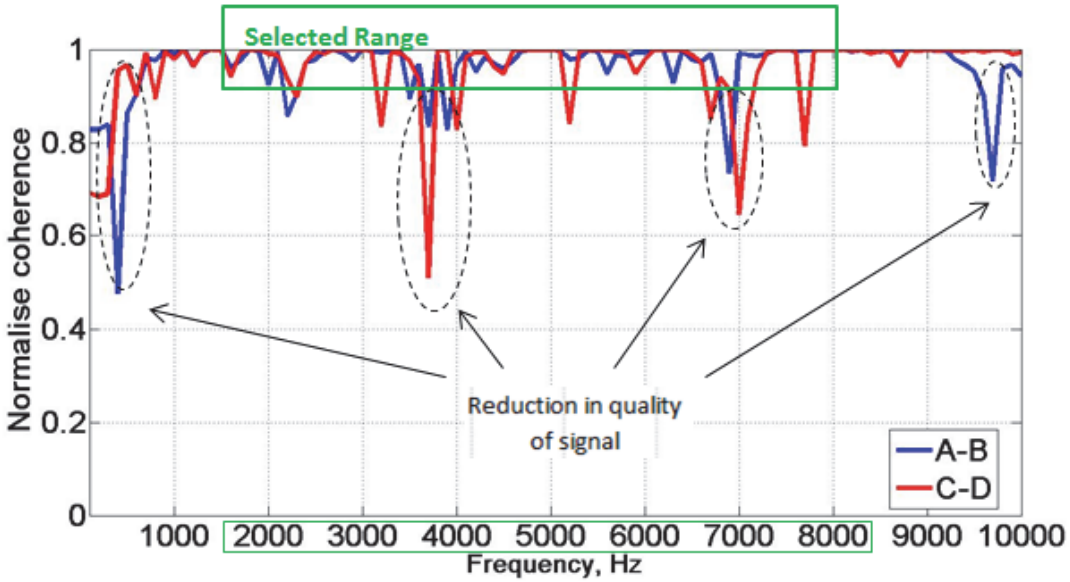

Figure 6.7: Normalised coherence for 2 sensor pairs for the Kaolin clay with a 28% moisture content (repeated test); selected frequency range 100Hz-10000.

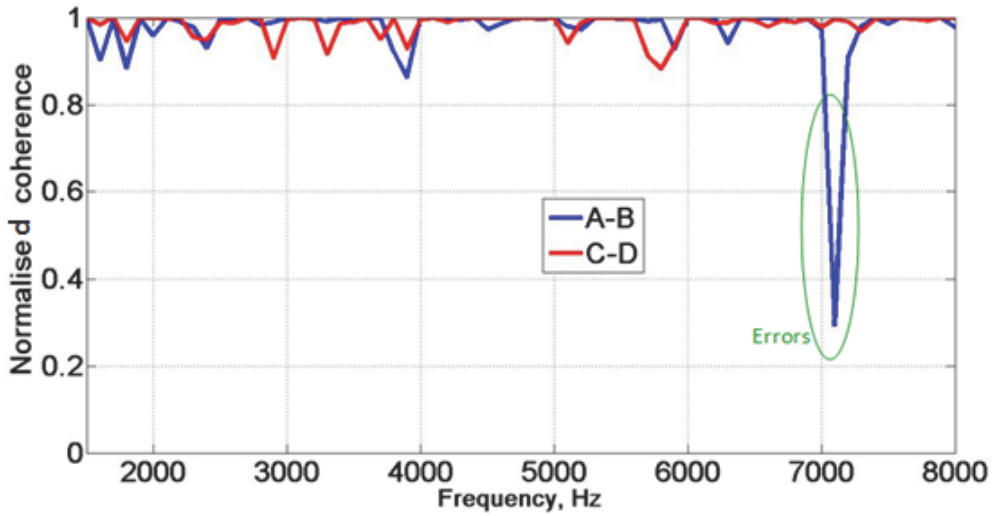

Figure 6.8: Normalised coherence for selected frequency range for 2 sensor pairs for the Kaolin clay with a 28% moisture content (repeated test); selected frequency range 1500Hz-8000Hz

Figure 6.9 shows the unwrapped phase difference versus frequency. The linear plots shows a deviation beyond frequency 5000Hz for both sensor pairs, but in contrast to the results obtained for the first test (Figure 6.4) it looks less corrupted.

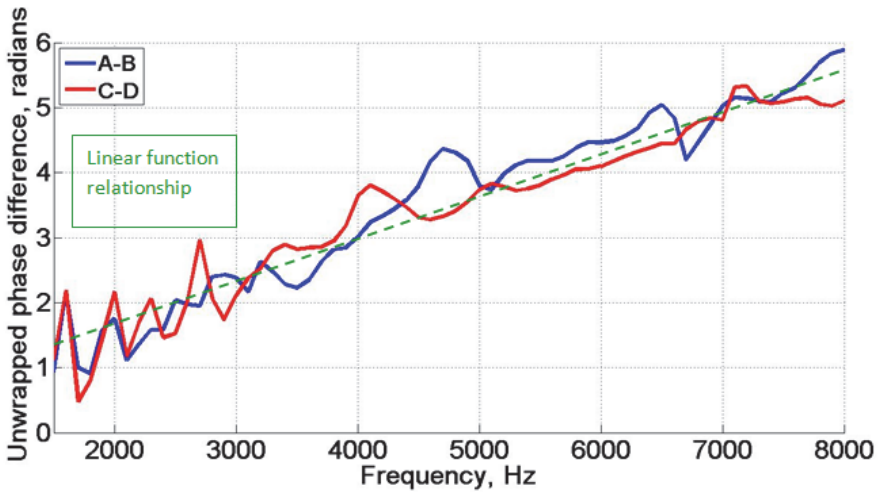

Figure 6.9: Unwrapped phase differences against frequency showing a linear function for A-B and C-D sensor pairs for Kaolin clay with a 28% moisture content (repeated test); selected frequency range 1500Hz-8000Hz

From the phase difference and distance between the sensors, the phase velocity can be calculated for each frequency as shown in Figure 6.10, which shows that the phase velocity

range for the frequency range of 1500Hz-8000Hz is approximately 120m/s to 230m/s for the Kaolin clay with a 28% moisture content. As shown in Figure 6.11, this range of phase velocity measurements is similar to the main test for Kaolin clay with a 28% moisture content.

Figure 6.12 shows the variation of the phase velocity with wavelength. For this test, the range of reliable wavelength is slightly larger than for the first test. Nevertheless the differences are small so that it can be assumed that the test is repeatable and the results reliable.

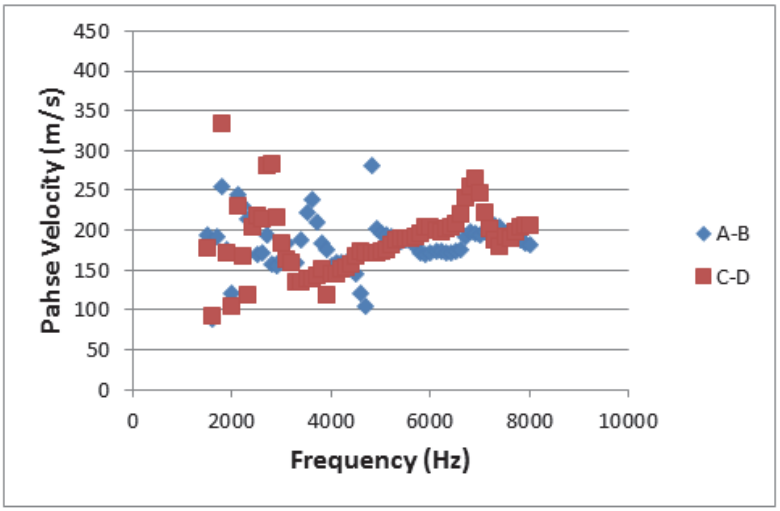

Figure 6.10: Phase velocity versus frequency showing the dispersive curve for the Kaolin clay with a 28% moisture content (repeated test); the frequency range was 1500Hz-8000Hz

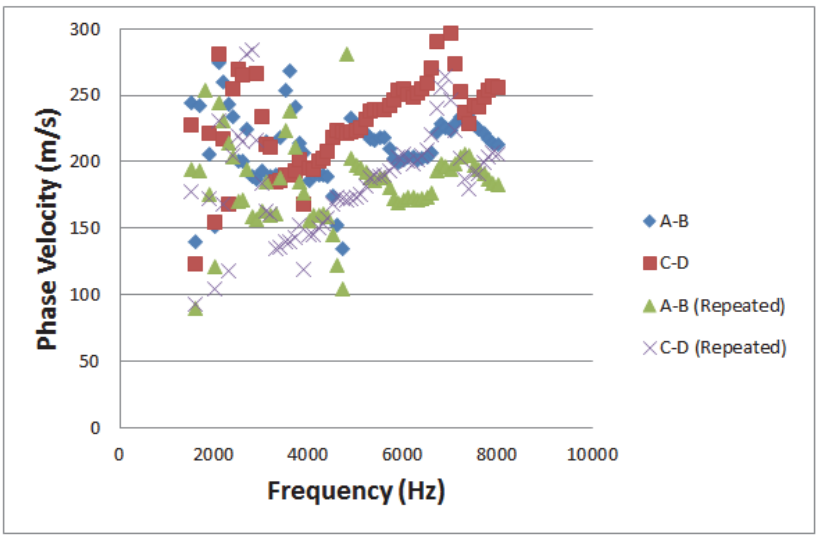

Figure 6.11: Phase velocity versus frequency showing the dispersive curve for the Kaolin clay with a 28% moisture content for main test and the repeated test; the frequency range was 1500Hz-8000Hz

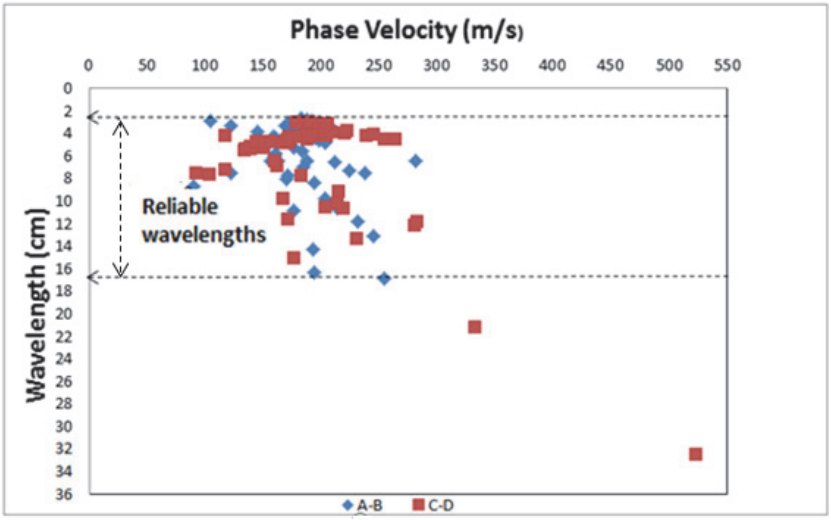

Figure 6.12: Wavelength versus phase velocity for Kaolin clay with a 28% moisture content (repeated test) for wavelengths between 2.75 and 16.50 cm; the frequency range was 1500Hz-8000Hz

6.2.2 Kaolin Clay, 24% and 33% Moisture Content

For Kaolin clay with a 24% moisture content, the excitation was initially done with a frequency range of 100Hz to 10000 Hz. The signal quality in terms of the signal-to-noise ratio showed degradation when the frequency was less than 3000Hz and above 6000Hz. This is illustrated in Figure 6.13.

Based on the results from Figure 6.13 the frequency range of 3000Hz-6000Hz was selected to provide good quality results and on closer inspection this was confirmed in Figure 6.14 .

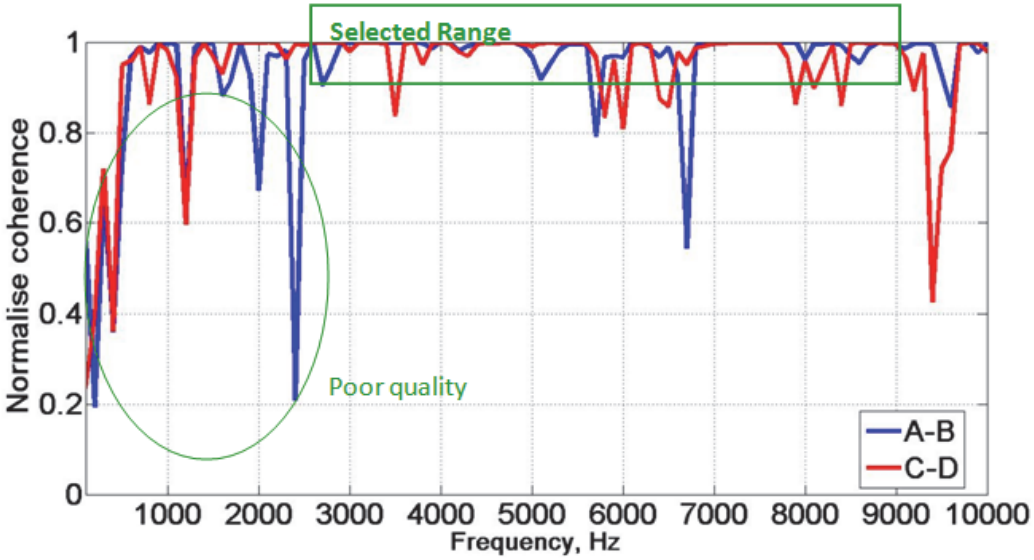

Figure 6.13: Normalised coherence for 2 sensor pairs for Kaolin clay with a 24% moisture content; selected frequency range 100Hz-10000Hz

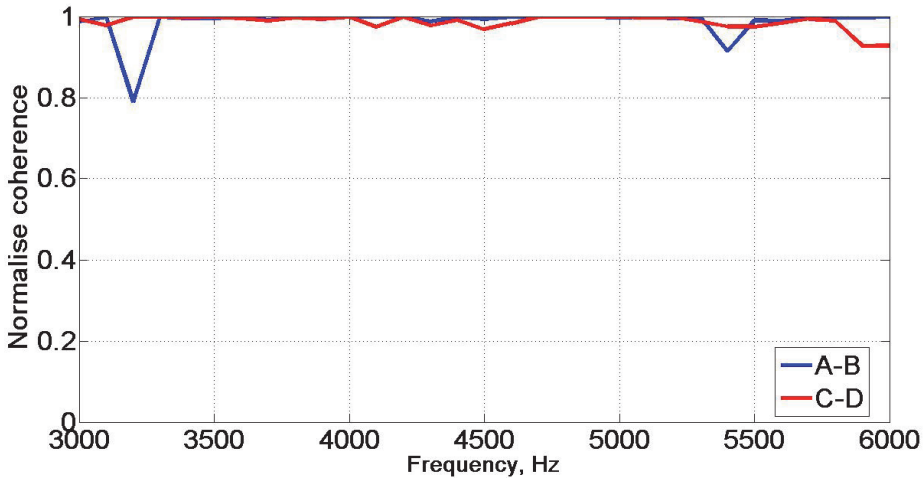

Figure 6.14: Normalised coherence for selected frequency range for 2 sensor pairs for the Kaolin clay with a 24% moisture content; selected frequency range 3000Hz-6000Hz

Figure 6.15 shows the unwrapped phase difference versus frequency. The linear plots show a deviation beyond frequency 4000Hz and above 5000Hz for both sensor pairs.

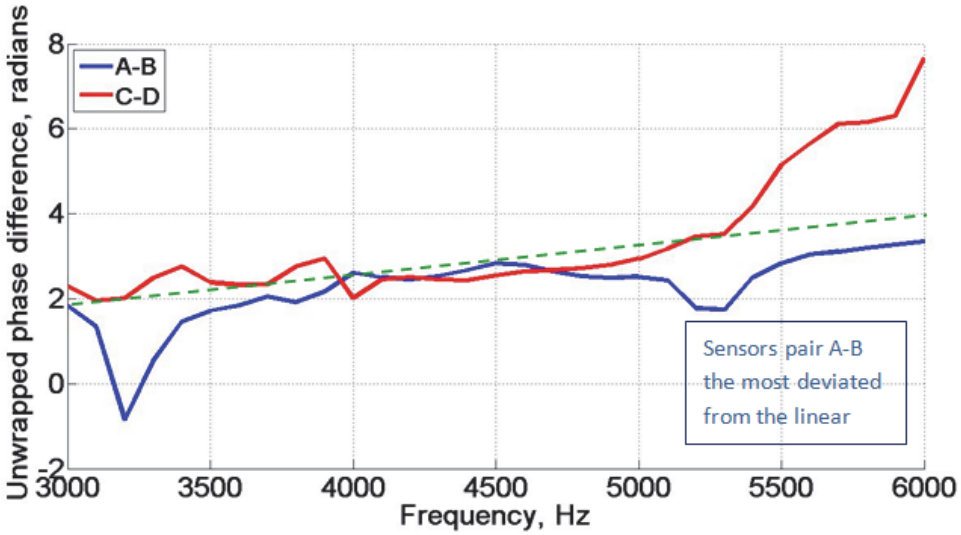

Figure 6.15: Unwrapped phase differences show linear function for A-B and C-D sensor pairs for Kaolin clay with a 24% moisture content; the frequency range was 3000Hz-6000Hz

As explained previously the phase velocity can be calculated from the phase difference and distance between the sensors, for each frequency. This is plotted in Figure 6.16, which shows that the phase velocity range for the frequency range of 3000Hz-6000Hz is approximately 200m/s to 300m/s for the Kaolin clay with a 24% moisture content. This is larger than the phase velocity range for Kaolin clay with a 28% moisture content.

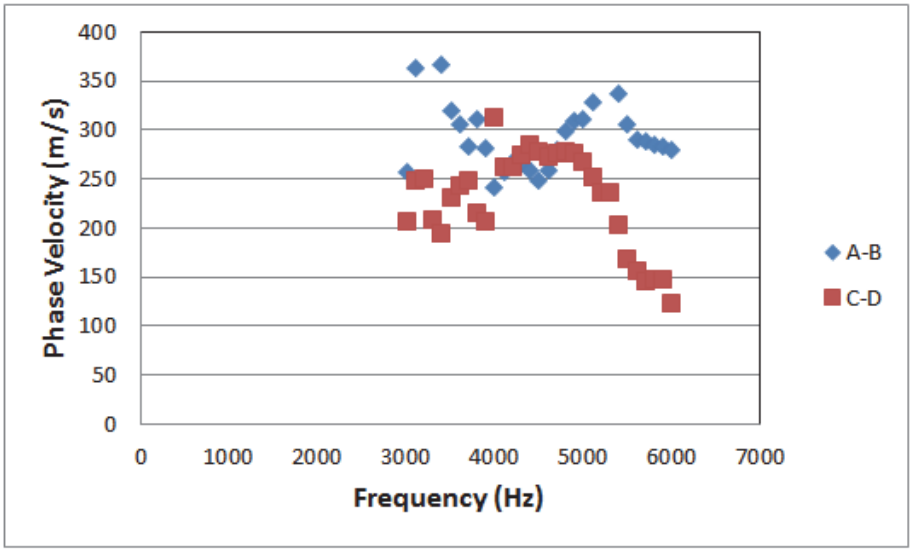

Figure 6.16: Phase velocity versus frequency showing dispersive curve for the Kaolin clay with a 24% moisture content; the frequency range was 3000Hz-6000Hz

Figure 6.17 shows the variation of the phase velocity with wavelength for the Kaolin clay with a 24% moisture content.

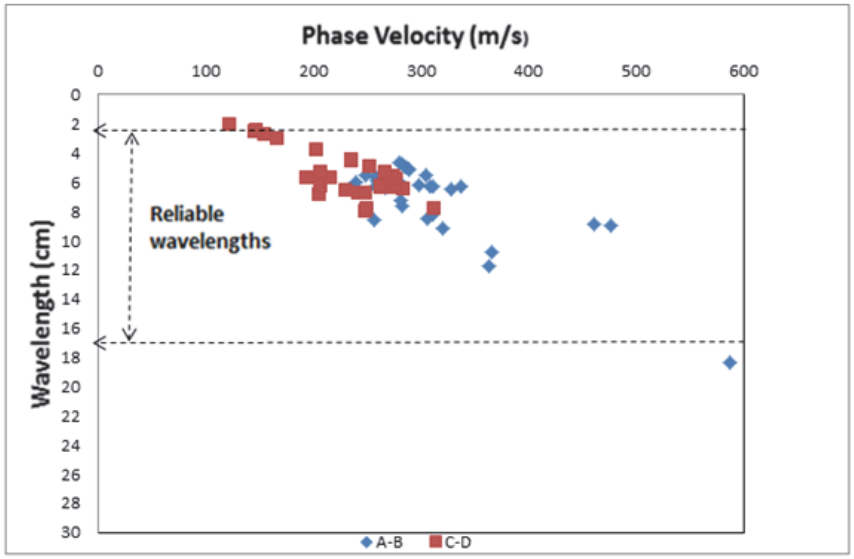

Figure 6.17: Wavelength versus phase velocity for Kaolin clay with a 24% moisture content for wavelengths between 2.75 and 16.50 cm; the frequency range was 3000Hz-6000Hz

For Kaolin clay with a 33% moisture content, the excitation was initially done with a frequency range of 100Hz to 10000 Hz. The signal quality in terms of the signal-to-noise ratio showed degradation when the frequency was less than 1000Hz and when it goes above 4000 Hz. This is illustrated in Figure 6.18.

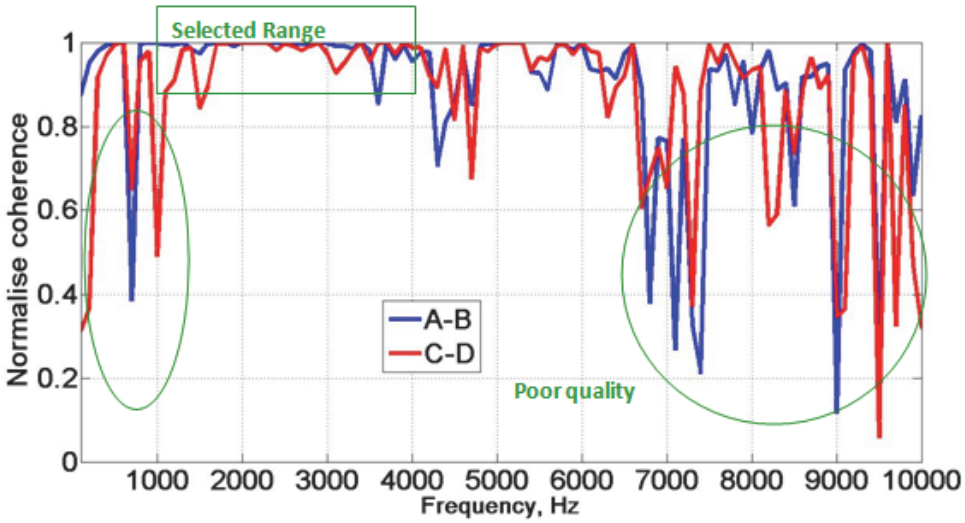

Figure 6.18: Normalised coherence for 2 sensor pairs for Kaolin clay with a 33% moisture content; selected frequency range 100Hz-10000Hz

The frequency range of 1000Hz-4000Hz was selected to provide good quality results based on the results from Figure 6.18 and on closer inspection this was confirmed, see Figure 6.19.

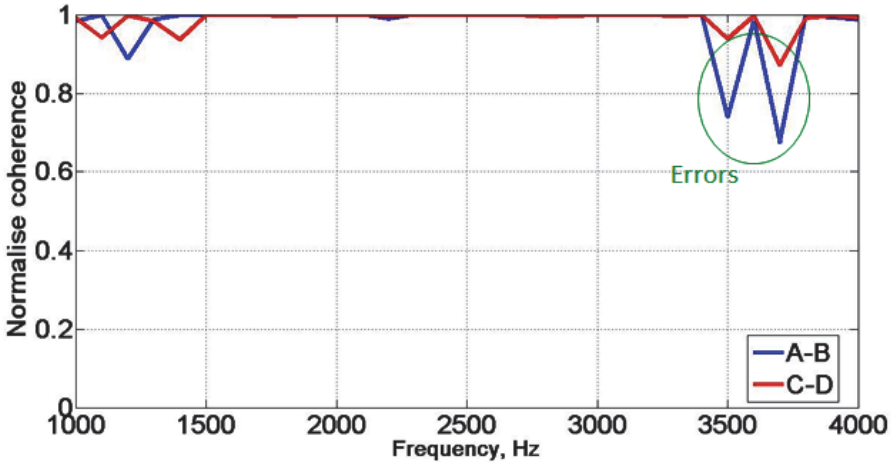

Figure 6.19: Normalised coherence for selected frequency range for 2 sensor pairs for the Kaolin clay with a 33% moisture content; selected frequency range 1000Hz-4000Hz

Figure 6.20, in which frequency is plotted against unwrapped phase difference for Kaolin clay with a 33% moisture content, shows a perfectly linear function relationship for sensor pairs A-B and C-D. This indicates a good quality sample and reflects the ability to create more consistent samples at higher water contents, i.e. compaction creates a more uniform sample when the moisture content is wet of the optimum moisture content, and better coupling of the

accelerometers to the surface. It also indicates that the preparation process and compaction procedure were appropriate, and that variation sample quality at lower moisture contents reflects the traditional problems in geotechnical physical modelling of compacting samples at lower moisture contents.

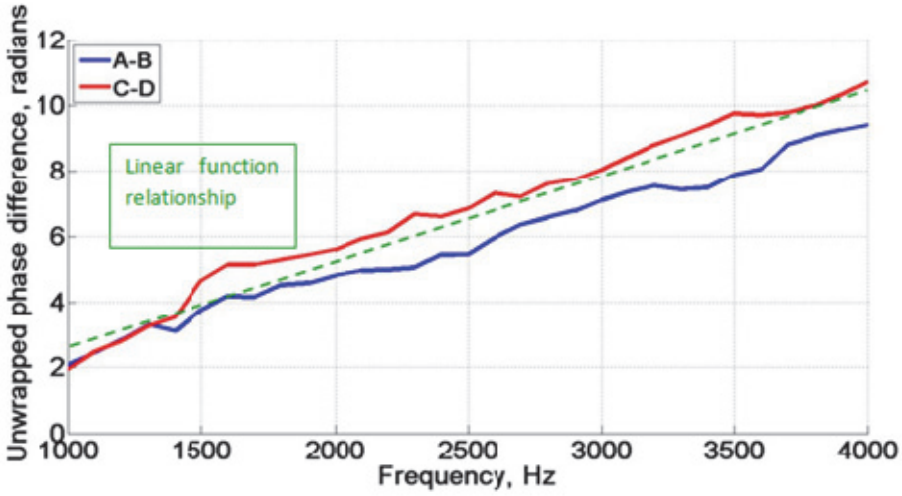

Figure 6.20: Unwrapped phase differences show linear function for A-B and C-D sensor pairs on for Kaolin clay with a 33% moisture content; the frequency range was 1000 Hz-4000Hz

The phase velocity versus frequency is shown in Figure 6.21 for Kaolin clay with a 33% moisture content. It shows that the phase velocity range for the frequency range of 1000Hz-4000Hz is approximately 50m/s to 70m/s, which is much less than phase velocity range for Kaolin clay with a 28% and a 24% moisture content.

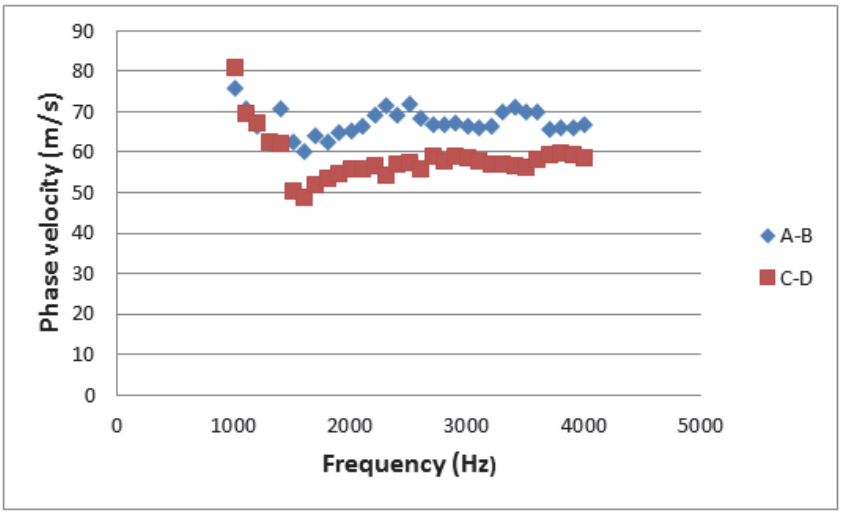

Figure 6.21: Phase velocity versus frequency showing dispersive curve for the Kaolin clay with a 33% moisture content (the dominant phase velocity range is 50m/s-70m/s); the frequency range was 1000Hz-4000Hz

Figure 6.22 shows the variation of the phase velocity with wavelength for the Kaolin clay with a 33% moisture content and again indicates better quality (i.e. more consistent) data than Kaolin clay with 28% and 24% moisture content.

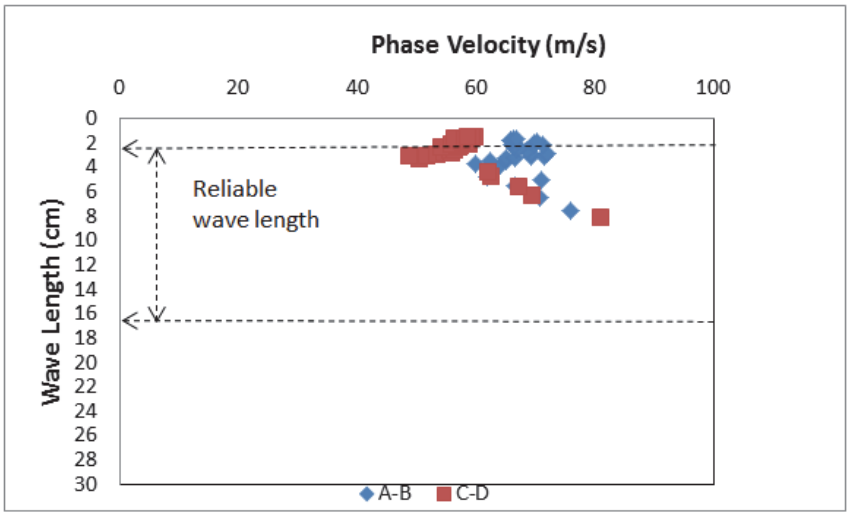

Figure 6.22: Wavelength versus phase velocity for Kaolin clay with a 33% moisture content for wavelengths between 2.75 and 16.50 cm; the frequency range was 1000Hz-4000Hz

As discussed previously, the primary differences between the results from sensor pairs A-B and C-D were attributed to difficulties in coupling the accelerometers (i.e. receivers) to the soil surface, thus exacerbating the frequencies/wavelength constraint that influences the near

and far-offset distance of the source from the receivers, as well as some reflected waves from the boundary of the clay container.

6.3 Homogeneous Oxford Clay – 32% Moisture Content

A second set of tests was carried out using Oxford Clay. The test set-up was identical to the one used for Kaolin clay, with the same dimensions of the container and arrangements of the acoustic sensors.

The signal quality in terms of the signal-to-noise ratio is shown in the normalised coherence plot for different arrays in Figure 6.23. It shows a degradation when the frequency is less than 1000Hz and more than 5000Hz and a better signal quality between these frequencies. As sensor-pairs were placed at a similar distance from the seismic source, an approximately similar normalised coherence relationship, as a function of frequency, was observed. Figure 6.23 shows in particular that the near offset constraint for the lower frequency (below 10000 Hz) and the far offset constraint (above 5000 Hz) had lower coherence values (Equation 2.10 and 2.11).

Based on the results from Figure 6.23 and based on the criterion of choosing the suitable frequencies as discussed in Chapters 3 and 4, a frequency range of 1000Hz-5000Hz has been selected as shown in Figure 6.24.

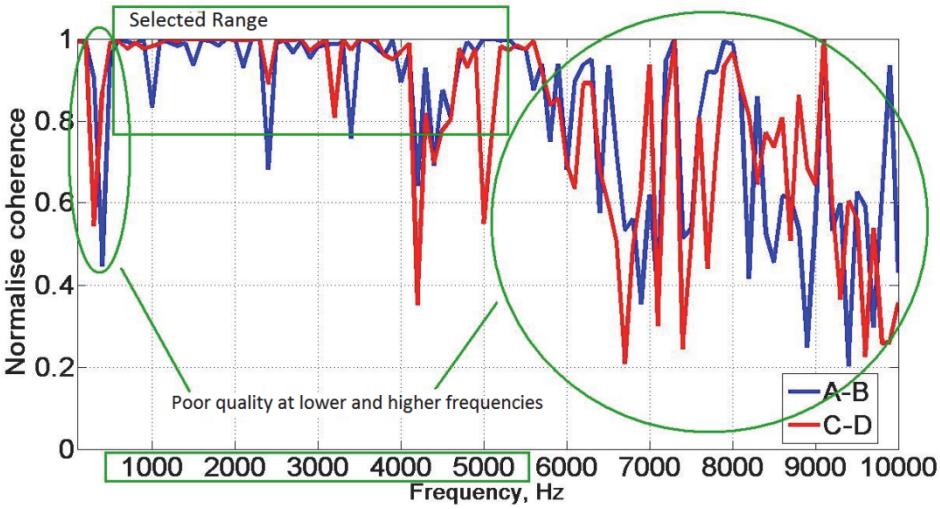

Figure 6.23: Typical coherence in the seismic wave testing for the Oxford Clay model with a 32% moisture content; selected frequency range 100Hz-10000Hz

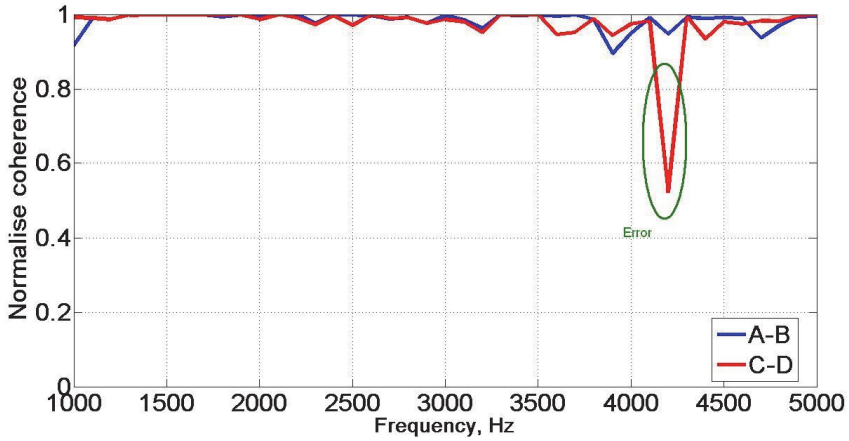

Figure 6.24: Normalised coherence for selected frequency range for 2 sensor pairs for the Oxford Clay with a 32% moisture content; selected frequency range 1000Hz-5000Hz

In general, the unwrapped phase difference as shown in Figure 6.25 should be a linear function. The plots indicate a larger deviation beyond the frequency of 3500 Hz for sensor pair C-D due to a reduction of signal quality.

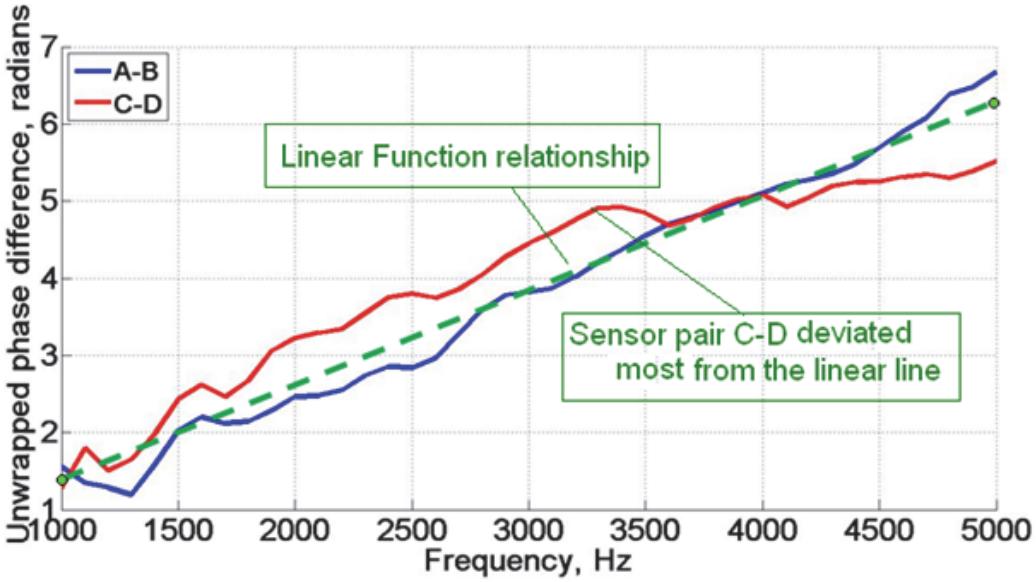

Figure 6.25: Unwrapped phase differences show and approximately linear function for A-B and C-D sensor pairs for the Oxford Clay with a 32% moisture content for a frequency range of 1000Hz-5000Hz

Figure 6.26 shows a typical phase dispersion plot for one set of tests indicating that the phase velocities are relatively consistent for frequencies between 1500Hz and 5000Hz. Uncommon clay phase velocities were observed for frequencies below 1500Hz, which was likely caused by the Rayleigh-waves being dominated by body waves and boundary reflections from a longer wavelength. It indicates that the phase velocity range for the frequency range of 1500Hz-5000Hz is approximately 100m/s to 150m/s for Oxford Clay with a 32% moisture content. Moreover based on these observations, phase velocities were reliable (i.e. close to the mean value of phase velocity) when the data comply with the frequency or wavelength requirement, even though the data have a low coherence threshold (0.9). It is worth to underline that the measured values of phase wave velocities agree with typical values reported in literature. MAdun et al., (2012), range phase wave velocity from 100 to 200 m/s.

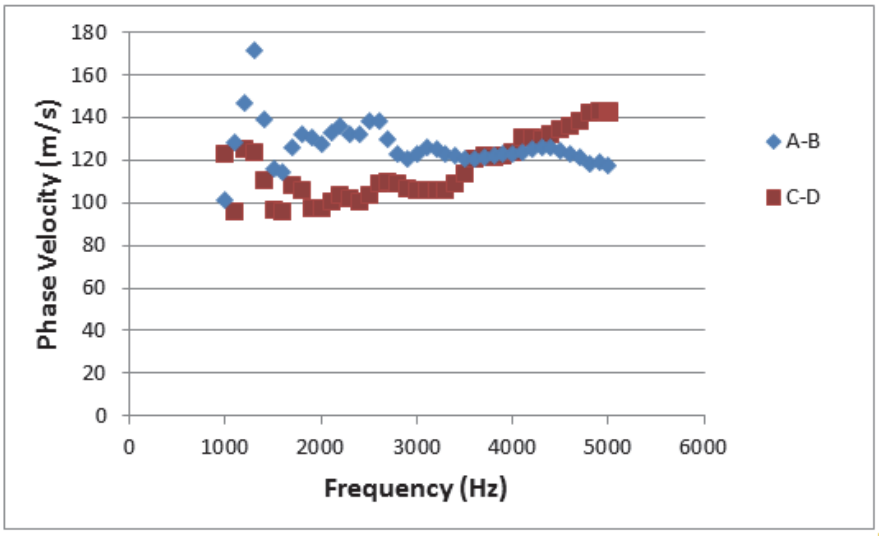

Figure 6.26: Phase velocity versus frequency showing the dispersive curve for the Oxford Clay with a 32% moisture content; the frequency range was1000Hz-5000Hz

As mentioned earlier, there are two possible arrangements of seismic source and sensor-receivers, namely seismic source at the one end of the array and seismic source at the middle of the sensor-pairs. Based on the work of Madun (2011), in cases where the seismic source is located at the middle of the array the source-receiver achieved higher signal-to-noise ratios because both pairs of receivers are located closed to seismic source, there is a better correlation of unwrapped phase difference between sensor-pairs and also observation of small standard deviations demonstrates that this is an optimal arrangement for array deployment to carry out the seismic surface wave test. This arrangement was therefore used in the test programme.

In the case where the source was set in the middle of the array, the expected useful frequencies for sensor pairs A-B and C-D were from 900Hz to 5400Hz based on calculations using Equations 2.10 and 2.11. This is in agreement with the selected frequency range obtained by trial and error in the first step of the test procedure.

Figure 6.27 is a plot of all data with no constraint on the coherence threshold. As was mentioned before, this plot is important to evaluate the reliability of the phase velocity. To avoid the far-offset constraint, the wavelengths should be larger than 2.75 cm (using Equation 2.11), and to avoid near-offset constraint the wavelengths should be below than 16.50 cm (using Equation 2.10). Using these constraints the variation of average phase velocity versus wavelength indicates a range of phase velocities between 100m/s and 150m/s.

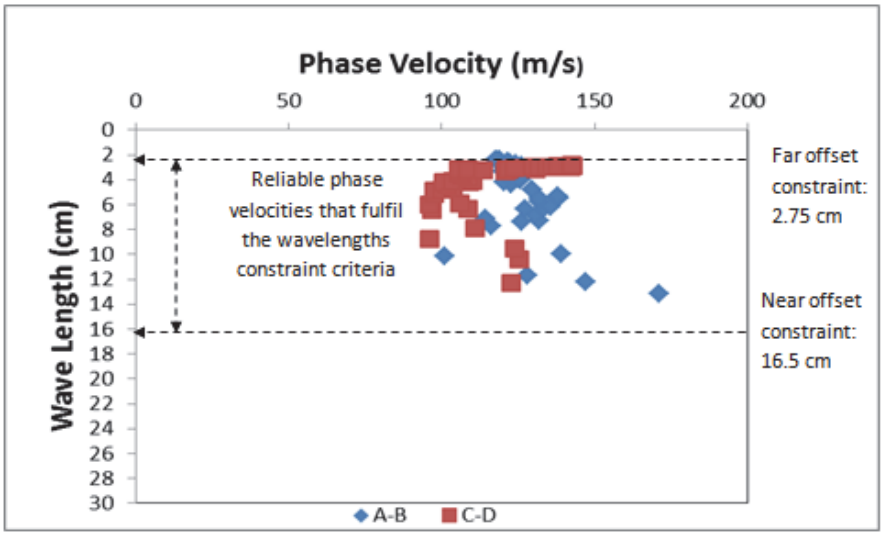

Figure 6.27: Wavelength versus phase velocity for Oxford clay with a 32% moisture content for wavelengths of 2.75cm to 16.50 cm, corresponding to a frequency range of 1000 Hz-5000Hz

This homogeneous soft clay is considered to have a constant phase velocity across its depth due to its relatively uniform density profile both laterally and vertically (with depth) and the phase velocities are therefore considered reliable. The phase velocities were converted into shear wave velocities using Equation 3.9 (V_s(shear wave)=1.047.V_r(Rayleigh wave)) based upon a Poisson's ratio of 0.5 for the clay.

6.3.1 Repeatability of the tests - Oxford Clay

In order to test the repeatability of the experiments (i.e. to demonstrate that the measurement system can give reliable results of phase velocities), a repeat test using Oxford Clay with a moisture content of 32% was carried out using the same procedure as the first test for Oxford

Clay. As for the Kaolin clay repeat test, the plastic box was emptied and a new sample of clay was mixed, and placed and compacted in the test bed. Figures 6.28 and 6.29 show the results for Oxford Clay with a 32% moisture content as a repeated test. In the first test, the acceptable frequency range was 1000Hz-5000Hz based on a coherence threshold of 0.9. Figure 6.28 indicates a slightly improved signal compared to the results in Figure 6.23.

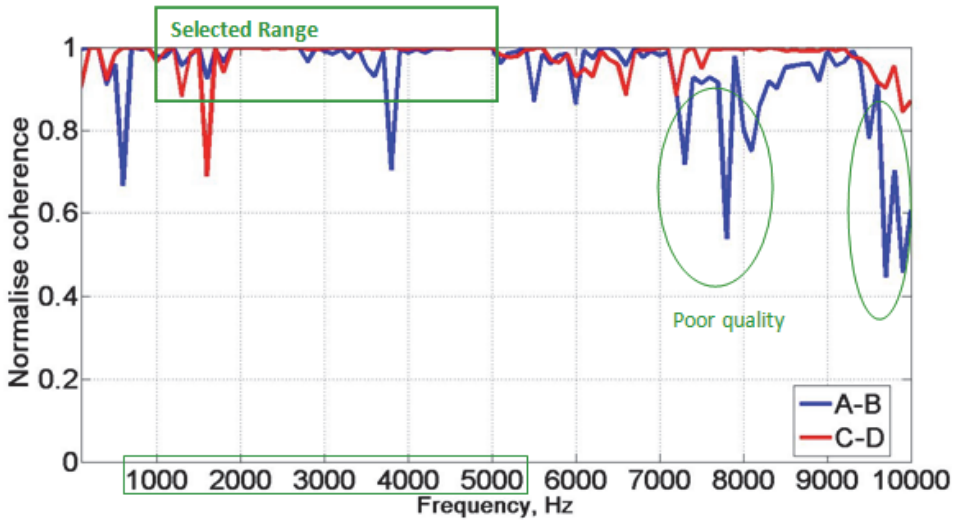

Figure 6.28: Normalised coherence for 2 sensor pairs for the Oxford Clay with a 32% moisture content (repeated test); selected frequency range 100Hz-10000Hz

Based on the results from Figure 6.28, the most appropriate frequency range is again 1000Hz to 5000Hz, although at frequencies of 3700Hz and 4300Hz the normalised coherence is low (Figure 6.29).

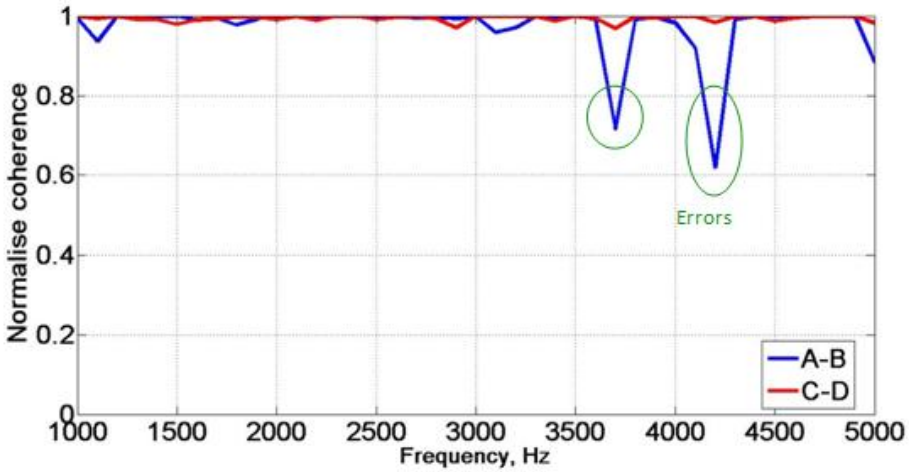

Figure 6.29: Normalised coherence for selected frequency range for 2 sensor pairs for the Oxford Clay with a 32% moisture content (repeated test); selected frequency range 1000Hz-5000Hz.

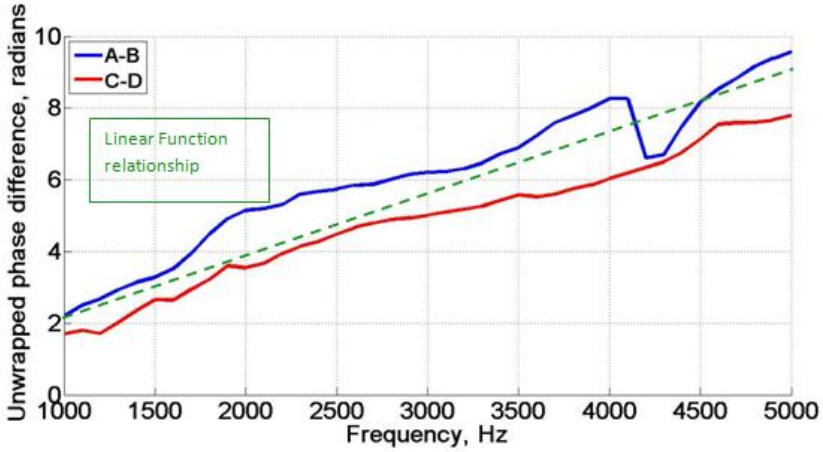

Figure 6.30: Unwrapped phase differences against frequency. It shows a linear function for A-B and C-D sensor pairs for Oxford Clay with a 32% moisture content (repeated test), selected frequency range 1000Hz-5000Hz

Figure 6.30 shows the unwrapped phase difference versus frequency. The linear plots show some minor deviation between frequencies 3000Hz and 4500Hz for both sensor pairs A-B and C-D, though it looks similar to the results obtained for the first test for Oxford Clay (Figure 6.25). Figure 6.31 indicates the phase velocity versus frequency for Oxford Clay with a 32% moisture content. It shows that the phase velocity

range for the frequency range of 1000Hz-5000Hz is approximately 100m/s to 150m/s and this range of phase velocity measurements is similar to the main test for Oxford Clay with a 32% moisture content.

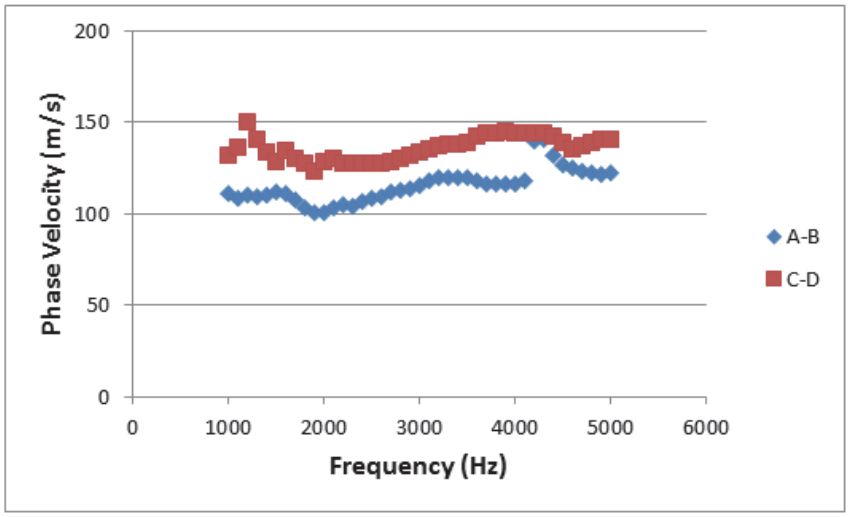

Figure 6.31: Phase velocity versus frequency showing the dispersive curve for the Oxford Clay with a 32% moisture content (repeated test); the frequency range was 1000Hz-5000Hz

Figure 6.32 shows more clearly that the range of phase velocity measurements is similar to the main test for Oxford Clay with a 32% moisture content.

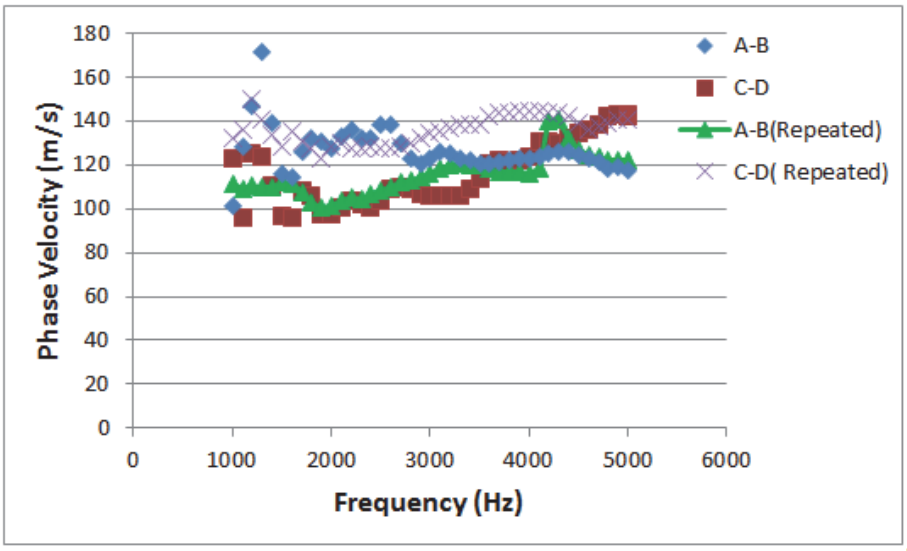

Figure 6.32: Phase velocity versus frequency showing the dispersive curve for the Oxford Clay with a 32% moisture content for main test and the repeated test, the frequency range was 1000Hz-5000Hz

Figure 6.33 shows the variation of the phase velocity with wavelength for Oxford Clay with a 32% moisture content. The range of reliable wavelengths is in the same range for this repeat test as the first test, and since the differences are minor it can be assumed the test is repeatable and the results reliable. It should be noted that the measured phase velocities for sensor pair C-D for the repeat test are closer to each other than the first test, and this is again related to the improvement in sample preparation and compaction of the sample.

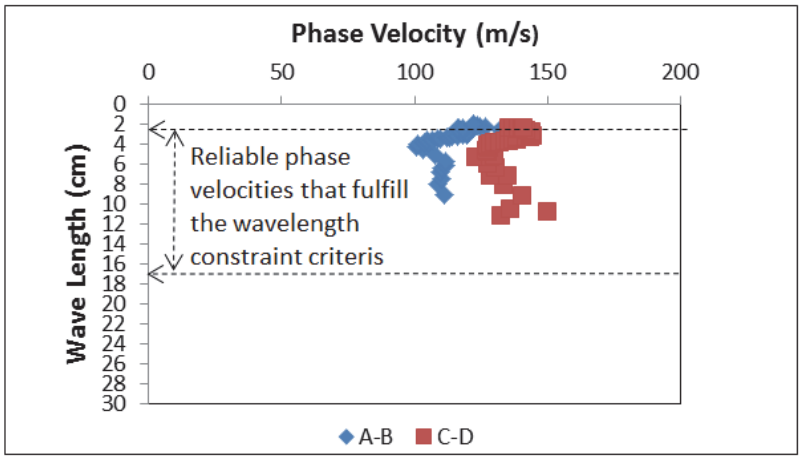

Figure 6.33: Wavelength versus phase velocity for Oxford Clay with a 32% moisture content (repeated test), throughout the wavelengths 2.75 to 16.50 cm; the frequency range was 1000Hz-5000Hz

6.3.2 Oxford Clay, 19% and 24% Moisture Content

For Oxford Clay with a 24% moisture content, the excitation was initially done with a frequency range of 100Hz to 10000Hz. The degradation in signal quality occurred when the frequency was less than 2000Hz and above 7000Hz. This is illustrated in Figure 6.34.

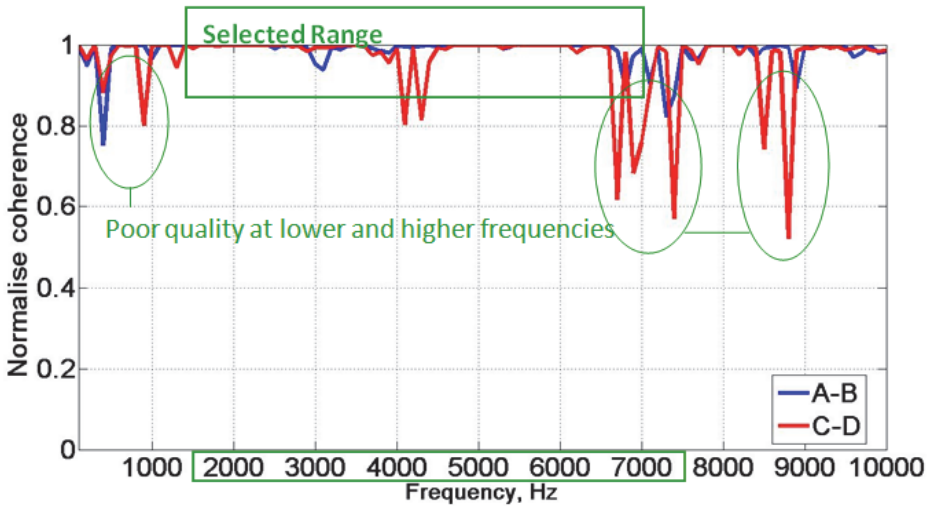

Figure 6.34: Normalised coherence for 2 sensor pairs for Oxford Clay with a 24% moisture content; selected frequency range 100Hz-10000Hz

As shown in Figure 6.35, the frequency range of 2000Hz-7000Hz was selected to achieve the best data quality, based on inspection of the results from Figure 6.34, although marked degradation of the signals for both pairs occurred at 4100 Hz.

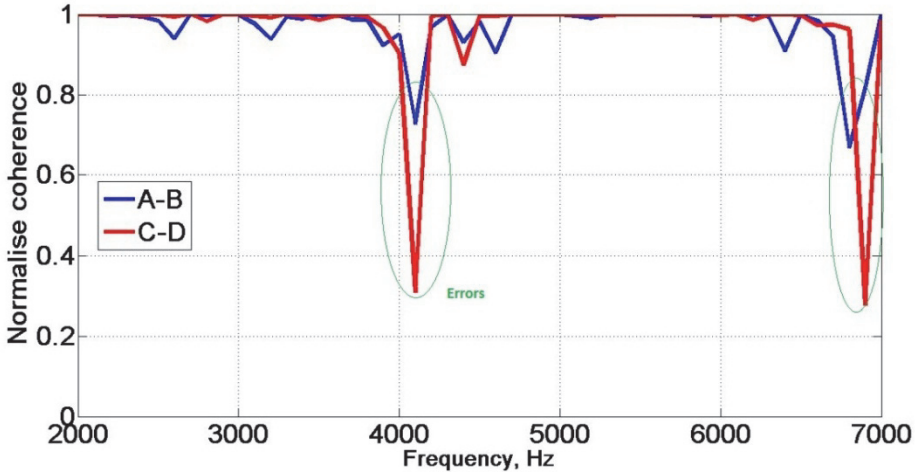

Figure 6.35: Normalised coherence for selected frequency range for 2 sensor pairs for the Oxford Clay with a 24% moisture content; selected frequency range 2000Hz-7000Hz

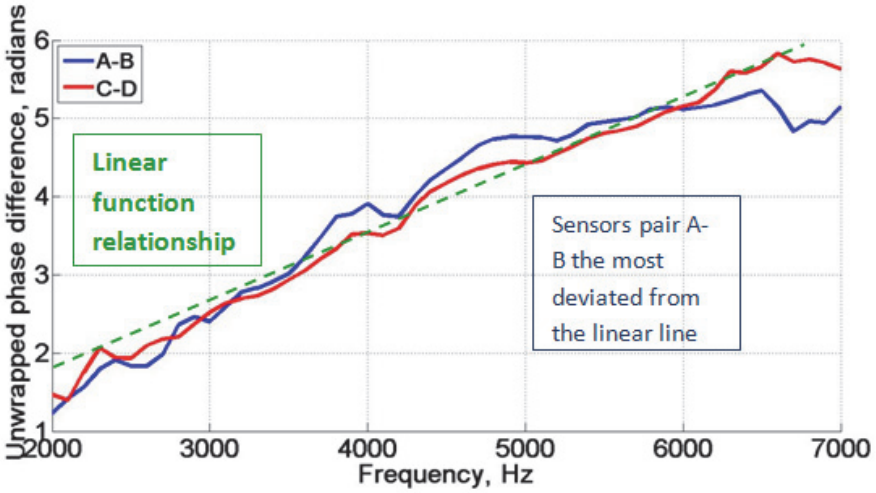

Figure 6.36: Unwrapped phase differences show linear function for A-B and C-D sensor pairs for Oxford Clay with a 24% moisture content; the frequency range was 2000 Hz-7000Hz

The unwrapped phase difference versus frequency is shown in Figure 6.36. The linear plots shows a deviation below a frequency of 3000Hz and above 6000Hz for both sensor pairs.

The phase velocities, which were calculated from the phase difference and distance between the sensors, is shown in Figure 6.37. It shows that the phase velocity range for the frequency range of 2000Hz-7000Hz is approximately 150m/s to 230m/s for the Oxford Clay with a 24% moisture content, which is larger than the phase velocity range for Oxford Clay with a 32% moisture content.

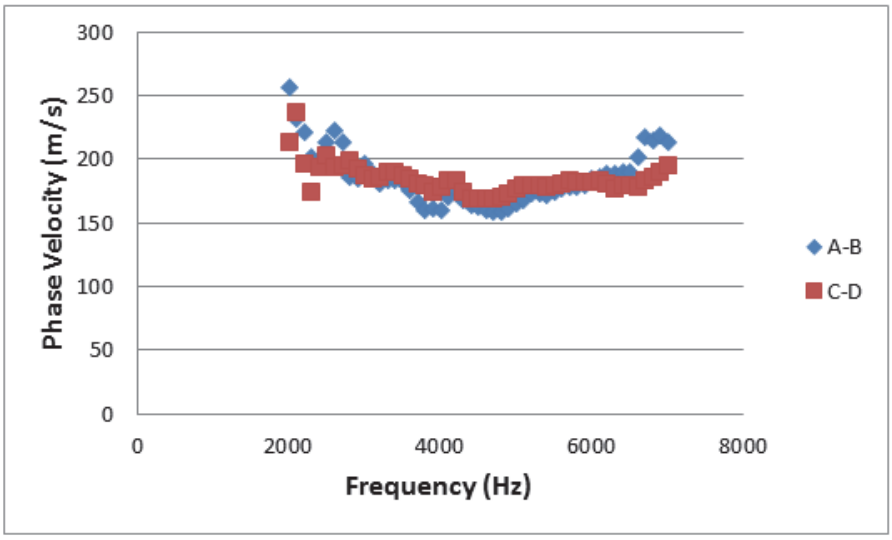

Figure 6.37: Phase velocity versus frequency showing dispersive curve for the Oxford Clay with a 24% moisture content (dominant phase velocity range: 150m/s-230m/s); the frequency range was 2000Hz-7000Hz

Figure 6.38 shows the variation of the phase velocity with wavelength for the Oxford Clay with a 24% moisture content.

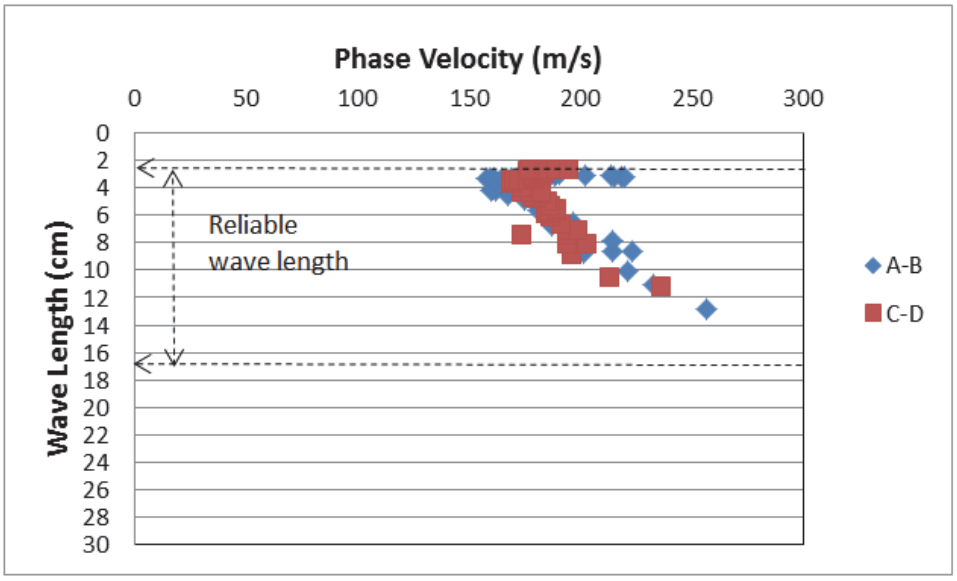

Figure 6.38: Wavelength versus phase velocity for Oxford Clay with a 24% moisture content for wavelengths of 2.75 to 16.50 cm; the frequency range was 2000Hz-7000Hz

For Oxford Clay with a 19% moisture content, the excitation was initially done with a frequency range of 100Hz to 10000Hz. The greatest degradation occurred when the frequency was less than 2000Hz and greater than 6000 Hz. This is illustrated in Figure 6.39. Figure 6.40

indicates the selected frequency range of 2000Hz-6000Hz, based on the results from Figure 6.39, provides the best quality data. It also shows, relatively, poorer quality in terms of the signal-to-noise in relation to the other tests as it was the first sample which was prepared – minor defects in the equipment operation and difficulties in coupling the piezo-ceramic accelerators to the surface were eradicated as experience in the experimental procedures increased and thus experimental techniques improved.

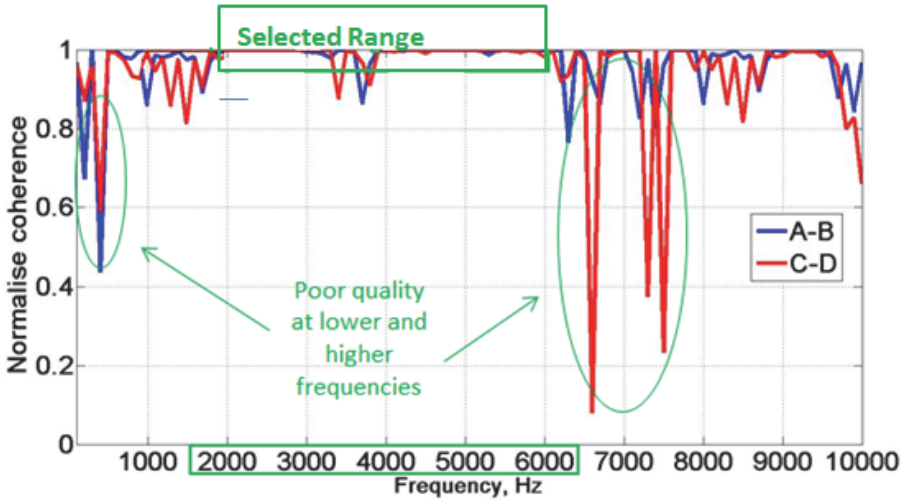

Figure 6.39: Normalised coherence for 2 sensor pairs for Oxford Clay with a 19% moisture content; selected frequency range 100Hz-10000Hz

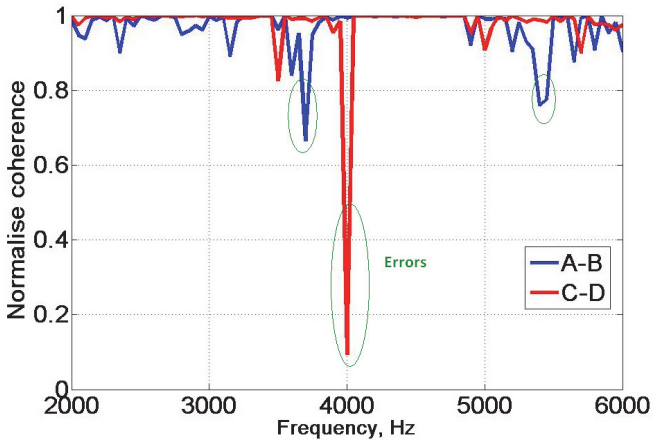

Figure 6.40: Normalised coherence for selected frequency range for 2 sensor pairs for the Oxford Clay with a 19% moisture content; selected frequency range 2000Hz-6000Hz

Figure 6.41 indicates frequency against unwrapped phase difference for Oxford Clay with a 19% moisture content. Although approximately linear, it shows a poorer quality relationship for sensor pairs A-B and C-D than for wetter samples, which as mentioned relates to difficulties in achieving uniformity in the preparation and compaction processes.

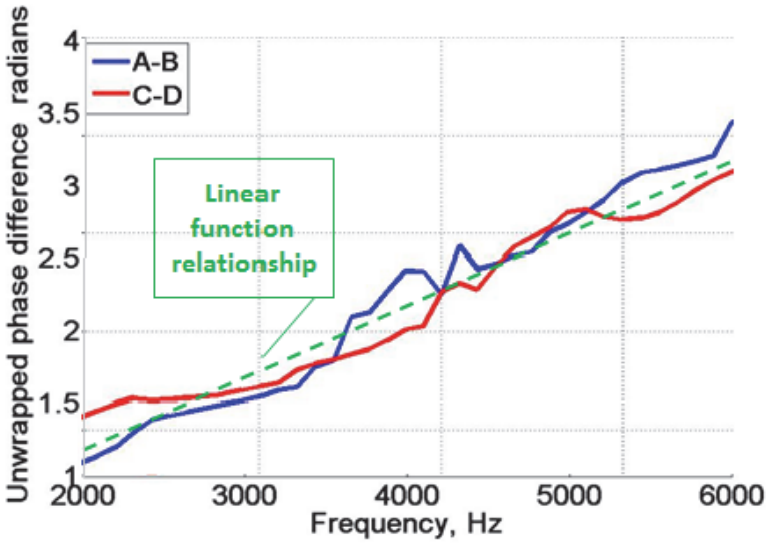

Figure 6.41: Unwrapped phase differences show linear function for A-B and C-D sensor pairs on for Oxford Clay with a 19% moisture content; the frequency range was 2000 Hz-6000Hz

The phase velocity versus frequency is shown in Figure 6.42 for Oxford Clay with a 19% moisture content. It shows that the phase velocity range for the frequency range of 2000Hz-6000Hz is approximately 250m/s to 320m/s, which as expected is more than the phase velocity range for Oxford Clay with a 24% and a 32% moisture content. Figure 6.43 shows the variation of the phase velocity with wavelength for the Oxford Clay with a 19% moisture content. Interestingly these two figures show that the results even at this low water content are more consistent than those for Kaolin clay at lower water contents.

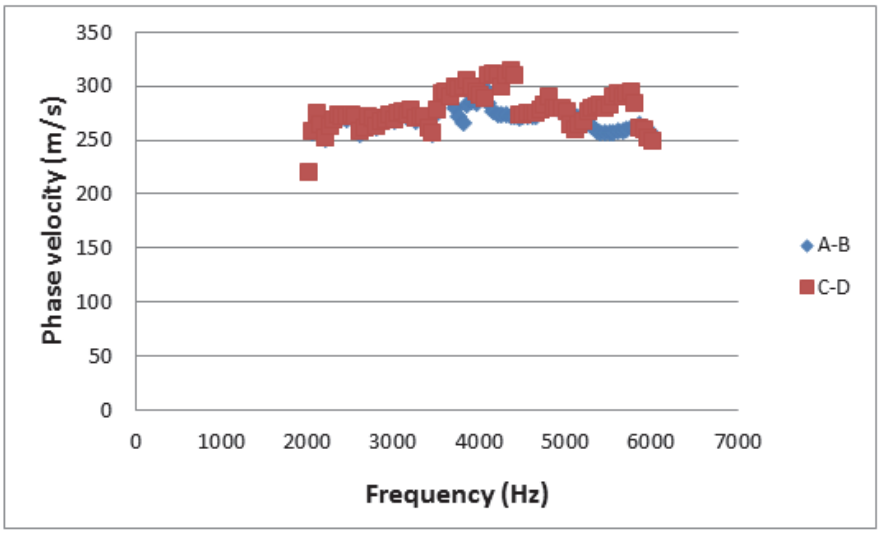

Figure 6.42: Phase velocity versus frequency showing dispersive curve for the Oxford Clay with a 19% moisture content (dominant phase velocity range: 250m/s-320m/s); the frequency range was 2000Hz-6000Hz

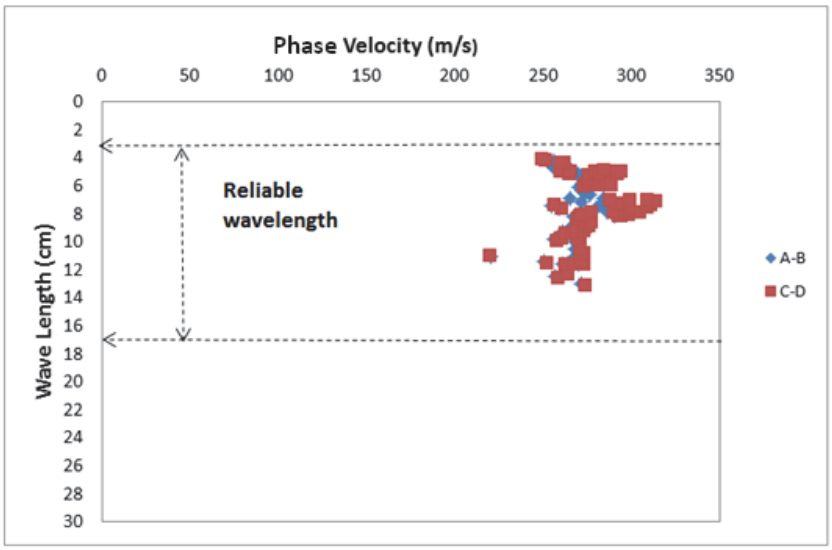

Figure 6.43: Wavelength versus phase velocity for Oxford Clay with a 19% moisture content for wavelengths of 2.75 to 16.50 cm; the frequency range was 2000Hz-6000Hz

6.4 Discussion

The range of phase velocities measured in Kaolin clay was 200m/s-300m/s, 150m/s-230 m/s, 120m/s-230 m/s and 50m/s-70 m/s for moisture contents of 24%, 28%, 28% and 33% respectively . The range of phase velocities measured in Oxford Clay was, 250m/s-320 m/s,

150m/s-230 m/s, 100m/s-150 m/s and100m/s-150m/s for moisture contents of 19%, 24%, 32% and 32% respectively. So in next chapter (Chapter 7) these phase velocities convert to shear wave velocities (Equation 3.7) As and the results show agreement with the past works by Mular (2007), Thitimakorn (2010) and Maheswari (2008) for clay soils. These results show strong trends of reduction of phase velocity with increasing water content of clay, which will be discussed in Chapter 7. The results also demonstrate that the values obtained from the repeated tests for velocity measurements are close to the phase velocity values obtained from the main tests in soft clay, and thus that the tests are repeatable.

A larger physical model would provide an increase in useful frequencies having a reliable phase velocity, since this would relate to a wavelength that is half of the model depth. Moreover the higher the coherence values, the less the deviation from the average value and the better the quality of the measurements. As explained in Section 6.3, a seismic source located in the middle of an array resulted in a smaller deviation from the average, due to both sensor-pairs receiving equal and higher amounts of energy when compared with the source placed at one end of the sensor array.

An acceptable range of phase velocity was observed for wavelengths from 2.75 to 16.50 cm. Thus, these phase velocities are considered reliable. The phase velocities were converted into shear wave velocities using Equation 3.9 (V_s=1.047.V_r) based upon a Poisson's ratio of 0.5 for the clay. The shear wave velocities were then converted into the shear modulus using the measured average bulk density for clay and the Equation 3.10 ($G_{max}=\rho.V_s^2$). These results are presented and discussed in Chapter 7.

Chapter 7

DISCUSSION

7.1 Introduction

This chapter discusses the results of the model testing for Kaolin Clay and Oxford Clay, which aimed to develop the most appropriate seismic wave method to find the relationship between geophysical and geotechnical properties of soil. Feasibility testing was conducted (see Chapter 4) to establish the equipment and its system for surface wave testing at the laboratory scale. Different materials were used in the main programme of testing in order to achieve the aim of the study.

7.2 Equipment and System

The equipment used to create a steady state vibration source was a National Instruments (NI) data acquisition system combined with an electromechanical vibrator and piezo-ceramic transducer, used to produce the seismic wave energy to generate the transmission waveform, which was amplified by the audio power amplifier. As reported in Chapter 3 the surface wave

was generated by a piezo-ceramic transducer with an electromechanical vibrator placed above it, creating a point energy source (see Figure 3.3), and this was positioned in the centre of the linear sequence of four receivers. On the output side four piezoelectric-accelerometers, connected to a four channel signal conditioner, were used. The conversion of the seismic wave energy to voltage was achieved using the NI analogue to digital converter module. This equipment was connected to a personal computer and controlled from within the Matlab environment. The outputs were stored for further processing.

The seismic surface wave system was designed to obtain a higher signal-to-noise ratio at a selected frequency range, thus a stepped-frequency approach was preferred. Each frequency step consisted of a few repetitive snapshots to improve the signal-to-noise ratio of the received signal (Clayton, 2011).\The Matlab script developed for this project to run the system is shown in Appendix B (1). Four sensors create two sensor-pairs, based on the symmetrical arrangement of the seismic source and receivers. The stepped-frequencies data were processed in Matlab environment as shown in Appendix B (2) and this was used to obtain phase difference between sensor-pairs. To obtain the phase velocity for each sensor-pair and an assessment of the quality of signal, which was represented by the coherence, further processing of the received signal was needed as shown in Appendix B (3). A repeated test was also introduced for improving the reliability of the calculated velocities.

7.3 Clay Model

7.3.1 Phase and Shear Wave Velocity Variations

7.3.1.1 Kaolin Clay

The initial water contents of Kaolin Clay were 24%, 28% and 33% and the associated range of phase velocities measured was 200m/s-300m/s, 150m/s-230m/s and 50m/s-70m/s, as discussed in Section 6.3. The experimental results of average phase velocity for Kaolin Clay

obtained from the surface wave tests for a frequency range of 3000Hz-4000Hz is also shown in Table 7.1.

Table 7.1: Results of average phase velocity for Kaolin Clay

Moisture content (%)	Frequency range (Hz)	Phase velocity range (m/s)	Average phase velocity (m/s) for a frequency range of 3000-4000Hz
24	3000-6000	200-300	282.5
28	1500-8000	150-230	172.5
28 (Repeated)	1500-8000	120-230	167.7
33	1000-4000	50-70	70.0

Figure 7.1 presents the results of the phase velocity for the frequency range of 1500Hz-8000Hz for four moisture contents of Kaolin Clay based on the results in Table 7.1. The figure shows that there is some significant scatter in the results, part of which might be attributed to specific frequency issues discussed in Chapter 6 (even though the frequency ranges have been selected to minimise these effects). Closer inspection, however, shows that the scatter is small for the highest water content (33%) and greatest at the water content well below optimum (24%), reflecting the greater difficulty in achieving uniform sample quality at such low water contents.

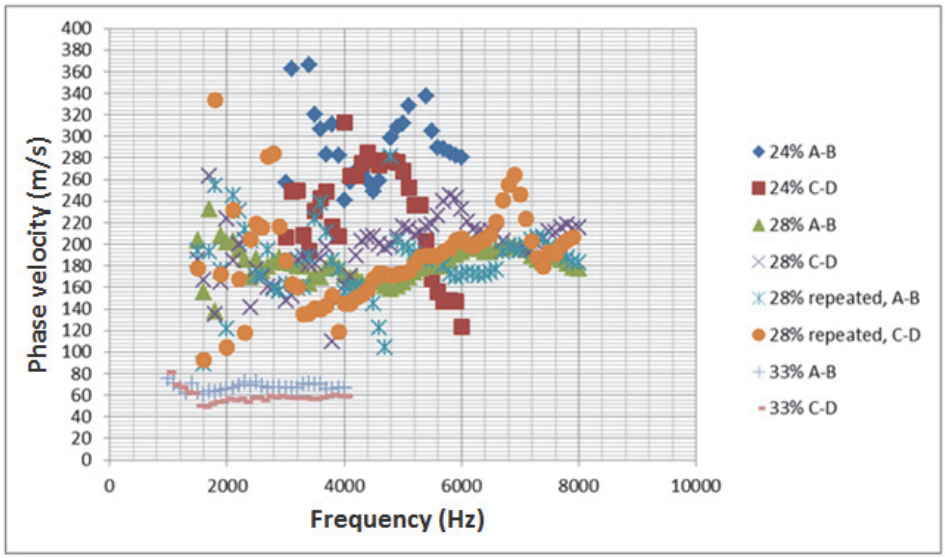

Figure 7.1: Results of the phase velocity versus frequency for the frequency range of 1500Hz-8000Hz for Kaolin Clay

Figure 7.2 shows the phase velocity variation for the frequency range of 3000Hz-4000Hz for four moisture contents of Kaolin Clay based on the results from Table 7.1. The average phase velocities are 282.5, 172.5 and 70.0m/s for moisture contents of 24%, 28% and 33% respectively, which indicates that the phase velocity is decreasing while the moisture content is increasing. The reason will be discussed later on this section.

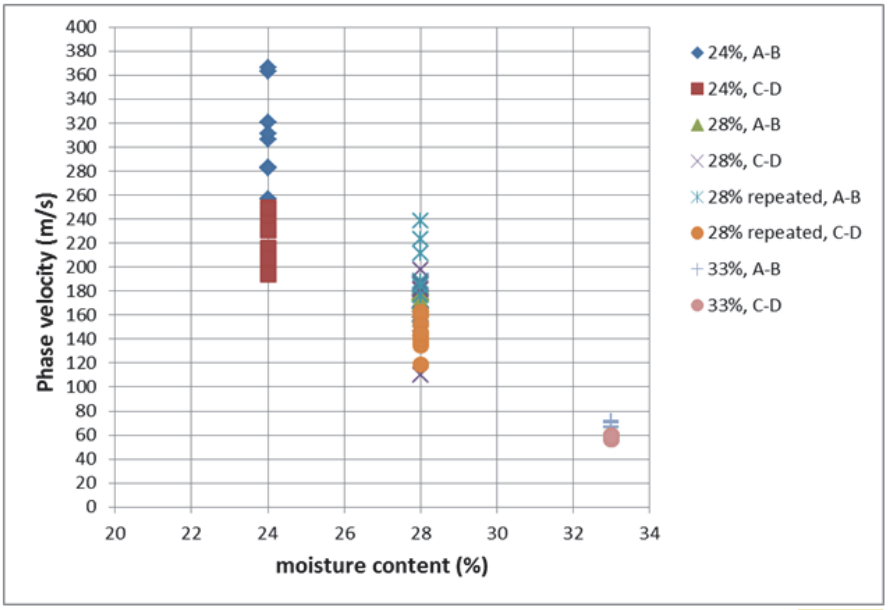

Figure 7.2: Phase velocity variation for the frequency range of 3000Hz-4000Hz for Kaolin Clay. As in mentioned before, the phase velocity can be converted to shear wave velocity

using a factor of 1.047 in Equation 3.7, with the assumption that the Poisson's ratio of Clay was 0.5. Table 7.2 show the results of shear wave velocity range and average of shear wave velocity for the frequency range of 3000Hz -4000Hz.

Table 7.2: Results of average shear wave velocity for Kaolin Clay

Moisture content (%)	Frequency range (Hz)	Shear wave velocity range (m/s)	Average shear wave velocity (m/s) for a frequency range of 3000-4000 Hz
24	3000-6000	210-315	279
28	1500-8000	157-240	180
28 (Repeated)	1500-8000	125-240	174
33	1000-4000	52.5-73.5	66

It is worth to underline that the measured values of shear wave velocities agree with typical values reported in literature. Molar et al., (2007), ranging shear wave velocity from 100 to 260 m/s for Victoria Clay at Greater Victoria site, Maheswari et al., (2008), ranging from 150 to 250 m/s for soil formation mainly consists of soft and stiff clay in Chennai city and Thitimakorn et al., (2010) ranging from 150 to 300 m/s for Bangkok soft clay.

Figure 7.3 shows the results of the shear wave velocity for the frequency range of 1500Hz-8000Hz for the four moisture contents of Kaolin Clay based on the results in Table 7.2.

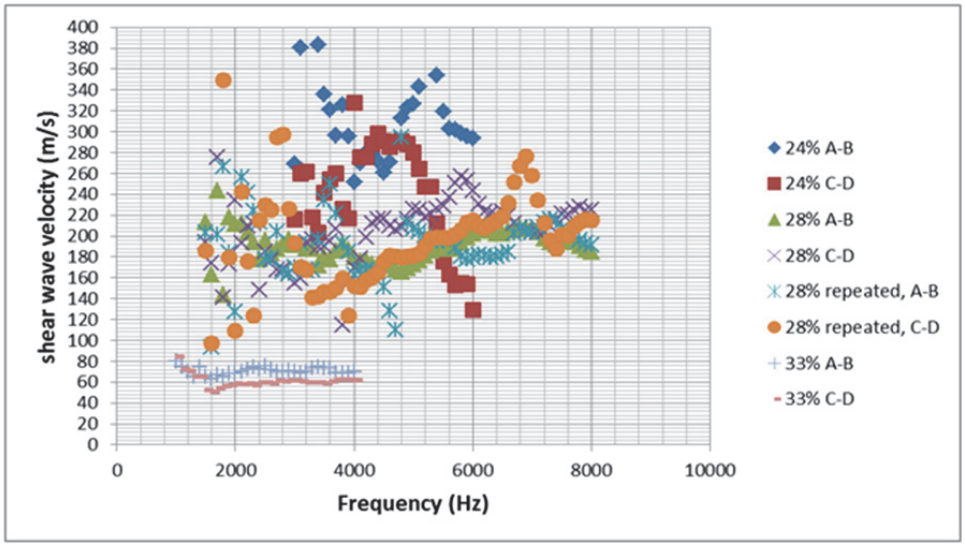

Figure 7.3: Shear wave velocity versus frequency for the frequency range of 1500Hz-8000Hz for Kaolin Clay

The average shear wave velocities for Kaolin Clay for a frequency range of 3000-4000Hz are shown in Figure 7.4, which again demonstrates that the shear wave velocity is decreasing while the moisture content is increasing.

From literature review Yung et al.,(2008), reported that shear wave velocity decreased with increasing moisture content and degree of saturation which is matched with the results of present work.

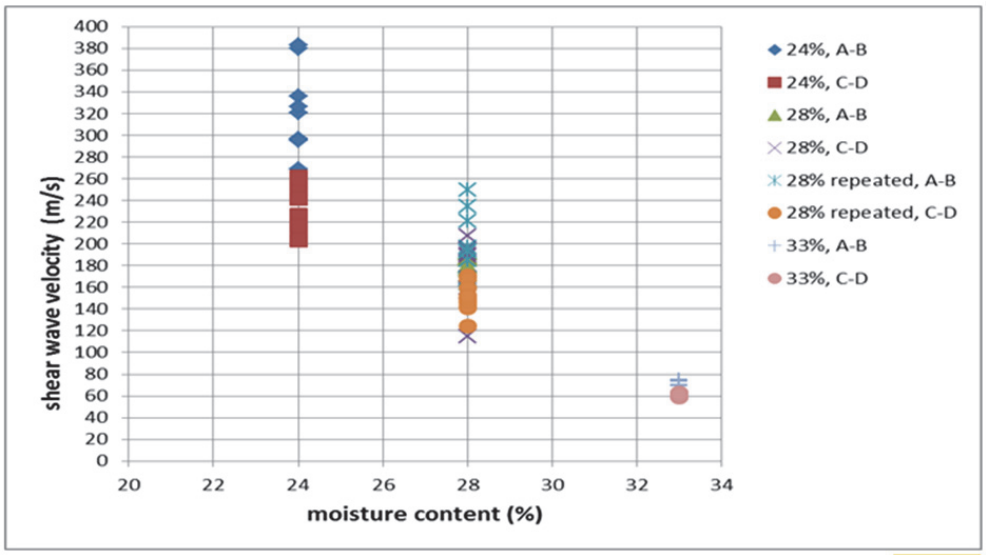

Figure 7.4: Shear wave velocity variation for the frequency range of 3000Hz-4000Hz for Kaolin Clay

7.3.1.2 Oxford Clay

Table 7.3 shows the experimental results of phase velocity range and average phase velocity for Oxford Clay for a frequency range of 2000Hz-5000Hz. The initial water contents of Oxford Clay were 19%, 24% and 32% and the range of phase velocities measured was 250m/s-330m/s, 150m/s-230m/s and 100m/s-150 m/s respectively.

Table 7.3: Results of average phase velocity for Oxford Clay

Moisture content (%)	Frequency range (Hz)	Phase velocity range (m/s)	Average phase velocity (m/s) for a frequency range of 2000-5000 Hz
19	2000-6000	250-330	275.5
24	2000-7000	150-230	185.2
32	1000-5000	100-150	121.6
32 (Repeated)	1000-5000	100-150	127.1

The full set of results of the phase velocity measurements for the frequency range of 1000Hz-6000Hz for the four moisture contents of Oxford Clay are shown in Figure 7.5, based on the results in Table 7.3.

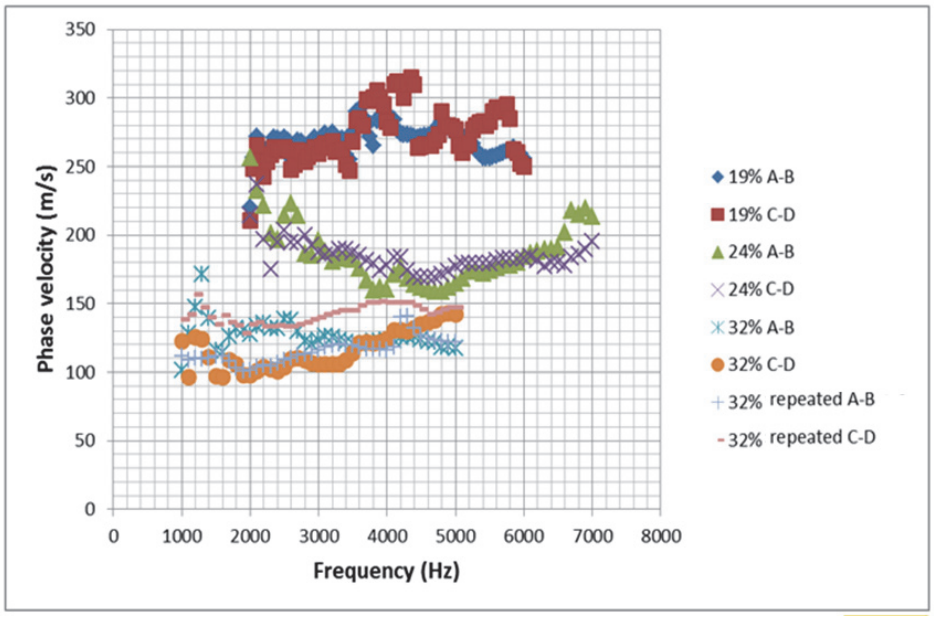

Figure 7.5: Results of the phase velocity measurements against frequency for the frequency range of 1000Hz -7000Hz for Oxford Clay

The phase velocity variation for the frequency range of 2000Hz-5000Hz for the four moisture contents of Oxford Clay is shown in Figure 7.6, again based on the results presented in Table 7.3 and it once more indicates that the phase velocity is reducing while the moisture content is increasing.

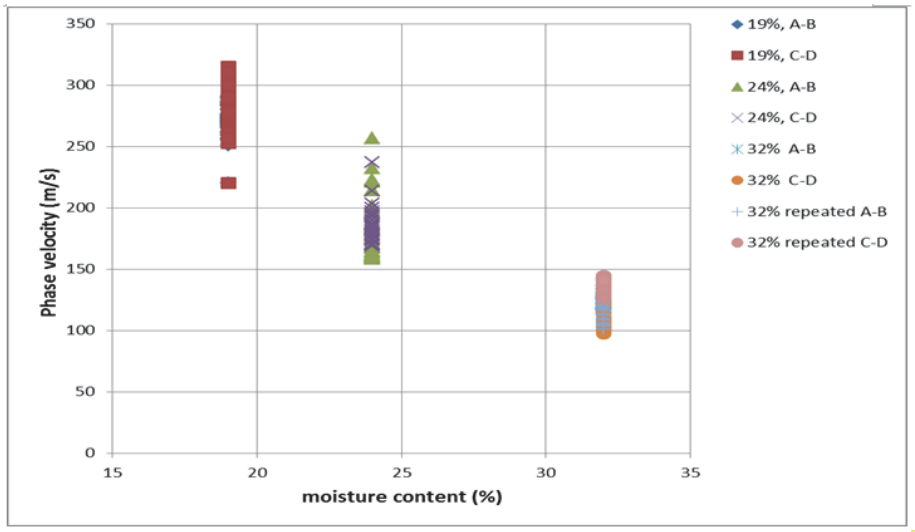

Figure 7.6: Results of the phase velocity variation for the frequency range of 2000Hz-5000Hz for Oxford Clay

As before, shear wave velocities were calculated from phase velocity measurements by using Equation 3.7 and the factor of 1.047, as is shown in Table 7.4, with the assumption that the value of Poisson's ratio of Clay was 0.5.

Table 7.4: Result of average shear wave velocity for Oxford Clay

Moisture content (%)	Frequency range (Hz)	Shear wave velocity range (m/s)	Average shear wave velocity (m/s) for a frequency range of 2000-5000Hz
19	2000-6000	260-360	288.5
24	2000-7000	160-250	194.0
32	1000-5000	110-160	127.3
32 (Repeated)	1000-5000	110-160	130.2

Same as Kaoli Clay table of results, the present table show a good match with the previous works results in the literature, Mular (2007), Thitimakorn (2010) and Maheswari (2008), which indicated range of 100 to 300 m/s for shear wave velocity for clay soils.

On the other hand Madun et al., (2012), measured shear wave velocity for Oxford clay with 32% moisture content at the same condition of sample preparation and testing method with present work and show good agreement with measured shear velocity and shear modulus with this work.

Figure 7.7 displays the results of the shear wave velocity for the frequency range of 1000Hz-6000Hz for the four moisture contents of Oxford Clay based on the results in Table 7.4.

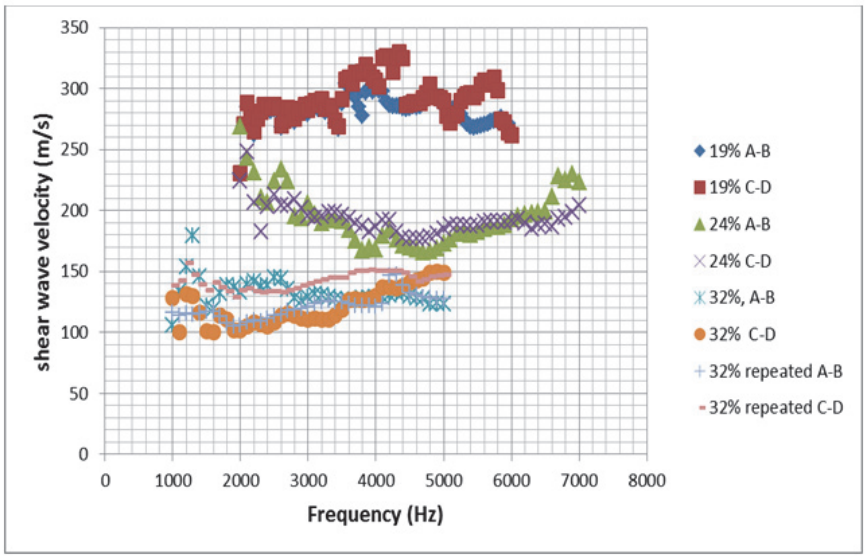

Figure 7.7: Results of shear wave velocity versus frequency for the frequency range of 1000Hz-7000Hz for Oxford Clay

The average shear wave velocities for Oxford Clay for the frequency range of 1000Hz-6000Hz is shown in Figure 7.8, which again shows an obvious pattern of decreasing shear wave velocity while the moisture content is increasing.

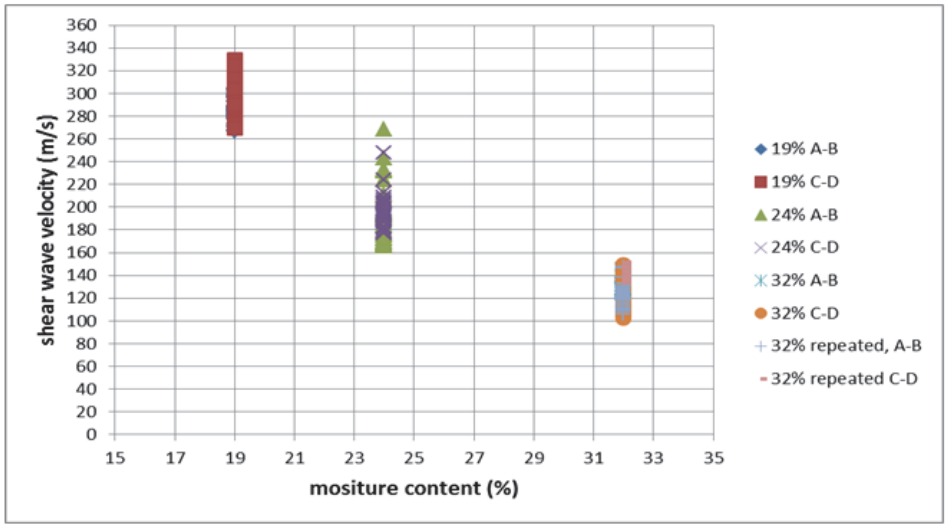

Figure 7.8: Results of the shear wave velocity for the frequency range of 2000Hz-5000Hz for Oxford Clay

And same as before, from literature review Yung et al.,(2008), reported that shear wave velocity decreased with increasing moisture content and degree of saturation which is matched with the results of present work.

Figure 7.2 plots the relationship between phase velocity and moisture content, and Figure 7.4 the shear wave velocity versus moisture content, for a frequency range of 3000Hz-4000Hz for Kaolin Clay. Figure 7.6 plots phase velocity against moisture content and Figure 7.8 shear wave velocity against moisture content for the frequency range 2000Hz-5000Hz for Oxford Clay. All these figures show phase velocity decreases with increasing moisture content of soil. This behaviour can be attributed to influences of both the pore water in the soil and the soil skeleton, i.e. wave propagation through saturated soils involves both the soil skeleton and water in the void spaces. For S-wave propagation, the pore water has no resistance to shear and thus the S-wave in soils is dependent only on the properties of the soil skeleton (Das, 1983), i.e. the 'interconnectedness' of the soil particles. Similar principles can be drawn from the field of unsaturated soils, since the ability to resist shearing decrease when moisture content in soils increases and because pore water has no capacity to resist shear then the effect must be due to soil particle interconnectivity (the relevant phenomena being friction and

dilation). However in the case of shear resistance, the pore water pressure within the soil has a direct influence on the amount of frictional resistance that is mobilised, whereas in the case of shear wave transmission it is solely density that is suggested in the literature to be the controlling feature; this would appear to be borne out by the results of this research. Thus, it might be concluded that if soils experience a significant change in the soil skeleton, usually accompanied by significant change in moisture content, the S-wave velocity is expected to exhibit significant changes, whereas if there are significant changes in pore water pressure yet these are accompanied by no significant change in the arrangement of the soil skeleton then no significant change in S-wave velocity occurs (Yang et al. 2008).

7.3.2 Shear Modulus

As stated above, the shear wave velocity of Clay was calculated by converting the average phase velocity to shear wave velocity using a factor of 1.047 in Equation 3.7, with the assumption that the Poisson's ratio of Clay was 0.5. The maximum shear modulus of material, G_{max}, is defined as the ratio of shear stress to the shear strain and is one of several quantities for measuring the stiffness of materials. G_{max} describes the material's response to shearing strains and in the case of soil it is related to the soil bulk density, ρ, and the shear wave velocity through Equation 3.8, i.e. $G_{max}=\rho V_s^2$. From this equation, shear wave velocity governs shear modulus, i.e. it is the dominant influence. The error in the maximum shear modulus arising from the approximation of the Poisson's ratio in the conversion of Rayleigh-wave phase velocity into shear wave velocity is usually less than 10% (Menzies 2001).

Figures 7.9 and 7.10 show the relationship between calculated the maximum shear modulus and shear wave velocity for the four moisture contents of Kaolin Clay and Oxford Clay. Based on Equation 3.8, there is a strong relationship between the shear modulus and shear wave velocity so as the shear wave velocity is increasing, the shear modulus will increase

also. On the other hand these figures indicate that the shear modulus for both Clays is decreasing while the moisture content is increasing. This relationship is shown more clearly in Figures 7.11 and 7.12 for Kaolin Clay and Oxford Clay respectively. Increase in modulus as the moisture content decreased in saturated Clay soil is similarly related to density effects, but is a phenomenon observed in other materials. For example, in timber the phenomenon was explained in terms of an increase in the effective number of hydrogen bonds available to maintain the saturated integrity of the cell wall, which is the tough, usually flexible but sometimes fairly rigid layer that located outside the cell membrane and provides these cells with structural support and protection. A major function of the cell wall is to act as a pressure vessel, preventing over-expansion when water enters the cell (Kretschmann and Green, 1996a, b).

It is worth to underline that the trend of mentioned figures agree with Yang et al.,(2008) which indicates that shear wave velocity decreases with increasing in moisture contents.

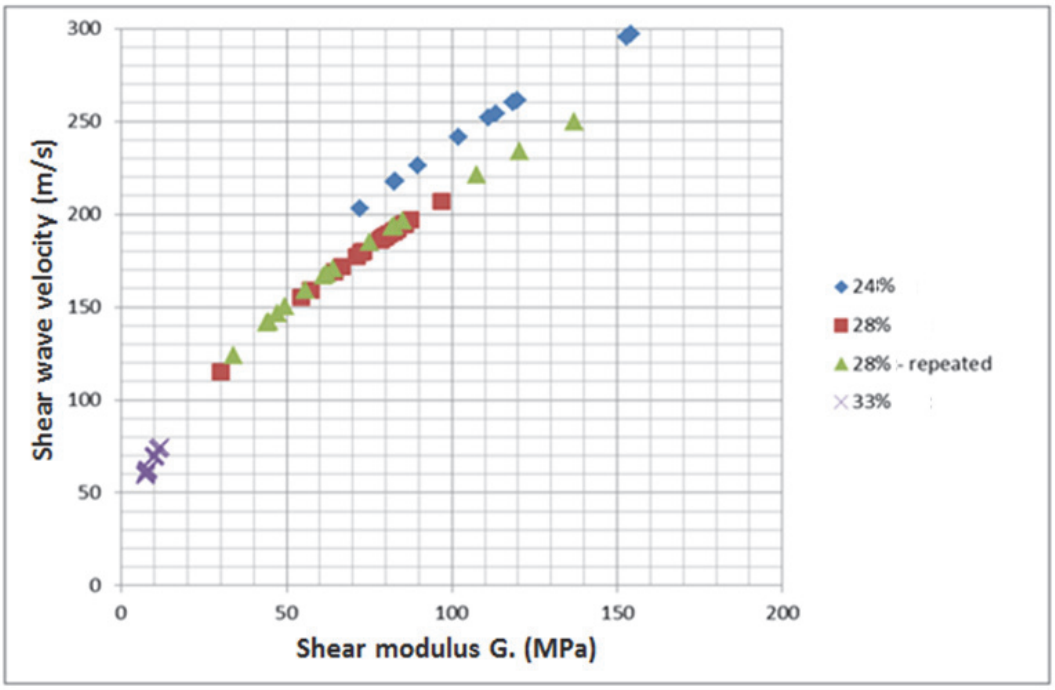

Figure 7.9: Relationships between shear wave velocity and the calculated shear modulus for Kaolin Clay with 24%, 28% and 33% moisture content

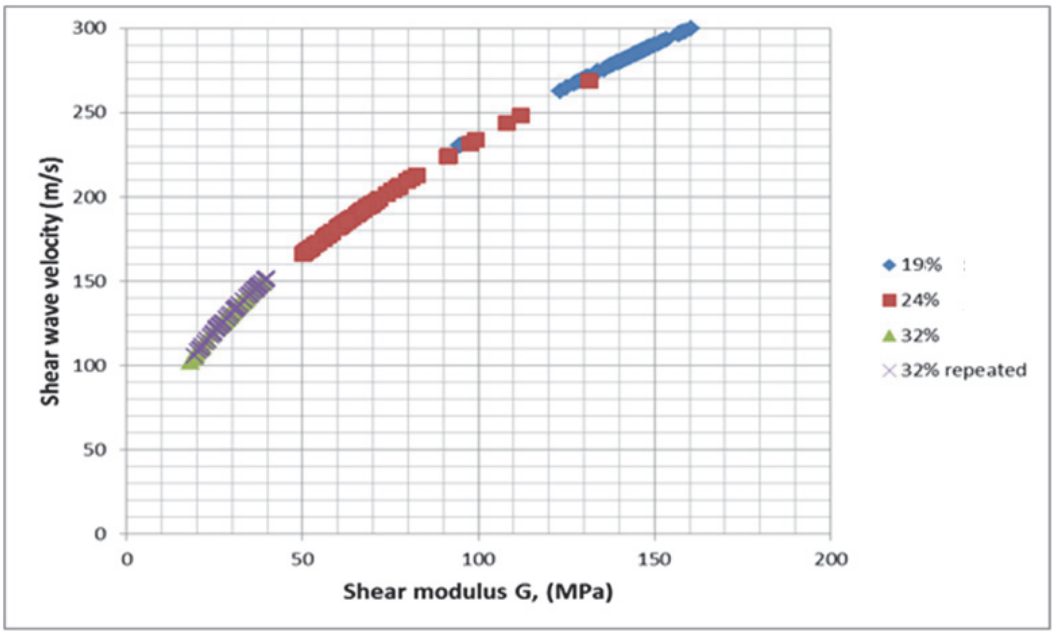

Figure 7.10: Relationship between shear wave velocity and the calculated shear modulus for Oxford Clay with 19%, 24% and 32% moisture content

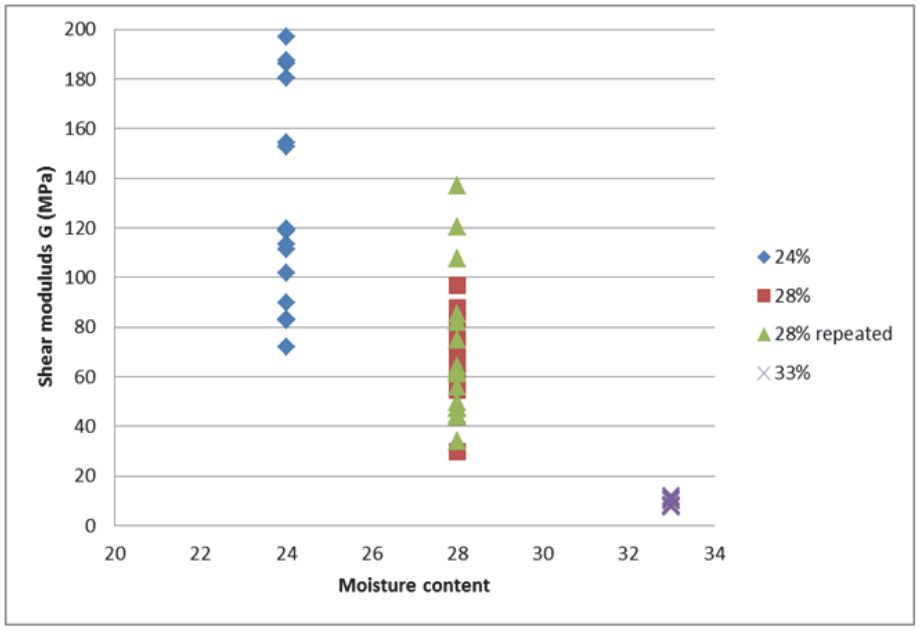

Figure 7.11: Variation of shear modulus for different moisture content of Kaolin Clay

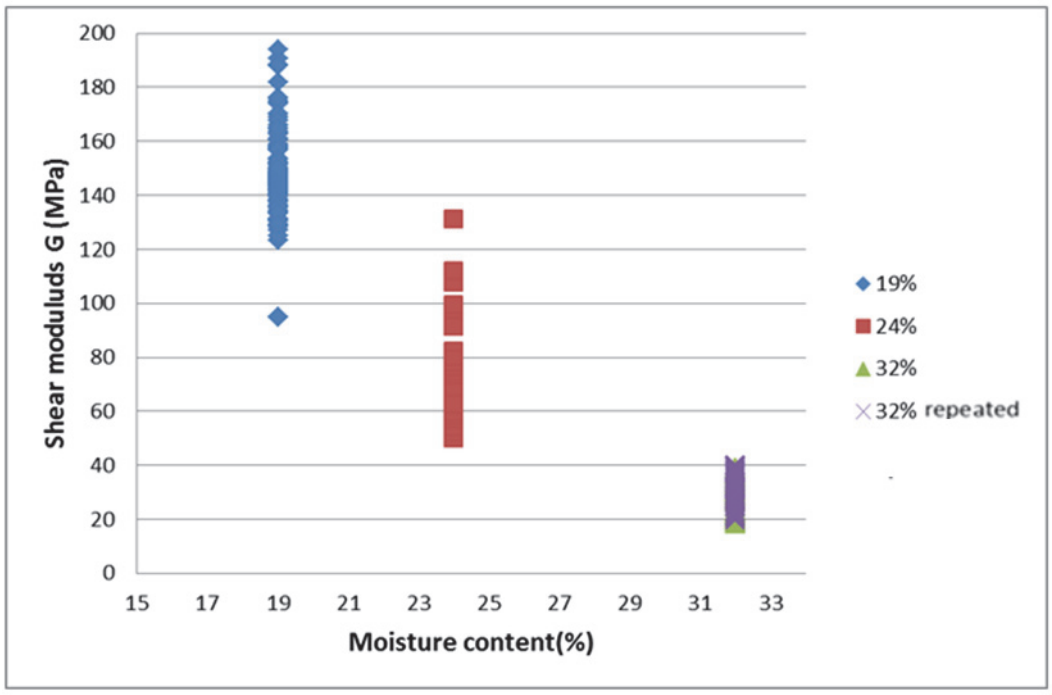

Figure 7.12: Variation of shear modulus for different moisture content of Oxford Clay

Figures 7.13 and 7.14 show the relationship of the shear modulus for Kaolin Clay and Oxford Clay for reliable wavelengths, i.e. between 2.75 cm and 16.50 cm (the shear modulus profile). These shear modulus profiles were related to phase velocity profiles in Chapter 6 and demonstrate that the shear modulus is increasing as the depth below the surface of the sample is increasing, while the shear modulus increases as the moisture content decreases agree with Yang et al., (2008) which indicates same conclusion as the shear modulus decreases with increasing moisture content. The profiles for both Clays show some variation, as expected for compacted Clay samples, although the variation is greater for the Oxford Clay. This is attributed to the greater plasticity of the mixed mineralogy in this Clay, in contrast to the relatively pure, lower plasticity kaolinite of the Kaolin Clay.

Regarding to literature review, Madun et al., (2012), indicates shear modulus versus wavelength for measurements conducted in a small container filled with Oxford clay atb32% moisture contents with the same conditions like present work and show the range of 15 to 40MPa for shear modulus which is almost same with the present results.

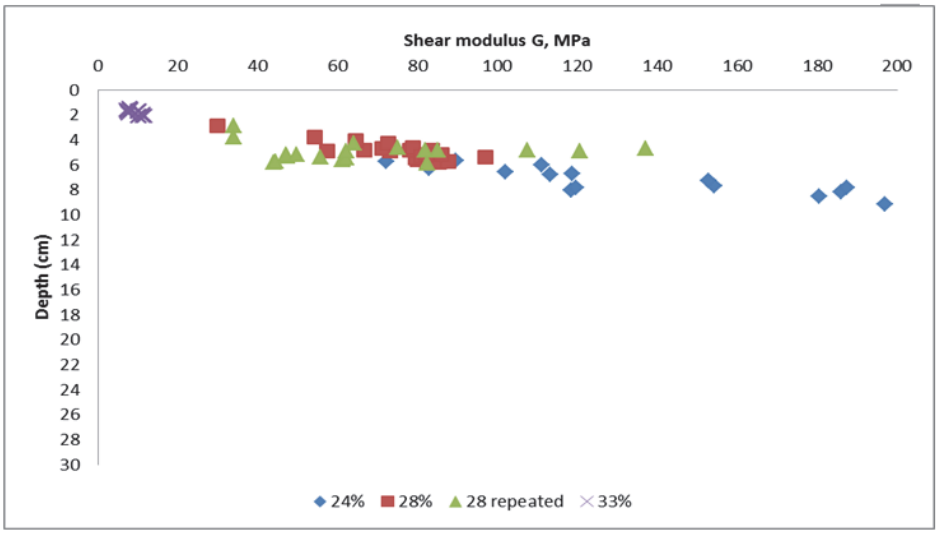

Figure 7.13: Shear modulus profile at different depths below the surface of the samples for Kaolin Clay at different moisture contents

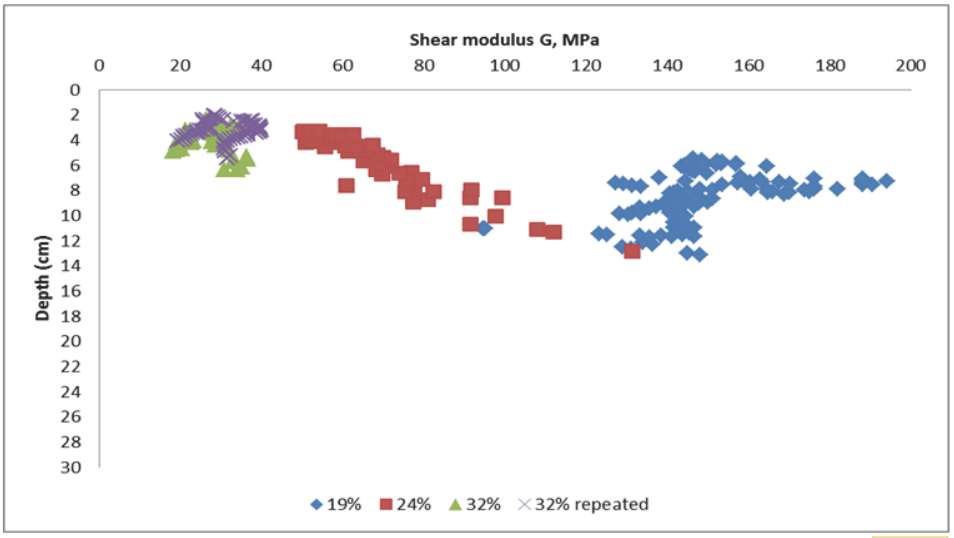

Figure 7.14: Shear modulus profile for Oxford Clay at different depths below the surface of the samples at four different moisture contents

7.3.4 Correlation Between Shear Wave Velocity, Density and Moisture Content

Figures 7.15 and 7.16 indicate the correlation between shear wave velocity of compacted Clayey soils, calculated water content and the density of Clay, which combine to form the main conclusion of the research along with the results from Figures 7.9 to 7.14, i.e. to achieve the last objective of this study: to establish a correlation between geophysical and geotechnical properties of artificial soil.

Water is sometimes described as acting as a lubricant within soil to enable the particles to slide past each other. While this is unhelpful in some senses of describing soil mechanics principles, essentially because the phenomena described relate to pore water pressure effects, an increase in water content of an artificial, compacted Clay soil causes particles to be separated by water and this separation facilitates undrained shear. Figure 7.15 shows that when the moisture content is increasing from 24% to 28% (the optimum moisture content) for Kaolin Clay, and in Figure 7.16 from 19% to 24% (optimum moisture content for Oxford Clay; Figure 5.1), so the particles can move past each other to achieve a greater density. In this case the issue of the 'lubrication effect' is an inaccurate description of the dominant behaviour since the Clay at a significantly lower water content than its optimum will sustain suctions, or negative pore water pressures, and these suctions resist undrained shearing, leading in turn to a reduced density. In this case the density increased from 2130kg/m^3 to 2260kg/m^3 for Kaolin Clay and from 1740 to 1820 for Oxford Clay. In this region the average shear wave velocity decreased from 279 m/s to 180m/s for Kaolin Clay and from 289 m/s to 194 m/s for Oxford Clay. The reduced ability to resist shearing as the moisture content increases causes an increase in density as long as the water content remains below the optimum water content; once the water content exceeds the optimum value (i.e. the point corresponding to the maximum dry density) – at 28% moisture content for Kaolin Clay and 24% moisture content for Oxford Clay (Figure 5.1) – then density no longer increases but reduces as the water content continues to increase. This additional water expands the size of water-filled voids and consequently weakens the soil (i.e. its shear resistance reduces) as the density of soil progressively decreases; however the shear wave velocity continues to decrease for same reasons as mentioned previously. [Here the 'lubrication' argument has greater relevance, though it is in reality greater Clay particle separation, and hence reduced frictional resistance, as the water content increases.] Therefore, the shear wave velocity has an inverse relationship with moisture content throughout the range tested (i.e. from well below to well

above the optimum water content), while it has an inverse relation with density before it reaches the optimum water content (or maximum dry density) after which they exhibit a direct relationship – which means that the shear wave velocity decreases while the density decreases.

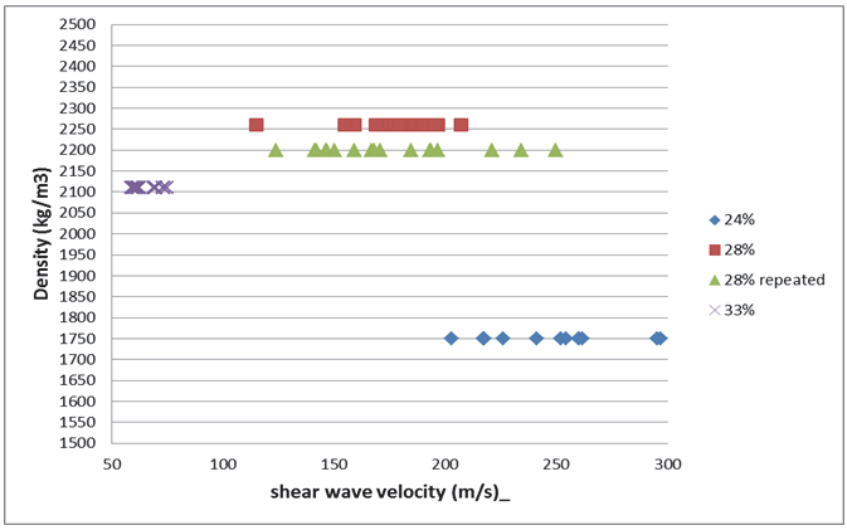

Figure 7.15: Variation of shear wave velocity related to moisture content and density of Kaolin Clay

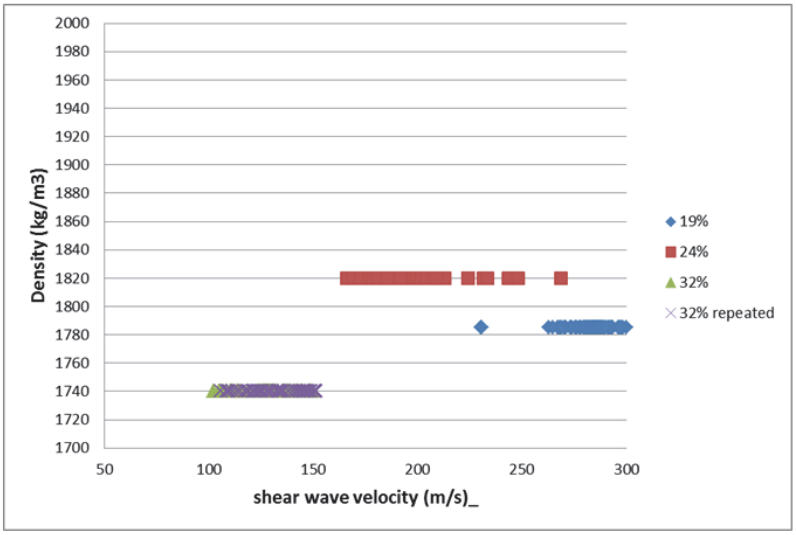

Figure 7.16: Variation of shear wave velocity related to moisture content and density of Oxford Clay

In the literature it is suggested that a strong direct relationship exists between shear wave velocity and density; $G_{max} = \rho v_s^2$ (Clayton et al., 1995; Menzies and Matthews, 1996; Massarsch, 2005), but it is contended that this is because of the limited range of water contents over which this is observed and in natural soils at water contents below the optimum

water content, yet for compacted soils at water contents well above optimum the relationship does not hold. In this research it is demonstrated that the strong relationship is in fact an inverse relationship with water content. It is for this reason that the shape of the relationship in Figures 7.15 and 7.16 resemble the typical shape of the standard compaction curves for Clay soil (Figure 5.1).

Chapter 8

CONCLUSIONS AND RECOMMENDATIONS FOR FURTHER RESEARCH

8.1 Introduction

In this thesis, the seismic surface wave technique has been described and relevant literature reviewed. By way of laboratory testing, alternative test arrangements were examined and a suitable testing programme was developed to meet the aim of developing an appropriate seismic surface wave experimental methodology to assess how soil properties influence seismic waves transmission and how they can be used to develop correlations between acoustic and geotechnical properties. A test bed was established using two different types of clay, Kaolin clay and Oxford Clay, with moisture contents varying from well above to well below the optimum moisture contents.

It was clear from the literature review that a detailed programme of work was needed, based in the laboratory, to assess the properties of soil in relation to surface shear wave characteristics over this range of moisture contents. The equipment and system reliability

performance were established and checked, prior to the models of Kaolin clay and Oxford Clay being tested.

Based on the results and experience gathered from the laboratory work, this chapter summarizes the main findings and gives recommendations for future research. This work focused on laboratory scale models, so providing essential parameter and boundary control. From this work ways to adapt approaches for full-scale field testing, and ultimately quality assurance testing, can be developed.

8.2 Main Outcomes

- From a laboratory point of view the selected size of the container/box was sufficiently large to enable clay samples of a suitable quality to be made, i.e. placed and compacted well and uniformly. Also it was acceptable from practical viewpoint, in terms of mixing and handling the clay, but there were limitations from the acoustic experimentation point of view so a specific frequency range for each clay type and water content had to be established to ensure reliable results as follows. Despite careful prior consideration with regard to the size of the container**,** some interference of the surface waves (these were the ones of interest in the experiments) with body waves (near offset constraint effect) occurred. In addition, attenuation of the surface waves (far offset constraint effect) was visible. These were identified via the anomalies in the phase-response of the coherence plot and unwrapped phase difference. A weaker signal quality at higher frequencies was due to a more rapid attenuation of the shorter wavelengths as well as the presence of relatively strong boundary reflections, thus reducing the signal quality at higher frequencies and deviation of associated phase velocities. The sensors which were located further from the source received less energy, which compromised signal quality under certain circumstances, and this problem was exacerbated by the interfering reflected wave from the boundary of the container. For this reason only reliable wavelengths, established via detailed initial analysis of the test data, were

considered when analyzing the results for this test model. A common problem with geotechnical model testing, this research showed that by minimizing the size of sample some parameters become more accurate, such as those associated with uniform compaction of the sample, while on the other hand there will be some limitation on the range of reliable wavelengths that can be used, e.g. because of the boundary reflections.

- The optimal arrangement of the sensor array on the test model was when the seismic source was located at the centre of the array with the receiver pairs at either side. This arrangement was based on the literature and previous work by Madun (2011). This arrangement ensures that both sensor-pairs receive an equal and relatively high amount of energy so that there is a relatively small deviation in the phase velocities. For the laboratory seismic surface wave array set-up, the optimal distances between the source and the first sensor (d) and sensors spacing (Δx) were 5.5cm and 2.5cm respectively. This array gave reliable wavelengths between 2.75cm and 16.50cm, which were derived from half d and three times d, respectively.
- During the tests it became apparent that a careful identification and selection of suitable frequencies for each test was essential. The coherence plots gave an initial indication of suitable frequencies, but closer inspection was required by looking at smaller frequency bands as well as the graph of frequency against unwrapped phase difference. This indicated frequency ranges where the confidence in the corresponding phase and ultimately shear wave velocities is reduced.

- The data were recorded by two receiver pairs A-B and C-D. As the receiver pairs were exactly the same distance from the seismic wave source, the signals should be identical assuming the clay was homogenous and all other boundary conditions were identical. However, looking at the data, and assuming that any differences were not due to experimental

influences such as sensor-clay coupling effects, it became apparent that there was some variation between the two signals received indicating that, despite every effort, the clay was not exactly homogenous with some variation throughout the container. The results were, however, sufficiently similar to give confidence in the accuracy of the outcomes.

- The measurements of shear wave velocity and moisture content of clay soil show a clear trend of reduction of shear wave velocity, and hence shear modulus, while the moisture content is increasing for both clay test models over the full range of water contents tested, i.e. from significantly wet through to significantly dry of the optimum water content.

- The measurements of shear wave velocity, moisture content and density of the clay soils tested show that the shear wave velocity, and hence shear modulus, has an inverse relationship with density before it reaches the optimum water content (or maximum dry density) after which it exhibits a direct relationship, i.e. the shear wave velocity decreases while the density decreases.

8.3 Recommendations for Future Research

- If the soil water contents and densities change with depth in a soil, as might occur with traditionally compacted clay soils, the wavelength might not be equal to the depth. Therefore, the relationship between the wavelength and the depth might be explored in a larger test programme in which larger soil samples are included. However the maximum information on the soil properties is limited to half of the model depth while the limitation arising from the arrangement of the equipment (the distance of seismic source to the first receiver, d, and the spacing between receivers, Δx) also needs consideration. The benefit from a larger d is the acquisition of information from a deeper layer, yet a larger d causes a lower signal-to-noise ratio and less information for the shallow layer.

- It would be beneficial to conduct seismic tests using bender elements to validate the seismic surface wave results. [This was an original intention of this research, but repeated equipment malfunctions precluded its use and the test programme presented herein was devised to achieve the project's objectives without bender elements.]
- Field measurements are ultimately required to validate the measurement technique established in the laboratory. These might be carried out under a programme of research such as Mapping the Underworld.
- The shear modulus profile established from the seismic test could be validated via computer modelling.

REFERENCES

Abu-Hassanein, Z.S., Benson, C.H. and Blotz, L.R. (1996) *Electrical resistivity of compacted clay*. Journal of Geotechnical Engineering, ASCE, 122(5):397-406.

Adamo, F., Andria, G., Attivissimo, F., Giaquinto, N. (2004) *An acoustic method for soil moisture measurement*, IEEE Trans. Instrum. Meas. 891-898.

Adamo, F., Attivissimo, F., Fabbiano, L., Giaquinto, N. (2009) *Velocity moisture relationship for sandy soil*: Experimental results and data analysis 58 (2), 311-317.

Addo, K.O. and Robertson, P.K. (1992) *Shear-wave velocity measurement of soils using Rayleigh waves*. Canadian Geotechnical Journal, 29(4): 558-568.

Andrus, RD, Stokoe, KH. *(2000). Liquefaction resistance of soils from shearwave velocity.* Geotech Geoenviron Eng 2000;126(11):1015–25.

Al-Hunaidi M.O. (1993*) Insight on the SASW non-destructive testing method*. Canadian Geotechnical Journal*,* 20: 940–950.

Arulanandan, K and Muraleetharan, K (1988) *Level ground soil-liquefaction analysis using in-situ properties*. Journal Geotechnical Engineering ASCE, 114(7): 753-770

Asaka, Y and Abe, T. (2011) *Non-destructive technique for assessing cement-treated ground. Ground Improvement*, 164 (G13): 179–187.

Ashford, S.A., W. Jakrapiyanun and P. Lukkunaprasit, (1997). *Amplification of earthquake ground motions in Bangkok*, Bangkok, Chulalonglongkorn University.

Atkinson, J. (2007) *The mechanics of soils and foundations*. 2nd edition. Oxon: Taylor and Francis.

BSI (1990) *Methods of Test for Soils for Civil Engineering Purposes BS1377*. London: British Standards Institution.

Cassidy, N.J. (2007) *Frequency-dependent attenuation and velocity characteristics of magnetically lossy materials*.In IEEE Proceedings of the 4th International Workshop on Advanced Ground Penetrating Radar, Naples, pp. 142–146.

Chan C.M. (2006) *A laboratory investigation of shear wave velocity in stabilized soft soils*. PhD thesis, University of Sheffield.

Chen Yunmin C., , Han k., Ren-peng c., (2005). *Correlation of shear wave velocity with liquefaction resistance based on laboratory tests*. Civil Engineering Department, Institute of Geotechnical Engineering, Zhejiang University, Hangzhou

Charles, J.A. and Watts, K.S. (2002) *Treated ground engineering properties* London: Construction Industry Research and Information Association, ClRlA C572.

Christopher D.P. Baxter, P.E., M.ASCE; M.S. Ravi Sharma , *Shear wave velocity of weakly cemented sand during drained and undrained triaxial compression* . Civil and Environmental Engineering, The University of Rhode Island, Narraganset

Clayton, C.R.I. (2011) *Stiffness at small strain: research and practice*. Géotechnique, 61 (1): 5-37.

Clayton, C.R.I., Matthews, M.C. and Simons, N.E. (1995) *Site Investigation*. 2nd edition. London: Blackwell Science Ltd.

Cosenza, P., Marmet, E., Rejiba F., Cui, Y.J., Tabbagh, A. and Charlery, Y. (2006) *Correlations between geotechnical and electrical data: A case study at Garchy in France*. Journal of Applied Geophysics, 60 (2006): 165–178.

Crice, D. (2005) *MASW: the wave of the future*. Journal of Environmental and Engineering Geophysics, 10(2): 77–79.

Das, B .M. (1983) *Fundamental of Soil Dynamics*: Elsevier, New York.

Davich, P., Labuz, F.L., Guzina, L. And Drescher (2004)*A small strain and resilient modulus testing of granular soils*. Department of Transportation, University of Minnesota, August 2004.

Finck, F. (2003) *Introduction of a ground penetrating radar system for investigations on concrete structures*. 35 Otto-Graf-Journal Vol. 14, 2003.

Garcia-Bengochea, I., Lovell, C. and Altschaeffl (1979) *Pore Distribution and permeability of silty clay*. Journal of Geotechnical Engineering, ASCE, 105 (7): 839-856.

Giao P.H., Chung S.G., Kim D.Y., and Tanaka, H. (2003) *Electric imaging and laboratory testing for geotechnical investigation of Pusan clay deposits*. Journal of Applied Geophysics, 52 (2003): 157-175.

Gordon, M.A., Clayton, C.R.I., Thomas, T.C. and Matthews, M.C. (1996) *The selection in interpretation of seismic geophysical methods for site investigation*.In: Craig, C. (ed) Advances in site investigation practice. London: Thomas Telford. pp. 727-738.

Griffiths, D.H. and King, R.F. (1965*) Applied geophysics for geologist and engineers*. 2nd edition. Pergamon press,Oxford, UK.

Hardin, B.O., Black, W.L., (1968). *Vibration modulus of normally consolidated clay.* Journals of Soil Mechanics and Foundations Division ASCE 94 (SM2), 353–369.

Hardin, B.O., Drnevich, V.P., (1972). *Shear modulus and damping in soils.* Journal of the Soil Mechanics and Foundations Division ASCE 98 (SM7), 667–692.

Head, K.H. (1986) *Manual of soil laboratory testing*. Volume 3.. London: Pentech Press.

Heisey, J.S., Stokoe, K.H., and Meyer, A.H. (1982) *Moduli of pavement systems from spectral analysis of surface waves*. In Strength and deformation characteristics of pavements. Transportation Research Record 852, Washington, D.C., pp. 22–31.

Hunter, J. A., H. A. Christian, J. B. Harris, J. R. Britton, and J. L. Luternauer, (199*9). Mapping shear-wave velocity structure beneath the Fraser River delta sediments – Preliminary results,* Proceedings 8 th Canadian Conference on Earthquake Engineering, 101-106.

Ifeachor E.C. and Jervis B.W. (1993) *Digital signal processing: a practical approach*. Addison: Wesley Publishing, 184-191.

Inazaki ,T. (2006) , *Relationship between S-Wave Velocities and Geotechnical Properties Of Alluvial Sediments*. Public Works Research Institute, Tsukuba, JAPAN

John, U.E. (2011) *Chemical performance of cement stabilised contaminated clay*. PhD thesis, University of Birmingham

Kramer, S.L. (1996)*Geotechnical Earthquake Engineering*. New JERSEY: Prentice-Hall International Series.

Keller, G. and Frischknecht, F. (1966) *Electrical methods in geophysical prospecting*. New York: Pergamon Press.

Kretschmann, D.E. and Green, D.W. (1996a)*Moisture Content-Specific Gravity Relationship for Clear Southern Pine*, In: Gopu, K.A. Vijaya, ed. Proceedings of the international wood engineering conference; 1996 October 28-31; New Orleans, LA. Baton Rouge, LA: Louisiana State University: Vol. 2: 536-542.

Kretschmann, D.E. and Green, D.W. (1996b). *Modelling Moisture Content-Mechanical Property Relationships for Clear Southern Pine, Wood and Fiber Science*, 28(3) : 320-337

Lankston, R.W. (1990) *High-resolution refraction seismic data acquisition and interpretation*. In Ward, S.H. (ed) Investigations in Geophysics no. 5, Volume 1: Review and Tutorial. Oklahoma: Society of Exploration Geophysicists. pp. 1-30.

Lee, L. (2001) *Soil-pile interaction of bored and case in-situ piles*. PhD Thesis, University of Birmingham.

Luke, B. (1999) *Site investigations function better with seismic waves*. IEEE Potentials, 18(1), Feb.-March 1999: 33-35.

Luna, R. and Jadi, H. (2000*) Determination of dynamic soil properties using geophysical methods*. In Proceedings of the First International Conference on the Application of Geophysical and NDT Methodologies to Transportation Facilities and Infrastructure, St. Louis, December 2000, pp. 1-15.

Madun, A. (2011)*Seismic evaluation of vibro-stone column*. PhD thesis, University of Birmingham.

Madun, A., Jefferson, I., Chapman, D.N., Culshaw, M.G., Foo K.Y. and Atkins, P.R. (2010a) *Evaluation of the multi-channel surface wave analysis approach for the monitoring of multiple soil-stiffening columns*. Near Surface Geophysics, 8(6): 611-621.

Madun, A., Jefferson, I., Foo, K.Y.,Chapman, D.N., Culshaw, M.G., Atikins, P.R. (2012) *Laboratory scale seismic surface wave testing for the determination of soil elastic profiles*, International Journal of Integrated Engeenireng, Vol. 4 No. 2 P 9-24

Massarsch K.R. (2005) *Deformation properties of stabilized soil columns*. In Proceedings International Conference on Deep Mixing, Stockhom, 23 - 25 May 2005.

Matthews M.C., Hope V.S. and Clayton C.R.I. (1995) *The geotechnical value of ground stiffness determined using seismic methods*. Geological Society, London, Engineering Geology Special

Publications, 12: 113-123.

Matthews, M.C. Hope, Y.S. and Clayton, C.R.I. (1996) *The use of surface waves in the determination of ground stiffness profiles*. Proceedings of the Institution of Civil Engineers Geotechnical Engineering, 119: 84-95.

Matthews, M.C., Clayton, C.R.I. and Own, Y. (2000) *The use of field geophysical techniques to determine geotechnical stiffness parameters*. Proceedings of the Institution of Civil Engineers Geotechnical Engineering, 143: 31-42.

Mattsson, H., Larsson, R., Holm, G., Dannewitz, N. and Eriksson, H. (2005) *Down-hole technique improves quality control on dry mix columns*. In Proceedings of the International Conference on Deep Mixing Best Practice and Recent Advances, Stockholm, Sweden, Vol. 1, pp. 581-592.

McDowell, P.W., Barker, R.D. and Butcher, A.P., et al. (2002) *Geophysics in engineering investigations*. London: Construction Industry Research and Information Association, ClRlA C562.

Menzies B.K. (2001) *Near-surface site characterisation by ground stiffness profiling using surface wave geophysics*. In Instrumentation in Geotechnical Engineering (eds K.R. Saxena and V.M. Sharma), H.C.Verma Commemorative Volume, 43-71. Oxford& IBH Publishing Co. Pvt. Ltd., New Delhi, Calcultta.

Menzies, B. and Matthews, M. (1996) *The continuous surface-wave system: A modern technique for site investigation.*In Special lecture: Indian Geotechnical Conference Madras, December 11-14th 1996.

Milsom, J. (1939) *Field geophysics, The geological field guide series*. 3rd edition. London,UK: John Wiley & sons Ltd. 12-13.

Molnar S., Cassidy J.F.,. Monahan P.A., and Dosso S.E. (2007). *Comparison Of Geophysical Shear-Wave Velocity Methods***,** Ninth Canadian Conference on Earthquake Engineering Ottawa, Ontario, Canada 26-29

Monahan, P. A., and V. M. Levson, (2001). *Development of a shear-wave velocity model of the near surface deposits of southwestern British Columbia, Canada,* 4th International Conference in Earthquake Engineering and Soil Dynamics, San Diego, California, 26-31

Monahan, P. A., and V. M. Levson,(2000). *Quaternary Geological Map of Greater Victoria.* British Columbia Geological Survey, Ministry of Energy and Mines, Victoria, B.C.

Moxhay, A.L., Tinsley, R.D. and Sutton J.A. (2001) *Monitoring of soil stiffness during ground improvement using seismic surface waves*. Ground Engineering Magazine, January: 34-37.

Moxhay, A.L., Tinsley, R.D., Redgers, J.D. and Gravell, D.C. (2008) *The prediction of ground settlement from continuous surface wave data*. Ground Engineering Magazine, July: 34-38.

Ohkubo, T., Terasaki, A., (1976). *Physical Property and Seismic Wave Velocity of Rock. Oyo Corp.*

Park, C.B., Miller, R.D. and Xia, J. (2007) *Multichannel Analysis Of Surface Waves (MASW)-Active And Passive Methods*. The Leading Edge, January 2007, 60-64.

Park, C.B., Miller, R.D., and Xia, J. (1999) *Multichannel analysis of surface waves*. Geophysics,

64(3): 800-808.

Park, C.B., Miller, R.D., Ryden, N., Xia, J., and Ivanov, J., (2005) *Combined use of active and passive surface waves*. Journal of Engineering and Environmental Geophysics, 10 (3): 323-334.

Parasnis, D.S. (1962) *Principles of applied geophysics*. 5th edition. Thomas Press, New Dehli.

Pickett, G.R., (1963). *Acoustic character logs and their applications in formation evaluation*. Journal of Petroleum Technology 15, 650–667.
Rampello. S., Viggiani, G. M. B. & Amorosi, A. (1997). *Small-strain stiffness of reconstituted clay compressed along constant triaxial effective stress ratio paths*. Geotechnique 47, No. 3, 475– 489.

Redges, J.D., Moxhay, A.L., Ghataora, G.S. and Jefferson, I. (2008) *Case histories of settlement performance comparisons on ground improvements using stiffness, seismic waves and traditional methods*. In Proc. 6th International Conference on Case Histories in Geotechnical Engineering, Arlington, VA, 11-16 August 2008, Expanded Abstracts.

Reynolds, J.M. (1997) *An introduction to applied and environmental geophysics*. John Wiley & Sons.

Rhazi, J., Hassaim, M., Ballivy, G. and Hunaidi, O. (2002) *Effects of concrete non-homogeneity on Rayleigh waves dispersion*. Magazine of Concrete Research, 2002, 54, No. 3, June, 193–201.

Richart, F.E., Wood, R.D., Hall, J.R. (1970) *Vibration of soils and foundations*. New Jersey: Prentice-Hall.

Roy, D.R.N. (2010) *Continuous surface wave testing of vibro-stonecolumn ground improvement*. MSc thesis, University of Birmingham.

Sheriff, R.E. and Geldart, L.P. (1982) *Exploration seismology*, volume 1. Cambridge University Press.

Shibuya, S. and Tanaka, H. (1996) *Estimate of elastic shear modulus in Holocene soil deposits*. Soil Fdns, 36(4): 45-55.

Socco, L.V. and Strobbia, C. (2004) *Surface wave method for near-surface characterization: a tutorial*. Near Surface Geophysics, 2004, 165-185.

Staab, D.A., Edil, T.B. and Alumbaugh, D.L. (2004) *Non-Destructive Evaluation of Cement-Mixed Soils*. In Drilled Shafts, Micropiling, Deep Mixing, Remedial and Specialty Foundation Systems, Geotechnical Special Publication No. 124, ASCE. Orlando, Florida: Geo-Support 2004. pp. 838-848.

Steeples, D.W., and Miller, R.D. (1990) *Seismic reflection methods applied to engineering, environmental, and groundwater problems*: In Ward, S.H. (ed) Investigations in Geophysics no. 5, Volume 1: Review and Tutorial. Oklahoma: Society of Exploration Geophysicists. pp. 1-30.

Stokoe, K.H., Wright, G.W., III, Bay, J.A., and Roesset, J.M. (1994) *Characterisation of geotechnical sites by SASW method*. In Woods, R.D. (ed) Geophysical Characterisation of Sites. New York: Oxford Publishers.

Sutton, J.A. and Snelling, K. (1998) *Assessment of ground improvement using the continuous surface wave method*. In 4th meeting of the environmental and engineering geophysical society, Barcelona, 14-17th September 1998.

Tallavo F., Cascante G. and Pandey M. (2009) *Experimental and numerical analysis of MASW tests for detection of buried timber trestles*. Soil Dynamics and Earthquake Engineering, 29: 91-102.

Teachavorasinskun, S. & Amornwithayalax, T. (2002). *Elastic shear modulus of Bangkok clay during undrained triaxial compression.* Geotechnique 52, No. 7, 537–540.

Teachavorasinskun, S. & Akkarakun, T. (2004). *Path of elastic shear modulus of clays.* Geotechnique 54, No. 5, 331–333.

Thanop Thitimakorn T.(2010). *Comparison of Shear -Wave Velocity Profiles of Bangkok Subsoils from Multi-Channel Analysis of Surface Wave and Down-hole Seismic Methods*. Department of Geology, Faculty of Science, Chulalongkorn University , Thailand.

Thevanayagam, S. (1993) Electrical response of two-phase soil: theory and applications. Geotechnical Engineering ASCE, 119 (8): 1250-1275.

Thomas, A.M. (2010) *Measurement of electromagnetic signal velocities in saturated fine-grained soils*. PhD thesis, University of Birmingham.

Uma Maheswari R; Boominathan A. and Dodagoudar G.R (2008). *Development Of Empirical Correlation Between Shear Wave Velocity And Standard Penetration Resistance In Soils Of Chennai City*. The 14 th World Conference on Earthquake Engineering October 12-17, 2008, Beijing, China

Uyanık O, (2011), *The porosity of saturated shallow sediments from seismic compressional and shear wave velocities*,Süleyman Demirel University, Earthquake and Geotechnical Research Center, Turkey

Uyanık, O., Ulugergerli, E.U., (2008). *Quality control of compacted grounds using seismic velocities.* Near Surface Geophysics 6 (5), 299–306.

Wightman, W. (2003) *Application of geophysical methods to highway related problems*

Xia, J., Miller, R.D. , Park, C.B. et al (2002) *Comparing shear wave velocity profiles inverted from multichannel surface wave with borehole measurements*. Soil Dynamics and Earthquake Engineering, 22: 181-190.

Yang, Shu-Rong ,Lin, Horn-Da, Sheng Kung, Johson Hsiang, Liao, Jr-Ying (2008) *Shear wave velocity and suction of unsaturated soil usimg bender elementary and filter paper method*, Journal of GeoEngineering Vol. 3 No. 2 PP. 67-74

Yang, S.R., Lin, H.D., Kung, J.H. and Liao, J. (2008) *Shear wave velocity and suction of unsaturated soil using Bender element and filter paper method*. Journal of GeoEngineering, August, Vol. 3: 67-74.

Zerwer, A., Polak, M.A. and Santamarina, J.C. (2000) *Wave propagation in thin Plexiglas plates: implications for Rayleigh waves*. NDT&E International, 33(2000): 33-41.

Zerwer, A., Polak, M.A. and Santamarina, J.C. (2002) *Effect of surface cracks on Rayleigh wave propagation: an experimental study*. Journal Structural Engineering, 128(2): 240-248.

Online Sources

Central Weather Bureau (CWB). (n.d). *The main types of seismic waves*. [Online]. Available at: <http://www.cwb.gov.tw/V7e/knowledge/>. [Accessed 15th January 2012.]

Cube Surveys Ltd. [Online] [Accessed 2013]

Mapping the underworld. (n.d).*Mapping the Underworld*. [online] Available at: <http://www.mappingtheunderworld.ac.uk/>. [Accessed 10th July 2011].

Michigan Technological University. (2007). *Introduction to Seismology*. [online] Available at: <http://www.geo.mtu.edu/UPSeis/waves.html> [Accessed 26th December 2011]

GeoVision. (2010). *Spectral Analysis of Surface Waves (SASW)*. [online] Available at: <http://www.geovision.com/>. [Accessed 2nd January 2012]

PT. Mitra Intimarga. (2010). *Signal Antenna-GPR system*. [Online]. Available at:<http://www.ptmitra.com/index.html>. [Accessed 20th October 2011]

PmPrestij. (n.d). *Ground Penetrating Radar (GPR)*. [Online]. Available at: <http://pmprestij.com/Makaleler/GPR.pdf>. [Accessed 20th October 2011]

Radar Solutions International (RSI). (1996). *Radar Solutions International (RSI)*.[online]. Available at: <http://www.radar-solutions.com/html/methods.html>. [Accessed October 2012].

APPENDICES

Appendix A. Detail results of seismic surface wave testing

A.1 Data of seismic test result for Kaolinclay

Test ID: China Clay 24% moisture content,13-oct-08
Date of test: 13 October 2011
Test frequency range / interval: 3000 Hz to 6000 Hz / 100 Hz

Frequency(Hz)	Vel A-B(m/s)	Wave L A-B (cm)	Vel C-D (m/s)	Wave L C-D(cm)
2999.87793	256.8950001	8.56351512	206.4900544	6.883281895
3099.822998	363.0604587	11.71229644	248.5960206	8.019684374
3200.149536	587.7482224	18.36627369	249.8484843	7.807400294
3300.094604	450.0215365	13.63662532	207.9098654	6.30011834
3400.039673	365.8168678	10.7591941	193.8796739	5.702276813
3499.984741	320.4037213	9.154431947	230.5380361	6.586829748
3599.92981	306.6668148	8.518688725	242.9396327	6.748454707
3699.874878	283.491978	7.662204462	248.6328958	6.720035245
3799.819946	311.4399634	8.196176866	216.0849159	5.686714606
3900.146484	282.2230572	7.236216853	207.4880632	5.320006929
4000.091553	240.6211227	6.015390386	312.5396158	7.813311562
4100.036621	257.7601935	6.286777834	262.9016777	6.412178768
4199.981689	267.7506575	6.375043448	263.0560939	6.263267637
4299.926758	265.9377018	6.184703061	275.1940928	6.399971634
4399.871826	259.1340909	5.889582723	284.6345288	6.469155013
4499.816895	249.1811466	5.537584138	277.9063334	6.175947598
4600.143433	258.6954794	5.623639419	273.0527268	5.935743761
4700.088501	279.1750145	5.939782079	276.8550233	5.890421494
4800.033569	298.5818385	6.220411466	277.4797412	5.780787513
4899.978638	308.7822368	6.301705775	275.4857526	5.622182727
4999.923706	311.7890999	6.23587715	267.4142927	5.348367464
5099.868774	327.9152044	6.429875334	252.6997896	4.955025331
5199.813843	461.483561	8.875001586	235.757899	4.533968064
5300.140381	477.3198277	9.005795949	236.3162482	4.458679039
5400.085449	337.6930403	6.253475866	202.9209549	3.757735999
5500.030518	305.0757155	5.546800414	167.6494748	3.048155356
5599.975586	289.3101337	5.166274911	155.6627008	2.779703204
5699.920654	288.3338888	5.058559694	146.4858276	2.569962575
5799.865723	285.2140049	4.917596692	147.9894882	2.551601973
5899.810791	282.6207019	4.790335011	147.031328	2.492136328
6000.137329	280.5302798	4.675397652	123.078369	2.0512592

frequency (Hz)	Surface Vel A-B(m/s)	Shear wave Vel A-B	Vs2 (m/s)	G(kg/ms2), N/m2	G (Mpa)
2999.87793	256.8950001	77.06850003	5939.553697	10394218.97	10.39421897
3099.822998	363.0604587	108.9181376	11863.1607	20760531.23	20.76053123
3200.149536	587.7482224	176.3244667	31090.31756	54408055.74	54.40805574
3300.094604	971.3937731	291.4181319	84924.52762	148617923.3	148.6179233
3400.039673	365.8168678	109.7450603	12043.97827	21076961.97	21.07696197
3499.984741	320.4037213	96.12111639	9239.269016	16168720.78	16.16872078
3599.92981	306.6668148	92.00004444	8464.008177	14812014.31	14.81201431
3699.874878	283.491978	85.0475934	7233.093143	12657913	12.657913
3799.819946	311.4399634	93.43198902	8729.536572	15276689	15.276689
3900.146484	282.2230572	84.66691716	7168.486861	12544852.01	12.54485201
4000.091553	240.6211227	72.18633681	5210.867222	9119017.639	9.119017639
4100.036621	257.7601935	77.32805805	5979.628562	10464349.98	10.46434998
4199.981689	267.7506575	80.32519725	6452.137313	11291240.3	11.2912403
4299.926758	265.9377018	79.78131054	6365.057511	11138850.65	11.13885065
4399.871826	259.1340909	77.74022727	6043.542936	10576200.14	10.57620014
4499.816895	249.1811466	74.75434398	5588.211944	9779370.902	9.779370902
4600.143433	258.6954794	77.60864382	6023.101596	10540427.79	10.54042779
4700.088501	279.1750145	83.75250435	7014.481985	12275343.47	12.27534347
4800.033569	298.5818385	89.57455155	8023.600285	14041300.5	14.0413005
4899.978638	308.7822368	92.63467104	8581.182279	15017068.99	15.01706899
4999.923706	311.7890999	93.53672997	8749.119853	15310959.74	15.31095974
5099.868774	327.9152044	98.37456132	9677.554315	16935720.05	16.93572005
5199.813843	461.483561	138.4450683	19167.03694	33542314.64	33.54231464
5300.140381	477.3198277	143.1959483	20505.07961	35883889.32	35.88388932
5400.085449	337.6930403	101.3079121	10263.29305	17960762.84	17.96076284
5500.030518	305.0757155	91.52271465	8376.407297	14658712.77	14.65871277
5599.975586	289.3101337	86.79304011	7533.031812	13182805.67	13.18280567
5699.920654	288.3338888	86.50016664	7482.278829	13093987.95	13.09398795
5799.865723	285.2140049	85.56420147	7321.232573	12812157	12.812157
5899.810791	282.6207019	84.78621057	7188.701503	12580227.63	12.58022763
6000.137329	280.5302798	84.15908394	7082.75141	12394814.97	12.39481497

frequency (Hz)	Surface Vel C-D (m/s)	Shear wave Vel C-D	Vs2 (m/s)	G(kg/ms2), N/m2, pa	G (Mpa)

Test ID: China Clay 28% moisture content, 06-sep-03
Date of test: 06 September 2011

		(m/s)			
2999.87793	206.4900544	61.94701632	3837.432831	6715507.454	6.715507454
3099.822998	248.5960206	74.57880618	5561.998331	9733497.08	9.73349708
3200.149536	249.8484843	74.95454529	5618.18386	9831821.754	9.831821754
3300.094604	207.9098654	62.37295962	3890.386092	6808175.661	6.808175661
3400.039673	193.8796739	58.16390217	3383.039516	5920319.152	5.920319152
3499.984741	230.5380361	69.16141083	4783.300748	8370776.309	8.370776309
3599.92981	242.9396327	72.88188981	5311.769862	9295597.259	9.295597259
3699.874878	248.6328958	74.58986874	5563.648519	9736384.908	9.736384908
3799.819946	216.0849159	64.82547477	4202.342179	7354098.814	7.354098814
3900.146484	207.4880632	62.24641896	3874.616673	6780579.178	6.780579178
4000.091553	312.5396158	93.76188474	8791.29103	15384759.3	15.3847593
4100.036621	262.9016777	78.87050331	6220.556292	10885973.51	10.88597351
4199.981689	263.0560939	78.91682817	6227.865768	10898765.09	10.89876509
4299.926758	275.1940928	82.55822784	6815.860984	11927756.72	11.92775672
4399.871826	284.6345288	85.39035864	7291.513349	12760148.36	12.76014836
4499.816895	277.9063334	83.37190002	6950.873713	12164029	12.164029
4600.143433	273.0527268	81.91581804	6710.201245	11742852.18	11.74285218
4700.088501	276.8550233	83.05650699	6898.383353	12072170.87	12.07217087
4800.033569	277.4797412	83.24392236	6929.55061	12126713.57	12.12671357
4899.978638	275.4857526	82.64572578	6830.31599	11953052.98	11.95305298
4999.923706	267.4142927	80.22428781	6435.936355	11262888.62	11.26288862
5099.868774	252.6997896	75.809936	5747.14653	10057506.43	10.05750643
5199.813843	235.757899	70.7273697	5002.360825	8754131.443	8.754131443
5300.140381	236.3162482	70.89487446	5026.083225	8795645.643	8.795645643
5400.085449	202.9209549	60.87628647	3705.922254	6485363.945	6.485363945
5500.030518	167.6494748	50.29484244	2529.571176	4426749.558	4.426749558
5599.975586	155.6627008	46.69881024	2180.778878	3816363.036	3.816363036
5699.920654	146.4858276	43.94574828	1931.228792	3379650.386	3.379650386
5799.865723	147.9894882	44.39684646	1971.079976	3449389.957	3.449389957
5899.810791	147.031328	44.1093984	1945.639027	3404868.298	3.404868298
6000.137329	123.078369	36.9235107	1363.345642	2385854.874	2.385854874

Test frequency range / interval: 1500 Hz to 8000 Hz / 100 Hz

Frequency(Hz)	Vel A-B(m/s)	Wave L A-B (cm)	Vel C-D (m/s)	Wave L C-D(cm)
1499.938965	204.0603297	13.60457555	185.5496193	12.37047798
1599.884033	155.4146807	9.714121614	166.3088354	10.39505564
1699.829102	232.2209259	13.66142783	263.3858855	15.49484505
1800.15564	137.8072657	7.655297281	134.8791233	7.492636767
1900.100708	208.3568743	10.96557006	165.1012074	8.689076674
2000.045776	202.0243753	10.10098757	223.5298042	11.17623441
2099.990845	202.6089825	9.64808885	184.2863141	8.775577026
2199.935913	194.4299866	8.837984116	200.0720937	9.094451001
2299.880981	185.4874673	8.065089839	203.2403438	8.836993979
2399.82605	169.7584305	7.07378064	141.6182205	5.901186899
2500.152588	186.7202499	7.468354165	176.6647324	7.06615801
2600.097656	175.8744189	6.764146666	169.0788403	6.502788074
2700.042725	179.5232323	6.648903393	160.2334106	5.934476855
2799.987793	183.928679	6.568910032	160.5841922	5.735174724
2899.932861	187.8336806	6.477173424	156.5899057	5.399776932
2999.87793	183.0392826	6.101557693	148.1154073	4.937381145
3099.822998	182.4155122	5.884707364	152.1028107	4.906822447
3200.149536	179.774019	5.61767558	185.5280482	5.797480589
3300.094604	179.2663286	5.432157259	187.9971179	5.696719046
3400.039673	164.0931198	4.826211915	180.6851781	5.314207936
3499.984741	171.9030535	4.911537227	182.0761878	5.202199474
3599.92981	169.4220592	4.706260069	186.2576822	5.173925384
3699.874878	177.6869986	4.80251372	197.7880896	5.345804821
3799.819946	183.6142484	4.832182867	109.8923927	2.892042103
3900.146484	178.471374	4.5760172	148.1360738	3.798218204
4000.091553	171.2718893	4.281699231	161.3941751	4.034762029
4100.036621	168.360558	4.106318397	170.5358431	4.159373656
4199.981689	169.0463298	4.024930162	189.6033391	4.514384897
4299.926758	165.205558	3.842055162	202.9412639	4.719644667
4399.871826	164.0354927	3.728187983	206.3957188	4.69094844
4499.816895	165.7733522	3.684002174	207.2445725	4.605622348
4600.143433	164.6931294	3.580173789	200.0158228	4.348034484
4700.088501	161.1294837	3.428222333	196.8897059	4.1890638
4800.033569	158.7050808	3.306332727	199.0117826	4.146049809
4899.978638	161.3807364	3.293498774	205.9495648	4.203070668
4999.923706	165.0578768	3.301207908	216.1167406	4.322400767
5099.868774	168.9663859	3.313151639	214.859221	4.213034306
5199.813843	173.514342	3.33693373	208.3893491	4.007630953
5300.140381	177.4611992	3.348235828	211.1638336	3.984117748
5400.085449	179.4866471	3.323774203	216.0414794	4.00070483
5500.030518	179.7448464	3.268069982	218.3873116	3.97065636

5599.975586	178.8610308	3.193960903	225.9730452	4.035250543
5699.920654	180.5195385	3.167053535	239.7942913	4.206975954
5799.865723	184.617503	3.18313409	245.3199594	4.229752397
5899.810791	189.6929788	3.215238345	242.3182366	4.107220472
6000.137329	193.1999674	3.219925759	232.8136828	3.880139238
6100.082397	195.8667645	3.210887194	220.6348377	3.616915696
6200.027466	197.104792	3.179095465	213.4075341	3.442041754
6299.972534	195.743262	3.107049451	211.7055542	3.360420273
6399.917603	193.0590548	3.016586569	210.2239364	3.284791296
6499.862671	193.1153116	2.971067565	212.9562291	3.276318898
6600.189209	195.7583284	2.965950251	209.887684	3.180025259
6700.134277	196.5242579	2.933139094	202.7122599	3.025495483
6800.079346	198.9123056	2.925146833	198.0657612	2.912697796
6900.024414	198.4634212	2.87627129	196.0892242	2.84186276
6999.969482	197.5444296	2.822075583	194.588444	2.779847033
7099.914551	194.9950891	2.746442759	194.6264408	2.741250467
7199.859619	189.2056485	2.627907467	194.9330454	2.707456197
7300.186157	185.5178016	2.541274943	200.2680619	2.743328151
7400.131226	183.5415354	2.480247036	206.0007338	2.783744335
7500.076294	187.6297555	2.501704624	211.8077343	2.824074396
7600.021362	187.3196218	2.464724938	211.0318127	2.776726572
7699.966431	185.4020175	2.407828906	215.204071	2.79487025
7799.911499	181.956716	2.332804879	217.7837061	2.792130477
7899.856567	178.4413459	2.258792225	214.3989691	2.713960275
8000.183105	177.0605574	2.213206311	215.0390928	2.687927139

frequency (Hz)	Surface Vel A-B(m/s)	Shear wave Vel A-B(m/s)	Vs2 (m/s)	G(kg/ms2), N/m2	G (Mpa)
1499.938965	204.0603297	213.6511652	45646.8204	103161814.1	103.1618141
1599.884033	155.4146807	162.7191707	26477.5285	59839214.41	59.83921441
1699.829102	232.2209259	243.1353094	59114.77867	133599399.8	133.5993998
1800.15564	137.8072657	144.2842072	20817.93246	47048527.35	47.04852735
1900.100708	208.3568743	218.1496474	47589.26864	107551747.1	107.5517471
2000.045776	202.0243753	211.5195209	44740.50773	101113547.5	101.1135475
2099.990845	202.6089825	212.1316047	44999.81772	101699588.1	101.6995881
2199.935913	194.4299866	203.5681959	41440.01039	93654423.48	93.65442348
2299.880981	185.4874673	194.2053783	37715.72896	85237547.46	85.23754746
2399.82605	169.7584305	177.7370767	31590.46845	71394458.7	71.3944587
2500.152588	186.7202499	195.4961017	38218.72577	86374320.25	86.37432025
2600.097656	175.8744189	184.1405166	33907.72986	76631469.48	76.63146948
2700.042725	179.5232323	187.9608242	35329.27145	79844153.47	79.84415347
2799.987793	183.928679	192.573327	37084.48625	83810938.93	83.81093893
2899.932861	187.8336806	196.6618636	38675.88859	87407508.21	87.40750821

2999.87793	183.0392826	191.6421289	36726.70556	83002354.56	83.00235456
3099.822998	182.4155122	190.9890413	36476.81391	82437599.43	82.43759943
3200.149536	179.774019	188.2233979	35428.04753	80067387.41	80.06738741
3300.094604	179.2663286	187.691846	35228.22907	79615797.7	79.6157977
3400.039673	164.0931198	171.8054964	29517.12861	66708710.65	66.70871065
3499.984741	171.9030535	179.982497	32393.69923	73209760.26	73.20976026
3599.92981	169.4220592	177.3848959	31465.40131	71111806.95	71.11180695
3699.874878	177.6869986	186.0382876	34610.24444	78219152.44	78.21915244
3799.819946	183.6142484	192.2441181	36957.80095	83524630.14	83.52463014
3900.146484	178.471374	186.8595285	34916.48341	78911252.5	78.9112525
4000.091553	171.2718893	179.3216681	32156.26063	72673149.03	72.67314903
4100.036621	168.360558	176.2735043	31072.34831	70223507.17	70.22350717
4199.981689	169.0463298	176.9915073	31325.99366	70796745.68	70.79674568
4299.926758	165.205558	172.9702192	29918.69673	67616254.61	67.61625461
4399.871826	164.0354927	171.7451609	29496.40028	66661864.63	66.66186463
4499.816895	165.7733522	173.5646998	30124.705	68081833.3	68.0818333
4600.143433	164.6931294	172.4337065	29733.38314	67197445.89	67.19744589
4700.088501	161.1294837	168.7025694	28460.55692	64320858.64	64.32085864
4800.033569	158.7050808	166.1642196	27610.54787	62399838.2	62.3998382
4899.978638	161.3807364	168.965631	28549.38445	64521608.86	64.52160886
4999.923706	165.0578768	172.815597	29865.23057	67495421.09	67.49542109
5099.868774	168.9663859	176.907806	31296.37182	70729800.32	70.72980032
5199.813843	173.514342	181.6695161	33003.81308	74588617.56	74.58861756
5300.140381	177.4611992	185.8018755	34522.33695	78020481.51	78.02048151
5400.085449	179.4866471	187.9225195	35314.87333	79811613.73	79.81161373
5500.030518	179.7448464	188.1928541	35416.55035	80041403.79	80.04140379
5599.975586	178.8610308	187.2674992	35069.11627	79256202.78	79.25620278
5699.920654	180.5195385	189.0039569	35722.49571	80732840.3	80.7328403
5799.865723	184.617503	193.2945256	37362.77364	84439868.43	84.43986843
5899.810791	189.6929788	198.6085488	39445.35567	89146503.8	89.1465038
6000.137329	193.1999674	202.2803659	40917.34643	92473202.92	92.47320292
6100.082397	195.8667645	205.0725024	42054.73126	95043692.64	95.04369264
6200.027466	197.104792	206.3687172	42588.04744	96248987.21	96.24898721
6299.972534	195.743262	204.9431953	42001.71331	94923872.09	94.92387209
6399.917603	193.0590548	202.1328304	40857.68113	92338359.35	92.33835935
6499.862671	193.1153116	202.1917312	40881.49618	92392181.36	92.39218136
6600.189209	195.7583284	204.9589698	42008.17931	94938485.24	94.93848524
6700.134277	196.5242579	205.760898	42337.54714	95682856.53	95.68285653
6800.079346	198.9123056	208.261184	43372.72075	98022348.89	98.02234889
6900.024414	198.4634212	207.791202	43177.18364	97580435.02	97.58043502
6999.969482	197.5444296	206.8290178	42778.2426	96678828.27	96.67882827
7099.914551	194.9950891	204.1598583	41681.24772	94199619.86	94.19961986
7199.859619	189.2056485	198.098314	39242.94202	88689048.97	88.68904897
7300.186157	185.5178016	194.2371383	37728.06589	85265428.9	85.2654289

7400.131226	183.5415354	192.1679875	36928.53543	83458490.08	83.45849008
7500.076294	187.6297555	196.448354	38591.95577	87217820.05	87.21782005
7600.021362	187.3196218	196.123644	38464.48375	86929733.27	86.92973327
7699.966431	185.4020175	194.1159123	37680.98741	85159031.55	85.15903155
7799.911499	181.956716	190.5086817	36293.55779	82023440.61	82.02344061
7899.856567	178.4413459	186.8280892	34904.73491	78884700.9	78.8847009
8000.183105	177.0605574	185.3824036	34366.63557	77668596.38	77.66859638

frequency (Hz)	Surface Vel C-D (m/s)	Shear wave Vel C-D (m/s)	Vs2 (m/s)	G(kg/ms2), N/m2	G (Mpa)
1499.938965	185.5496193	194.2704514	37741.00829	85294678.73	85.29467873
1599.884033	166.3088354	174.1253506	30319.63773	68522381.27	68.52238127
1699.829102	263.3858855	275.7650221	76046.3474	171864745.1	171.8647451
1800.15564	134.8791233	141.2184421	19942.64839	45070385.36	45.07038536
1900.100708	165.1012074	172.8609641	29880.91293	67530863.21	67.53086321
2000.045776	223.5298042	234.035705	54772.71122	123786327.4	123.7863274
2099.990845	184.2863141	192.9477709	37228.84229	84137183.57	84.13718357
2199.935913	200.0720937	209.4754821	43879.97759	99168749.36	99.16874936
2299.880981	203.2403438	212.79264	45280.70764	102334399.3	102.3343993
2399.82605	141.6182205	148.2742768	21985.26116	49686690.23	49.68669023
2500.152588	176.6647324	184.9679748	34213.15169	77321722.82	77.32172282
2600.097656	169.0788403	177.0255458	31338.04386	70823979.13	70.82397913
2700.042725	160.2334106	167.7643809	28144.88749	63607445.72	63.60744572
2799.987793	160.5841922	168.1316492	28268.25147	63886248.32	63.88624832
2899.932861	156.5899057	163.9496312	26879.48159	60747628.38	60.74762838
2999.87793	148.1154073	155.0768314	24048.82364	54350341.43	54.35034143
3099.822998	152.1028107	159.2516428	25361.08573	57316053.75	57.31605375
3200.149536	185.5280482	194.2478664	37732.23362	85274847.98	85.27484798
3300.094604	187.9971179	196.8329824	38743.22296	87559683.9	87.5596839
3400.039673	180.6851781	189.1773815	35788.08167	80881064.57	80.88106457
3499.984741	182.0761878	190.6337686	36341.23374	82131188.25	82.13118825
3599.92981	186.2576822	195.0117933	38029.59952	85946894.92	85.94689492
3699.874878	197.7880896	207.0841298	42883.83681	96917471.2	96.9174712
3799.819946	109.8923927	115.0573352	13238.19037	29918310.24	29.91831024
3900.146484	148.1360738	155.0984692	24055.53516	54365509.45	54.36550945
4000.091553	161.3941751	168.9797013	28554.13946	64532355.18	64.53235518
4100.036621	170.5358431	178.5510277	31880.46951	72049861.09	72.04986109
4199.981689	189.6033391	198.514696	39408.08453	89062271.04	89.06227104
4299.926758	202.9412639	212.4795033	45147.53932	102033438.9	102.0334389
4399.871826	206.3957188	216.0963176	46697.61846	105536617.7	105.5366177
4499.816895	207.2445725	216.9850674	47082.51949	106406494	106.406494
4600.143433	200.0158228	209.4165664	43855.2983	99112974.15	99.11297415
4700.088501	196.8897059	206.1435221	42495.15171	96039042.87	96.03904287
4800.033569	199.0117826	208.3653364	43416.11341	98120416.32	98.12041632

4899.978638	205.9495648	215.6291944	46495.94947	105080845.8	105.0808458
4999.923706	216.1167406	226.2742274	51200.026	115712058.7	115.7120587
5099.868774	214.859221	224.9576044	50605.92379	114369387.8	114.3693878
5199.813843	208.3893491	218.1836485	47604.10447	107585276.1	107.5852761
5300.140381	211.1638336	221.0885338	48880.13976	110469115.9	110.4691159
5400.085449	216.0414794	226.1954289	51164.37206	115631480.9	115.6314809
5500.030518	218.3873116	228.6515152	52281.5154	118156224.8	118.1562248
5599.975586	225.9730452	236.5937783	55976.61595	126507152	126.507152
5699.920654	239.7942913	251.064623	63033.44494	142455585.6	142.4555856
5799.865723	245.3199594	256.8499975	65971.92124	149096542	149.096542
5899.810791	242.3182366	253.7071937	64367.34015	145470188.8	145.4701888
6000.137329	232.8136828	243.7559259	59416.95143	134282310.2	134.2823102
6100.082397	220.6348377	231.0046751	53363.1599	120600741.4	120.6007414
6200.027466	213.4075341	223.4376882	49924.40053	112829145.2	112.8291452
6299.972534	211.7055542	221.6557153	49131.25611	111036638.8	111.0366388
6399.917603	210.2239364	220.1044614	48445.97393	109487901.1	109.4879011
6499.862671	212.9562291	222.9651718	49713.46785	112352437.3	112.3524373
6600.189209	209.887684	219.7524052	48291.11957	109137930.2	109.1379302
6700.134277	202.7122599	212.2397361	45045.70558	101803294.6	101.8032946
6800.079346	198.0657612	207.374852	43004.32925	97189784.1	97.1897841
6900.024414	196.0892242	205.3054178	42150.31457	95259710.92	95.25971092
6999.969482	194.588444	203.7341009	41507.58386	93807139.51	93.80713951
7099.914551	194.6264408	203.7738835	41523.79559	93843778.03	93.84377803
7199.859619	194.9330454	204.0948985	41654.72761	94139684.4	94.1396844
7300.186157	200.2680619	209.6806608	43965.97952	99363113.71	99.36311371
7400.131226	206.0007338	215.6827683	46519.05653	105133067.8	105.1330678
7500.076294	211.8077343	221.7626978	49178.69412	111143848.7	111.1438487
7600.021362	211.0318127	220.9503079	48819.03854	110331027.1	110.3310271
7699.966431	215.204071	225.3186623	50768.49959	114736809.1	114.7368091
7799.911499	217.7837061	228.0195403	51992.91076	117503978.3	117.5039783
7899.856567	214.3989691	224.4757206	50389.34914	113879929.1	113.8799291
8000.183105	215.0390928	225.1459302	50690.68988	114560959.1	114.5609591

Test ID: China Clay 28% moisture content-Repeated, 26-oct-04
Date of test: 26 October 2011
Test frequency range / interval: 1500 Hz to 8000 Hz / 100 Hz

Frequency(Hz)	Vel A-B(m/s)	Wave L A-B (cm)	Vel C-D (m/s)	Wave L C-D(cm)
1499.938965	204.0603297	13.60457555	185.5496193	12.37047798

1599.884033	155.4146807	9.714121614	166.3088354	10.39505564
1699.829102	232.2209259	13.66142783	263.3858855	15.49484505
1800.15564	137.8072657	7.655297281	134.8791233	7.492636767
1900.100708	208.3568743	10.96557006	165.1012074	8.689076674
2000.045776	202.0243753	10.10098757	223.5298042	11.17623441
2099.990845	202.6089825	9.64808885	184.2863141	8.775577026
2199.935913	194.4299866	8.837984116	200.0720937	9.094451001
2299.880981	185.4874673	8.065089839	203.2403438	8.836993979
2399.82605	169.7584305	7.07378064	141.6182205	5.901186899
2500.152588	186.7202499	7.468354165	176.6647324	7.06615801
2600.097656	175.8744189	6.764146666	169.0788403	6.502788074
2700.042725	179.5232323	6.648903393	160.2334106	5.934476855
2799.987793	183.928679	6.568910032	160.5841922	5.735174724
2899.932861	187.8336806	6.477173424	156.5899057	5.399776932
2999.87793	183.0392826	6.101557693	148.1154073	4.937381145
3099.822998	182.4155122	5.884707364	152.1028107	4.906822447
3200.149536	179.774019	5.61767558	185.5280482	5.797480589
3300.094604	179.2663286	5.432157259	187.9971179	5.696719046
3400.039673	164.0931198	4.826211915	180.6851781	5.314207936
3499.984741	171.9030535	4.911537227	182.0761878	5.202199474
3599.92981	169.4220592	4.706260069	186.2576822	5.173925384
3699.874878	177.6869986	4.80251372	197.7880896	5.345804821
3799.819946	183.6142484	4.832182867	109.8923927	2.892042103
3900.146484	178.471374	4.5760172	148.1360738	3.798218204
4000.091553	171.2718893	4.281699231	161.3941751	4.034762029
4100.036621	168.360558	4.106318397	170.5358431	4.159373656
4199.981689	169.0463298	4.024930162	189.6033391	4.514384897
4299.926758	165.205558	3.842055162	202.9412639	4.719644667
4399.871826	164.0354927	3.728187983	206.3957188	4.69094844
4499.816895	165.7733522	3.684002174	207.2445725	4.605622348
4600.143433	164.6931294	3.580173789	200.0158228	4.348034484
4700.088501	161.1294837	3.428222333	196.8897059	4.1890638
4800.033569	158.7050808	3.306332727	199.0117826	4.146049809
4899.978638	161.3807364	3.293498774	205.9495648	4.203070668
4999.923706	165.0578768	3.301207908	216.1167406	4.322400767
5099.868774	168.9663859	3.313151639	214.859221	4.213034306
5199.813843	173.514342	3.33693373	208.3893491	4.007630953
5300.140381	177.4611992	3.348235828	211.1638336	3.984117748
5400.085449	179.4866471	3.323774203	216.0414794	4.00070483
5500.030518	179.7448464	3.268069982	218.3873116	3.97065636
5599.975586	178.8610308	3.193960903	225.9730452	4.035250543
5699.920654	180.5195385	3.167053535	239.7942913	4.206975954
5799.865723	184.617503	3.18313409	245.3199594	4.229752397
5899.810791	189.6929788	3.215238345	242.3182366	4.107220472

6000.137329	193.1999674	3.219925759	232.8136828	3.880139238
6100.082397	195.8667645	3.210887194	220.6348377	3.616915696
6200.027466	197.104792	3.179095465	213.4075341	3.442041754
6299.972534	195.743262	3.107049451	211.7055542	3.360420273
6399.917603	193.0590548	3.016586569	210.2239364	3.284791296
6499.862671	193.1153116	2.971067565	212.9562291	3.276318898
6600.189209	195.7583284	2.965950251	209.887684	3.180025259
6700.134277	196.5242579	2.933139094	202.7122599	3.025495483
6800.079346	198.9123056	2.925146833	198.0657612	2.912697796
6900.024414	198.4634212	2.87627129	196.0892242	2.84186276
6999.969482	197.5444296	2.822075583	194.588444	2.779847033
7099.914551	194.9950891	2.746442759	194.6264408	2.741250467
7199.859619	189.2056485	2.627907467	194.9330454	2.707456197
7300.186157	185.5178016	2.541274943	200.2680619	2.743328151
7400.131226	183.5415354	2.480247036	206.0007338	2.783744335
7500.076294	187.6297555	2.501704624	211.8077343	2.824074396
7600.021362	187.3196218	2.464724938	211.0318127	2.776726572
7699.966431	185.4020175	2.407828906	215.204071	2.79487025
7799.911499	181.956716	2.332804879	217.7837061	2.792130477
7899.856567	178.4413459	2.258792225	214.3989691	2.713960275
8000.183105	177.0605574	2.213206311	215.0390928	2.687927139

frequency (Hz)	Surface Vel A-B (m/s)	Shear wave Vel A-B (m/s)	Vs2 (m/s)	G(kg/ms2), N/m2	G (Mpa)
1499.938965	204.0603297	213.6511652	45646.8204	103161814.1	103.1618141
1599.884033	155.4146807	162.7191707	26477.5285	59839214.41	59.83921441
1699.829102	232.2209259	243.1353094	59114.77867	133599399.8	133.5993998
1800.15564	137.8072657	144.2842072	20817.93246	47048527.35	47.04852735
1900.100708	208.3568743	218.1496474	47589.26864	107551747.1	107.5517471
2000.045776	202.0243753	211.5195209	44740.50773	101113547.5	101.1135475
2099.990845	202.6089825	212.1316047	44999.81772	101699588.1	101.6995881
2199.935913	194.4299866	203.5681959	41440.01039	93654423.48	93.65442348
2299.880981	185.4874673	194.2053783	37715.72896	85237547.46	85.23754746
2399.82605	169.7584305	177.7370767	31590.46845	71394458.7	71.3944587
2500.152588	186.7202499	195.4961017	38218.72577	86374320.25	86.37432025
2600.097656	175.8744189	184.1405166	33907.72986	76631469.48	76.63146948
2700.042725	179.5232323	187.9608242	35329.27145	79844153.47	79.84415347
2799.987793	183.928679	192.573327	37084.48625	83810938.93	83.81093893
2899.932861	187.8336806	196.6618636	38675.88859	87407508.21	87.40750821
2999.87793	183.0392826	191.6421289	36726.70556	83002354.56	83.00235456
3099.822998	182.4155122	190.9890413	36476.81391	82437599.43	82.43759943
3200.149536	179.774019	188.2233979	35428.04753	80067387.41	80.06738741
3300.094604	179.2663286	187.691846	35228.22907	79615797.7	79.6157977
3400.039673	164.0931198	171.8054964	29517.12861	66708710.65	66.70871065

3499.984741	171.9030535	179.982497	32393.69923	73209760.26	73.20976026
3599.92981	169.4220592	177.3848959	31465.40131	71111806.95	71.11180695
3699.874878	177.6869986	186.0382876	34610.24444	78219152.44	78.21915244
3799.819946	183.6142484	192.2441181	36957.80095	83524630.14	83.52463014
3900.146484	178.471374	186.8595285	34916.48341	78911252.5	78.9112525
4000.091553	171.2718893	179.3216681	32156.26063	72673149.03	72.67314903
4100.036621	168.360558	176.2735043	31072.34831	70223507.17	70.22350717
4199.981689	169.0463298	176.9915073	31325.99366	70796745.68	70.79674568
4299.926758	165.205558	172.9702192	29918.69673	67616254.61	67.61625461
4399.871826	164.0354927	171.7451609	29496.40028	66661864.63	66.66186463
4499.816895	165.7733522	173.5646998	30124.705	68081833.3	68.0818333
4600.143433	164.6931294	172.4337065	29733.38314	67197445.89	67.19744589
4700.088501	161.1294837	168.7025694	28460.55692	64320858.64	64.32085864
4800.033569	158.7050808	166.1642196	27610.54787	62399838.2	62.3998382
4899.978638	161.3807364	168.965631	28549.38445	64521608.86	64.52160886
4999.923706	165.0578768	172.815597	29865.23057	67495421.09	67.49542109
5099.868774	168.9663859	176.907806	31296.37182	70729800.32	70.72980032
5199.813843	173.514342	181.6695161	33003.81308	74588617.56	74.58861756
5300.140381	177.4611992	185.8018755	34522.33695	78020481.51	78.02048151
5400.085449	179.4866471	187.9225195	35314.87333	79811613.73	79.81161373
5500.030518	179.7448464	188.1928541	35416.55035	80041403.79	80.04140379
5599.975586	178.8610308	187.2674992	35069.11627	79256202.78	79.25620278
5699.920654	180.5195385	189.0039569	35722.49571	80732840.3	80.7328403
5799.865723	184.617503	193.2945256	37362.77364	84439868.43	84.43986843
5899.810791	189.6929788	198.6085488	39445.35567	89146503.8	89.1465038
6000.137329	193.1999674	202.2803659	40917.34643	92473202.92	92.47320292
6100.082397	195.8667645	205.0725024	42054.73126	95043692.64	95.04369264
6200.027466	197.104792	206.3687172	42588.04744	96248987.21	96.24898721
6299.972534	195.743262	204.9431953	42001.71331	94923872.09	94.92387209
6399.917603	193.0590548	202.1328304	40857.68113	92338359.35	92.33835935
6499.862671	193.1153116	202.1917312	40881.49618	92392181.36	92.39218136
6600.189209	195.7583284	204.9589698	42008.17931	94938485.24	94.93848524
6700.134277	196.5242579	205.760898	42337.54714	95682856.53	95.68285653
6800.079346	198.9123056	208.261184	43372.72075	98022348.89	98.02234889
6900.024414	198.4634212	207.791202	43177.18364	97580435.02	97.58043502
6999.969482	197.5444296	206.8290178	42778.2426	96678828.27	96.67882827
7099.914551	194.9950891	204.1598583	41681.24772	94199619.86	94.19961986
7199.859619	189.2056485	198.098314	39242.94202	88689048.97	88.68904897
7300.186157	185.5178016	194.2371383	37728.06589	85265428.9	85.2654289
7400.131226	183.5415354	192.1679875	36928.53543	83458490.08	83.45849008
7500.076294	187.6297555	196.448354	38591.95577	87217820.05	87.21782005
7600.021362	187.3196218	196.123644	38464.48375	86929733.27	86.92973327
7699.966431	185.4020175	194.1159123	37680.98741	85159031.55	85.15903155
7799.911499	181.956716	190.5086817	36293.55779	82023440.61	82.02344061

7899.856567	178.4413459	186.8280892	34904.73491	78884700.9	78.8847009
8000.183105	177.0605574	185.3824036	34366.63557	77668596.38	77.66859638

frequency (Hz)	Surface Vel C-D (m/s)	Shear wave Vel C-D (m/s)	Vs2 (m/s)	G(kg/ms2), N/m2	G (Mpa)
1499.938965	185.5496193	194.2704514	37741.00829	85294678.73	85.29467873
1599.884033	166.3088354	174.1253506	30319.63773	68522381.27	68.52238127
1699.829102	263.3858855	275.7650221	76046.3474	171864745.1	171.8647451
1800.15564	134.8791233	141.2184421	19942.64839	45070385.36	45.07038536
1900.100708	165.1012074	172.8609641	29880.91293	67530863.21	67.53086321
2000.045776	223.5298042	234.035705	54772.71122	123786327.4	123.7863274
2099.990845	184.2863141	192.9477709	37228.84229	84137183.57	84.13718357
2199.935913	200.0720937	209.4754821	43879.97759	99168749.36	99.16874936
2299.880981	203.2403438	212.79264	45280.70764	102334399.3	102.3343993
2399.82605	141.6182205	148.2742768	21985.26116	49686690.23	49.68669023
2500.152588	176.6647324	184.9679748	34213.15169	77321722.82	77.32172282
2600.097656	169.0788403	177.0255458	31338.04386	70823979.13	70.82397913
2700.042725	160.2334106	167.7643809	28144.88749	63607445.72	63.60744572
2799.987793	160.5841922	168.1316492	28268.25147	63886248.32	63.88624832
2899.932861	156.5899057	163.9496312	26879.48159	60747628.38	60.74762838
2999.87793	148.1154073	155.0768314	24048.82364	54350341.43	54.35034143
3099.822998	152.1028107	159.2516428	25361.08573	57316053.75	57.31605375
3200.149536	185.5280482	194.2478664	37732.23362	85274847.98	85.27484798
3300.094604	187.9971179	196.8329824	38743.22296	87559683.9	87.5596839
3400.039673	180.6851781	189.1773815	35788.08167	80881064.57	80.88106457
3499.984741	182.0761878	190.6337686	36341.23374	82131188.25	82.13118825
3599.92981	186.2576822	195.0117933	38029.59952	85946894.92	85.94689492
3699.874878	197.7880896	207.0841298	42883.83681	96917471.2	96.9174712
3799.819946	109.8923927	115.0573352	13238.19037	29918310.24	29.91831024
3900.146484	148.1360738	155.0984692	24055.53516	54365509.45	54.36550945
4000.091553	161.3941751	168.9797013	28554.13946	64532355.18	64.53235518
4100.036621	170.5358431	178.5510277	31880.46951	72049861.09	72.04986109
4199.981689	189.6033391	198.514696	39408.08453	89062271.04	89.06227104
4299.926758	202.9412639	212.4795033	45147.53932	102033438.9	102.0334389
4399.871826	206.3957188	216.0963176	46697.61846	105536617.7	105.5366177
4499.816895	207.2445725	216.9850674	47082.51949	106406494	106.406494
4600.143433	200.0158228	209.4165664	43855.2983	99112974.15	99.11297415
4700.088501	196.8897059	206.1435221	42495.15171	96039042.87	96.03904287
4800.033569	199.0117826	208.3653364	43416.11341	98120416.32	98.12041632
4899.978638	205.9495648	215.6291944	46495.94947	105080845.8	105.0808458
4999.923706	216.1167406	226.2742274	51200.026	115712058.7	115.7120587
5099.868774	214.859221	224.9576044	50605.92379	114369387.8	114.3693878
5199.813843	208.3893491	218.1836485	47604.10447	107585276.1	107.5852761
5300.140381	211.1638336	221.0885338	48880.13976	110469115.9	110.4691159

5400.085449	216.0414794	226.1954289	51164.37206	115631480.9	115.6314809
5500.030518	218.3873116	228.6515152	52281.5154	118156224.8	118.1562248
5599.975586	225.9730452	236.5937783	55976.61595	126507152	126.507152
5699.920654	239.7942913	251.064623	63033.44494	142455585.6	142.4555856
5799.865723	245.3199594	256.8499975	65971.92124	149096542	149.096542
5899.810791	242.3182366	253.7071937	64367.34015	145470188.8	145.4701888
6000.137329	232.8136828	243.7559259	59416.95143	134282310.2	134.2823102
6100.082397	220.6348377	231.0046751	53363.1599	120600741.4	120.6007414
6200.027466	213.4075341	223.4376882	49924.40053	112829145.2	112.8291452
6299.972534	211.7055542	221.6557153	49131.25611	111036638.8	111.0366388
6399.917603	210.2239364	220.1044614	48445.97393	109487901.1	109.4879011
6499.862671	212.9562291	222.9651718	49713.46785	112352437.3	112.3524373
6600.189209	209.887684	219.7524052	48291.11957	109137930.2	109.1379302
6700.134277	202.7122599	212.2397361	45045.70558	101803294.6	101.8032946
6800.079346	198.0657612	207.374852	43004.32925	97189784.1	97.1897841
6900.024414	196.0892242	205.3054178	42150.31457	95259710.92	95.25971092
6999.969482	194.588444	203.7341009	41507.58386	93807139.51	93.80713951
7099.914551	194.6264408	203.7738835	41523.79559	93843778.03	93.84377803
7199.859619	194.9330454	204.0948985	41654.72761	94139684.4	94.1396844
7300.186157	200.2680619	209.6806608	43965.97952	99363113.71	99.36311371
7400.131226	206.0007338	215.6827683	46519.05653	105133067.8	105.1330678
7500.076294	211.8077343	221.7626978	49178.69412	111143848.7	111.1438487
7600.021362	211.0318127	220.9503079	48819.03854	110331027.1	110.3310271
7699.966431	215.204071	225.3186623	50768.49959	114736809.1	114.7368091
7799.911499	217.7837061	228.0195403	51992.91076	117503978.3	117.5039783
7899.856567	214.3989691	224.4757206	50389.34914	113879929.1	113.8799291
8000.183105	215.0390928	225.1459302	50690.68988	114560959.1	114.5609591

Test ID: China Clay 33% moisture content, 25-Agu-02
Date of test: 25 August 2011
Test frequency range / interval: 1000 Hz to 4000 Hz / 100 Hz

Frequency(Hz)	Vel A-B(m/s)	Wave L A-B (cm)	Vel C-D (m/s)	Wave L C-D(cm)
999.8321533	75.875766	7.588850363	81.0379549	8.105155913
1100.158691	70.8165959	6.436943728	69.6229592	6.328446957
1200.10376	66.447315	5.536797498	67.2536423	5.603985636
1300.048828	61.961702	4.766105757	62.5951987	4.814834439
1399.993896	70.9556478	5.068282654	62.112059	4.436594983
1499.938965	62.6387264	4.176085019	50.4430734	3.363008402

1599.884033	60.0246634	3.751813394	48.8012347	3.050298253
1699.829102	64.0635884	3.768825251	51.8669313	3.051302699
1800.15564	62.410619	3.466956833	53.4246654	2.967780355
1900.100708	64.9809211	3.419867211	54.7956349	2.883827927
2000.045776	65.1464834	3.257249619	56.0337064	2.801621194
2099.990845	66.4980689	3.166588512	55.7621016	2.655349749
2199.935913	69.3012354	3.150147921	56.504116	2.56844373
2299.880981	71.392966	3.104202632	54.1303066	2.353613382
2399.82605	69.1651304	2.882089326	57.0799168	2.378502259
2500.152588	71.9753029	2.878836406	57.3699309	2.294657182
2600.097656	68.5374595	2.635957128	55.8460653	2.147844914
2700.042725	66.7660726	2.472778376	58.8730142	2.180447505
2799.987793	66.9998654	2.392862768	57.8614328	2.066488751
2899.932861	67.2910346	2.320434224	58.8613227	2.029747772
2999.87793	66.4009166	2.213453951	58.5780501	1.952681123
3099.822998	66.170738	2.134661819	57.8058254	1.86481052
3200.149536	66.6281041	2.082030959	57.1535093	1.785963706
3300.094604	69.8523631	2.116677594	57.0229346	1.727918179
3400.039673	71.3220956	2.097684217	56.8672344	1.672546201
3499.984741	69.817634	1.994798241	56.3863029	1.611044249
3599.92981	70.1319299	1.948147148	58.2431217	1.617896037
3699.874878	65.8299688	1.779248514	59.4008112	1.605481621
3799.819946	65.8879549	1.733975711	59.8051155	1.573893404
3900.146484	66.2398437	1.698393738	59.4345716	1.523906137
4000.091553	66.8085275	1.670174959	58.7802767	1.469473284

frequency (Hz)	Surface Vel A-B (m/s)	Shear wave Vel A-B (m/s)	Vs2 (m/s)	G(kg/ms2), N/m2	G (Mpa)
999.8322	75.875766	22.7627298	518.141868	1108823.597	1.108823597
1100.159	70.81659588	21.24497876	451.349123	965887.1225	0.965887123
1200.104	66.44731495	19.93419449	397.37211	850376.3149	0.850376315
1300.049	61.96170204	18.58851061	345.532727	739440.0353	0.739440035
1399.994	70.95564781	21.28669434	453.123356	969683.982	0.969683982
1499.939	62.6387264	18.79161792	353.124904	755687.2947	0.755687295
1599.884	60.02466344	18.00739903	324.26642	693930.1386	0.693930139
1699.829	64.0635884	19.21907652	369.372902	790458.0109	0.790458011
1800.156	62.41061896	18.72318569	350.557682	750193.4401	0.75019344
1900.101	64.98092108	19.49427632	380.026809	813257.3721	0.813257372

2000.046	65.14648343	19.54394503	381.965787	817406.7848	0.817406785
2099.991	66.49806885	19.94942066	397.979384	851675.8828	0.851675883
2199.936	69.30123544	20.79037063	432.239511	924992.5536	0.924992554
2299.881	71.39296595	21.41788979	458.726003	981673.6461	0.981673646
2399.826	69.16513043	20.74953913	430.543374	921362.8205	0.921362821
2500.153	71.97530291	21.59259087	466.239981	997753.5585	0.997753559
2600.098	68.53745951	20.56123785	422.764502	904716.0344	0.904716034
2700.043	66.76607263	20.02982179	401.193761	858554.6483	0.858554648
2799.988	66.99986541	20.09995962	404.008377	864577.9265	0.864577926
2899.933	67.2910346	20.18731038	407.5275	872108.8508	0.872108851
2999.878	66.40091656	19.92027497	396.817355	849189.1393	0.849189139
3099.823	66.17073799	19.8512214	394.070991	843311.9206	0.843311921
3200.15	66.62810408	19.98843122	399.537383	855009.9992	0.855009999
3300.095	69.85236309	20.95570893	439.141737	939763.3164	0.939763316
3400.04	71.3220956	21.39662868	457.815719	979725.6384	0.979725638
3499.985	69.81763404	20.94529021	438.705182	938829.0896	0.93882909
3599.93	70.13192992	21.03957898	442.663883	947300.7107	0.947300711
3699.875	65.8299688	19.74899064	390.022631	834648.431	0.834648431
3799.82	65.88795493	19.76638648	390.710034	836119.4737	0.836119474
3900.146	66.23984367	19.8719531	394.89452	845074.2729	0.845074273
4000.092	66.80852747	20.04255824	401.704141	859646.8614	0.859646861

frequency (Hz)	Surface Vel C-D (m/s)	Shear wave Vel C-D (m/s)	Vs2 (m/s)	G(kg/ms2), N/m2	G (Mpa)
999.8321533	81.03795489	24.31138647	591.0435119	1264833.116	1.264833116
1100.158691	69.62295923	20.88688777	436.2620807	933600.8526	0.933600853
1200.10376	67.25364232	20.1760927	407.0747165	871139.8933	0.871139893
1300.048828	62.5951987	18.77855961	352.634301	754637.4042	0.754637404
1399.993896	62.11205898	18.63361769	347.2117084	743033.0559	0.743033056
1499.938965	50.44307341	15.13292202	229.005329	490071.404	0.490071404
1599.884033	48.80123471	14.64037041	214.3404458	458688.5541	0.458688554
1699.829102	51.86693125	15.56007938	242.1160702	518128.3901	0.51812839
1800.15564	53.42466544	16.02739963	256.877539	549717.9334	0.549717933
1900.100708	54.79563486	16.43869046	270.230544	578293.3641	0.578293364
2000.045776	56.03370637	16.81011191	282.5798625	604720.9057	0.604720906
2099.990845	55.76210162	16.72863049	279.8470779	598872.7468	0.598872747
2199.935913	56.50411603	16.95123481	287.3443615	614916.9337	0.614916934
2299.880981	54.13030655	16.23909197	263.7081078	564335.3508	0.564335351
2399.82605	57.07991681	17.12397504	293.2305213	627513.3155	0.627513316
2500.152588	57.36993092	17.21097928	296.2178076	633906.1083	0.633906108
2600.097656	55.84606527	16.75381958	280.6904706	600677.607	0.600677607
2700.042725	58.87301421	17.66190426	311.9428622	667557.7251	0.667557725
2799.987793	57.86143276	17.35842983	301.3150861	644814.2842	0.644814284
2899.932861	58.86132265	17.6583968	311.8189774	667292.6116	0.667292612

2999.87793	58.57805005	17.57341502	308.8249153	660885.3187	0.660885319
3099.822998	57.80582536	17.34174761	300.7362101	643575.4896	0.64357549
3200.149536	57.15350926	17.14605278	293.9871259	629132.4494	0.629132449
3300.094604	57.02293458	17.10688037	292.6453561	626261.0621	0.626261062
3400.039673	56.86723439	17.06017032	291.0494112	622845.7401	0.62284574
3499.984741	56.3863029	16.91589087	286.1473639	612355.3588	0.612355359
3599.92981	58.24312172	17.47293652	305.3035105	653349.5125	0.653349512
3699.874878	59.40081115	17.82024335	317.5610729	679580.696	0.679580696
3799.819946	59.80511549	17.94153465	321.8986655	688863.1441	0.688863144
3900.146484	59.43457164	17.83037149	317.9221475	680353.3957	0.680353396
4000.091553	58.7802767	17.63408301	310.9608836	665456.2909	0.665456291

A.2 Data of seismic test result for Oxfordclay

Test ID: OxfordClay 19% moisture, 16-June-01
Date of test: 16 June 2011
Test frequency range / interval: 2000 Hz to 6000 Hz / 100 Hz

Frequency(Hz)	Vel A-B(m/s)	Wave L A-B (cm)	Vel C-D (m/s)	Wave L C-D(cm)
2000.045776	219.9575946	10.99762801	220.2956016	230.6494948
2050.018311	256.679302	12.52082973	258.7432292	270.904161
2099.990845	272.1624088	12.96017121	274.954042	287.876882
2149.963379	261.734848	12.17392122	264.0363859	276.446096
2199.935913	251.852126	11.40942327	252.797	264.678459
2249.908447	261.65223	11.60047202	263.267	275.640549
2299.880981	266.215365	11.56581589	268.502	281.121594
2349.853516	271.584639	11.53263377	273.737	286.602639
2399.82605	270.593254	11.25081545	272.69	285.50643

2450.180054	269.523654	10.97878499	271.643	284.410221
2500.152588	271.548563	10.83933842	273.737	286.602639
2550.125122	269.5684526	10.54850202	271.643	284.410221
2600.097656	256.548712	9.845784038	258.032	270.159504
2650.07019	259.890254	9.77332604	261.173	273.448131
2700.042725	269.521045	9.962805312	271.643	284.410221
2750.015259	268.536021	9.745400472	270.596	283.314012
2799.987793	261.008546	9.32146921	263.267	275.640549
2849.960327	265.4128027	9.29837505	267.455	280.025385
2899.932861	267.536982	9.207109708	269.549	282.217803
2949.905396	271.2536001	9.18673529	273.737	286.602639
2999.87793	267.586203	8.900362157	269.549	282.217803
3049.850464	272.101452	8.918470044	274.784	287.698848
3099.822998	274.518202	8.839214374	276.878	289.891266
3150.177002	271.0879963	8.602691209	273.737	286.602639
3200.149536	275.203698	8.593348432	277.925	290.987475
3250.12207	268.102546	8.245844131	270.596	283.314012
3300.094604	269.085479	8.15128147	271.643	284.410221
3350.067139	270.302587	8.059539968	272.69	285.50643
3400.039673	259.54893	7.617558173	261.173	273.448131
3450.012207	255.485693	7.391278195	256.985	269.063295
3499.984741	275.0719894	7.859233959	278.0003729	291.0663904
3549.957275	290.1384254	8.173011755	293.7749314	307.5823532
3599.92981	291.1145132	8.086671923	294.7968953	308.6523494
3649.902344	286.6597798	7.853902728	290.1327894	303.7690305
3699.874878	280.1200115	7.571067151	299.26359	313.053466
3749.847412	271.7956717	7.248179509	298.325471	312.006454
3799.819946	265.5276043	6.987899638	300.320145	314.124454
3850.17395	283.5519725	7.364653549	305.321475	319.3354454
3900.146484	286.4296491	7.344074133	300.201471	314.11145
3950.119019	284.26845	7.196452783	295.21493	308.865545
4000.091553	293.8042152	7.344937267	292.583	306.334401
4050.064087	297.4643534	7.344682628	288.395	301.949565
4100.036621	284.2085446	6.931853806	310.361725	324.5754
4150.009155	276.55754	6.664022407	312.980321	326.664245
4199.981689	274.0378162	6.524738355	310.0017633	324.577572
4249.954224	273.2473271	6.429418124	300.367152	314.12447
4299.926758	273.1851625	6.353251529	310.571201	324.576687
4349.899292	272.5781939	6.266310449	315.971503	329.805431
4399.871826	271.5197047	6.171082145	310.3471205	324.5775463
4449.84436	270.917851	6.088254534	273.65099	286.5125866
4499.816895	271.5768414	6.035286496	274.3409529	287.2349777
4550.170898	272.8981959	5.997537279	275.7244111	288.6834584
4600.143433	272.5261366	5.924296505	275.334865	288.2756037
4650.115967	272.6990849	5.864350197	275.5159418	288.4651911
4700.088501	275.8402863	5.868831752	278.8047798	291.9086044
4750.061035	279.8875201	5.892293131	283.0422335	296.3452185
4800.033569	283.0695939	5.897241963	290.621752	303.63463
4850.006104	283.2523021	5.840246301	280.345268	293.166456
4899.978638	280.1140002	5.716637172	280.7802549	293.16145
4949.951172	275.4860285	5.565429213	279.624105	292.113238

4999.923706	273.4123924	5.468331288	277.8701253	290.0196843
5049.89624	272.2456994	5.391114716	265.620514	277.4550456
5099.868774	271.5877457	5.325386941	260.32759	272.224362
5149.841309	270.7870972	5.258163911	265.378941	277.45501231
5199.813843	269.3206382	5.179428462	267.39425	279.54916401
5250.167847	266.490585	5.075848864	277.712543	290.019442
5300.140381	262.5941983	4.954476286	280.697082	293.16001
5350.112915	259.1451024	4.84373146	282.647125	295.254454
5400.085449	256.8784456	4.756932978	283.975142	296.301454
5450.057983	256.3741355	4.70406253	280.364102	293.16162
5500.030518	256.6016604	4.665458848	283.445236	296.301213
5550.003052	257.3364243	4.63668978	290.714982	303.630456
5599.975586	258.2130258	4.610966991	293.36352	306.771785
5649.94812	259.123866	4.586305228	290.02351	303.634546
5699.920654	260.5001428	4.570241564	293.201402	306.7715464
5749.893188	261.3264652	4.544892516	295.317402	308.8650134
5799.865723	261.2507241	4.504427112	285.65485	298.3951035
5849.838257	263.9378616	4.511883065	262.678219	274.3145601
5899.810791	261.7556619	4.436678924	260.634825	272.2246478
5950.164795	259.096604	4.354444169	252.541023	263.8443145
6000.137329	255.7237392	4.261964771	250.659725	261.7579301

frequency (Hz)	Surface Vel A-B (m/s)	Shear wave Vel A-B (m/s)	Vs2 (m/s)	G(kg/ms2), N/m2	G (Mpa)
2000.04578	219.9575946	65.98727838	4354.320908	10102.02451	0.010102025
2050.01831	256.679302	77.0037906	5929.583767	13756.63434	0.013756634
2099.99084	272.1624088	81.64872264	6666.513909	15466.31227	0.015466312
2149.96338	261.734848	78.5204544	6165.461759	14303.87128	0.014303871
2199.93591	247.1152811	74.13458433	5495.936594	12750.5729	0.012750573
2249.90845	239.3135603	71.79406809	5154.388213	11958.18065	0.011958181
2299.88098	244.7325273	73.41975819	5390.460893	12505.86927	0.012505869
2349.85352	257.350633	77.2051899	5960.641347	13828.68793	0.013828688
2399.82605	267.9878441	80.39635323	6463.573613	14995.49078	0.014995491
2450.18005	266.5851412	79.97554236	6396.087376	14838.92271	0.014838923
2500.15259	261.6132054	78.48396162	6159.732232	14290.57878	0.014290579
2550.12512	254.596241	76.3788723	5833.732134	13534.25855	0.013534259
2600.09766	243.1379792	72.94139376	5320.446924	12343.43686	0.012343437
2650.07019	230.4873239	69.14619717	4781.196583	11092.37607	0.011092376
2700.04272	219.8703443	65.96110329	4350.867147	10094.01178	0.010094012

2750.01526	212.5682594	63.77047782	4066.673841	9434.683312	0.009434683
2799.98779	213.4900211	64.04700633	4102.01902	9516.684126	0.009516684
2849.96033	220.9503969	66.28511907	4393.71701	10193.42346	0.010193423
2899.93286	232.3352578	69.70057734	4858.170482	11270.95552	0.011270956
2949.9054	243.106222	72.9318666	5319.057166	12340.21262	0.012340213
2999.87793	248.730089	74.6190267	5567.999146	12917.75802	0.012917758
3049.85046	255.8319416	76.74958248	5890.498411	13665.95631	0.013665956
3099.823	260.0472499	78.01417497	6086.211496	14120.01067	0.014120011
3150.177	261.6405704	78.49217112	6161.020927	14293.56855	0.014293569
3200.14954	261.3940152	78.41820456	6149.414806	14266.64235	0.014266642
3250.12207	257.4469322	77.23407966	5965.103061	13839.0391	0.013839039
3300.0946	252.5891785	75.77675355	5742.116379	13321.71	0.01332171
3350.06714	245.5377562	73.66132686	5425.991075	12588.29929	0.012588299
3400.03967	240.6452499	72.19357497	5211.912267	12091.63646	0.012091636
3450.01221	259.9344421	77.98033263	6080.932277	14107.76288	0.014107763
3499.98474	275.0719894	82.52159682	6809.813942	15798.76834	0.015798768
3549.95728	290.1384254	87.04152762	7576.22753	17576.84787	0.017576848
3599.92981	291.1145132	87.33435396	7627.289382	17695.31137	0.017695311
3649.90234	286.6597798	85.99793394	7395.644642	17157.89557	0.017157896
3699.87488	280.1200115	84.03600345	7062.049876	16383.95571	0.016383956
3749.84741	271.7956717	81.53870151	6648.559844	15424.65884	0.015424659
3799.81995	265.5276043	79.65828129	6345.441778	14721.42493	0.014721425
3850.17395	283.5519725	85.06559175	7236.1549	16787.87937	0.016787879
3900.14648	286.4296491	85.92889473	7383.77495	17130.35788	0.017130358
3950.11902	284.26845	85.280535	7272.76965	16872.82559	0.016872826
4000.09155	293.8042152	88.14126456	7768.882518	18023.80744	0.018023807
4050.06409	297.4643534	89.23930602	7963.653739	18475.67667	0.018475677
4100.03662	284.2085446	85.26256338	7269.704714	16865.71494	0.016865715
4150.00916	276.55754	82.967262	6883.566564	15969.87443	0.015969874
4199.98169	274.0378162	82.21134486	6758.705224	15680.19612	0.015680196
4249.95422	273.2473271	81.97419813	6719.769159	15589.86445	0.015589864
4299.92676	273.1851625	81.95554875	6716.711971	15582.77177	0.015582772
4349.89929	272.5781939	81.77345817	6686.898461	15513.60443	0.015513604
4399.87183	271.5197047	81.45591141	6635.065504	15393.35197	0.015393352
4449.84436	270.917851	81.2753553	6605.683379	15325.18544	0.015325185
4499.81689	271.5768414	81.47305242	6637.858271	15399.83119	0.015399831
4550.1709	272.8981959	81.86945877	6702.608279	15550.05121	0.015550051
4600.14343	272.5261366	81.75784098	6684.344562	15507.67938	0.015507679
4650.11597	272.6990849	81.80972547	6692.831181	15527.36834	0.015527368
4700.0885	275.8402863	82.75208589	6847.907719	15887.14591	0.015887146
4750.06104	279.8875201	83.96625603	7050.332152	16356.77059	0.016356771
4800.03357	283.0695939	84.92087817	7211.555549	16730.80887	0.016730809
4850.0061	283.2523021	84.97569063	7220.867998	16752.41376	0.016752414
4899.97864	280.1140002	84.03420006	7061.74678	16383.25253	0.016383253
4949.95117	275.4860285	82.64580855	6830.329671	15846.36484	0.015846365
4999.92371	273.4123924	82.02371772	6727.890269	15608.70542	0.015608705
5049.89624	272.2456994	81.67370982	6670.594876	15475.78011	0.01547578
5099.86877	271.5877457	81.47632371	6638.391325	15401.06787	0.015401068

5149.84131	270.7870972	81.23612916	6599.308681	15310.39614	0.015310396
5199.81384	269.3206382	80.79619146	6528.024554	15145.01697	0.015145017
5250.16785	266.490585	79.9471755	6391.55087	14828.39802	0.014828398
5300.14038	262.5941983	78.77825949	6206.014168	14397.95287	0.014397953
5350.11292	259.1451024	77.74353072	6044.056569	14022.21124	0.014022211
5400.08545	256.8784456	77.06353368	5938.788223	13777.98868	0.013777989
5450.05798	256.3741355	76.91224065	5915.492762	13723.94321	0.013723943
5500.03052	256.6016604	76.98049812	5925.997091	13748.31325	0.013748313
5550.00305	257.3364243	77.20092729	5959.983174	13827.16096	0.013827161
5599.97559	258.2130258	77.46390774	6000.657002	13921.52425	0.013921524
5649.94812	259.123866	77.7371598	6043.066014	14019.91315	0.014019913
5699.92065	260.5001428	78.15004284	6107.429196	14169.23573	0.014169236
5749.89319	261.3264652	78.39793956	6146.236927	14259.26967	0.01425927
5799.86572	261.2507241	78.37521723	6142.674676	14251.00525	0.014251005
5849.83826	263.9378616	79.18135848	6269.687531	14545.67507	0.014545675
5899.81079	261.7556619	78.52669857	6166.442388	14306.14634	0.014306146
5950.16479	259.096604	77.7289812	6041.794518	14016.96328	0.014016963
6000.13733	255.7237392	76.71712176	5885.516771	13654.39891	0.013654399

frequency (Hz)	Surface Vel C-D (m/s)	Shear wave Vel C-D (m/s)	Vs2 (m/s)	G(kg/ms2), N/m2	G (Mpa)
2000.045776	282.773594	84.8320782	7196.481492	16695.83706	0.016695837
2050.018311	275.9336143	82.78008429	6852.542355	15897.89826	0.015897898
2099.990845	282.8127606	84.84382818	7198.47518	16700.46242	0.016700462
2149.963379	296.8543892	89.05631676	7931.027555	18399.98393	0.018399984
2199.935913	312.2160429	93.66481287	8773.09717	20353.58543	0.020353585
2249.908447	322.6403031	96.79209093	9368.708867	21735.40457	0.021735405
2299.880981	333.222676	99.9668028	9993.361662	23184.59906	0.023184599
2349.853516	349.785862	104.9357586	11011.51343	25546.71116	0.025546711
2399.82605	366.0877559	109.8263268	12061.82205	27983.42716	0.027983427
2450.180054	374.1937352	112.2581206	12601.88563	29236.37467	0.029236375
2500.152588	365.7758038	109.7327411	12041.27448	27935.75679	0.027935757
2550.125122	346.1015427	103.8304628	10780.76501	25011.37482	0.025011375
2600.097656	331.0115752	99.30347256	9861.179662	22877.93682	0.022877937
2650.07019	326.3778463	97.91335389	9587.02487	22241.8977	0.022241898
2700.042725	328.1620643	98.44861929	9692.13064	22485.74309	0.022485743
2750.015259	330.1189115	99.03567345	9808.064616	22754.70991	0.02275471
2799.987793	338.6491056	101.5947317	10321.48951	23945.85565	0.023945856
2849.960327	338.2810114	101.4843034	10299.06384	23893.82811	0.023893828
2899.932861	344.7290433	103.418713	10695.4302	24813.39806	0.024813398
2949.905396	345.7263141	103.7178942	10757.40158	24957.17167	0.024957172
2999.87793	357.2152191	107.1645657	11484.24415	26643.44642	0.026643446
3049.850464	370.0402153	111.0120646	12323.67848	28590.93408	0.028590934
3099.822998	367.5669466	110.270084	12159.49142	28210.0201	0.02821002
3150.177002	352.9189923	105.8756977	11209.66336	26006.419	0.026006419
3200.149536	333.3210604	99.99631812	9999.263638	23198.29164	0.023198292
3250.12207	317.4321895	95.22965685	9068.687544	21039.3551	0.021039355
3300.094604	307.5087127	92.25261381	8510.544755	19744.46383	0.019744464
3350.067139	300.962197	90.2886591	8152.041962	18912.73735	0.018912737

3400.039673	307.1074053	92.13222159	8488.346255	19692.96331	0.019692963
3450.012207	316.8321059	95.04963177	9034.4325	20959.8834	0.020959883
3499.984741	300.1648045	90.04944135	8108.901887	18812.65238	0.018812652
3549.957275	282.487846	84.7463538	7181.944482	16662.1112	0.016662111
3599.92981	292.8328429	87.84985287	7717.596649	17904.82423	0.017904824
3649.902344	310.6470034	93.19410102	8685.140465	20149.52588	0.020149526
3699.874878	322.7546252	96.82638756	9375.349328	21750.81044	0.02175081
3749.847412	326.8595624	98.05786872	9615.345618	22307.60183	0.022307602
3799.819946	320.0119298	96.00357894	9216.687169	21382.71423	0.021382714
3850.17395	303.7643136	91.12929408	8304.54824	19266.55192	0.019266552
3900.146484	291.9110846	87.57332538	7669.087318	17792.28258	0.017792283
3950.119019	261.5906085	78.47718255	6158.668181	14288.11018	0.01428811
4000.091553	218.7230757	65.61692271	4305.580546	9988.946867	0.009988947
4050.064087	393.6556342	118.0966903	13946.82825	32356.64154	0.032356642
4100.036621	371.9615716	111.5884715	12451.98697	28888.60976	0.02888861
4150.009155	342.5060005	102.7518002	10557.93243	24494.40325	0.024494403
4199.981689	331.7162945	99.51488835	9903.213003	22975.45417	0.022975454
4249.954224	326.0173258	97.80519774	9565.856705	22192.78756	0.022192788
4299.926758	322.4590095	96.73770285	9358.183153	21710.98491	0.021710985
4349.899292	320.7275724	96.21827172	9257.955813	21478.45749	0.021478457
4399.871826	320.0685227	96.02055681	9219.94733	21390.27781	0.021390278
4449.84436	319.2770471	95.78311413	9174.404952	21284.61949	0.021284619
4499.816895	317.1731731	95.15195193	9053.893956	21005.03398	0.021005034
4550.170898	316.2064405	94.86193215	8998.786171	20877.18392	0.020877184
4600.143433	316.380868	94.9142604	9008.716827	20900.22304	0.020900223
4650.115967	314.9534903	94.48604709	8927.613095	20712.06238	0.020712062
4700.088501	310.8966836	93.26900508	8699.107309	20181.92896	0.020181929
4750.061035	305.3742244	91.61226732	8392.807524	19471.31345	0.019471313
4800.033569	297.5310812	89.25932436	7967.226985	18483.96661	0.018483967
4850.006104	286.541576	85.9624728	7389.54673	17143.74841	0.017143748
4899.978638	276.4534368	82.93603104	6878.385245	15957.85377	0.015957854
4949.951172	265.7208245	79.71624735	6354.680092	14742.85781	0.014742858
4999.923706	255.8422845	76.75268535	5890.974708	13667.06132	0.013667061
5049.89624	248.7904176	74.63712528	5570.70047	12924.02509	0.012924025
5099.868774	253.2730299	75.98190897	5773.250491	13393.94114	0.013393941
5149.841309	265.1751832	79.55255496	6328.609001	14682.37288	0.014682373
5199.813843	284.5311954	85.35935862	7286.220104	16904.03064	0.016904031
5250.167847	311.1951715	93.35855145	8715.819129	20220.70038	0.0202207
5300.140381	328.3326826	98.49980478	9702.211542	22509.13078	0.022509131
5350.112915	347.5824683	104.2747405	10873.2215	25225.87389	0.025225874
5400.085449	339.5361424	101.8608427	10375.63128	24071.46457	0.024071465
5450.057983	332.85014	99.855042	9971.029413	23132.78824	0.023132788
5500.030518	329.3150824	98.79452472	9760.358115	22644.03083	0.022644031
5550.003052	323.0416425	96.91249275	9392.031251	21789.5125	0.021789513
5599.975586	327.2858496	98.18575488	9640.442461	22365.82651	0.022365827
5649.94812	319.1519115	95.74557345	9167.214835	21267.93842	0.021267938
5699.920654	307.2995302	92.18985906	8498.970114	19717.61066	0.019717611
5749.893188	326.6675978	98.00027934	9604.054751	22281.40702	0.022281407
5799.865723	292.6137262	87.78411786	7706.051348	17878.03913	0.017878039
5849.838257	270.5903985	81.17711955	6589.724738	15288.16139	0.015288161
5899.810791	252.4803949	75.74411847	5737.171483	13310.23784	0.013310238

5950.164795	242.0720188	72.62160564	5273.897606	12235.44245	0.012235442
6000.137329	239.420672	71.8262016	5159.003236	11968.88751	0.011968888

Test ID: OxfordClay 24% moisture, 14-Nov-01
Date of test: 14 November 2011
Test frequency range / interval: 2000 Hz to 7000 Hz / 100 Hz

Frequency(Hz)	Vel A-B(m/s)	Wave L A-B (cm)	Vel C-D (m/s)	Wave L C-D(cm)
2000.045776	256.618913	12.83065197	213.9992366	10.69971693
2099.990845	232.562663	11.07446083	236.9057662	11.28127615
2199.935913	221.249744	10.0570995	197.038663	8.956563771
2299.880981	201.333167	8.754068968	174.770224	7.599098623
2399.82605	197.133796	8.214503528	194.5177501	8.105493733
2500.152588	214.116822	8.564150173	203.2767207	8.130572575
2600.097656	223.071508	8.579351137	194.7663542	7.49073227
2700.042725	214.275352	7.935998572	194.7963669	7.214566093
2799.987793	186.854935	6.673419632	199.7090575	7.132497434
2899.932861	185.072639	6.381962889	192.5661511	6.64036584
2999.87793	196.400135	6.546937564	186.9953229	6.233431068
3099.822998	188.286287	6.074098002	184.9100897	5.965182201
3200.149536	180.977958	5.655296908	186.3572836	5.823392984

3300.094604	183.295317	5.55424431	189.8312954	5.752298589
3400.039673	183.613061	5.400321133	189.8490791	5.583731291
3499.984741	182.504507	5.214437209	187.3055898	5.351611611
3599.92981	175.611924	4.87820411	185.4092881	5.15035842
3699.874878	167.231537	4.519924132	181.4967055	4.905482252
3799.819946	159.580513	4.199686178	179.2891541	4.718359201
3900.146484	162.060009	4.155228773	174.2735681	4.468385196
4000.091553	160.712245	4.017714162	178.0086639	4.450114741
4100.036621	171.23988	4.176545124	183.6931569	4.480280882
4199.981689	176.104062	4.192972137	183.6150117	4.371805052
4299.926758	168.533615	3.919453156	174.2277752	4.051877742
4399.871826	163.97355	3.726780158	169.9135733	3.861784617
4499.816895	162.19131	3.604397995	169.3759855	3.76406395
4600.143433	160.666801	3.492647636	169.0845852	3.675637242
4700.088501	158.628333	3.375007357	169.4177258	3.604564591
4800.033569	159.099567	3.314551129	170.972023	3.561892236
4899.978638	161.525745	3.29645814	173.2604712	3.535943399
4999.923706	164.933762	3.298725576	177.094451	3.541943066
5099.868774	168.476799	3.303551652	179.674386	3.523117828
5199.813843	173.243943	3.331733561	179.6427488	3.454791926
5300.140381	173.652882	3.276382684	179.5110441	3.386911124
5400.085449	172.215862	3.189132174	178.9669398	3.314150146
5500.030518	174.421931	3.171290237	179.6280175	3.265945833
5599.975586	176.646978	3.15442407	181.707715	3.244794771
5699.920654	178.602331	3.133417845	183.0912683	3.212172229
5799.865723	177.869154	3.06678055	182.6919207	3.149933627
5899.810791	179.999156	3.050930988	182.0248894	3.085266559
6000.137329	184.518087	3.075231065	182.9899578	3.049762827
6100.082397	186.427451	3.056146433	184.2058256	3.019726844
6200.027466	188.406865	3.038806943	181.5715497	2.928560409
6299.972534	189.159369	3.002542753	176.8129867	2.80656758
6399.917603	189.630799	2.963019378	180.0575409	2.813435299
6499.862671	190.744999	2.934600447	180.2672212	2.77340046
6600.189209	201.737253	3.056537428	177.8605007	2.694778817
6700.134277	217.759303	3.250073718	183.9907912	2.746076176
6800.079346	215.156453	3.164028562	185.6694007	2.730400504
6900.024414	219.263071	3.177714424	189.7440774	2.749904435
6999.969482	213.631575	3.051892949	195.1125662	2.787334526

frequency (Hz)	Surface Vel A-B (m/s)	Shear wave Vel A-B (m/s)	Vs2 (m/s)	G(kg/ms2), N/m2	G (Mpa)
2000.046	256.6189128	268.6800017	72188.94333	131383876.9	131.3838769
2099.991	232.5626635	243.4931087	59288.89397	107905787	107.905787
2199.936	221.2497437	231.6484817	53661.01906	97663054.69	97.66305469

2299.881	201.3331673	210.7958262	44434.88033	80871482.2	80.8714822
2399.826	197.1337955	206.3990839	42600.58184	77533058.95	77.53305895
2500.153	214.1168222	224.1803128	50256.81266	91467399.03	91.46739903
2600.098	223.0715078	233.5558687	54548.3438	99277985.72	99.27798572
2700.043	214.2753521	224.3462936	50331.25946	91602892.22	91.60289222
2799.988	186.8549351	195.637117	38273.88156	69658464.44	69.65846444
2899.933	185.072639	193.771053	37547.221	68335942.22	68.33594222
2999.878	196.4001351	205.6309414	42284.08407	76957033	76.957033
3099.823	188.2862868	197.1357423	38862.50088	70729751.59	70.72975159
3200.15	180.9779578	189.4839218	35904.15661	65345565.03	65.34556503
3300.095	183.2953168	191.9101967	36829.52359	67029732.93	67.02973293
3400.04	183.613061	192.2428748	36957.32293	67262327.73	67.26232773
3499.985	182.5045067	191.0822185	36512.41422	66452593.88	66.45259388
3599.93	175.6119239	183.8656844	33806.58989	61527993.59	61.52799359
3699.875	167.2315375	175.0914197	30657.00527	55795749.58	55.79574958
3799.82	159.5805131	167.0807972	27915.99279	50807106.88	50.80710688
3900.146	162.0600089	169.6768293	28790.22641	52398212.06	52.39821206
4000.092	160.7122448	168.2657203	28313.35264	51530301.8	51.5303018
4100.037	171.2398796	179.2881539	32144.24214	58502520.69	58.50252069
4199.982	176.104062	184.3809529	33996.3358	61873331.16	61.87333116
4299.927	168.533615	176.4546949	31136.25936	56667992.03	56.66799203
4399.872	163.9735502	171.6803071	29474.12783	53642912.65	53.64291265
4499.817	162.1913099	169.8143015	28836.89699	52483152.52	52.48315252
4600.143	160.6668008	168.2181405	28297.34278	51501163.87	51.50116387
4700.089	158.6283327	166.0838643	27583.84998	50202606.97	50.20260697
4800.034	159.0995669	166.5772465	27747.97905	50501321.88	50.50132188
4899.979	161.5257447	169.1174547	28600.71347	52053298.52	52.05329852
4999.924	164.9337621	172.6856489	29820.33333	54273006.66	54.27300666
5099.869	168.4767992	176.3952087	31115.26966	56629790.79	56.62979079
5199.814	173.2439429	181.3864082	32901.02909	59879872.94	59.87987294
5300.14	173.6528817	181.8145671	33056.53682	60162897.01	60.16289701
5400.085	172.2158625	180.310008	32511.69899	59171292.17	59.17129217
5500.031	174.4219308	182.6197616	33349.97732	60696958.72	60.69695872
5599.976	176.6469778	184.9493858	34206.2753	62255421.04	62.25542104
5699.921	178.6023309	186.9966405	34967.74355	63641293.26	63.64129326
5799.866	177.8691539	186.2290042	34681.24199	63119860.42	63.11986042
5899.811	179.9991556	188.459116	35516.83839	64640645.86	64.64064586
6000.137	184.5180871	193.1904372	37322.54501	67927031.92	67.92703192
6100.082	186.4274506	195.1895408	38098.95682	69340101.41	67.35030933
6200.027	188.4068651	197.2619878	38912.29183	70820371.12	65.788515
6299.973	189.1593687	198.0498591	39223.74668	71387218.96	64.76126446
6399.918	189.6307988	198.5434463	39419.50007	71743490.13	63.95878177
6499.863	190.744999	199.7100139	39884.08967	72589043.19	63.54627689
6600.189	201.7372535	211.2189044	44613.42557	81196434.55	63.20513586

6700.134	217.7593032	227.9939905	51981.2597	94605892.65	62.51581237
6800.079	215.1564527	225.268806	50746.03496	92357783.62	61.61917399
6900.024	219.2630711	229.5684354	52701.66654	95917033.1	60.88786379
6999.969	213.6315751	223.6722591	50029.2795	91053288.7	60.6739467

frequency (Hz)	Surface Vel C-D (m/s)	Shear wave Vel C-D (m/s)	Vs2 (m/s)	G(kg/ms2), N/m2	G (Mpa)
2000.04578	213.9992366	224.0572007	50201.6292	91366965.13	91.36696513
2099.99084	236.9057662	248.0403373	61524.0089	111973696.2	111.9736962
2199.93591	197.038663	206.2994801	42559.4755	77458245.42	77.45824542
2299.88098	174.770224	182.9844245	33483.2996	60939605.3	60.9396053
2399.82605	194.5177501	203.6600843	41477.4299	75488922.5	75.4889225
2500.15259	203.2767207	212.8307265	45296.9182	82440391.04	82.44039104
2600.09766	194.7663542	203.9203728	41583.5185	75682003.59	75.68200359
2700.04272	194.7963669	203.9517962	41596.3352	75705329.99	75.70532999
2799.98779	199.7090575	209.0953832	43720.8793	79572000.27	79.57200027
2899.93286	192.5661511	201.6167602	40649.318	73981758.75	73.98175875
2999.87793	186.9953229	195.7841031	38331.415	69763175.31	69.76317531
3099.823	184.9100897	193.600864	37481.2945	68215956.04	68.21595604
3200.14954	186.3572836	195.1160759	38070.2831	69287915.19	69.28791519
3300.0946	189.8312954	198.7533663	39502.9006	71895279.09	71.89527909
3400.03967	189.8490791	198.7719858	39510.3024	71908750.28	71.90875028
3499.98474	187.3055898	196.1089525	38458.7213	69994872.68	69.99487268
3599.92981	185.4092881	194.1235246	37683.9428	68584775.91	68.58477591
3699.87488	181.4967055	190.0270506	36110.28	65720709.56	65.72070956
3799.81995	179.2891541	187.7157443	35237.2007	64131705.2	64.1317052
3900.14648	174.2735681	182.4644258	33293.2667	60593745.39	60.59374539
4000.09155	178.0086639	186.3750711	34735.6671	63218914.14	63.21891414
4100.03662	183.6931569	192.3267353	36989.5731	67321023.03	67.32102303
4199.98169	183.6150117	192.2449172	36958.1082	67263756.91	67.26375691
4299.92676	174.2277752	182.4164807	33275.7724	60561905.8	60.5619058
4399.87183	169.9135733	177.8995113	31648.2361	57599789.73	57.59978973
4499.81689	169.3759855	177.3366569	31448.2899	57235887.55	57.23588755
4600.14343	169.0845852	177.0315607	31340.1735	57039115.74	57.03911574
4700.0885	169.4177258	177.380359	31463.7917	57264100.97	57.26410097
4800.03357	170.972023	179.0077081	32043.7596	58319642.41	58.31964241
4899.97864	173.2604712	181.4037133	32907.3072	59891299.12	59.89129912
4999.92371	177.094451	185.4178902	34379.794	62571225.1	62.5712251
5099.86877	179.674386	188.1190822	35388.7891	64407596.11	64.40759611
5199.81384	179.6427488	188.085958	35376.3276	64384916.21	64.38491621
5300.14038	179.5110441	187.9480632	35324.4745	64290543.53	64.29054353
5400.08545	178.9669398	187.378386	35110.6595	63901400.36	63.90140036
5500.03052	179.6280175	188.0705343	35370.5259	64374357.12	64.37435712
5599.97559	181.707715	190.2479776	36194.293	65873613.24	65.87361324

5699.92065	183.0912683	191.696558	36747.5703	66880578.01	66.88057801
5799.86572	182.6919207	191.278441	36587.442	66589144.43	66.58914443
5899.81079	182.0248894	190.5800592	36320.759	66103781.32	66.10378132
6000.13733	182.9899578	191.5904858	36706.9143	66806583.95	66.80658395
6100.0824	184.2058256	192.8634995	37196.3294	67697319.55	67.69731955
6200.02747	181.5715497	190.1054125	36140.0679	65774923.52	65.77492352
6299.97253	176.8129867	185.123197	34270.5981	62372488.52	62.37248852
6399.9176	180.0575409	188.5202454	35539.8829	64682586.9	64.6825869
6499.86267	180.2672212	188.7397806	35622.7048	64833322.69	64.83332269
6600.18921	177.8605007	186.2199442	34677.8676	63113719.1	63.1137191
6700.13428	183.9907912	192.6383584	37109.5371	67539357.54	67.53935754
6800.07935	185.6694007	194.3958626	37789.7514	68777347.52	68.77734752
6900.02441	189.7440774	198.662049	39466.6097	71829229.7	71.8292297
6999.96948	195.1125662	204.2828568	41731.4856	75951303.76	75.95130376

Test ID: OxfordClay 30% moisture, 25-July-01
Date of test: 25 July 2011
Test frequency range / interval: 1000 Hz to 5000 Hz / 100 Hz

Frequency(Hz)	Vel A-B(m/s)	Wave L A-B (cm)	Vel C-D (m/s)	Wave L C-D(cm)
999.8321533	101.1292882	10.11462653	122.863074	12.28836995
1100.158691	128.2139408	11.65413152	96.0938103	8.73454085
1200.10376	146.9821178	12.24745083	125.258279	10.43728743
1300.048828	171.2272322	13.17083086	123.969344	9.535745248
1399.993896	139.0189473	9.929968102	110.860373	7.918632617
1499.938965	116.0607814	7.737700273	96.7084521	6.447492487
1599.884033	114.3019231	7.144388015	96.0449007	6.003241402
1699.829102	126.153479	7.421538958	108.505855	6.38333906
1800.15564	132.0454446	7.33522378	105.88321	5.881891962
1900.100708	130.7638093	6.881940979	97.6697643	5.140241456
2000.045776	127.4345209	6.37158021	97.5383705	4.876806904
2099.990845	133.2560669	6.345554659	100.357018	4.778926454
2199.935913	135.8262225	6.17409906	103.481563	4.703844433
2299.880981	131.8694597	5.733751474	101.845339	4.428287374
2399.82605	132.0481709	5.502405933	100.532296	4.189149289

2500.152588	138.2984756	5.531601404	103.480206	4.138955629
2600.097656	137.8886209	5.303209306	109.087496	4.195515352
2700.042725	129.4761766	4.795338068	110.093088	4.077457241
2799.987793	122.608828	4.378905804	108.795041	3.885554102
2899.932861	120.4895906	4.15490966	106.530306	3.673543859
2999.87793	123.128992	4.104466746	105.807936	3.52707471
3099.822998	125.8247161	4.059093573	106.136794	3.423963051
3200.149536	125.1086751	3.909463406	105.733572	3.304019738
3300.094604	123.1329975	3.73119599	105.6035	3.200014321
3400.039673	122.0737319	3.590361985	108.634537	3.195096151
3499.984741	120.7573289	3.450224439	113.543408	3.244111522
3599.92981	120.2349532	3.33992493	120.869747	3.357558444
3699.874878	121.2837171	3.278049153	121.707387	3.289500073
3799.819946	122.1982778	3.215896531	121.261302	3.1912381
3900.146484	122.4799187	3.140392782	121.79363	3.122796299
4000.091553	123.0358067	3.075824769	123.810359	3.09518814
4100.036621	123.3032152	3.007368631	130.771026	3.189508736
4199.981689	125.0934756	2.978429072	130.658745	3.110936069
4299.926758	126.0563717	2.931593463	130.009938	3.023538437
4399.871826	126.0059791	2.863855677	131.728643	2.99392001
4499.816895	124.1891808	2.759871873	134.550884	2.990141312
4600.143433	122.497712	2.662910706	136.01688	2.95679651
4700.088501	121.5443642	2.586001608	138.092142	2.938075361
4800.033569	118.1210386	2.46083776	142.316819	2.964912991
4899.978638	118.8783942	2.426100254	142.738819	2.913049828
4999.923706	117.725491	2.354545748	142.481371	2.849670909

frequency (Hz)	Surface Vel A-B (m/s)	Shear wave Vel A-B (m/s)	Vs2 (m/s)	G(kg/ms2), N/m2	G (Mpa)
999.8322	101.1292882	105.8823648	11211.0752	20964710.56	20.96471056
1100.159	128.2139408	134.239996	18020.3765	33698104.1	33.6981041
1200.104	146.9821178	153.8902774	23682.2175	44285746.66	44.28574666
1300.049	130	136.11	18525.9321	34643493.03	34.64349303
1399.994	139.0189473	145.5528379	21185.6286	39617125.51	39.61712551
1499.939	116.0607814	121.5156381	14766.0503	27612514.07	27.61251407
1599.884	114.3019231	119.6741135	14321.8934	26781940.74	26.78194074
1699.829	126.153479	132.0826925	17445.8377	32623716.42	32.62371642
1800.156	132.0454446	138.2515805	19113.4995	35742244.06	35.74224406
1900.101	130.7638093	136.9097083	18744.2682	35051781.59	35.05178159
2000.046	127.4345209	133.4239434	17801.9487	33289643.99	33.28964399
2099.991	133.2560669	139.519102	19465.5798	36400634.28	36.40063428
2199.936	135.8262225	142.210055	20223.6997	37818318.51	37.81831851
2299.881	131.8694597	138.0673243	19062.586	35647035.89	35.64703589

2399.826	132.0481709	138.254435	19114.2888	35743720.04	35.74372004
2500.153	138.2984756	144.798504	20966.6068	39207554.64	39.20755464
2600.098	137.8886209	144.3693861	20842.5196	38975511.71	38.97551171
2700.043	129.4761766	135.5615569	18376.9357	34364869.8	34.3648698
2799.988	122.608828	128.3714429	16479.2274	30816155.15	30.81615515
2899.933	120.4895906	126.1526013	15914.4788	29760075.41	29.76007541
2999.878	123.128992	128.9160547	16619.3492	31078182.91	31.07818291
3099.823	125.8247161	131.7384777	17355.0265	32453899.59	32.45389959
3200.15	125.1086751	130.9887828	17158.0612	32085574.47	32.08557447
3300.095	123.1329975	128.9202484	16620.4305	31080204.95	31.08020495
3400.04	122.0737319	127.8111973	16335.7021	30547763.02	30.54776302
3499.985	120.7573289	126.4329234	15985.2841	29892481.29	29.89248129
3599.93	120.2349532	125.885996	15847.284	29634421.04	29.63442104
3699.875	121.2837171	126.9840518	16124.9494	30153655.41	30.15365541
3799.82	122.1982778	127.9415969	16369.0522	30610127.64	30.61012764
3900.146	122.4799187	128.2364748	16444.5935	30751389.81	30.75138981
4000.092	123.0358067	128.8184897	16594.2033	31031160.13	31.03116013
4100.037	123.3032152	129.0984663	16666.414	31166194.19	31.16619419
4199.982	125.0934756	130.972869	17153.8924	32077778.81	32.07777881
4299.927	126.0563717	131.9810212	17418.99	32573511.22	32.57351122
4399.872	126.0059791	131.9282601	17405.0658	32547473.06	32.54747306
4499.817	124.1891808	130.0260723	16906.7795	31615677.63	31.61567763
4600.143	122.497712	128.2551044	16449.3718	30760325.29	30.76032529
4700.089	121.5443642	127.2569494	16194.3312	30283399.27	30.28339927
4800.034	118.1210386	123.6727274	15294.9435	28601544.35	28.60154435
4899.979	118.8783942	124.4656787	15491.7052	28969488.68	28.96948868
4999.924	117.725491	123.2585891	15192.6798	28410311.21	28.41031121

frequency (Hz)	Surface Vel C-D (m/s)	Shear wave Vel C-D (m/s)	Vs2 (m/s)	G(kg/ms2), N/m2	G (Mpa)
999.8322	122.8630739	128.6376383	16547.642	30944090.53	30.94409053
1100.159	96.09381031	100.6102194	10122.416	18928918.38	18.92891838
1200.104	125.2582789	131.145418	17199.121	32162355.64	32.16235564
1300.049	123.9693444	129.7959035	16846.977	31503846.2	31.5038462
1399.994	110.8603733	116.0708109	13472.433	25193449.96	25.19344996
1499.939	96.70845207	101.2537493	10252.322	19171841.67	19.17184167
1599.884	96.04490067	100.559011	10112.115	18909654.48	18.90965448
1699.829	108.505855	113.6056302	12906.239	24134667.32	24.13466732
1800.156	105.8832099	110.8597207	12289.878	22982071.26	22.98207126
1900.101	97.66976429	102.2602432	10457.157	19554884.23	19.55488423
2000.046	97.5383705	102.1226739	10429.041	19502305.78	19.50230578
2099.991	100.357018	105.0737978	11040.503	20645740.6	20.6457406
2199.936	103.481563	108.3451964	11738.682	21951334.57	21.95133457

2299.881	101.8453391	106.6320701	11370.398	21262644.94	21.26264494
2399.826	100.5322959	105.2573138	11079.102	20717920.95	20.71792095
2500.153	103.4802063	108.343776	11738.374	21950758.99	21.95075899
2600.098	109.0874963	114.2146087	13044.977	24394106.67	24.39410667
2700.043	110.0930876	115.2674627	13286.588	24845919.48	24.84591948
2799.988	108.7950405	113.9084074	12975.125	24263484.28	24.26348428
2899.933	106.5303055	111.5372299	12440.554	23263835.33	23.26383533
2999.878	105.8079358	110.7809088	12272.41	22949406.22	22.94940622
3099.823	106.1367941	111.1252234	12348.815	23092284.58	23.09228458
3200.15	105.7335723	110.7030502	12255.165	22917159.17	22.91715917
3300.095	105.6034999	110.5668644	12225.032	22860808.93	22.86080893
3400.04	108.6345367	113.7403599	12936.869	24191945.93	24.19194593
3499.985	113.5434083	118.8799484	14132.442	26427666.81	26.42766681
3599.93	120.8697473	126.5506254	16015.061	29948163.68	29.94816368
3699.875	121.7073868	127.427634	16237.802	30364689.56	30.36468956
3799.82	121.2613018	126.960583	16118.99	30142510.64	30.14251064
3900.146	121.7936301	127.5179307	16260.823	30407738.35	30.40773835
4000.092	123.8103593	129.6294462	16803.793	31423093.51	31.42309351
4100.037	130.7710262	136.9172644	18746.337	35055650.75	35.05565075
4199.982	130.6587453	136.7997063	18714.16	34995478.53	34.99547853
4299.927	130.0099383	136.1204054	18528.765	34648790.12	34.64879012
4399.872	131.728643	137.9198892	19021.896	35570945.23	35.57094523
4499.817	134.5508839	140.8747755	19845.702	37111463.43	37.11146343
4600.143	136.0168805	142.4096738	20280.515	37924563.43	37.92456343
4700.089	138.0921422	144.5824729	20904.091	39090651.04	39.09065104
4800.034	142.3168189	149.0057094	22202.701	41519051.67	41.51905167
4899.979	142.7388193	149.4475438	22334.568	41765642.8	41.7656428
4999.924	142.4813713	149.1779958	22254.074	41615119.17	41.61511917

Test ID: OxfordClay 30% moisture-Repeated, 15-Sep-05
Date of test: 15 September 2011
Test frequency range / interval: 1000 Hz to 5000 Hz / 100 Hz

Frequency(Hz)	Vel A-B(m/s)	Wave L A-B (cm)	Vel C-D (m/s)	Wave L C-D(cm)
999.8321533	111.265583	11.12842622	132.4457678	13.24680021
1100.158691	108.857729	9.894729749	136.0532004	12.36668868
1200.10376	110.364986	9.196286971	150.0512253	12.50318767
1300.048828	109.500836	8.422824896	140.4875963	10.80633229
1399.993896	109.93986	7.852881382	133.4707005	9.533663026
1499.938965	111.885003	7.459303697	128.5938281	8.573270721
1599.884033	111.478848	6.967933024	134.9981752	8.437997531
1699.829102	107.718455	6.337016744	130.5829014	7.682119412
1800.15564	102.990097	5.721177386	127.8495496	7.102138658
1900.100708	100.718581	5.300696964	122.904055	6.468291627
2000.045776	101.051313	5.052450018	128.6101878	6.430362209
2099.990845	103.451521	4.926284371	129.9284796	6.187097432
2199.935913	105.169633	4.780577136	127.6191661	5.801040175
2299.880981	104.438046	4.541019608	127.2521429	5.532988183
2399.82605	106.434415	4.43508876	127.9619546	5.332134579
2500.152588	108.466702	4.338403281	127.5776151	5.102793153
2600.097656	109.824592	4.223864119	127.4078007	4.900115979
2700.042725	112.226294	4.156463653	128.5895095	4.762499066

2799.987793	113.15516	4.041273338	129.9972073	4.642777644
2899.932861	114.092235	3.934306096	132.1883266	4.558323688
2999.87793	115.897438	3.863405151	134.0347456	4.468006657
3099.822998	118.182644	3.81256105	135.4924829	4.370974828
3200.149536	119.671482	3.739559051	137.0529312	4.282703968
3300.094604	120.15673	3.641008643	138.5208514	4.197481224
3400.039673	119.444375	3.513028873	138.5522361	4.075018219
3499.984741	119.654431	3.418712922	138.6102927	3.960311344
3599.92981	118.243047	3.284593127	142.3055586	3.953009257
3699.874878	116.521326	3.149331525	143.8278475	3.887370579
3799.819946	116.56014	3.067517443	143.9090818	3.787260551
3900.146484	116.606869	2.989807431	144.6509225	3.708858708
4000.091553	115.979357	2.899417555	144.218241	3.605373506
4100.036621	117.936459	2.876473301	144.1011263	3.514630224
4199.981689	139.818968	3.329037552	143.9966023	3.428505477
4299.926758	140.805448	3.274601084	143.8878819	3.34628681
4399.871826	132.118339	3.002776995	142.1173657	3.230034222
4499.816895	126.586724	2.813152789	139.0987906	3.091210017
4600.143433	124.674977	2.710241077	135.671789	2.949294756
4700.088501	123.577719	2.629263656	137.2890032	2.920987619
4800.033569	122.288924	2.547668091	139.2373198	2.900757209
4899.978638	122.0031	2.489870036	140.3951521	2.865219677
4999.923706	122.055811	2.441153472	140.9169246	2.818381497

frequency (Hz)	Surface Vel A-B (m/s)	Shear wave Vel A-B (m/s)	Vs2 (m/s)	G(kg/ms2), N/m2	G (Mpa)
999.8322	111.2656	116.4951	13571.1	23613715	23.61371
1100.159	108.8577	113.974	12990.08	22602743	22.60274
1200.104	110.365	115.5521	13352.3	23232997	23.233
1300.049	109.5008	114.6474	13144.02	22870596	22.8706
1399.994	109.9399	115.107	13249.63	23054355	23.05435
1499.939	111.885	117.1436	13722.62	23877363	23.87736
1599.884	111.4788	116.7184	13623.17	23704323	23.70432
1699.829	107.7185	112.7812	12719.6	22132111	22.13211
1800.156	102.9901	107.8306	11627.45	20231755	20.23175
1900.101	100.7186	105.4524	11120.2	19349146	19.34915
2000.046	101.0513	105.8007	11193.79	19477201	19.4772
2099.991	103.4515	108.3137	11731.87	20413448	20.41345
2199.936	105.1696	110.1126	12124.79	21097128	21.09713
2299.881	104.438	109.3466	11956.69	20804634	20.80463
2399.826	106.4344	111.4368	12418.17	21607612	21.60761
2500.153	108.4667	113.5646	12896.93	22440653	22.44065
2600.098	109.8246	114.9863	13221.86	23006037	23.00604
2700.043	112.2263	117.5009	13806.47	24023255	24.02326

2799.988	113.1552	118.4735	14035.96	24422569	24.42257
2899.933	114.0922	119.4546	14269.39	24828746	24.82875
2999.878	115.8974	121.3446	14724.52	25620658	25.62066
3099.823	118.1826	123.7372	15310.9	26640969	26.64097
3200.15	119.6715	125.296	15699.1	27316430	27.31643
3300.095	120.1567	125.8041	15826.67	27538407	27.53841
3400.04	119.4444	125.0583	15639.57	27212849	27.21285
3499.985	119.6544	125.2782	15694.62	27308647	27.30865
3599.93	118.243	123.8005	15326.56	26668208	26.66821
3699.875	116.5213	121.9978	14883.47	25897238	25.89724
3799.82	116.5601	122.0385	14893.39	25914494	25.91449
3900.146	116.6069	122.0874	14905.33	25935277	25.93528
4000.092	115.9794	121.4304	14745.34	25656889	25.65689
4100.037	117.9365	123.4795	15247.18	26530093	26.53009
4199.982	139.819	146.3905	21430.17	37288490	37.28849
4299.927	140.8054	147.4233	21733.63	37816517	37.81652
4399.872	132.1183	138.3279	19134.61	33294218	33.29422
4499.817	126.5867	132.5363	17565.87	30564615	30.56462
4600.143	124.675	130.5347	17039.31	29648396	29.6484
4700.089	123.5777	129.3859	16740.7	29128825	29.12882
4800.034	122.2889	128.0365	16393.35	28524422	28.52442
4899.979	122.0031	127.7372	16316.8	28391239	28.39124
4999.924	122.0558	127.7924	16330.91	28415777	28.41578

frequency (Hz)	Surface Vel C-D (m/s)	Shear wave Vel C-D (m/s)	Vs2 (m/s)	G(kg/ms2), N/m2	G (Mpa)
999.8322	132.4458	138.6707	19229.57	33459449	33.45945
1100.159	136.0532	142.4477	20291.35	35306945	35.30694
1200.104	150.0512	157.1036	24681.55	42945900	42.9459
1300.049	140.4876	147.0905	21635.62	37645977	37.64598
1399.994	133.4707	139.7438	19528.34	33979305	33.9793
1499.939	128.5938	134.6377	18127.32	31541538	31.54154
1599.884	134.9982	141.3431	19977.87	34761492	34.76149
1699.829	130.5829	136.7203	18692.44	32524845	32.52485
1800.156	127.8495	133.8585	17918.09	31177481	31.17748
1900.101	122.9041	128.6805	16558.68	28812108	28.81211
2000.046	128.6102	134.6549	18131.93	31549564	31.54956
2099.991	129.9285	136.0351	18505.55	32199663	32.19966
2199.936	127.6192	133.6173	17853.57	31065219	31.06522
2299.881	127.2521	133.233	17751.03	30886793	30.88679
2399.826	127.962	133.9762	17949.61	31232327	31.23233
2500.153	127.5776	133.5738	17841.95	31044993	31.04499
2600.098	127.4078	133.396	17794.48	30962402	30.9624

2700.043	128.5895	134.6332	18126.1	31539419	31.53942
2799.988	129.9972	136.1071	18525.14	32233737	32.23374
2899.933	132.1883	138.4012	19154.89	33329502	33.3295
2999.878	134.0347	140.3344	19693.74	34267104	34.2671
3099.823	135.4925	141.8606	20124.44	35016523	35.01652
3200.15	137.0529	143.4944	20590.65	35827728	35.82773
3300.095	138.5209	145.0313	21034.09	36599312	36.59931
3400.04	138.5522	145.0642	21043.62	36615898	36.6159
3499.985	138.6103	145.125	21061.26	36646590	36.64659
3599.93	142.3056	148.9939	22199.19	38626587	38.62659
3699.875	143.8278	150.5878	22676.67	39457410	39.45741
3799.82	143.9091	150.6728	22702.3	39501994	39.50199
3900.146	144.6509	151.4495	22936.96	39910303	39.9103
4000.092	144.2182	150.9965	22799.94	39671900	39.6719
4100.037	144.1011	150.8739	22762.93	39607494	39.60749
4199.982	143.9966	150.7644	22729.92	39550056	39.55006
4299.927	143.8879	150.6506	22695.61	39490356	39.49036
4399.872	142.1174	148.7969	22140.51	38524491	38.52449
4499.817	139.0988	145.6364	21209.97	36905349	36.90535
4600.143	135.6718	142.0484	20177.74	35109263	35.10926
4700.089	137.289	143.7416	20661.64	35951260	35.95126
4800.034	139.2373	145.7815	21252.24	36978894	36.97889
4899.979	140.3952	146.9937	21607.15	37596450	37.59645
4999.924	140.9169	147.54	21768.06	37876420	37.87642

Appendix B. Matlab script

B.1. Matlab script for run the test using step frequency;

```
% AzimanCompactDAQmxSteppedFrequency
% Matlab interface script to communicate with a NI 9172 chassis populated
with a 9263 signal source
% and multiple 9239 4-channel A/Ds
% Step through the frequencies

% Warning: the transpose function ' is actually the complex conjugate
transpose!

% Status is int32 value error code returned by the function in the event of
an error or warning.
% A value of 0 indicates success.   A positive value indicates a warning. A
negative value indicates an error.

clear all
%clear global
count=0;
NumberOfRXChannels = 4; % Define the number of RX channels being used
NumberOfTXChannels = 1; % Define the number of TX channels being used
InputSamplesPerChannel = 2^17; % Samples to be collected per channel
OutputSamplesPerChannel = 2^17; % Samples to be output per channel
BufferSize = InputSamplesPerChannel;
InputSamplingRate = double(50000);% Input Sampling rate
OutputSamplingRate = double(50000); % Output Sampling rate - normally the
same
ZeroPaddingTime = 0.00; % Zero pad transmission signal to there is a dead-
time to allow for signal to be received and processed without aliasses
StartingFrequency =100; % sweep from 0Hz to one third of the available
bandwidth
StepFrequency =10;
StopFrequency =10000;
SensorSpacing = 0.03; % accelerometer spacing (assume uniform) in meter
Vmax = 9.99;
```

```
NumOfPhaseRotation=1;
EstimatedVelocity=50;

LoopThroughTest = 0; % Test delay from transmit to receive
CrossSpectrumMeasurements = 1;% Collect data for velocity/phase coherence
measurements

NumberOfSnapshots =5; % Number of data collection operations to measure
real data

PassBandFraction = 0.50; % A/D converter passband as a ratio of the
sampling frequency
Bandwidth = OutputSamplingRate*PassBandFraction; % Bandwidth of
transmission signal

% Add experiment information here
Comment1 = 'One current measuring channel and four accelerometer. Order
from Department: REF,Chan1,Chan2...Chan4';
Comment2 = 'Chan0 measures voltage across 10 0hm resistor, Chans 1 - 4
measure voltage from accelerometers';
Comment3 = 'Add specific comments here';

% Check out valid sampling rate
ValidSamplingRates = 50e3./(1:31); % Search for best fit of sampling rate
[ActualInputSamplingRate ActualInputSamplingRateIndex] =
min(abs(InputSamplingRate-ValidSamplingRates));
ActualInputSamplingRate = ValidSamplingRates(ActualInputSamplingRateIndex);
if ActualInputSamplingRate~=InputSamplingRate,
    fprintf('Program input sampling rate replaced with actual sampling rate
of %f Hz\n',ActualInputSamplingRate);
    InputSamplingRate = ActualInputSamplingRate;
end
[ActualOutputSamplingRate ActualOutputSamplingRateIndex] =
min(abs(OutputSamplingRate-ValidSamplingRates));
ActualOutputSamplingRate =
ValidSamplingRates(ActualOutputSamplingRateIndex);
if ActualOutputSamplingRate~=OutputSamplingRate,
    fprintf('Program output sampling rate replaced with actual sampling
rate of %f Hz\n',ActualOutputSamplingRate);
    OutputSamplingRate = ActualOutputSamplingRate;
end

fprintf('Observation period = %f
s\n',InputSamplesPerChannel/ActualOutputSamplingRate);


% Predicted input A/D channel latency
PredictedInputLatency = 38.4/InputSamplingRate + 3e-6; % latency measured
in seconds

% Predict output D/A latency
OutputLatency = [3e-6 5e-6 7.5e-6 9.5e-6];
PredictedOutputLatency = OutputLatency(NumberOfTXChannels);

% Measurements imply an extra few samples of delay
AdditionalDelaySamples = 2;
TotalPredictedLatency = PredictedOutputLatency + PredictedInputLatency +
AdditionalDelaySamples/InputSamplingRate + 1.8e-6;
```

```
% The IDAQmx DLL functions appear to exist in 'nicaiu.dll'
if ~libisloaded('nicaiu') % checks if library is loaded
    %hfile  =  'C:\Program Files\National Instruments\NI-DAQ\DAQmx ANSI C
Dev\include\NIDAQmx.h';
    %hfile  =  'C:\\Program Files\\National Instruments\\NI-DAQ\\DAQmx ANSI
C Dev\\include\\NIDAQmx.h';
    hfile  =  'NIDAQmx.h';
    [notfound,warnings] = loadlibrary('nicaiu.dll', hfile, 'mfilename',
'mxproto');
    % mxproto contains the function prototypes
end

%% required constants (see NIDAQmx.h)
% Terminal Configuration
DAQmx_Val_Cfg_Default = int32(-1);              % Default
DAQmx_Val_RSE = int32(10083);                   % RSE
DAQmx_Val_NRSE = int32(10078);                  % NRSE
DAQmx_Val_Diff = int32(10106);                  % Differential
DAQmx_Val_PseudoDiff = int32(12529);            % Pseudodifferential
                                                % Units
DAQmx_Val_Volts = int32(10348);                 % Volts
DAQmx_Val_FromCustomScale = int32(10065);       % From Custom Scale
                                                % Active Edge
DAQmx_Val_Rising = int32(10280);                % Rising
DAQmx_Val_Falling = int32(10171);               % Falling
                                                % Sample Mode
DAQmx_Val_FiniteSamps = int32(10178);           % Finite Samples
DAQmx_Val_ContSamps = int32(10123);             % Continuous Samples
DAQmx_Val_HWTimedSinglePoint = int32(12522);    % Hardware Timed Single
Point
                                                % Fill Mode
DAQmx_Val_GroupByChannel = uint32(0);           % Group by Channel
DAQmx_Val_GroupByScanNumber = uint32(1);        % Group by Scan Number
                                                     % Device ID
DAQmx_Val_CompactDAQChassis = uint32(14658);    % CompactDAQ chassis


%% Try getting names of NI cards
DeviceNames = libpointer('stringPtr',blanks(60));
[Status, DeviceNames] =
calllib('nicaiu','DAQmxGetSysDevNames',DeviceNames,uint32(60));
%DAQmxGetSysDevNames(char *data, uInt32 bufferSize);
if isempty(DeviceNames),
    fprintf('No NI DAQ devices found\n');
    unloadlibrary 'nicaiu';                 % unload library
    return
end
% There may be multiple device in a comma-separated list
CommaSeparatedVariableCell = textscan(DeviceNames, '%s', 'delimiter', ',');
% Convert to a list of CSV names
% Process each name in-turn
IndividualDeviceNameList = cell(numel(CommaSeparatedVariableCell{1}),1);
for DeviceNameIndex = 1:numel(CommaSeparatedVariableCell{1}),
    IndividualDeviceName =
char(CommaSeparatedVariableCell{1}(DeviceNameIndex));
    fprintf('Device Name = %s    ',IndividualDeviceName);
    ProductType = libpointer('stringPtr',blanks(60));
```

```
    [Status,IndividualDeviceName,ProductType] =
calllib('nicaiu','DAQmxGetDevProductType',IndividualDeviceName,ProductType,
uint32(60));
    %int32 DAQmxGetDevProductType(const char device[], char *data, uInt32
bufferSize);
    IndividualDeviceNameList{DeviceNameIndex,1} = char(ProductType);
    fprintf('Product Type = %s\n',ProductType);
end

% Check if required chassis exists in list
DeviceComparison = strcmp(IndividualDeviceNameList,'cDAQ-9172');
if sum(DeviceComparison) == 0,
    fprintf('cDAQ-9172 compact device chassis not found\n');
    unloadlibrary 'nicaiu';                 % unload library
    return
end
% Recover device name of chassis
IndividualChassisName =
char(CommaSeparatedVariableCell{1}(DeviceComparison));

% Check if required input modules exists in list
DeviceComparison = strcmp(IndividualDeviceNameList,'NI 9239');
if sum(DeviceComparison) == 0,
    fprintf('No NI 9239 A/D modules found\n');
    unloadlibrary 'nicaiu';                 % unload library
    return
end
% Recover device name of A/D modules
IndividualADNames = char(CommaSeparatedVariableCell{1}(DeviceComparison));

% Check if required output modules exists in list
DeviceComparison = strcmp(IndividualDeviceNameList,'NI 9263');
if sum(DeviceComparison) == 0,
    fprintf('No NI 9263 D/A modules found\n');
    unloadlibrary 'nicaiu';                 % unload library
    return
end
% Recover device name of D/A modules
IndividualDANames = char(CommaSeparatedVariableCell{1}(DeviceComparison));
%% Determine which input channels are available in device - there may be
multiple modules
for ModuleIndex = 1:size(IndividualADNames,1),
    PhysicalChannels = libpointer('stringPtr',blanks(200));
    [Status,IndividualDeviceName,PhysicalChannels] =
calllib('nicaiu','DAQmxGetDevAIPhysicalChans',IndividualADNames(ModuleIndex
,:),PhysicalChannels,uint32(200));
    %int32  DAQmxGetDevAIPhysicalChans(const char device[], char *data,
uInt32 bufferSize);
    if Status ~= 0,
        fprintf('Error in DAQmxGetDevAIPhysicalChans.   Status =
%d\n',Status);
        return
    end

    % There may be multiple physical channels in a comma-separated list
    CommaSeparatedVariableCell = textscan(PhysicalChannels, '%s',
'delimiter', ',');     % Convert to a list of CSV names
    % Convert to a full list
    if ModuleIndex == 1,
```

```
        IndividualPhysicalChannelName =
cell(numel(CommaSeparatedVariableCell{1}),size(IndividualADNames,1));
    end
    for PhysicalChannelIndex = 1:numel(CommaSeparatedVariableCell{1}),
        IndividualPhysicalChannelName{PhysicalChannelIndex,ModuleIndex} =
char(CommaSeparatedVariableCell{1}(PhysicalChannelIndex));
    end
end

%% Analogue Input configuration string generation
% Make a single string determined by the 'NumberOfRXChannels' requested
if NumberOfRXChannels > numel(IndividualPhysicalChannelName),
    fprintf('Request number of A/D channels exceeds the number
available\n');
    return
end

% Assume A/D modules are obtained in groups of four
CompleteADModules = floor((NumberOfRXChannels-1)/4);        % e.g.
0,0,0,0,1,1,1,1,2,2,2,2,3,3,3,3
PartialADChannels = mod((NumberOfRXChannels-1),4);          % e.g.
1,2,3,4,1,2,3,4,1,2,3,4,1,2,3,4
if NumberOfRXChannels == 1,
    % single channel
    AIConfigString ={IndividualPhysicalChannelName{1,1}};
else
    % multiple channels
    AIConfigString = '';
    if CompleteADModules >= 1,
        for ModulesIndex = 1:CompleteADModules,
            % Complete group of four channels
            AIConfigString =
strcat(AIConfigString,cellstr([IndividualPhysicalChannelName{1,ModulesIndex
} ':' IndividualPhysicalChannelName{4,ModulesIndex}]),',');
        end
    end
    % Add in last group
    if PartialADChannels == 0,
        AIConfigString =
strcat(AIConfigString,{IndividualPhysicalChannelName{1,CompleteADModules+1}
},',');
    else
        AIConfigString =
strcat(AIConfigString,cellstr([IndividualPhysicalChannelName{1,CompleteADMo
dules+1} ':'
IndividualPhysicalChannelName{PartialADChannels+1,CompleteADModules+1}]));
    end
end
AIConfigString = char(AIConfigString);
fprintf('A/D Configuration String = %s\n',AIConfigString);

%% Determine which output channels are available in device - there may be
multiple modules
for ModuleIndex = 1:size(IndividualDANames,1),
    PhysicalChannels = libpointer('stringPtr',blanks(200));
    [Status,IndividualDeviceName,PhysicalChannels] =
calllib('nicaiu','DAQmxGetDevAOPhysicalChans',IndividualDANames(ModuleIndex
,:),PhysicalChannels,uint32(200));
```

```
    %int32  DAQmxGetDevAIPhysicalChans(const char device[], char *data,
uInt32 bufferSize);
    if Status ~= 0,
        fprintf('Error in DAQmxGetDevAOPhysicalChans.   Status =
%d\n',Status);
        return
    end

    % There may be multiple physical channels in a comma-separated list
    CommaSeparatedVariableCell = textscan(PhysicalChannels, '%s',
'delimiter', ',');     % Convert to a list of CSV names
    % Convert to a full list
    if ModuleIndex == 1,
        IndividualPhysicalChannelName =
cell(numel(CommaSeparatedVariableCell{1}),size(IndividualDANames,1));
    end
    for PhysicalChannelIndex = 1:numel(CommaSeparatedVariableCell{1}),
        IndividualPhysicalChannelName{PhysicalChannelIndex,ModuleIndex} =
char(CommaSeparatedVariableCell{1}(PhysicalChannelIndex));
    end
end
% Re-arrange into a single row vector
IndividualPhysicalChannelName =
reshape(IndividualPhysicalChannelName,[],1);

%% Analogue Output configuration string generation
% Make a single string determined by the 'NumberOfTXChannels' requested
if NumberOfTXChannels > numel(IndividualPhysicalChannelName),
    fprintf('Request number of D/a channels exceeds the number
available\n');
    return
end

% Assume D/A modules are obtained in groups of four
CompleteDAModules = floor((NumberOfTXChannels-1)/4);        % e.g.
0,0,0,0,1,1,1,1,2,2,2,2,3,3,3,3
PartialDAChannels = mod((NumberOfTXChannels-1),4);          % e.g.
1,2,3,4,1,2,3,4,1,2,3,4,1,2,3,4
if NumberOfTXChannels == 1,
    % single channel
    AOConfigString ={IndividualPhysicalChannelName{1,1}};
else
    % multiple channels
    AOConfigString = '';
    if CompleteDAModules >= 1,
        for ModulesIndex = 1:CompleteDAModules,
            % Complete group of four channels
            AOConfigString =
strcat(AOConfigString,cellstr([IndividualPhysicalChannelName{1,ModulesIndex
} ':' IndividualPhysicalChannelName{4,ModulesIndex}]),',');
        end
    end
    % Add in last group
    if PartialDAChannels == 0,
        AOConfigString =
strcat(AOConfigString,{IndividualPhysicalChannelName{1,CompleteDAModules+1}
},',');
    else
```

```
        AOConfigString =
strcat(AOConfigString,cellstr([IndividualPhysicalChannelName{1,CompleteDAMo
dules+1} ':'
IndividualPhysicalChannelName{PartialDAChannels+1,CompleteDAModules+1}]));
    end
end
AOConfigString = char(AOConfigString);
fprintf('D/A Configuration String = %s\n',AOConfigString);

%% Create new tasks
TaskHandle1 = libpointer('uint32Ptr',0);        % VOID task handle pointers
TaskHandle2 = libpointer('uint32Ptr',0);
InputTaskName = 'AITask';
OutputTaskName = 'AOTask';
[Status,TaskNameText,TaskHandle1]  =
calllib('nicaiu','DAQmxCreateTask',InputTaskName,TaskHandle1);     % Create
a NIDAQmx Task TaskHandle1
% int32 DAQmxCreateTask (const char taskName[], TaskHandle, *taskHandle);
if Status ~= 0,
    fprintf('Error in DAQmxCreateTask - Input Task.   Status =
%d\n',Status);
    return
end
TaskHandle1Numeric = TaskHandle1;
TaskHandle1 = libpointer('uint32Ptr',TaskHandle1);

[Status,TaskNameText,TaskHandle2]  =
calllib('nicaiu','DAQmxCreateTask',OutputTaskName,TaskHandle2);     %
Create a NIDAQmx Task TaskHandle2
% int32 DAQmxCreateTask (const char taskName[], TaskHandle, *taskHandle);
if Status ~= 0,
    fprintf('Error in DAQmxCreateTask - Output Task.   Status =
%d\n',Status);
    return
end
TaskHandle2Numeric = TaskHandle2;
TaskHandle2 = libpointer('uint32Ptr',TaskHandle2);

% Generate a D/A output channels and A/D input channel to be referred to
% later
minVal = double(-10);
maxVal = double(10);

% Generate a D/A output channel
[Status,ChannelNameText,c,d]  =
calllib('nicaiu','DAQmxCreateAOVoltageChan',TaskHandle2Numeric,AOConfigStri
ng,'',minVal,maxVal,DAQmx_Val_Volts,'');
% int32 DAQmxCreateAOVoltageChan (TaskHandle taskHandle, const char
physicalChannel[], const char nameToAssignToChannel[], float64 minVal,
float64 maxVal, int32 units, const char customScaleName[]);
if Status ~= 0,
    fprintf('Error in DAQmxCreateAOVoltageChan.   Status = %d\n',Status);
    return
end

[Status,ChannelNameText,c,d]  =
calllib('nicaiu','DAQmxCreateAIVoltageChan',TaskHandle1Numeric,AIConfigStri
ng,'',DAQmx_Val_Diff,minVal,maxVal,DAQmx_Val_Volts,'');
```

```
% int32 DAQmxCreateAIVoltageChan (TaskHandle taskHandle, const char
physicalChannel[], const char nameToAssignToChannel[],
% int32 terminalConfig, float64 minVal, float64 maxVal, int32 units, const
char customScaleName[]);
if Status ~= 0,
    fprintf('Error in DAQmxCreateAIVoltageChan.   Status = %d\n',Status);
    return
end


%%
% Set up the on-board timing with internal clock source
ActiveEdge = DAQmx_Val_Rising;          % Samplig edge
SampleMode = DAQmx_Val_FiniteSamps;     % Collect a finite number of
samples
%SampleMode = DAQmx_Val_ContSamps;       % Collect samples continuously
%SamplesToAcquire = uint64(InputSamplesPerChannel*NumberOfRXChannels);
% Make buffer size large - several times expected window size
SamplesToAcquire = uint64(BufferSize);
[Status,ClockSource] =
calllib('nicaiu','DAQmxCfgSampClkTiming',TaskHandle1Numeric,'OnboardClock',
InputSamplingRate,ActiveEdge,SampleMode,SamplesToAcquire);
% int32 DAQmxCfgSampClkTiming (TaskHandle taskHandle, const char
source[],float64 rate, int32 ActiveEdge, int32 SampleMode, uInt64
% sampsPerChanToAcquire);
if Status ~= 0,
    fprintf('Error in DAQmxCfgSampClkTiming for TaskHandle1   Status =
%d\n',Status);
    Status = calllib('nicaiu','DAQmxClearTask',TaskHandle1);           %
Clear the task
    return
end


TerminalName = 'ai/StartTrigger';

%  Define the parameters for a digital edge start trigger for output.  Set
the analog output to trigger off the AI start trigger. This is an internal
trigger signal.
[Status,a] =
calllib('nicaiu','DAQmxCfgDigEdgeStartTrig',TaskHandle2Numeric,TerminalName
,DAQmx_Val_Rising);
% [int32] DAQmxCfgDigEdgeStartTrig (TaskHandle taskHandle, const char
triggerSource[], int32 triggerEdge);
if Status ~= 0,
    fprintf('Error in DAQmxCfgDigEdgeStartTrig.   Status = %d\n',Status);
    Status = calllib('nicaiu','DAQmxClearTask',TaskHandle2Numeric);
% Clear the task
    return
end

%% Make an LFM transmission signal
ZeroPaddingPoints = round(OutputSamplingRate.*ZeroPaddingTime);     % This
is the number of zeros to be added after the transmission has finished
ActiveTXPoints = OutputSamplesPerChannel - ZeroPaddingPoints;       % This
is the number of samples within the active region of the TX signal
% Weight received signals with a suitable window
WeightingFunction = tukeywin(ActiveTXPoints,0.005)';  % Tukey Window
```

```
% Make a single chirp signal for transmission
% Make a complex chirp signal - zero padded
TXSignal = zeros(1,OutputSamplesPerChannel);
TXTimeIndex = 0:ActiveTXPoints-1;

%TXSignal(1,1:ActiveTXPoints) =
exp(j.*(StartingFrequency*2*pi*TXTimeIndex/OutputSamplingRate +
Bandwidth*2*pi*TXTimeIndex.^2./(2*ActiveTXPoints*OutputSamplingRate)));
FixedFrequency = 500;
TXSignal(1,1:ActiveTXPoints) =
exp(j.*(FixedFrequency*2*pi*TXTimeIndex/OutputSamplingRate));

% scale result
TXSignal(1:ActiveTXPoints) = Vmax .*
WeightingFunction.*TXSignal(1:ActiveTXPoints) / max(abs(TXSignal));
TXSignal('last') = 0;     % Last sample should be zero

% Make a one-sided spectral estimate of the complex TX signal - including
zero padding
DriveFFT2N = conj(fft(TXSignal,2*InputSamplesPerChannel) ./
InputSamplesPerChannel);

% If the signal was generated in a complex form then convert back to a real
number
if ~isreal(TXSignal),
    % Convert back to a real signal (start at zero voltage)
    TXSignal = -imag(TXSignal);
end

% Calculate the spectrum of the transmitted signal
TXSignalFFT = conj(fft(TXSignal));

% Time index for display purposes
TimeIndex = (0:(OutputSamplesPerChannel-1))/OutputSamplingRate;
% Frequency index for display purposes - assuming zero padded
FrequencyIndex = (0:(OutputSamplesPerChannel -
1)).*OutputSamplingRate./OutputSamplesPerChannel;

DisplayThis = 0;
if DisplayThis == 1,
    figure(1)
    plot(TimeIndex,real(TXSignal),'r')
    title('Transmitted waveform')
    xlabel('Time (s)')
    ylabel('Voltage (V)')
    figure(2)

plot(FrequencyIndex,20*log10(abs(fft(TXSignal)./OutputSamplesPerChannel)));
    title('Spectrum of transmitted signal')
    xlabel('Frequency (Hz)')
    ylabel('Spectrum Level (dB)')
    xlim([0 OutputSamplingRate*PassBandFraction])
end
%%
% Make buffer size same as number of samples transmitted -
SamplesToTx = uint64(BufferSize);
```

```
[Status,ClockSource] =
calllib('nicaiu','DAQmxCfgSampClkTiming',TaskHandle2Numeric,'ai/SampleClock
',OutputSamplingRate,ActiveEdge,SampleMode,SamplesToTx);
if Status ~= 0,
    fprintf('Error in DAQmxCfgSampClkTiming for TaskHandle2.   Status =
%d\n',Status);
    Status = calllib('nicaiu','DAQmxClearTask',TaskHandle2Numeric);
% Clear the task
    return
end

%%
LoopThroughLatency = zeros(1,NumberOfRXChannels);
if LoopThroughTest == 1,
    %% Write samples to task
    SamplesPerChannelWritten = libpointer('int32Ptr',0);
    [Status,DAQmxWriteAnalogF64Return1,DAQmxWriteAnalogF64Return2] =
calllib('nicaiu','DAQmxWriteAnalogF64',TaskHandle2Numeric,int32(OutputSampl
esPerChannel),int32(0),double(-
1),DAQmx_Val_GroupByScanNumber,TXSignal,SamplesPerChannelWritten,[]);
    % int32 DAQmxWriteAnalogF64 (TaskHandle taskHandle, int32
numSampsPerChan, bool32 autoStart, float64 timeout, bool32 dataLayout,
float64 writeArray[], int32 *sampsPerChanWritten, bool32 *reserved);
    if Status ~= 0,
        fprintf('Error in DAQmxWriteAnalogF64.   Status = %d\n',Status);
        Status = calllib('nicaiu','DAQmxClearTask',TaskHandle1Numeric);
%#ok<NASGU> % Clear the tasks
        Status = calllib('nicaiu','DAQmxClearTask',TaskHandle2Numeric);
        return
    end
    % Perform loop-through latency check
    for InputSensorIndex = 1:NumberOfRXChannels,
        % Scan through each input channel
        % Prompt user to connect desired loop through
        fprintf('Testing input channel %d\n',InputSensorIndex-1)
        UserReply = input('Connect output to desired input channel and
press enter','s');
        % Collect data
        % Start the tasks - start output before input as the input task
would trigger the output task
        Status = calllib('nicaiu','DAQmxStartTask',TaskHandle2Numeric);
        % int32 DAQmxStartTask (TaskHandle taskHandle);
        if Status ~= 0,
            fprintf('Error in DAQmxStartTask.   Status = %d\n',Status);
            Status = calllib('nicaiu','DAQmxClearTask',TaskHandle2Numeric);
% Clear the task
            return
        end

        Status = calllib('nicaiu','DAQmxStartTask',TaskHandle1Numeric);
        % int32 DAQmxStartTask (TaskHandle taskHandle);
        if Status ~= 0,
            fprintf('Error in DAQmxStartTask.   Status = %d\n',Status);
            Status = calllib('nicaiu','DAQmxClearTask',TaskHandle1Numeric);
%#ok<NASGU> % Clear the tasks
            Status = calllib('nicaiu','DAQmxClearTask',TaskHandle2Numeric);
            return
        end
        %FillMode = DAQmx_Val_GroupByChannel;
```

```
        FillMode = DAQmx_Val_GroupByScanNumber;                         %
Interleaved samples
        RecoveredInputData =
zeros(InputSamplesPerChannel*NumberOfRXChannels,1);
        Timeout = double(-1);                       % maximum waiting time
before timeout (in secs)
        RecoveredInputDataPtr  =
libpointer('doublePtr',zeros(InputSamplesPerChannel*NumberOfRXChannels,1));
        ReadPtr = libpointer('int32Ptr',0);
        ReservedPtr = libpointer('uint32Ptr',[]);


[Status,RecoveredData,DAQmxReadAnalogF64Return1,DAQmxReadAnalogF64Return2]
=
calllib('nicaiu','DAQmxReadAnalogF64',TaskHandle1Numeric,int32(InputSamples
PerChannel),Timeout,FillMode,RecoveredInputDataPtr,uint32(InputSamplesPerCh
annel*NumberOfRXChannels),ReadPtr,ReservedPtr);
        % int32 DAQmxReadAnalogF64 (TaskHandle taskHandle, int32
numSampsPerChan, float64 timeout, bool32 fillMode, float64 readArray[],
uInt32 arraySizeInSamps,int32 *sampsPerChanRead, bool32 *reserved);
        if Status ~= 0,
            fprintf('Error in DAQmxReadAnalogF64.   Status = %d\n',Status);
        end

        % Stop the tasks
        Status = calllib('nicaiu','DAQmxStopTask',TaskHandle1Numeric);
        % int32 DAQmxStopTask(uint32)
        % int32 DAQmxStopTask (TaskHandle taskHandle);
        if Status ~= 0,
            fprintf('Error/warning in DAQmxStopTask.   Status =
%d\n',Status);
        end
        Status = calllib('nicaiu','DAQmxStopTask',TaskHandle2Numeric);
        if Status ~= 0,
            fprintf('Error/warning in DAQmxStopTask.   Status =
%d\n',Status);
        end

        % If more than one A/D channel is used, then the sampes should be
separated
        RecoveredData =
reshape(RecoveredData,NumberOfRXChannels,InputSamplesPerChannel);



        figure(3)
        plot(TimeIndex,RecoveredData(InputSensorIndex,:))
        title('Raw Input Data')
        xlabel('Time (s)')
        ylabel('Voltage (V)')
        ylim([-1 1])

        RecoveredDataFFT =
fft(RecoveredData(InputSensorIndex,:),2*InputSamplesPerChannel);
        % Calculate the covariance
        RecoveredDataFFT(1) = 0;       % Remove any DC component
        DisplayThis = 1;
        if DisplayThis == 1,
            figure(4)
```

```
            PaddedFrequencyIndex = (0:(2*OutputSamplesPerChannel -
1)).*OutputSamplingRate/OutputSamplesPerChannel/2;
            plot(PaddedFrequencyIndex,20*log10(abs(DriveFFT2N)),'r')
            hold on
            plot(PaddedFrequencyIndex,20*log10(abs(RecoveredDataFFT) ./
InputSamplesPerChannel),'k');
            hold off
            legend('Drive Signal','Sense Signal',0)
            ylabel('Spectral Amplitude (dB)')
            xlabel('Frequency (Hz)')
            title('Linear Spectra of Transmit and Received Signals');
            xlim([0 InputSamplingRate*PassBandFraction]);
            drawnow
        end
        % Calculate the correlation function
        CrossSpectrum = RecoveredDataFFT .* DriveFFT2N;
        CrossCorrelation = ifft(CrossSpectrum);
        [maxval LoopThroughLatency(InputSensorIndex)] =
max(abs(CrossCorrelation));
        % Re-order data - swap frequency portions
        %CrossCorrelation =
[CrossCorrelation(NumberSamples+1:2*NumberSamples) ;
CrossCorrelation(1:NumberSamples)];
        figure(5)
        DisplayTimeIndex2N = (0:(2*InputSamplesPerChannel-
1))/InputSamplingRate;
        plot(DisplayTimeIndex2N,abs(CrossCorrelation),'k')
        title('Cross Correlation Function')
        ylabel('Magnitude')
        xlabel('Time (s)')
        %xlim([0 RXSamplingFrequency/(2*NumberRXChannels)])
        drawnow

        % select a small bit of the correlation output
        SegmentLength = 1000;
        SegmentCrossCorrelation = CrossCorrelation(1:SegmentLength);
        SegmentCrossCorrelation = abs(SegmentCrossCorrelation);
        SegmentTime = DisplayTimeIndex2N(1:SegmentLength);
        % Normalise correlation value
        SegmentCrossCorrelation = SegmentCrossCorrelation ./
max(SegmentCrossCorrelation);
        figure(6)
        plot(SegmentTime,SegmentCrossCorrelation,'k')
        title('Cross Correlation Function')
        ylabel('Magnitude')
        xlabel('Time (s)')

        % Plot the cross spectrum
        % First correct by the guess
        DisplayFrequencyIndex2N =
InputSamplingRate*(0:(2*InputSamplesPerChannel-
1))/(2*InputSamplesPerChannel);
        CompensationFunction =
exp(j*2*pi*DisplayFrequencyIndex2N*TotalPredictedLatency);
        CompensatedCrossSpectrum = CompensationFunction .* CrossSpectrum;
        figure(7)

plot(DisplayFrequencyIndex2N/1000,angle(CrossSpectrum),DisplayFrequencyInde
x2N/1000,angle(CompensatedCrossSpectrum))
```

```
        title('Cross Spectrum Function')
        ylabel('Phase (rads)')
        xlabel('Frequency (kHz)')
        figure(8)
        plot(DisplayFrequencyIndex2N/1000,abs(CrossSpectrum))
        title('Cross Spectrum Function')
        ylabel('Magnitude)')
        xlabel('Frequency (kHz)')
        %xlim([0 RXSamplingFrequency/(2*NumberRXChannels)])
        drawnow

    end
    % Convert sample values into time
    LoopThroughLatencyTime = DisplayTimeIndex2N(LoopThroughLatency);
    fprintf('Measured Latency = %e secs \n',LoopThroughLatencyTime);
end


%% Normal data collection operation
if CrossSpectrumMeasurements == 1,
    % Prompt user to connect desired loop through
    UserReply = input('Connect output to desired input channel and press
enter','s');
    % Predict effects of D/A sampling zero-order-hold
    % Predicted amplitude & phase compensation value
    AmplitudeFunction = sinc(FrequencyIndex/OutputSamplingRate);
    CompensationFunction = AmplitudeFunction .*
exp(j*2*pi*FrequencyIndex*TotalPredictedLatency);
    % Modify predicted TX spectrum
    TXSignalFFT = TXSignalFFT .* AmplitudeFunction;
    %FillMode = DAQmx_Val_GroupByChannel;
    FillMode = DAQmx_Val_GroupByScanNumber;                    %
Interleaved samples


   %for SteppedFrequencyIndex =
StartingFrequency:StepFrequency:StartingFrequency,
   for SteppedFrequencyIndex =
StartingFrequency:StepFrequency:StopFrequency,

        CrossSpectrum = zeros(NumberOfRXChannels,InputSamplesPerChannel);
        PowerSpectrum = zeros(NumberOfRXChannels,InputSamplesPerChannel);

        % Generate a CW signal
        WeightingFunction = tukeywin(OutputSamplesPerChannel,0.005)';
% Tukey Window

        % Make a single CW signal for transmission
        TXSignal = zeros(1,OutputSamplesPerChannel);
        TXTimeIndex = 0:OutputSamplesPerChannel-1;

        TXSignal =
exp(j.*(SteppedFrequencyIndex*2*pi*TXTimeIndex/OutputSamplingRate));

        % scale result
        TXSignal = Vmax .* WeightingFunction.*TXSignal /
max(abs(TXSignal));
        TXSignal('last') = 0;     % Last sample should be zero
```

```
        % Make a one-sided spectral estimate of the complex TX signal -
including zero padding
        DriveFFT2N = conj(fft(TXSignal,2*InputSamplesPerChannel) ./
InputSamplesPerChannel);

        % If the signal was generated in a complex form then convert back
to a real number
        if ~isreal(TXSignal),
            % Convert back to a real signal (start at zero voltage)
            TXSignal = -imag(TXSignal);
        end

        % Calculate the spectrum of the transmitted signal
        TXSignalFFT = conj(fft(TXSignal));

        % Time index for display purposes
        TimeIndex = (0:(OutputSamplesPerChannel-1))/OutputSamplingRate;
        % Frequency index for display purposes - assuming zero padded
        FrequencyIndex = (0:(OutputSamplesPerChannel -
1)).*OutputSamplingRate./OutputSamplesPerChannel;

        DisplayThis = 1;
        if DisplayThis == 1,
            figure(1)
            plot(TimeIndex,real(TXSignal),'r')
            title('Transmitted waveform')
            xlabel('Time (s)')
            ylabel('Voltage (V)')
            figure(2)

plot(FrequencyIndex,20*log10(abs(fft(TXSignal)./OutputSamplesPerChannel)));
            title('Spectrum of transmitted signal')
            xlabel('Frequency (Hz)')
            ylabel('Spectrum Level (dB)')
            xlim([0 OutputSamplingRate*PassBandFraction])
        end
        % Write samples to task
        SamplesPerChannelWritten = libpointer('int32Ptr',0);
        [Status,DAQmxWriteAnalogF64Return1,DAQmxWriteAnalogF64Return2] =
calllib('nicaiu','DAQmxWriteAnalogF64',TaskHandle2Numeric,int32(OutputSampl
esPerChannel),int32(0),double(-
1),DAQmx_Val_GroupByScanNumber,TXSignal,SamplesPerChannelWritten,[]);
        % int32 DAQmxWriteAnalogF64 (TaskHandle taskHandle, int32
numSampsPerChan, bool32 autoStart, float64 timeout, bool32 dataLayout,
float64 writeArray[], int32 *sampsPerChanWritten, bool32 *reserved);
        if Status ~= 0,
            fprintf('Error in DAQmxWriteAnalogF64.   Status =
%d\n',Status);
            Status = calllib('nicaiu','DAQmxClearTask',TaskHandle1Numeric);
%#ok<NASGU> % Clear the tasks
            Status = calllib('nicaiu','DAQmxClearTask',TaskHandle2Numeric);
            return
        end

        RecoveredInputData =
zeros(InputSamplesPerChannel*NumberOfRXChannels,1);
        Timeout = double(-1);                    % maximum waiting time
before timeout (in secs)
```

```
        RecoveredInputDataPtr  =
libpointer('doublePtr',zeros(InputSamplesPerChannel*NumberOfRXChannels,1));
        ReadPtr = libpointer('int32Ptr',0);
        ReservedPtr = libpointer('uint32Ptr',[]);

        InputSensorIndex = 1;       % Process for channel one - this can be
updated later
        for SnapShotNumber = 1:NumberOfSnapshots,
            fprintf('Snapshot number = %d\n',SnapShotNumber);
            % Start the tasks - start output before input as the input task
would trigger the output task
            Status = calllib('nicaiu','DAQmxStartTask',TaskHandle2Numeric);
            % int32 DAQmxStartTask (TaskHandle taskHandle);
            if Status ~= 0,
                fprintf('Error in DAQmxStartTask.   Status = %d\n',Status);
                Status =
calllib('nicaiu','DAQmxClearTask',TaskHandle2Numeric);           % Clear
the task
                return
            end

            Status = calllib('nicaiu','DAQmxStartTask',TaskHandle1Numeric);
            % int32 DAQmxStartTask (TaskHandle taskHandle);
            if Status ~= 0,
                fprintf('Error in DAQmxStartTask.   Status = %d\n',Status);
                Status =
calllib('nicaiu','DAQmxClearTask',TaskHandle1Numeric);
%#ok<NASGU> % Clear the tasks
                Status =
calllib('nicaiu','DAQmxClearTask',TaskHandle2Numeric);
                return
            end

            % Collect the data
            [Status,RecoveredData,e,f] =
calllib('nicaiu','DAQmxReadAnalogF64',TaskHandle1Numeric,int32(InputSamples
PerChannel),Timeout,FillMode,RecoveredInputDataPtr,uint32(InputSamplesPerCh
annel*NumberOfRXChannels),ReadPtr,ReservedPtr);
            % [int32, doublePtr, int32Ptr, uint32Ptr]
DAQmxReadAnalogF64(uint32, int32, double, uint32, doublePtr, uint32,
int32Ptr, uint32Ptr)
            % int32 DAQmxReadAnalogF64 (TaskHandle taskHandle, int32
numSampsPerChan, float64 timeout, bool32 fillMode, float64 readArray[],
uInt32 arraySizeInSamps,int32 *sampsPerChanRead, bool32 *reserved);
            if Status ~= 0,
                fprintf('Error in DAQmxReadAnalogF64.   Status =
%d\n',Status);
            end
            % If more than one A/D channel is used, then the sampes should
be separated
            RecoveredData =
reshape(RecoveredData,NumberOfRXChannels,InputSamplesPerChannel);

            % Stop the tasks
            Status = calllib('nicaiu','DAQmxStopTask',TaskHandle1Numeric);
            % int32 DAQmxStopTask(uint32)
            % int32 DAQmxStopTask (TaskHandle taskHandle);
            if Status ~= 0,
                fprintf('Error in DAQmxStopTask.   Status = %d\n',Status);
```

```
            end
            Status = calllib('nicaiu','DAQmxStopTask',TaskHandle2Numeric);
            if Status ~= 0,
                fprintf('Error in DAQmxStopTask.   Status = %d\n',Status);
            end

            % Save results structure to disc for later use
            Date = now;
            FileName = datestr(Date);
            % Replace colons
            for i=1:length(FileName),
                if (FileName(i) == ':')||(FileName(i) == ' '),
                    FileName(i) = '-';
                end
            end
            % Add extra Pre-fix
            FileName = strcat('Aziman-', FileName);
            fprintf('File name to be used = %s\n',FileName);
            save(FileName,
'RecoveredData','Date','TXSignalFFT','NumberOfRXChannels','InputSamplesPerC
hannel','InputSamplingRate','NumberOfSnapshots','SteppedFrequencyIndex','Co
mment1','Comment2','Comment3')

            DoThis = 1;
            if DoThis == 1,
                % Fourier transform - normally an fft operates on each
colum on the matrix
                RecoveredDataFFT =
fft(RecoveredData,InputSamplesPerChannel,2);
                % Calculate the averaged cross-spectrum
                CrossSpectrum = CrossSpectrum +
RecoveredDataFFT.*repmat(TXSignalFFT,NumberOfRXChannels,1);
                % Calculate the averaged power-spectrum
                PowerSpectrum = PowerSpectrum +
RecoveredDataFFT.*conj(RecoveredDataFFT);
                % Only display on single snapshot usage - takes up too much
time otherwise
                DisplayThis = 1;
                if DisplayThis == 1,
                    % Display data for channel 1
                    InputSensorIndex = 1;
                    figure(3)
                    plot(TimeIndex,RecoveredData)
                    title('Raw Input Data')
                    xlabel('Time (s)')
                    ylabel('Voltage (V)')
                    %ylim([-1 1])
                    legend('RX0','RX1',0)
                    drawnow

                end
            end
        end

        DoThis = 1;
        if DoThis == 1,
            count=count+1;
            % Normalise by the number of snapshots
            CrossSpectrum = CrossSpectrum ./ NumberOfSnapshots;
```

```
            PowerSpectrum = PowerSpectrum ./ NumberOfSnapshots;

            % normalise the cross-spectrum
            %CrossSpectrum = CrossSpectrum ./
(PowerSpectrum.*repmat(TXSignalFFT.*conj(TXSignalFFT),NumberOfRXChannels,1)
).^0.5;
            index=round(SteppedFrequencyIndex/FrequencyIndex(2))+1;
            Rec1(count)=RecoveredDataFFT(1,index);
            Rec2(count)=RecoveredDataFFT(2,index);
            Rec3(count)=RecoveredDataFFT(3,index);
            Rec4(count)=RecoveredDataFFT(4,index);
            CRec1(count)=CrossSpectrum(1,index);
            CRec2(count)=CrossSpectrum(2,index);
            CRec3(count)=CrossSpectrum(3,index);
            CRec4(count)=CrossSpectrum(4,index);
            RecIndex(count)=index;

            phaseDiff1=abs(angle(RecoveredDataFFT(1,index))-
angle(RecoveredDataFFT(2,index)));
            phaseDiff2=abs(angle(RecoveredDataFFT(2,index))-
angle(RecoveredDataFFT(3,index)));
            phaseDiff3=abs(angle(RecoveredDataFFT(3,index))-
angle(RecoveredDataFFT(4,index)));

            phaseDiff1=abs(angle(CrossSpectrum(1,index))-
angle(CrossSpectrum(2,index)));
            phaseDiff2=abs(angle(CrossSpectrum(2,index))-
angle(CrossSpectrum(3,index)));
            phaseDiff3=abs(angle(CrossSpectrum(3,index))-
angle(CrossSpectrum(4,index)));


                DisplayThis = 1; % ctrl R % remove ctrl T
            if  DisplayThis == 1,
                figure(21)
                hold on
                plot(SteppedFrequencyIndex,phaseDiff1,'x','color','blue');
                plot(SteppedFrequencyIndex,phaseDiff2,'x','color','red');
                plot(SteppedFrequencyIndex,phaseDiff3,'x','color','green');
                title('PhaseDiff')
                xlabel('Frequency (Hz)')
                ylabel('Phase Diffrent (Rad')
                drawnow;
            end

           RotationThreshold=EstimatedVelocity/(2*SensorSpacing);

NumOfPhaseRotation=floor(SteppedFrequencyIndex/RotationThreshold);

            if phaseDiff1>pi,
                phaseDiff1=((NumOfPhaseRotation+1)*2*pi)-phaseDiff1;
            else
                phaseDiff1=(NumOfPhaseRotation*2*pi)-phaseDiff1;
            end
            if phaseDiff2>pi,
                 phaseDiff2=((NumOfPhaseRotation+1)*2*pi)-phaseDiff2;
            else
                phaseDiff2=(NumOfPhaseRotation*2*pi)-phaseDiff2;
```

```
            end
            if phaseDiff3>pi,
                 phaseDiff3=((NumOfPhaseRotation+1)*2*pi)-phaseDiff3;
            else
                phaseDiff3=(NumOfPhaseRotation*2*pi)-phaseDiff3;
            end

             phaseDiff1=abs(phaseDiff1);
             phaseDiff2=abs(phaseDiff2);
             phaseDiff3=abs(phaseDiff3);


estVelocity1=2*pi*SteppedFrequencyIndex*SensorSpacing/phaseDiff1;

estVelocity2=2*pi*SteppedFrequencyIndex*SensorSpacing/phaseDiff2;

estVelocity3=2*pi*SteppedFrequencyIndex*SensorSpacing/phaseDiff3;
             RecEstVelocity1(count)=estVelocity1;
             RecEstVelocity2(count)=estVelocity2;
             RecEstVelocity3(count)=estVelocity3;
             disp(['Estimated velocity: ' num2str(estVelocity1)]);
             % plot magnitude and phase of cross-spectrum
             DisplayThis = 0;
             if DisplayThis == 1,
                 figure(5)
                 plot(FrequencyIndex,abs(CrossSpectrum));
                 title('Normalised Cross-Spectrum')
                 xlabel('Frequency (Hz)')
                 ylabel('Spectrum Level')
                 xlim([0 OutputSamplingRate*PassBandFraction])
                 ylim([0 1.01])
                 figure(6)
                 plot(FrequencyIndex,angle(CrossSpectrum));
                 title('Cross-Spectrum Phase')
                 xlabel('Frequency (Hz)')
                 ylabel('Phase (rads)')
                 xlim([0 OutputSamplingRate*PassBandFraction])
                 figure(7)

plot(FrequencyIndex,angle(CrossSpectrum.*repmat(CompensationFunction,Number
OfRXChannels,1)));
                 title('Compensated Cross-Spectrum Phase')
                 xlabel('Frequency (Hz)')
                 ylabel('Phase (rads)')
                 xlim([0 OutputSamplingRate*PassBandFraction])
             end
             figure(20)
             hold on;
             if estVelocity1<500,
                 plot(SteppedFrequencyIndex,
estVelocity1,'x','color','blue');
             end
             if estVelocity2<500,
                 plot(SteppedFrequencyIndex,
estVelocity2,'x','color','red');
             end
             if estVelocity3<500,
                 plot(SteppedFrequencyIndex,
estVelocity3,'x','color','green');
```

```
            end
            xlabel('Frequency, Hz'); ylabel('Velocity, m/s');
            drawnow;


        end
    end
end

%% Clear the tasks
Status = calllib('nicaiu','DAQmxClearTask',TaskHandle1Numeric);
% int32 DAQmxClearTask(uint32)
% int32 DAQmxClearTask (TaskHandle taskHandle);
if Status ~= 0,
    fprintf('Error in DAQmxClearTask.   Status = %d\n',Status);
    return
end
Status = calllib('nicaiu','DAQmxClearTask',TaskHandle2Numeric);
if Status ~= 0,
    fprintf('Error in DAQmxClearTask.   Status = %d\n',Status);
    return
end

unloadlibrary 'nicaiu';                 % unload library


return
```

B(2). Matlab script for processing data captured from step frequency;

```
% AnalyseAzimanStepFrequency
% Script to analyse data collected with Aziman Soil Exp

clear

DisplayCompensatedPhase = 0;
pingCount=1;
SnapShotNumber=1;
if exist('C:\Users\aziman\Documents\MATLAB\AzimanData\','file'),
    PathName = 'C:\Users\aziman\Documents\MATLAB\AzimanData\';
end

FileNameStub = 'Aziman-15-Nov-2011';
% Load data files generated on that day
FileNameList = dir([PathName FileNameStub '*.mat']);

NumberOfFiles = numel(FileNameList);
if NumberOfFiles == 0,
    disp('No files found');
```

```
    return
end
disp(NumberOfFiles)
for FileNameIndex = 1:NumberOfFiles,
    % Extract file name
    FileName = [PathName FileNameList(FileNameIndex).name];
    % Open file
    if exist(FileName,'file'),
        fprintf('Processing file %s\n',FileName);
        load(FileName);
    else
        disp('File not found')
        return
    end
    dotPos=strfind(FileName,'.');
    hh(FileNameIndex)=str2double(FileName(dotPos-8:dotPos-7));
    mm(FileNameIndex)=str2double(FileName(dotPos-5:dotPos-4));
    ss(FileNameIndex)=str2double(FileName(dotPos-2:dotPos-1));
    % Reserve and initialise variables on the first data load
    if FileNameIndex == 1,
        NumberOfTXChannels = 1; % Define the number of TX channels being
used
        OutputSamplesPerChannel = InputSamplesPerChannel; % Samples to be
output per channel
        % Predicted input A/D channel latency
        PredictedInputLatency = 38.4/InputSamplingRate + 3e-6;     %
latency measured in seconds

        % Predict output D/A latency
        OutputLatency = [3e-6 5e-6 7.5e-6 9.5e-6];
        PredictedOutputLatency = OutputLatency(NumberOfTXChannels);

        % Measurements imply an extra few samples of delay
        AdditionalDelaySamples = 2;
        TotalPredictedLatency = PredictedOutputLatency +
PredictedInputLatency + AdditionalDelaySamples/InputSamplingRate + 1.8e-6;


        % Time index for display purposes
        TimeIndex = (0:(InputSamplesPerChannel-1))/InputSamplingRate;
        % Frequency index for display purposes - assuming zero padded
        FrequencyIndex = (0:(InputSamplesPerChannel -
1)).*InputSamplingRate./InputSamplesPerChannel;

        PhaseSpectrum = zeros(NumberOfRXChannels,InputSamplesPerChannel);
        CrossSpectrum = zeros(NumberOfRXChannels,InputSamplesPerChannel);
        PowerSpectrum = zeros(NumberOfRXChannels,InputSamplesPerChannel);
        AvgDataFFT = zeros(NumberOfRXChannels,InputSamplesPerChannel);
    end

    % Fourier transform - normally fft operates on each column on the
matrix
    RecoveredDataFFT = fft(RecoveredData,InputSamplesPerChannel,2);
    Sensor1Max(SnapShotNumber)=max(RecoveredData(1,:));
    Sensor1Min(SnapShotNumber)=min(RecoveredData(1,:));
    AmplitudeSensor1(SnapShotNumber)=Sensor1Max(SnapShotNumber)-
Sensor1Min(SnapShotNumber);
```

```
    Sensor2Max(SnapShotNumber)=max(RecoveredData(2,:));
    Sensor2Min(SnapShotNumber)=min(RecoveredData(2,:));
    AmplitudeSensor2(SnapShotNumber)=Sensor2Max(SnapShotNumber)-
Sensor2Min(SnapShotNumber);

    Sensor3Max(SnapShotNumber)=max(RecoveredData(3,:));
    Sensor3Min(SnapShotNumber)=min(RecoveredData(3,:));
    AmplitudeSensor3(SnapShotNumber)=Sensor3Max(SnapShotNumber)-
Sensor3Min(SnapShotNumber);

    Sensor4Max(SnapShotNumber)=max(RecoveredData(4,:));
    Sensor4Min(SnapShotNumber)=min(RecoveredData(4,:));
    AmplitudeSensor4(SnapShotNumber)=Sensor4Max(SnapShotNumber)-
Sensor4Min(SnapShotNumber);

    RecoveredData1 = fft(RecoveredData,InputSamplesPerChannel,2);

    if SnapShotNumber==NumberOfSnapshots,


        AvgDataFFT = AvgDataFFT + RecoveredDataFFT;

        AvgAmplitudeSensor1=mean(AmplitudeSensor1);
        AvgAmplitudeSensor2=mean(AmplitudeSensor2);
        AvgAmplitudeSensor3=mean(AmplitudeSensor3);
        AvgAmplitudeSensor4=mean(AmplitudeSensor4);

        AmpSensor1(pingCount)=AvgAmplitudeSensor1;
        AmpSensor2(pingCount)=AvgAmplitudeSensor2;
        AmpSensor3(pingCount)=AvgAmplitudeSensor3;
        AmpSensor4(pingCount)=AvgAmplitudeSensor4;


NormalisedWithSensor11(pingCount)=20*log10(AvgAmplitudeSensor1./AvgAmplitud
eSensor1);

NormalisedWithSensor12(pingCount)=20*log10(AvgAmplitudeSensor2./AvgAmplitud
eSensor1);

NormalisedWithSensor13(pingCount)=20*log10(AvgAmplitudeSensor3./AvgAmplitud
eSensor1);

NormalisedWithSensor14(pingCount)=20*log10(AvgAmplitudeSensor4./AvgAmplitud
eSensor1);

        index=round(SteppedFrequencyIndex/FrequencyIndex(2))+1;

        for chanNum=1:NumberOfRXChannels,
            RecordDataFFT(chanNum, pingCount,
SnapShotNumber)=RecoveredDataFFT(chanNum, index);
        end

        Frequency(pingCount)=FrequencyIndex(index);

        ResultTXSignalFFT(pingCount)=TXSignalFFT(index);

        for chanNum=1:NumberOfRXChannels,
```

```
            ResultAvgDataFFT(chanNum,pingCount)=AvgDataFFT(chanNum,index);
        end

        AvgDataFFT = zeros(NumberOfRXChannels,InputSamplesPerChannel);

        pingCount=pingCount+1;
        SnapShotNumber=1;
    else
        index=round(SteppedFrequencyIndex/FrequencyIndex(2))+1;

        for chanNum=1:NumberOfRXChannels,
            RecordDataFFT(chanNum, pingCount,
SnapShotNumber)=RecoveredDataFFT(chanNum, index);
        end
        SnapShotNumber=SnapShotNumber+1;

        AvgDataFFT = AvgDataFFT + RecoveredDataFFT;

% Only display on single snapshot usage - takes up too much time otherwise
        DisplayThis = 0;
        if DisplayThis == 1,
            % Display data for channel 1
            InputSensorIndex = 1;
            figure(3)
            plot(TimeIndex,RecoveredData)
            title('Raw Input Data')
            xlabel('Time (s)')
            ylabel('Voltage (V)')
            ylim([-1 1])
            drawnow

            figure(4)
            plot(FrequencyIndex,20*log10(abs(TXSignalFFT)),'r')
            hold on
            plot(FrequencyIndex,20*log10(abs(RecoveredDataFFT)),'k');
            hold off
            legend('Drive Signal','Sense Signals',0)
            ylabel('Spectral Amplitude (dB)')
            xlabel('Frequency (Hz)')
            title('Linear Spectra of Transmit and Received Signals');
            xlim([0 InputSamplingRate*PassBandFraction]);
            drawnow
        end
    end
end

% AmplitudeFunction = sinc(Frequency/InputSamplingRate);
 CompensationFunction =  exp(j*2*pi*Frequency*TotalPredictedLatency);
 CrossSpectrum =
ResultAvgDataFFT.*repmat(ResultTXSignalFFT,NumberOfRXChannels,1);
 PowerSpectrum = ResultAvgDataFFT.*conj(ResultAvgDataFFT);
 CompCrossSpectrum =
CrossSpectrum.*repmat(CompensationFunction,NumberOfRXChannels,1);

 phaseCross1=CrossSpectrum(1,:).*conj(CrossSpectrum(2,:));
 phaseCross2=CrossSpectrum(2,:).*conj(CrossSpectrum(3,:));
 phaseCross3=CrossSpectrum(3,:).*conj(CrossSpectrum(4,:));
 figure(18);
```

```
 plot(Frequency,angle(phaseCross1));
save('ProcessedData.mat','CrossSpectrum','ResultTXSignalFFT','ResultAvgData
FFT','RecordDataFFT','CompensationFunction','Frequency')
```

B.3. Matlab script for calculated coherences and phase velocities for each sensor-pair;

```
clear all
%load ProcessedData3000_10_100004Acc1_2Bar3_4NoBarSrc_MidBar
%load ProcessedData3000_10_100004Acc1_2NoBar3_4Bar
%load ProcessedData3000_10_100004AccSrcFarNoBarHoriNew
%load ProcessedData3000_10_100004Acc1_2NoBar3_4BarSrc_Bet2_3
%load ProcessedData3000_10_100004Acc1_2NoBar3_4BarSrcBet2_3Redo
%load ProcessedData3000_10_100004acc1_2Bar3_4NoBarSrc2_3_26Nov
load ProcessedData122.mat%14Jun7cm3cmSrcStart_01  %12Clay34ColSrcMid_04
%12Col34ColSrcMid_01 %23AprSplitSrc1234column03 %06Aug12Clay34ColSrcMid_01
%n   %  %12Col34ClaySrcMid_01  %SrcMid_02
cohThresh=0.9;
minFreq=2000;
maxFreq=7000;
depthFreqStep=5;
SensorSpacingCol=0.025;
SensorSpacingClay=0.025;

% LOAD SETNUM ONLY
for setNum=1,
    phaseCross(1,:)=ResultAvgDataFFT(1,:).*conj(ResultAvgDataFFT(2,:));
    phaseCross(2,:)=ResultAvgDataFFT(2,:).*conj(ResultAvgDataFFT(3,:));
    phaseCross(3,:)=ResultAvgDataFFT(3,:).*conj(ResultAvgDataFFT(4,:));

phaseD(1,:)=angle(ResultAvgDataFFT(1,:))-angle(ResultAvgDataFFT(2,:));
phaseD(2,:)=angle(ResultAvgDataFFT(2,:))-angle(ResultAvgDataFFT(3,:));
phaseD(3,:)=angle(ResultAvgDataFFT(3,:))-angle(ResultAvgDataFFT(4,:));

    [chanNum,freqIndexTotal,avgNum]=size(RecordDataFFT);

    for index=1:freqIndexTotal,
        myCrossCoh(1,index)=(1/(avgNum-1))*(sum((RecordDataFFT(1,index,:)-
mean(RecordDataFFT(1,index,:))).*conj((RecordDataFFT(2,index,:)-
mean(RecordDataFFT(2,index,:))))))/(var(RecordDataFFT(1,index,:))*var(Recor
dDataFFT(2,index,:)))^0.5;
        myCrossCoh(2,index)=(1/(avgNum-1))*(sum((RecordDataFFT(2,index,:)-
mean(RecordDataFFT(2,index,:))).*conj((RecordDataFFT(3,index,:)-
mean(RecordDataFFT(3,index,:))))))/(var(RecordDataFFT(2,index,:))*var(Recor
dDataFFT(3,index,:)))^0.5;
        myCrossCoh(3,index)=(1/(avgNum-1))*(sum((RecordDataFFT(3,index,:)-
mean(RecordDataFFT(3,index,:))).*conj((RecordDataFFT(4,index,:)-
mean(RecordDataFFT(4,index,:))))))/(var(RecordDataFFT(3,index,:))*var(Recor
dDataFFT(4,index,:)))^0.5;
    end



    for comp=1:3,
        for index=1:freqIndexTotal,
            if (abs(myCrossCoh(comp,index))>cohThresh),
                phaseCoh(comp,index)=angle(phaseCross(comp,index));
            else
```

```
                phaseCoh(comp,index)=0;
            end
        end
    end

    count=0;
    phaseCross1unwrap=unwrap(angle(phaseCross(1,:)));
    for index=1:freqIndexTotal,
        if (abs(myCrossCoh(1,index))>cohThresh) &
(Frequency(index)>minFreq) & (Frequency(index)<maxFreq)
            count=count+1;
            phaseCoh1(count)=phaseCross1unwrap(1,index);
            freq1(count)=Frequency(index);
        end
    end
    if count>0,
        P1=polyfit(freq1,phaseCoh1,1);
    end
    count=0;
    phaseCross3unwrap=unwrap(angle(phaseCross(3,:)));
    for index=1:freqIndexTotal,
        if (abs(myCrossCoh(3,index))>cohThresh) &
(Frequency(index)>minFreq) & (Frequency(index)<maxFreq)
            count=count+1;
            phaseCoh3(count)=phaseCross3unwrap(1,index);
            freq3(count)=Frequency(index);
        end
    end
    if count>0,
        P3=polyfit(freq3,phaseCoh3,1);
    end


Vph(1,:)=abs(2*pi*Frequency*SensorSpacing./unwrap(angle(phaseCross(1,:))));
%
Vph(2,:)=abs(2*pi*Frequency*SensorSpacing./unwrap(angle(phaseCross(2,:))));
% (off Vph(2,:) if seismic source in the middle of array)

Vph(3,:)=abs(2*pi*Frequency*SensorSpacing./unwrap(angle(phaseCross(3,:))));
        VphCoh12=abs(2*pi*freq1*SensorSpacing./phaseCoh1);
%         VphCoh23=abs(2*pi*freq2*SensorSpacing./phaseCoh2); % (off
VphCoh23 if seismic source in the middle of array)
        VphCoh34=abs(2*pi*freq3*SensorSpacing./phaseCoh3);
        Vph1=transpose(Vph);
        Frequency1=transpose(Frequency);
        xlswrite('Frequency1.xls',Frequency1)
        xlswrite('Vph1.xls',Vph1);
        VphCoh12=transpose(VphCoh12);
        VphCoh34=transpose(VphCoh34);
        xlswrite('VphCoh12.xls',VphCoh12);
%         xlswrite('VphCoh23.xls',VphCoh23);
        xlswrite('VphCoh34.xls',VphCoh34);
        freq12=transpose(freq1);
        xlswrite('freq12.xls',freq12);
%         xlswrite('freq2.xls',freq2);
        freq34=transpose(freq3);
        xlswrite('freq34.xls',freq34);
```

```
% this plot for all velocity across the frequency without considered
coherence
drawthis=1;
    if drawthis==1,
        figure(30);

plot(Frequency,abs(2*pi*Frequency*SensorSpacing./unwrap(angle(phaseCross(1,
:)))),'b','linewidth',2);
        hold on
%
plot(Frequency,abs(2*pi*Frequency*SensorSpacing./unwrap(angle(phaseCross(2,
:)))),'g','linewidth',2);
%         hold on

plot(Frequency,abs(2*pi*Frequency*SensorSpacing./unwrap(angle(phaseCross(3,
:)))),'m','linewidth',2);
        hold off
        legend('A-B','C-D',0)
        titleH=title('');
        xLabelH=xlabel('Frequency, Hz');
        yLabelH=ylabel('Phase Velocity, m/s');
        set(xLabelH,'FontSize',18);
        set(xLabelH,'FontWeight','Demi');
        set(yLabelH,'FontSize',18);
        set(yLabelH,'FontWeight','Demi');
        set(titleH,'FontSize',18);
        set(titleH,'FontWeight','Demi');
        set(gca,'XLim',[minFreq,maxFreq]);
        set(gca,'FontSize',18);
        set(gca,'FontWeight','Demi');
        set(gcf,'PaperUnits','inches','PaperPosition',[0 0 7 4])
        grid on
end


% this plot for only velocity that higher than stated coherence
 drawthis=1;
    if drawthis==1,
        figure(40);

plot(freq1,abs(2*pi*freq1*SensorSpacing./phaseCoh1),'b','linewidth',2);
        hold on
%
plot(freq2,2*pi*freq2*SensorSpacing./abs(phaseCoh2),'g','linewidth',2);
%         hold on

plot(freq3,abs(2*pi*freq3*SensorSpacing./phaseCoh3),'m','linewidth',2);
        hold off
        legend('A-B','C-D',0)
        %titleH=title('Phase velocity of clay');
        xLabelH=xlabel('Frequency, Hz');
        yLabelH=ylabel('Phase Velocity, m/s');
        set(xLabelH,'FontSize',18);
        set(xLabelH,'FontWeight','Demi');
        set(yLabelH,'FontSize',18);
        set(yLabelH,'FontWeight','Demi');
        set(titleH,'FontSize',18);
        set(titleH,'FontWeight','Demi');
        set(gca,'XLim',[minFreq,maxFreq]);
```

```
        set(gca,'FontSize',18);
        set(gca,'FontWeight','Demi');
        set(gcf,'PaperUnits','inches','PaperPosition',[0 0 7 4])
        grid on
 end

  drawthis=1;
    if drawthis==1,
        figure(5);
        plot(Frequency,abs(myCrossCoh(1,:)),'b','linewidth',2);
        hold on
%         plot(Frequency,abs(myCrossCoh(2,:)),'g','linewidth',2);
%         hold on
        plot(Frequency,abs(myCrossCoh(3,:)),'m','linewidth',2);
        hold off
        legend('A-B','C-D',0)
        %titleH=title('Typical normalised coherence for both receiver');
        xLabelH=xlabel('Frequency, Hz');
        yLabelH=ylabel('Normalise coherence');
        set(xLabelH,'FontSize',18);
        set(xLabelH,'FontWeight','Demi');
        set(yLabelH,'FontSize',18);
        set(yLabelH,'FontWeight','Demi');
        set(titleH,'FontSize',18);
        set(titleH,'FontWeight','Demi');
        set(gca,'XLim',[minFreq,maxFreq]);
        set(gca,'YLim',[0,1]);
        set(gca,'FontSize',18);
        set(gca,'FontWeight','Demi');
        set(gcf,'PaperUnits','inches','PaperPosition',[0 0 7 4])
        grid on
    end

  drawthis=1;
    if drawthis==1,
        figure(10)
        hold on
        plot(Frequency,angle(phaseCross(1,:)),'blue','linewidth',2);
%       plot(Frequency,angle(phaseCross(2,:)),'green','linewidth',2);
        plot(Frequency,angle(phaseCross(3,:)),'red','linewidth',2);
        legendH=legend('A-B','C-D',1);
        %titleH=title('Phase difference');
        xLabelH=xlabel('Frequency (Hz)');
        yLabelH=ylabel('Phase difference (radians)');
        set(legendH,'FontSize',14);
        set(legendH,'FontWeight','Demi');
        set(xLabelH,'FontSize',18);
        set(xLabelH,'FontWeight','Demi');
        set(yLabelH,'FontSize',18);
        set(yLabelH,'FontWeight','Demi');
        set(titleH,'FontSize',18);
        set(titleH,'FontWeight','Demi');
        set(gca,'XLim',[minFreq,maxFreq]);
        set(gca,'FontSize',18);
        set(gca,'FontWeight','Demi');
        set(gcf,'PaperUnits','inches','PaperPosition',[0 0 7 4])
        grid on
    end
```

```
    drawthis=1;
    if drawthis==1,
        figure(12)
        hold on
   plot(Frequency,unwrap(angle(phaseCross(1,:))),'blue','linewidth',2);

%plot(Frequency,unwrap(angle(phaseCross(2,:))),'green','linewidth',2);
        plot(Frequency,unwrap(angle(phaseCross(3,:))),'red','linewidth',2);
        legendH=legend('A-B','C-D',2);
        %titleH=title('Phase difference');
        xLabelH=xlabel('Frequency, Hz');
        yLabelH=ylabel('Unwrapped phase difference, radians');
        set(legendH,'FontSize',14);
        set(legendH,'FontWeight','Demi');
        set(xLabelH,'FontSize',18);
        set(xLabelH,'FontWeight','Demi');
        set(yLabelH,'FontSize',18);
        set(yLabelH,'FontWeight','Demi');
        set(titleH,'FontSize',18);
        set(titleH,'FontWeight','Demi');
        set(gca,'XLim',[minFreq,maxFreq]);
        set(gca,'FontSize',18);
        set(gca,'FontWeight','Demi');
        set(gcf,'PaperUnits','inches','PaperPosition',[0 0 7 4])
        %print(gcf,'-dtiffnocompression',tiffFileName,'-r600');
        grid on
    end

    drawthis=1;
    if drawthis==1,
        figure(15);
        plot(Frequency, abs(myCrossCoh(1,:)),'linewidth',2);
        titleH=title('Typical normalised coherence (1st set receiver)');
        xLabelH=xlabel('Frequency (Hz)');
        yLabelH=ylabel('Normalised coherence');
        set(xLabelH,'FontSize',18);
        set(xLabelH,'FontWeight','Demi');
        set(yLabelH,'FontSize',18);
        set(yLabelH,'FontWeight','Demi');
        set(titleH,'FontSize',18);
        set(titleH,'FontWeight','Demi');
        set(gca,'XLim',[minFreq,maxFreq]);
        set(gca,'YLim',[0,1]);
        set(gca,'FontSize',18);
        set(gca,'FontWeight','Demi');
        set(gcf,'PaperUnits','inches','PaperPosition',[0 0 7 4])
        grid on
    end
%  drawthis=1;
%     if drawthis==1,
%         figure(15);
%         plot(Frequency, abs(myCrossCoh(2,:)),'linewidth',2);
%         titleH=title('Typical Normalised Coherence (Set with Sand)');
%         xLabelH=xlabel('Frequency (Hz)');
%         yLabelH=ylabel('Normalised Coherence');
%         set(xLabelH,'FontSize',18);
%         set(xLabelH,'FontWeight','Demi');
%         set(yLabelH,'FontSize',18);
%         set(yLabelH,'FontWeight','Demi');
%         set(titleH,'FontSize',18);
```

```
%         set(titleH,'FontWeight','Demi');
%         set(gca,'XLim',[490,1410]);
%         set(gca,'YLim',[0,1]);
%         set(gca,'FontSize',18);
%         set(gca,'FontWeight','Demi');
%         set(gcf,'PaperUnits','inches','PaperPosition',[0 0 7 4])
%         print(gcf,'-dtiffnocompression',tiffFileName,'-r600');
%         grid on
%     end

    drawthis=1;
    if drawthis==1,
        figure(20);
        plot(Frequency, abs(myCrossCoh(3,:)),'linewidth',2);
        titleH=title('Typical normalised coherence (2nd set receiver)');
        xLabelH=xlabel('Frequency (Hz)');
        yLabelH=ylabel('Normalised coherence');
        set(xLabelH,'FontSize',18);
        set(xLabelH,'FontWeight','Demi');
        set(yLabelH,'FontSize',18);
        set(yLabelH,'FontWeight','Demi');
        set(titleH,'FontSize',18);
        set(titleH,'FontWeight','Demi');
        set(gca,'XLim',[minFreq,maxFreq]);
        set(gca,'YLim',[0,1]);
        set(gca,'FontSize',18);
        set(gca,'FontWeight','Demi');
        set(gcf,'PaperUnits','inches','PaperPosition',[0 0 7 4])
        %print(gcf,'-dtiffnocompression',tiffFileName,'-r600');
        grid on
    end
         return
```

Appendix C. Bender Element

Quantification of soil properties is of primary value to geotechnical design and field work. The classical use of triaxial compression and oedometer consolidation tests has been the usual methods for routine estimations of soil properties such as stiffness, strength and compressibility. In recent years, there have been many dynamic methods of measuring and assessing soil stiffness properties, especially using shear wave velocities generated by piezo-ceramic plate transducers known as ‘bender elements’.

The bender element test was probably the first test used rigorously to uncover the relationship between geotechnical and geophysical properties of soil. To realize this objective, bender element sensors were applied in the triaxial apparatus. This made it possible to apply isotropic stress conditions on a soil specimen and then measure the shear wave velocity. The

shear wave was generated and received by the bender element sensors located at opposite ends of the soil specimen. The shear wave velocity was then calculated from the tip to tip distance between both transducers.

The principle of using the bender elements is based on the properties of piezoelectric materials. When a voltage is applied to the combination of two piezoelectric materials, it causes one to expand while the other contracts thus causing the entire element to bend as shown in Figure C.1.

In the similar manner, a lateral disturbance of the bender element will create a voltage so as to enable the bender elements to be used as both shear wave transmitter and receiver. By measuring the time delay between sending and receiving of the shear wave, the shear wave velocity can be determined. This defines the bender element as a two layer piezoelectric transducer that consists of two conductive outer electrodes, two piezo-ceramic sheets and a conductive metal shim at the centre (Kramer, 1996).

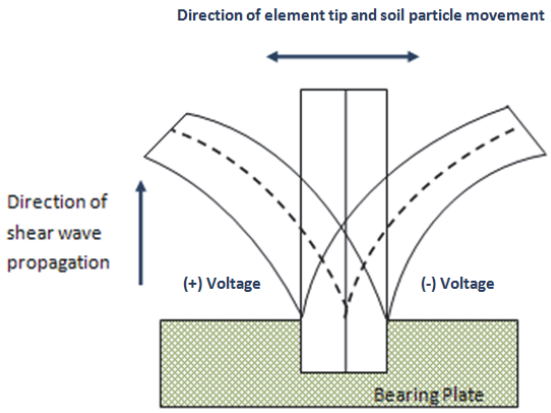

Figure C.1: Operation of a bender element (after Kramer, 1996)

Figure C.2 shows a classical arrangement for the triaxial apparatus with bender elements set up. A personal computer generates the signal which is amplified by an amplifier and a voltage pulse is applied to the transmitter which causes it to produce a shear wave. The shear

wave on reaching the other end of the soil specimen causes distortion of the receiver, and thus produces another voltage pulse. The receiver is directly connected to an analyser to compare the time gap between the transmitter and the receiver as illustrated in Figure C.3.

In this study, the initial test arrangement used a laptop to run a signal processor, which was connected to the bender elements. Both elements sent and received the voltage pulses and record the time delay. The shear wave velocity in the soil specimen can be computed by subtracting the time delay by the system as measured by the calibration test.

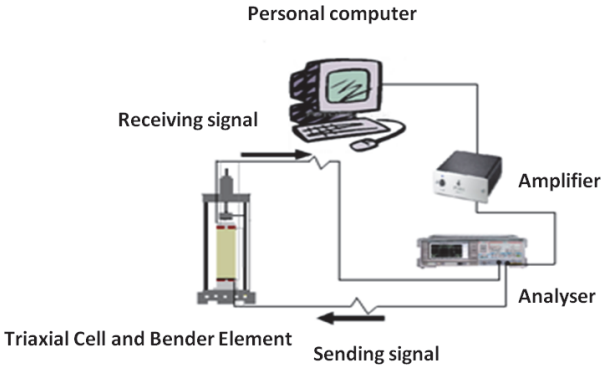

Figure C.2: Set-up of bender elements in triaxial apparatus

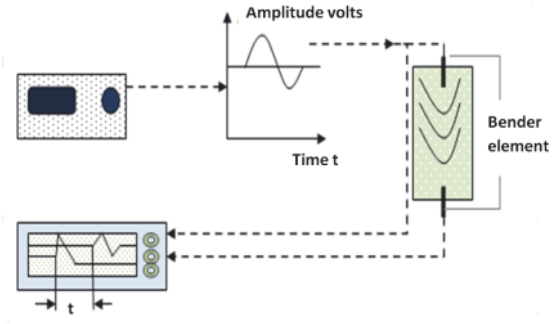

Figure C.3: Bender element and associated electronics

FiguresC.4 and C.5 show the construction and design for the bender elements to be fitted in the triaxial apparatus.

Figures C.4.a and C.4.b show the schematic plan for the bottom cap instrument for both top and seated view. In the top view the yellow circles are threaded for clamping the plinth onto the base. The bender element which has a diameter of 20 mm is located at the centre of the

cap with 100 mm diameter to be suitable for the specimen which also has a diameter of 100 mm. Figures C.4.c and C.4.d show the constructed bottom cap which was used in this research.

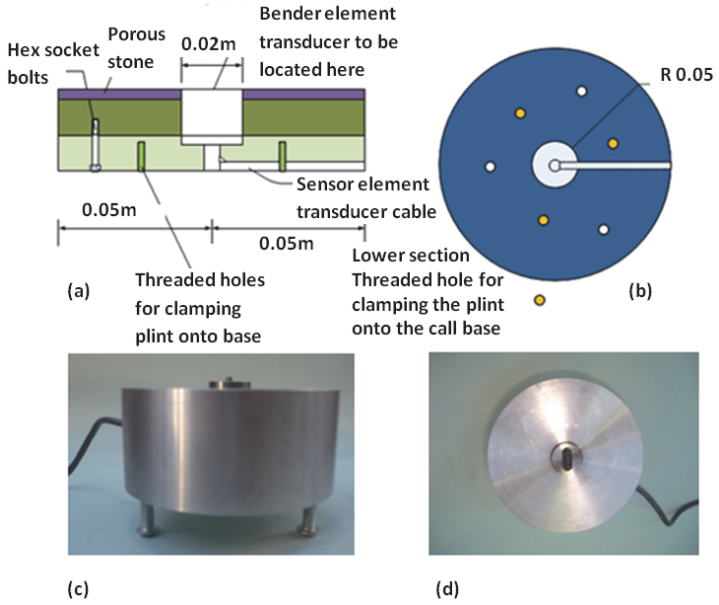

Figure C.4: Bottom cap for the bender element test; (a) schematic design seated view, (b) schematic design top view, (c) constructed bottom cap with bender element at the centre front view, (d) constructed bottom cap with bender element at the centre top view

Figures C.5.a and C.5.b indicate the top cap for the bender element for top and seated view. In Figure C.5.a, there is a small hole found at the top of this cap which is for locating the loading shaft of the triaxial apparatus. as with the bottom cap, the blender element which has a diameter of 20 mm is located at the centre of the cap with 100 mm diameter to be suitable for the specimen which also has a diameter of 100 mm. Figures C.5.c and C.5.d are the actual constructed top cap for the triaxial apparatus which was used in this research.

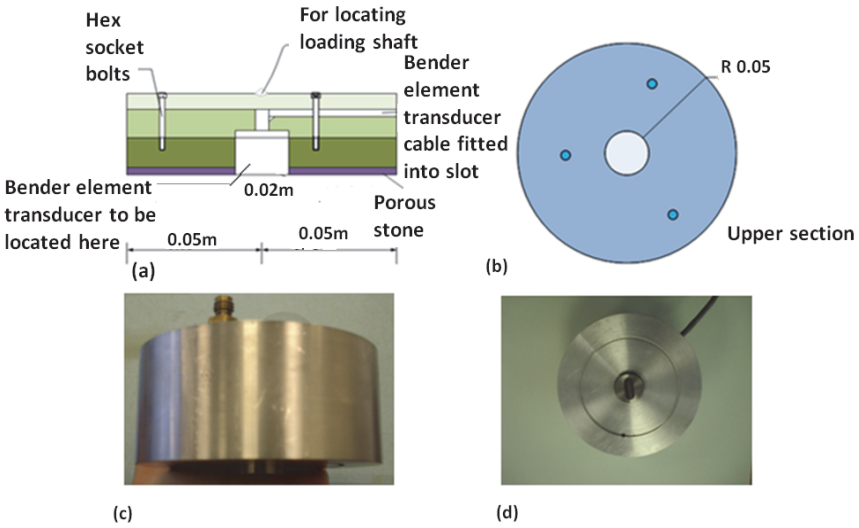

Figure C.5: Top cap for the bender element test; (a) schematic design seated view, (b) schematic design top view (c) constructed top cap with bender element at the centre front view, (d) constructed top cap with bender element at the centre top view

The recommended methodology was the routine procedure of a drained consolidation sequence in a triaxial cell followed by undrained shearing (Head, 1986). The only additional process is that S-wave velocity measurements are to be taken at each stage of the test using bender element with top cap and bottom pedestal as shown in Figures C.4 and C.5.

Bender element test was an original intention of this research, but repeated equipment malfunctions precluded its use and the test programme presented herein was devised to achieve the project's objectives.]

Methods of Analysis for Acoustic Properties

The analysis of the test results for the Kaolin Clay sample under isotropic stress conditions are outlined here. In triaxial test and the relation between them is the Poisson's ratio in undrained test conditions. In the analysis of bender element tests the time delay between the transducer and receiver signals allows the calculation of the shear wave velocity , V_s, and then the shear modulus, G (Equation 3.8). The equipment for this test was created and the

preliminary tests and the geotechnical properties of the Kaolin were carried out and established respectively, but due to some difficulties with the equipment, the results were not reliable so an alternative suitable seismic surface wave method has been considered.